Design and Synthesis of Acene Oligomers for the Study of Photophysical Processes

by

Yuxuan Hou

A thesis submitted in partial fulfillment of the requirements for the degree of

Doctor of Philosophy

Department of Chemistry
University of Alberta

Abstract

A variety of organic molecules have been used to study photophysical processes, such as singlet fission (SF) and triplet-triplet annihilation upconversion (TTA-UC), which are proposed strategies to improve the power conversion efficiencies of photovoltaics. Despite extensive study on these photophysical concepts over the past decades, the underlying molecular mechanisms are not well defined yet, and applications to photovoltaics remain to be achieved. Of the chromophores suited for photophysical studies, acene-based molecules have been the most common candidates to answer specific underlying questions about the mechanisms of SF and TTA-UC.

This thesis focuses on the design, synthesis, and characterization of tetracene and pentacene derivatives. Chapter 1 introduces acenes and the synthesis of acene derivatives, in particular *peri*-alkyne-functionalized acenes. This chapter also gives a brief introduction of the photophysical processes that are key to the studies of molecules in the thesis, SF and TTA-UC. Then, the state-of-the-art designs of acene-based molecules using the heavy-atom effect (HAE) and chromophore multiplication to promote more efficient materials for SF are described. Furthermore, the representative spacers used in dimeric acenes are presented, particularly with respect to the influence of electronic coupling on SF and TTA-UC.

Chapter 2 focuses on the synthesis of sterically hindered pyridyl ligands either with or without a pentacene moiety. Subsequently, these ligands are used to coordinate with Pt(II) and Pd(II) for the construction of pentacene dimers. The synthesis of tetramers with Ru(II) is presented using the same ligands. The successful formation of these complexes is supported by mass spectrometric and NMR spectroscopic analyses.

These compounds serve as model compounds for our collaborators to study the electronic influence of the heavy atoms and the impact on the mechanism of SF. Besides the study of the HAE, the pentacene tetramer is used to determine the prospect of triplet diffusion via chromophore multiplication.

Chapter 3 presents a stepwise and modular synthesis of covalently linked tetracene dimers featuring tunable electronic coupling using a common building block, which is obtained by mono-addition of acetylides into 5,12-naphthacenequinone. The electronic coupling of the tetracene derivatives has been examined with UV-vis spectroscopy analysis and photophysical analysis by our collaborators. These compounds are designed to unravel the interplay between SF and TTA-UC in dimeric systems.

Chapter 4 presents the synthesis of two sterically hindered pyridyl-endcapped tetracene dimers with identical structures, except that the intramolecular distance between the tetracene moiety and a pendent photosensitizer is varied via the spacer. These dimers are accessed through stepwise nucleophilic addition reactions using the common building blocks developed in Chapter 3. Moreover, pyridyl-endcapped tetracene dimers linked by a butadiyne or a *meta*-diethynylphenylene spacer have been synthesized. These dimers have been coordinated to a ruthenium phthalocyanine to form complexes with the potential to achieve intramolecular sensitization in addition to intramolecular upconversion. All molecules have been sent to our collaborators in Germany to study the process of TTA-UC.

Chapter 5 describes several syntheses as part of projects that are in various stages of exploration. Attempts to synthesize a twisted pentacene dimer are presented,

followed by the synthesis of an azobenzene linked pentacene dimer, and finally, the synthesis of a tetracenyl pyridyl ligand for the formation of tetracene dimers with Pt(II) and Pd(II). While the attempts to synthesize the twisted pentacene dimer are, to date, unsuccessful, a [5]cumulene endcapped with pentacenequinone has been obtained. The pentacene dimer linked by azobenzene has been synthesized successfully and preliminary studies of photoswitching have been conducted on both the unaromatized precursor and targeted pentacene dimer. With irradiation, the unaromatized precursor shows trans to cis isomerization. Studies of the pentacene dimer, however, reveal that the decomposition of the pentacene chromophore effectively competes with switching. In the final section of this chapter, the successful synthesis of tetracene dimers via the coordination of the sterically hindered pyridyl ligand with a tetracene moiety to Pt(II) and Pd(II) is outlined. These compounds serve as models for our collaborators for additional studies of the influence of the HAE on SF.

Chapter 6 gives a summary and an outlook for the design of acene-based molecules for the study of diffusion of triplets in SF and more efficient TTA-UC. Chapter 7 provides the synthetic procedures and the spectroscopic characterization data of the compounds discussed in this thesis.

Preface

Chapter 2 of this thesis has been published as Y. Hou,† I. Papadopoulos,† Y. Bo, A.-S. Wollny, M. J. Fergusen, L. A. Mai, R. R. Tykwinski, D.M. Guldi, "*Catalyzing Singlet Fission by Transition Metals: Second versus Third Row Effects,*" *Precis. Chem.* **2023**, *1*, 555–564 and Y. Hou,† I. Papadopoulos,† M. J. Ferguson, N. Jux, R. R. Tykwinski, D. M. Guldi, "*Photophysical Characterization of a Ruthenium-based Tetrameric Pentacene Complex,*" *J. Porphyrins Phthalocyanines* **2023**, *27*, 686–693. R. R. Tykwinski and I wrote the paper with the contribution of I. Papadopoulos, Y. Bo, and D. M. Guldi. R. R. Tykwinski and I designed the molecules. I synthesized and characterized the molecules. I. Papadopoulos, Y. Bo, A.-S. Wollny, and L. A. Mai carried out photophysical characterization. M. J. Ferguson conducted X-ray crystallographic characterization, refinement, and analysis.

Chapter 3 of this thesis has been published as Y. Bo,† Y. Hou,† D. Thiel,† R. Weiß, M. J. Fergusen, D. M. Guldi, R. R. Tykwinski, "*Tetracene Dimers: A Platform for Intramolecular Down- and Up-conversion,*" *J. Am. Chem. Soc.* **2023**, *145*, 18260–18275. D. M. Guldi, R. R. Tykwinski, Y. Bo and I wrote the paper. R. R. Tykwinski and I designed the molecules. I synthesized and characterized the molecules. Y. Bo, D. Thiel, and R. Weiß carried out photophysical characterization. M. J. Ferguson conducted X-ray crystallographic characterization, refinement, and analysis.

The synthesis of tetracene dimers in Chapter 5 was carried out in collaboration with M. Matabuena at the University of Alberta, who completed his CHEM 401/403 project under my supervision.

The remaining contents of this thesis are my original work and have not been published. Parts of them are joint projects with the research groups of T. Torres at the Autonomous University of Madrid and D. M. Guldi at the University of Erlangen-Nuremberg.

Acknowledgements

I would like to express my deepest gratitude to my supervisor, Dr. Rik R. Tykwinski, who consistently encouraged and supported me in every aspect of my life and shaped my academic journey. Thanks for having me in the group as a research assistant during my undergrad and then continue as a PhD student. The guidance and mentorship from Rik have inspired me to be not only a more independent researcher but also a better human being. I can not image how I could reach this point without Rik.

I would like to thank my group members for always being around and providing helpful suggestions whenever I needed. Big thanks to Yueze, Bob, Parisa, Henrik, Mohamad, David, Mattew, Lan, Miriam, Kévin, Davood, Sebastian, Zachary, Munashe, Kate, Yanwen, Lanting, Dominic, Shedrack, Jakob, Álvaro, Valentin, and Melchor. Special thanks to Yueze for teaching me the techniques and tricks needed to be an organic chemist and always being a role model for me.

I would like to thank the collaborators, including Dr. Dirk M. Guldi, Dr. Tomas Torres, Yifan Bo, Ilias Papadopoulos for all the excellent photophysical analysis. Special thanks to Yifan Bo for all the excellent measurements and countless online discussions. Hope we can meet in person in the future.

Furthermore, I would like to express my gratitude to the X-ray crystallographer, Dr. Michael J. Ferguson, for conducting X-ray crystallographic characterization, refinement, and analysis; the mass spectrometry lab, including Dr. Randy Whittal, Bela Reiz, Jing Zheng, and Dr. Angelina Morales-Izquierdo for all the MS measurements; the analytical lab, including Wayne Moffat and Jennifer Jones for all the IR and DSC measurements; the NMR spectroscopy facility, including Dr. Ryan McKay, Nupur Dabral, and Mark Miskolzie for the training and measurements. I also want to thank my supervisory committee members Dr. Jeffrey M. Stryker and Dr. Lingzi Sang for their suggestions and feedback. Huge thanks to Dr. Anna Jordan for editing my thesis and all the professional writing guides.

Finally, I would like to thank my family and friends for their endless support and love. I could not have done this without you.

Table of Contents

List of Tables

List of Figures

List of Schemes

List of Abbreviations

Å	Ångstrom(s)
An	annihilator
APPI	atmospheric pressure photoionization
aq	aqueous
Ar	aromatic group
bp	boiling point
br	broad
calcd	calculated
CCDC	Cambridge Crystallographic Data Center
CIF	crystallographic information file
cm	centimeter(s)
d	day(s)
d	doublet (NMR spectra)
DCE	1,2-dichloroethane
decomp	decomposition
DMF	*N,N*-dimethylformamide
DSC	differential scanning calorimetry
equiv	equivalent(s)
E	energy
ESI	electrospray ionization
Et	ethyl
eV	electron volt(s)
fs	femtosecond(s)
FTIR	Fourier transformation infrared spectroscopy
g	gram(s)
h	hour(s)
HAE	heavy-atom effect
HOMO	highest occupied molecular orbital

HSQC	heteronuclear single quantum coherence
Hz	hertz
*i*Bu	*iso*-butyl
*i*Pr	*iso*-propyl
ISC	intersystem crossing
iSF	intramolecular singlet fission
iTTA-UC	intramolecular triplet-triplet annihilation upconversion
IR	infrared
L	liter(s)
LiHMDS	lithium hexamethyldisilazide
LUMO	lowest unoccupied molecular orbital
m	medium (IR spectra)
m	multiplet (NMR spectra)
m	*meta*
M	intermediate (kinetic models)
M	molar
MALDI	matrix-assisted laser desorption ionization
Me	methyl
mg	milligram(s)
min	minute(s)
MHz	megahertz
mL	milliliter(s)
mmol	millimole(s)
mol	mole(s)
mp	melting point
MS	mass spectrometry
m/z	mass-to-charge ratio
*n*BuLi	*n*-butyllithium
NC	nanocrystal
NEt_3	triethylamine

NIR	near-infrared
nm	nanometer(s)
NMR	nuclear magnetic resonance
ns	nanosecond(s)
OLED	organic light emitting diode
ORTEP	Oak Ridge thermal ellipsoid plot
OSC	organic solar cell
p	*para*
PCE	pow conversion efficiency
Ph	phenyl
ppm	parts per million
ps	picosecond(s)
q	quartet (NMR spectra)
quint	quintet (NMR spectra)
R_f	retention factor
rt	room temperature
s	singlet (NMR spectra)
s	strong (IR spectra)
S_0	ground state
S_1	first singlet excited state
satd	saturated
Sen	sensitizer
sept	septet (NMR spectra)
sh	shoulder (absorption)
t	triplet (NMR spectra)
T_1	first triplet excited state
*t*Bu	*tert*-butyl
TAS	transient absorption spectroscopy
TBAF	tetrabutylammonium fluoride
TDA-1	tris[2-(2-methoxyethoxy)ethyl]amine

TET	triplet energy transfer
THF	tetrahydrofuran
TIBS	tri*iso*butylsilyl
TIPS	tri*iso*propylsilyl
TLC	thin layer chromatography
TMEDA	*N,N,N',N'*-tetramethylethylenediamine
TMS	trimethylsilyl
TTA	triplet-triplet annihilation
TTA-UC	triplet-triplet annihilation upconversion
UC	upconversion
UV-vis	ultraviolet-visible
w	weak (IR spectra)
δ	chemical shift in parts per million
ε	molar absorption coefficient
λ	absorption wavelength
λ_{max}	lowest energy absorption wavelength with maximum absorption
μs	microsecond(s)

CHAPTER 1

Introduction

1.1 Acenes

Acenes are polycyclic aromatic hydrocarbons comprised of linearly fused benzene rings. Among the families of acenes, anthracene, tetracene, and pentacene (Figure 1.1), as well as their derivatives, have been used widely for the study of photophysical processes since their excited states fulfill the necessary energy requirements (e.g., the singlet and triplet state energies).[1–7] However, the applications of unsubstituted acenes in organic electronic devices can be hindered by stability and solubility issues, and functionalized acenes have thus gained more attention in recent years.[8–11]

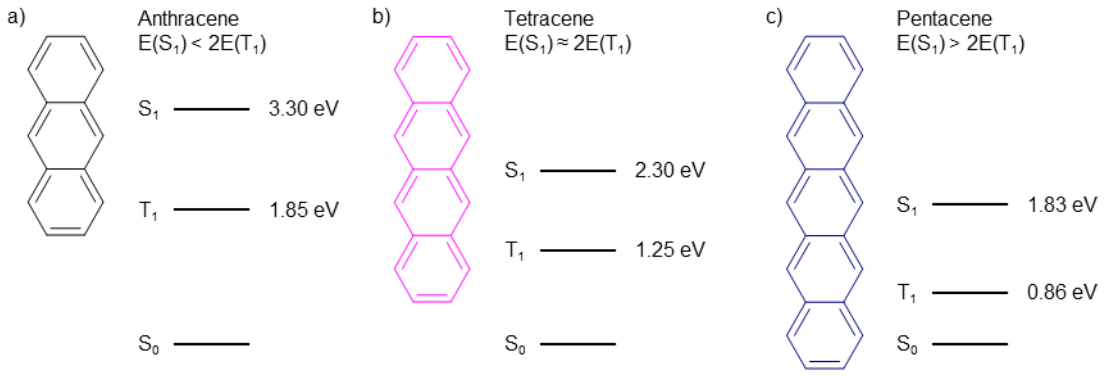

Figure 1.1. Structure and energy levels of T_1 and S_1 for a) anthracene, b) tetracene, and c) pentacene.

1.1.1 Anthracene

Anthracene, first discovered from coal tar in 1832 by Dumas and Laurent, is available commercially in large quantities as it is now isolated from petroleum.[12] The first singlet excited state (S_1) energy of anthracene is 3.10 eV;[13] and, thus, crystalline anthracene has been used as a wide band-gap semiconductor in devices like organic field-effect transistors.[14–16] As shown in Scheme 1.1, anthracene can dimerize under light through a [4 + 4] cycloaddition reaction at the central ring and form dianthracene (**1.1**).[17–19] Anthracene also can react with singlet oxygen through a [4 + 2] cycloaddition and form endoperoxide **1.2**.[20]

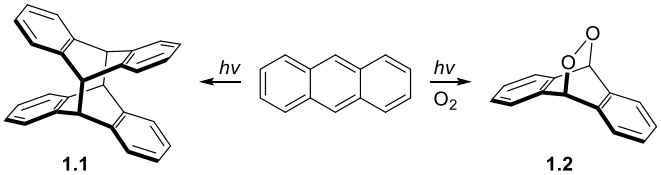

Scheme 1.1. Photoreactions of anthracene, including dimerization (**1.1**) and endoperoxide formation (**1.2**).

1.1.2 Tetracene

Tetracene, also known as naphthacene, is an orange solid with S_1 and triplet (T_1) excited state energies of 2.30 and 1.25 eV, respectively. Tetracene has been explored widely in organic electronic devices, including organic light emitting diodes (OLEDs)[21] and organic solar cells (OSCs).[22] As shown in Scheme 1.2, a suspension of tetracene in benzene can undergo photodimerization under irradiation and form two photodimers **1.3** (head-to-head) and **1.4** (head-to-tail).[23] The photooxidation of tetracene with singlet oxygen gives compound **1.5**.[8]

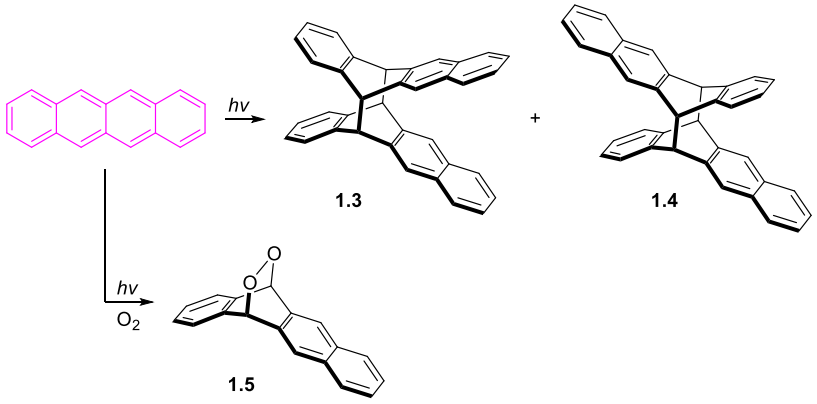

Scheme 1.2. Photoreactions of tetracene, including dimerization (**1.3** and **1.4**) and endoperoxide formation (**1.5**).

1.1.3 Pentacene

Pentacene was synthesized first in 1929 by Clar et al. through a Friedel–Crafts acylation reaction of *m*-xylene and benzoyl chloride.[24–25] Alternatively, it can be obtained as a dark blue solid by reductive aromatization of 6,13-pentacenequinone, which was synthesized through a four-fold aldol condensation reaction with *o*-phthaladehyde (**1.6**) and 1,4-cyclohexanedione (**1.7**, Scheme 1.3).[26]

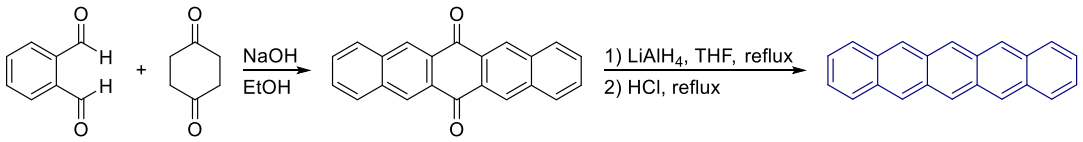

Scheme 1.3. Synthesis of pentacene.

Theoretically, photodimerization of pentacene should afford multiple isomers. By irradiating a solution of pentacene in oxygen free 1-chloronaphthalene at 120 °C, the symmetric dimer **1.8** was obtained as a major product, and a small amount of unsymmetrical dimer **1.9** was detected as well.[27] In the presence of O_2 and light, pentacene undergoes photooxidation at the central aromatic ring and forms compound **1.10** (Scheme 1.4). [28–29]

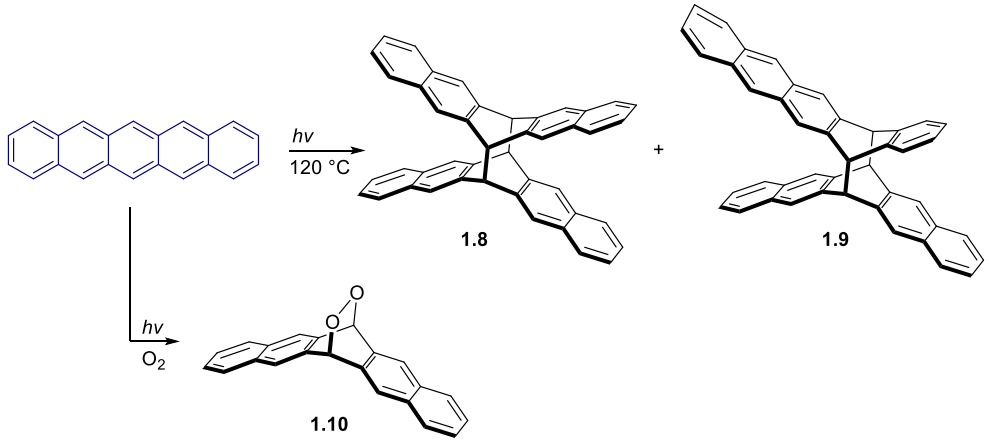

Scheme 1.4. Photoreactions of pentacene, including dimerization (**1.8** and **1.9**) and endoperoxide formation (**1.10**).

Comparatively, the reactivity of anthracene, tetracene, and pentacene increases with length as the π electron system increases and the HOMO–LUMO gap decreases.[9,23,30] Moreover, acenes typically are used as donors in organic electronic devices in conjunction with [60]fullerene as an acceptor. However, acenes can react with [60]fullerene via Diels–Alder [4 + 2] cycloadditions, which leads to problems for device performance.[28,31–32] Therefore, functionalized acenes with better solubility and stability are required for more optimal incorporation into devices.

1.2 Two Photophysical Processes Toward More Efficient Solar Energy Capture

Solar energy is an essential renewable energy resource, which can be converted into electricity with photovoltaic devices. While abundant, the solar radiation reaching the earth's surface covers a broad spectrum of energies, from high-energy ultraviolet, through the visible region, to low-energy infrared (Figure 1.2).[33–34] For a single-junction solar cell, the maximum power conversion efficiency (PCE) is determined mainly by the optical band-gap of the absorbing material. For photons with energies above the bandgap of the absorbing material, excess energy is lost predominantly as heat, so-called thermalization loss. In contrast, photons with energies below the optical band-gap are not absorbed, leading to so-called transmission loss.[35–36] Therefore, the theoretical efficiency limit of single-junction solar cells is approximately 33%, known as the detailed balance limit.[37–38] One strategy to reduce thermalization losses is down-conversion (i.e., singlet fission, SF).[39–43] Alternatively, one strategy to reduce transmission losses is upconversion (i.e., triplet-triplet annihilation upconversion, TTA-UC).[44–46] Both processes have the potential to increasing PCEs beyond current limitations by increasing the window of the solar spectrum that a single junction device can harvest efficiently.

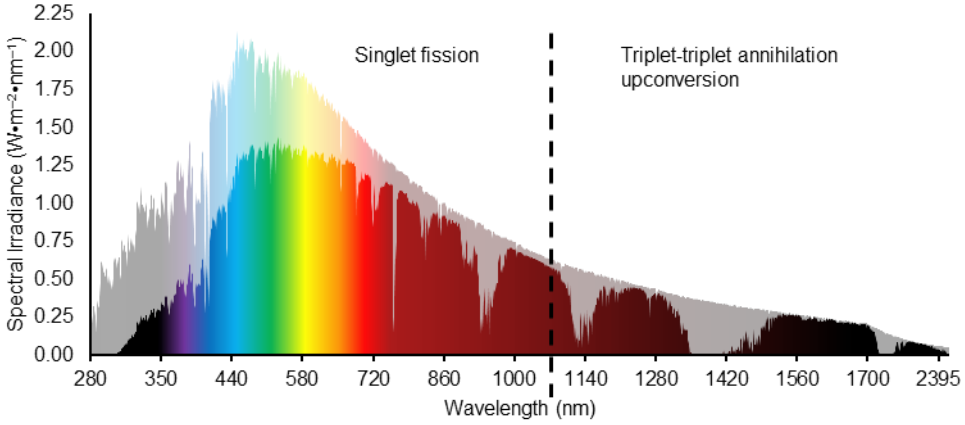

Figure 1.2. Solar spectrum at the sea level (data plotted from National Renewable Energy Laboratory).

1.2.1 Singlet Fission

Singlet fission (SF), a spin-allowed process involving the generation of two triplet excitons (T_1) from one excited singlet exciton (S_1), has been first observed in

anthracene crystals in 1965.[1] SF allows the generation of two pairs of charges from absorption of a single photon and provides an avenue to break the detailed balance limit of single junction solar cells from ~33% to over 45% through reducing thermalization losses.[37,47] As shown in Figure 1.3, when SF occurs, a chromophore in its singlet excited state (S_1) interacts with a nearby chromophore in its ground state (S_0), forming a spin-correlated triplet pair state $^1(T_1T_1)$.[39–40,48–50] Subsequently, the triplet pair undergoes decorrelation, resulting in two non-interacting, free triplet states ($T_1 + T_1$). These triplets are then available for completing the process of solar energy conversion.[39,50–54] En route towards ($T_1 + T_1$), the quintet form of the correlated triplet pair $^5(T_1T_1)$ may be generated, which is a key intermediate towards decorrelation.[47,51,55–59] One competitive pathway that competes with decorrelation of $^1(T_1T_1)$ is triplet-triplet annihilation (TTA), which is quite common in the case of strongly coupled chromophores.[13,59–63]

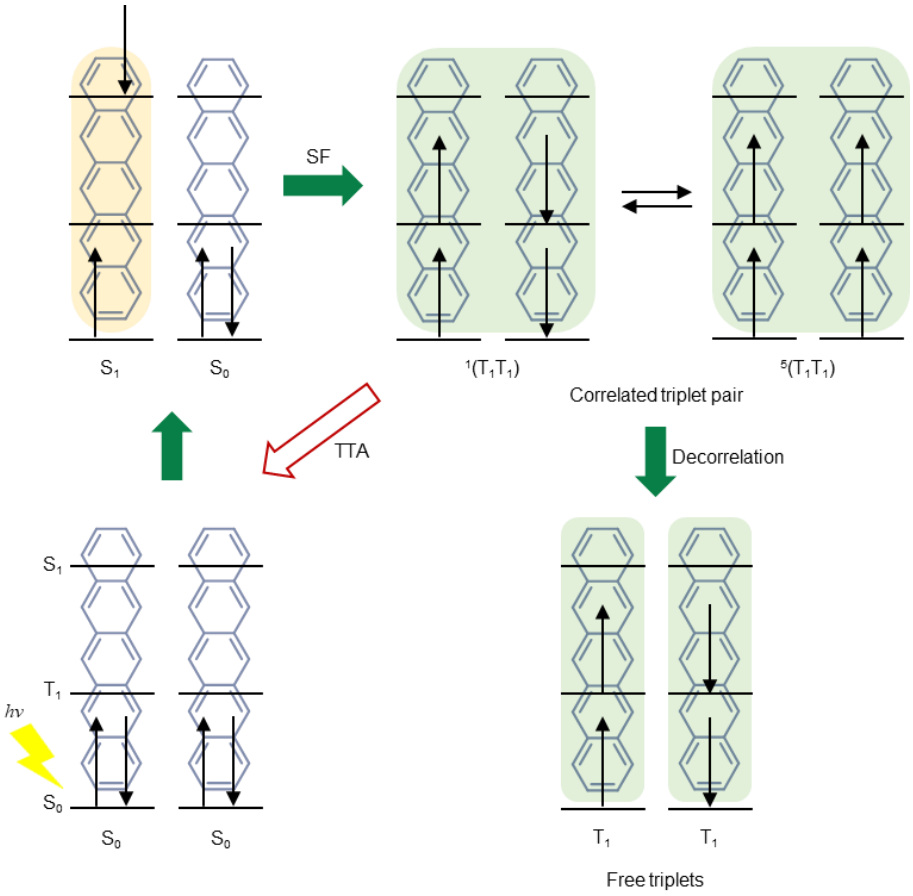

Figure 1.3. Schematic diagram of the mechanism of SF.

Singlet and triplet excited-state energies of the chromophores are essential for SF. For exothermic SF, the energy level of S_1 must be larger than twice that of T_1, namely $E(S_1) > 2E(T_1)$. Alternatively, if S_1 is equal to or slightly below $2E(T_1)$, isoergic or endothermic SF is possible.[41,64–65] Despite extensive studies on SF over the past decade, fundamental questions concerning the mechanism of SF remain unanswered, not to mention challenges toward applying SF to practical solar energy applications.[39,65–66]

1.2.2 Triplet-triplet Annihilation Upconversion

TTA-UC, first observed by Parker and Hatchard in 1962, is the reverse process of SF and involves the formation of one high-energy exciton from two lower energy photons.[6,67–70] By utilizing the lower-energy, sub-band-gap photons that normally cannot be absorbed by the light absorbing materials (i.e., silicon), TTA-UC potentially could benefit photovoltaics.[45,66,71–75] As shown in Figure 1.4, the low-energy incident light selectively excites the ground state photo sensitizer ([Sen]) to its singlet excited state ($^1[Sen]^*$). $^1[Sen]^*$ then undergoes intersystem crossing (ISC) to give the sensitizer in its triplet excited state ($^3[Sen]^*$). When $^3[Sen]^*$ encounters an annihilator molecule in its ground state ([An]), triplet energy transfer (TET) occurs, forming an annihilator triplet exciton ($^3[An]^*$). Finally, one higher energy singlet exciton ($^1[An]^*$) forms via the annihilation of two $^3[An]^*$. TTA-UC is typically a bimolecular process, and thus high concentrations of both sensitizer and annihilator are needed for an efficient process.[66,68–69,76]

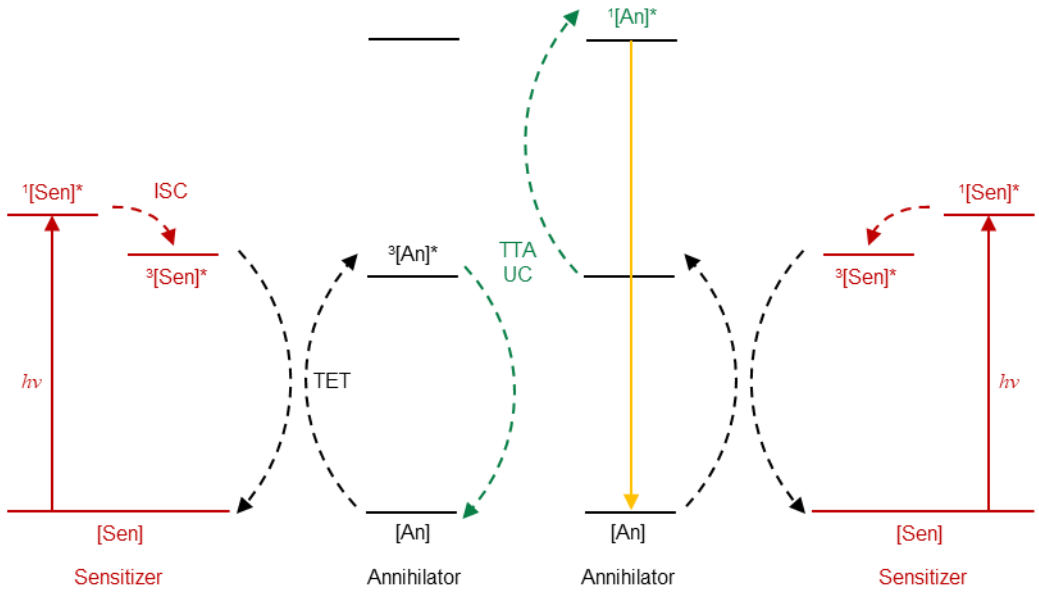

Figure 1.4. Schematic diagram of the mechanism of TTA-UC.

Careful tuning of the singlet and triplet excited state energies of the annihilator and sensitizer are critical to achieve efficient TTA-UC.[69,76] First of all, in order to selectively irradiate the sensitizer, the energy of $^1[Sen]^*$ needs to be lower than $^1[An]^*$, otherwise, the annihilator can absorb the photon directly and form $^1[An]^*$. For efficient exothermic TET, the energy of $^3[Sen]^*$ should be higher than the energy of $^3[An]^*$. Moreover, the energy of $^1[An]^*$ must be equal or lower than twice the energy of $^3[An]^*$ for TTA-UC to occur spontaneously.

1.3 Acenes for the Study of SF and TTA-UC

Even though SF was first discovered in anthracene, the efficiency of SF in anthracene is low, as $E(S_1)$ and $2E(T_1)$ values are 3.30 and 3.70 eV, respectively, resulting in endothermic SF.[1,77–78] However, anthracene is an ideal annihilator for TTA-UC, as it nicely fulfills the energy requirement of this process.[13] Thus, anthracene derivatives are used frequently as annihilators in the studies of TTA-UC.[6,66,69,79–81]

Conversely, pentacene typically undergoes exothermic SF since the energy of S_1 (1.83 eV) exceeds twice that of T_1 (0.86 eV). The energy excess between $2E(T_1)$ and $E(S_1)$ serves as a thermodynamic driving force for SF, leading to a typically fast and efficient process.[41 ,64,82–86] Such an exoergic process comes, however, at the expense

of thermal losses that lead to overall inefficient solar energy conversion.[87] Meanwhile, the excess energy renders the reverse process, TTA-UC, unfavored and undetected. Therefore, pentacene derivatives have been used widely as models for the study of the underlying process and mechanism of SF.[11,41,52,61,83,85,88]

Tetracene, with $E(S_1)$ at approximately the same energy as $2E(T_1)$, exhibits the possibility of both SF and TTA-UC.[65,85,89–92] SF in tetracene is effectively isoergic, and the energy loss is lower compared to exothermic SF in pentacene, leading to more efficient solar energy conversion.[78,93–95] Therefore, tetracene derivatives also are used frequently as models for the studies of SF.[11,65–66,85,89,91–92,96–98] However, the decorrelation of the correlated triplet pair in tetracene may be hindered by thermally activated TTA-UC.[5,65,85] While tetracene exhibits low TTA-UC efficiency, derivatives of tetracene have gained attention in recent years for the study of TTA-UA, as the excited-state energy levels can be modified by functionalization, and the high triplet excited state energy of tetracene allows for utilization of visible and near-infrared light.[99–101]

1.4 General Synthesis of Alkyne-functionalized Acenes

Acenes suffer from a lack of solubility in organic solvents as well as limited kinetic stability, and functionalized acenes have therefor been developed to tune the properties of the molecules via synthetic methods. For example, the solubility of acenes can be improved by installing alkynyltrialkylsilyl groups.[102–104] Depending on the position of the substitution, substitution can be classified into two groups, including *peri*-functionalized acenes (red substituents in Figure 1.5) and *pro-cata*-functionalized acenes (green substituents in Figure 1.5).[32] The *peri*-functionalized acenes have substituents on the central aromatic ring, most often the 5,12-positions for tetracene and the 6,13-positions for pentacene. The *pro-cata*-functionalized acenes have substituents on the end aromatic rings, namely 2,3,8,9-positions for tetracene and 2,3,9,10-positions for pentacene.

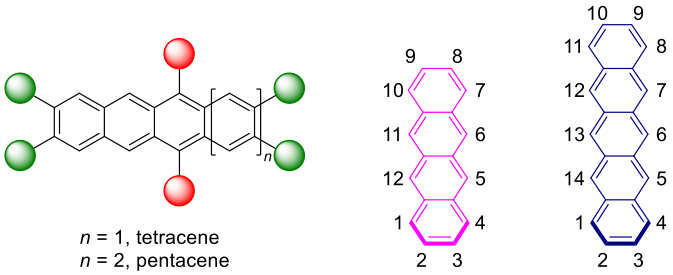

Figure 1.5. Schematic substitution of substituted tetracene and pentacene with red spheres illustrating the *peri*-positions and green spheres illustrating the *pro-cata*-positions (left). Numbering scheme for tetracene and pentacene (right).

The *peri*-positions of acenes (**1.11**) can be decorated with different functional groups, such as silylethynyl,[102–104] arylethynyl,[104–106] aryl,[28,107] and alkyl[108] groups, which are normally through nucleophilic addition into the corresponding quinone (Scheme 1.5a), while the 2-substituted acenes (**1.12**) usually are synthesized using a Suzuki–Miyaura cross-coupling reaction between acene bromides (**1.13**) and boronic pinacol esters (**1.14**) and vice versa (Scheme 1.5b).[53,109–110] Compared to *peri*-functionalized acenes, the *pro-cata*-functionalized acenes normally have different electronic properties and can be more reactive towards photoreactions.[29,40,52–53,100–101,111–117]

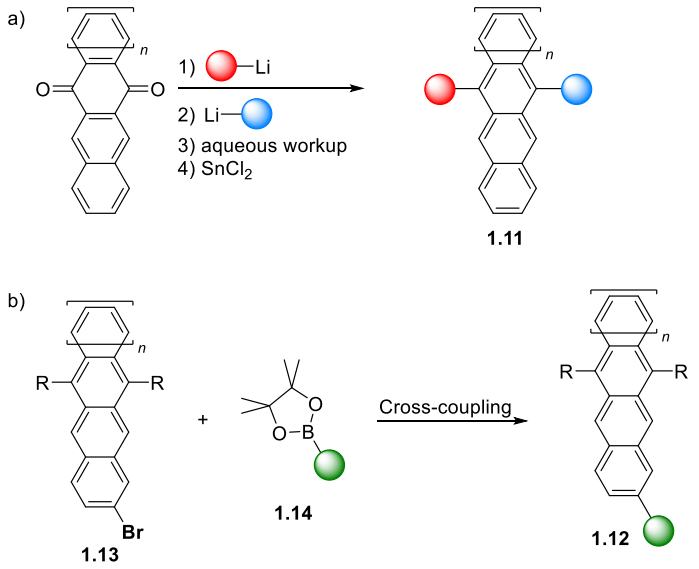

Scheme 1.5. Schematic synthesis of *peri*-substituted and *pro-cata*-substituted acenes.

Particularly, studies have shown that the alkynyl substitution of acenes at *peri*–positions often increase stability toward photoinduced cycloadditions, particularly endoperoxide formation, as both the LUMO energy and the energy of triplet state are lower compared to unprotected acenes.[29,107,115–116,118–121] Therefore, alkyne-functionalized tetracene and pentacene at the *peri*-positions are the focus of this section.

1.4.1 Synthesis of Symmetrical Alkyne-functionalized Acenes

The bis(phenylethynyl)-substituted acenes **1.15** and **1.21** are examples of the earliest reports of functionalized acenes.[106,122] One of the most famous symmetrical alkyne-functionalized acenes is 6,13-bis(tri*iso*propylsilylethynyl)pentacene (**1.15**), which was studied first by Anthony and co-workers in 2001.[102,123] This derivative shows greatly improved stability under ambient conditions and is much more soluble in common organic solvents compared to unsubstituted pentacene.

In general, the symmetrical alkyne-functionalized acenes are typically obtained through a two-step process including nucleophilic addition to acenequinone, followed by a reductive aromatization (Scheme 1.6,). When adding two or more equivalents of a lithium (or magnesium) acetylide to acenequinone, following an aqueous workup step, a diol intermediate would be formed. Then, the symmetric ethynyl substituted acenes (**1.15**–**1.23**) are generated by reductive aromatization of the diol intermediate with $SnCl_2$ in the presence of acid.[104,123–125]

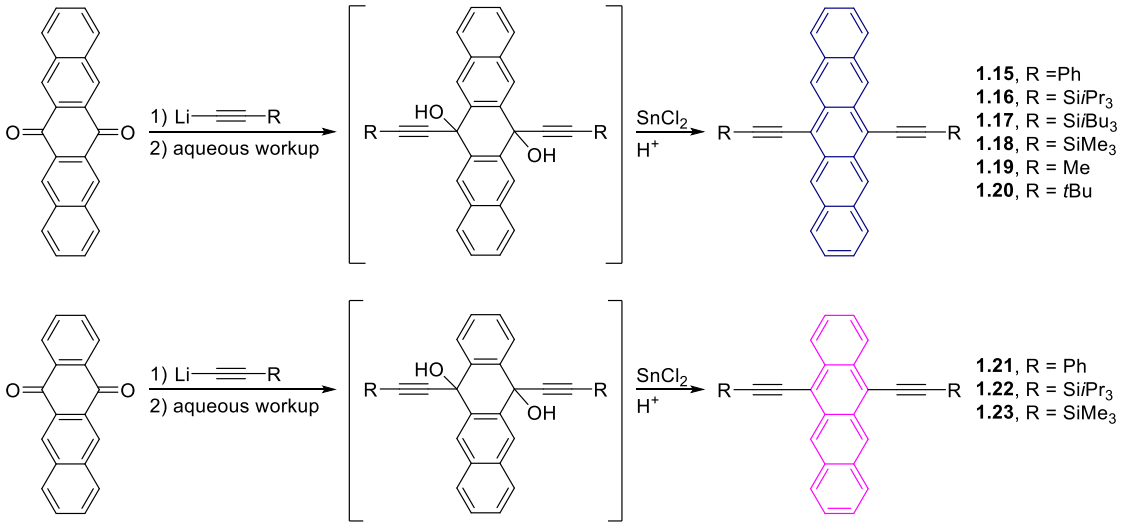

Scheme 1.6. General synthesis of symmetrical *peri*-substituted acenes.

1.4.2 Synthesis of Unsymmetrical Alkyne-functionalized Acenes

As shown in Scheme 1.7, a stepwise and modular synthesis of unsymmetrical 6,13-disubstituted pentacene derivatives has been developed by Tykwinski and co-workers,[124,126] and a similar approach to achieve unsymmetrical 5,12-disubstituted tetracene derivatives has been subsequently developed by Toyota and co-workers.[104] When using one equivalent of ethynyllithium in the nucleophilic addition of acenequinone, mono-substituted ketone **1.24** is obtained. The ketone **1.24** is treated with a second ethynyllithium to provide the diol intermediate with two different substituents. Then, the diol intermediate is subjected to $SnCl_2$-mediated reductive aromatization to give unsymmetrical alkyne-functionalized acenes.

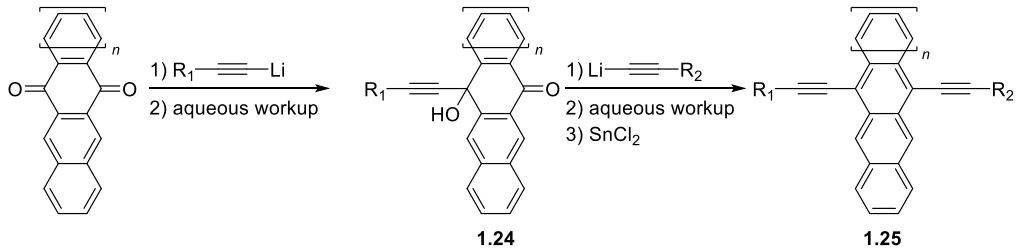

Scheme 1.7. General synthesis of unsymmetrical *peri*-substituted acenes via nucleophilic additions to acenequinones.

This stepwise nucleophilic addition method is not, however, particular successful for installing strong electron-rich or -deficient substitutes, which can be achieved alternatively by a procedure shown in Scheme 1.8 based on Pd-catalyzed cross coupling (the Sonogashira reaction).[105] The intermediate **1.26**, with two different silyl groups, can be deprotected selectively at the trimethylsilylalkynly group to form the key building block **1.27** bearing a terminal acetylene. Compound **1.27** is subjected to a Pd-catalyzed Sonogashira cross-coupling reaction with an aryl iodide to form **1.28**. The unsymmetrical substituted pentacene derivatives with strong electron-rich or deficient groups (**1.29**) are obtained after reductive aromatization of compound **1.28**.

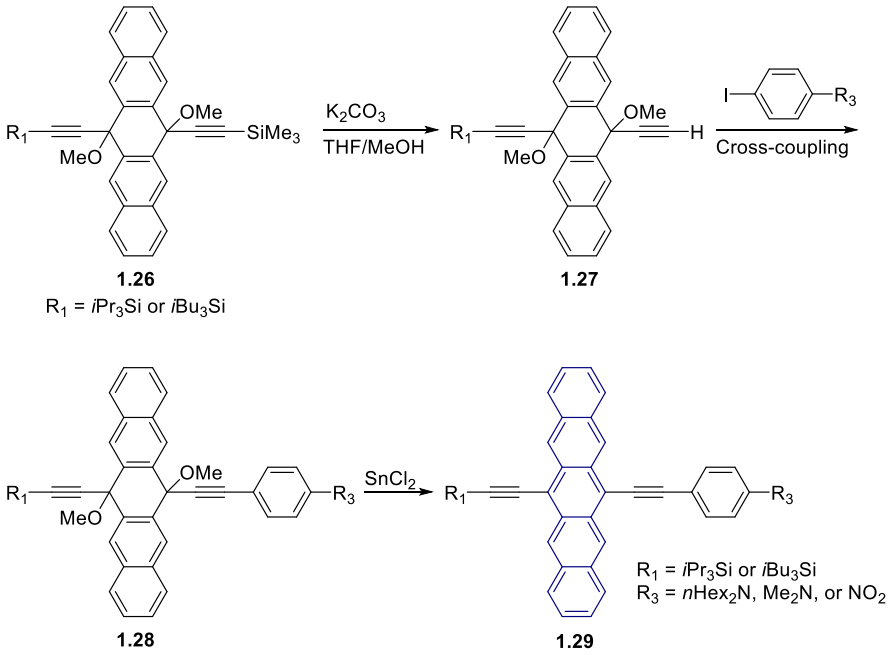

Scheme 1.8. Synthesis of unsymmetrical 6,13-substituted pentacenes via the Sonogashira reaction.

1.5 Acene Oligomers for The Study of Intramolecular Photophysical Processes

As discussed in Section 1.3, acenes have been used frequently as models for the study of SF and TTA-UC since their excited states energy level fulfil the necessary requirements. Acene oligomers, especially dimers, are targeted specifically because intramolecular processes can occur. Acene dimers allow intramolecular singlet fission (iSF) and intramolecular triplet-triplet annihilation upconversion (iTTA-UC) and are convenient systems to study these processes in dilute solution. From a synthetic perspective, the major advantage of the dimeric structure is the ability to modify the spacer. The spacer between interacting chromophores is the key to control the geometry, distance, and electronic coupling between the two chromophores of a the dimer, which allows detailed investigation of the mechanism of iSF and iTTA-UC.[51–52,61]

1.5.1 Electronic Coupling and Spacers in Acene Dimers

To achieve SF, sufficient electronic interaction(s) between the interacting chromophores needs to be assured. Monomer acenes can be used for intermolecular SF, and coupling typically is realized by either high concentrations of the molecule in solution or through control of the crystal packing in the solid state.[127–132] However,

iSF is possible in oligomers, which can be studied spectroscopically in dilute solution and avoids complications that arise from the concentrations requisite for intermolecular SF in monomers.

Control over spatial overlap and degree of coupling between interacting chromophores is one of the merits of dimers, and this aspect offers the ability to fine-tune and analyze the impact of coupling via the synthetic design of the spacer on the intricacies of the mechanism, kinetics, and efficiency of iSF and iTTA-UC.[58,63,85,133–136] The most representative examples are a series of pentacene dimers with different electronic coupling between interacting chromophores for the study of iSF (Figure 1.6). The dimers are linked by either a conjugated *para*-diethynylphenylene (**pPhPc2**), a cross-conjugated *meta*-diethynylphenylene (**mPhPc2**), or a non-conjugated 1,3-diethynyladamantyl spacer (**mAdPc2**). The compounds **pPhPc2** and **mPhPc2** are synthesized through a Sonogashira cross-coupling reaction between *m*- or *p*-diiodobenzene and **1.26**, analogous to that shown in Scheme 1.8, while compound **mAdPc2** is synthesized through the stepwise nucleophilic addition of lithiated 1,3-diethynyladamantane to ketone **1.24**, as described in Scheme 1.7. The subsequent photophysical studies of these dimers show that the formation of the correlated triplet pair (T_1T_1), as well as the following decorrelation to free triplets ($T_1 + T_1$), are impacted strongly by the level of electronic coupling imparted by the spacer.

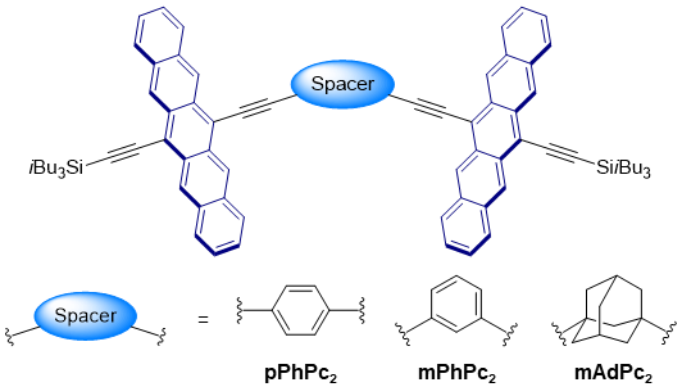

Figure 1.6. Structures of pentacene dimers with different spacers to control electronic coupling.

In conjugated dimer **pPhTc2**, the triplet pair formed after irradiation decays quickly via TTA as the generation of $^5(T_1T_1)$ is suppressed due to the strong coupling

between two pentacenes (see Figure 1.3 for mechanistic description).[60–62] The cross-conjugated dimer **mPhPc2** shows efficient iSF with a triplet yield for ($T_1 + T_1$) of 156% in benzonitrile, as the electronic coupling is weaker through the cross-conjugated *meta*-phenylene spacer than the linearly conjugated *para*-phenylene spacer. The non-conjugated dimer **mAdPc2** has a very similar spatial arrangement of the pentacene moieties as found in **mPhPc2**, but the electronic coupling is weaker through the non-conjugated spacer, leading to an increased triplet yield (188% in benzonitrile). In combination, these results suggest that sufficient while weak electronic coupling between interacting chromophores is important for sufficient SF.

TTA-UC measurements typically are conducted in the high-concentration regime since it is a bimolecular process in most cases and therefore diffusion-controlled. Studies using oligomeric annihilators have been explored with a hypothesis that iTTA-UC can occur and help to circumvent the need for high concentrations.[80,99,101,137] The electronic coupling between interacting chromophores has been studied in anthracene dimers (Figure 1.7), for example, by Albinsson and co-workers.[80]

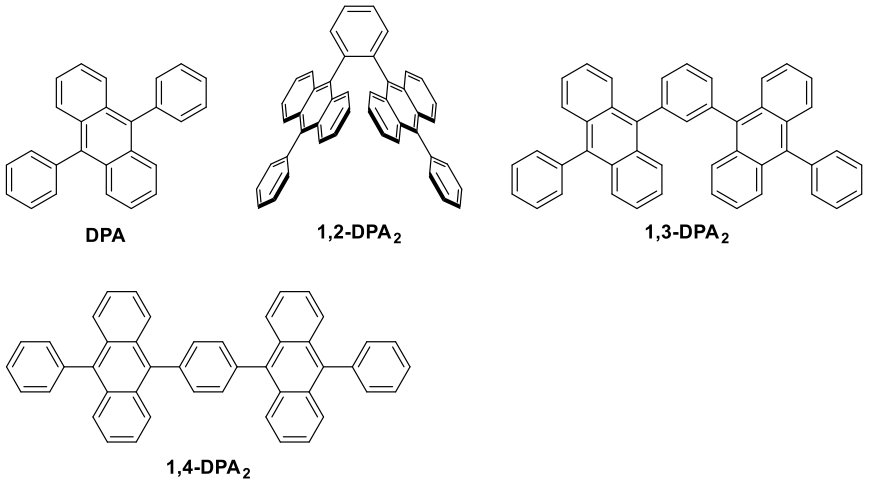

Figure 1.7. Structures of anthracene dimers with varied electronic coupling and corresponding monomer **DPA**.

The three dimers **1,2-**, **1,3-**, and **1,4-DPA2** with different conjugation give efficient TTA-UC when using platinum octaethylporphyrin as a photosensitizer. The cross-conjugated dimer **1,3-DPA2** shows an upconversion quantum yield of 21%, which is the highest in the dimer series (14% for **1,2-DPA2** and 15% for **1,4-DPA2**).

However, the yields of UC do not increase in the dimers relative to the reference monomer **DPA** (24%). Therefore, the study does not offer straightforward evidence that iTTA-UC can occur in the dimers, and the underlying mechanism of intramolecular UC is still not clear.

Unlike derivatives of pentacene or anthracene, derivatives of tetracene are capable of both SF and TTA-UC, as the energy of their lowest singlet excited state is about twice of the energy of their triplet excited state. However, previous investigations of tetracene dimers have been focused predominantly on the individual study of either iSF or iTTA-UC, respectively, rather than combining the two competitive processes into a single system. Insight into the interplay between iSF and iTTA-UC thus remains elusive.[66,138–139]

1.5.2 Heavy-atom Effect and SF

One potential means to influence or control decorrelation of (T_1T_1) and form ($T_1 + T_1$) involves exploiting heavy-atom effects (HAEs). Conventionally, the design of SF materials excludes heavy atoms since spin-orbit coupling often facilitate intersystem crossing (ISC). As well, the synthesis of heavy-atom chromophores can be more challenging when compared to small organic molecules.[47,140–141] Triplets born from ISC are fundamentally different from triplets of SF, as ISC is spin-forbidden while SF is a spin-allowed process. Thus, triplets of SF and ISC are clearly distinguishable.[142–145] Studies have shown that spin-orbit coupling enhancement produced by a heavy atom, the so called heavy-atom effect (HAE), can impart profound effects on the decorrelation of the spin-correlated triplet pair (T_1T_1). Musser and co-workers have shown that the spin evolution within (T_1T_1) is faster through replacing sulfur in polythienylenevinylene with the heavy atoms selenium and tellurium. Their results suggest that the presence of heavy atoms may manipulate the dynamics of triplets formed by SF.[146] Pt-bridged pentacene dimers have been synthesized, and the impact of the HAE has been investigated.[143,147] It is reported that the presence of Pt had no impact on the formation of the singlet correlated triplet pair $^1(T_1T_1)$ from (S_1S_0) via iSF, but Pt did influence subsequent transitions. The enhanced spin-orbit coupling on $^1(T_1T_1)$ caused by Pt leads to a spin-flip of $^1(T_1T_1)$ into both the triplet correlated triplet pair

$^3(T_1T_1)$ and quintet correlated triplet pair $^5(T_1T_1)$. This mixing could, in principle, facilitate decorrelation to yield free triplets ($T_1 + T_1$), although deactivation via intersystem crossing to (S_0T_1) must be prevented.[143–144,147] Ultimately, the population of the triplet excited states (S_0T_1) and ($T_1 + T_1$) results from $^3(T_1T_1)$ and $^5(T_1T_1)$, respectively. Thus, the enhanced spin-orbit coupling (SOC) produced by a heavy atom may improve the yield of decorrelation. However, the influence of HAE on triplet decorrelation in SF remains unpredictable.

1.5.3 Chromophore Multiplication for Triplet Diffusion

Decorrelation of $^1(T_1T_1)$ into free triplets ($T_1 + T_1$) is the essential step for SF to complete the energy conversion from sunlight to electricity.[64–65,148–149] When decorrelation to ($T_1 + T_1$) is achieved within dimeric acenes, however, the free triplets are unable to diffuse from the molecular system as would be possible in the solid. As a result, the spin-correlated and decorrelated triplet pairs usually decay back to ground state through TTA.[61,150] To explore the events for SF beyond formation of ($T_1 + T_1$), extended model systems for the study of SF are needed, and oligo- and polymeric systems have been considered to study triplet diffusion.[65,109,151–153] A series of oligoacene dendrimers (Figure 1.8a) have been synthesized to mimic SF in amorphous solids.[153] In these dendrimers, only short-lived triplet pairs are found due to the strong through-bond and through-space coupling between the chromophores. Even though rapid SF can occur in polymers to form long-lived triplet pairs, rapid recombination tends to occur due to strong coupling as diffusion of triplets is insufficient.[152–154]

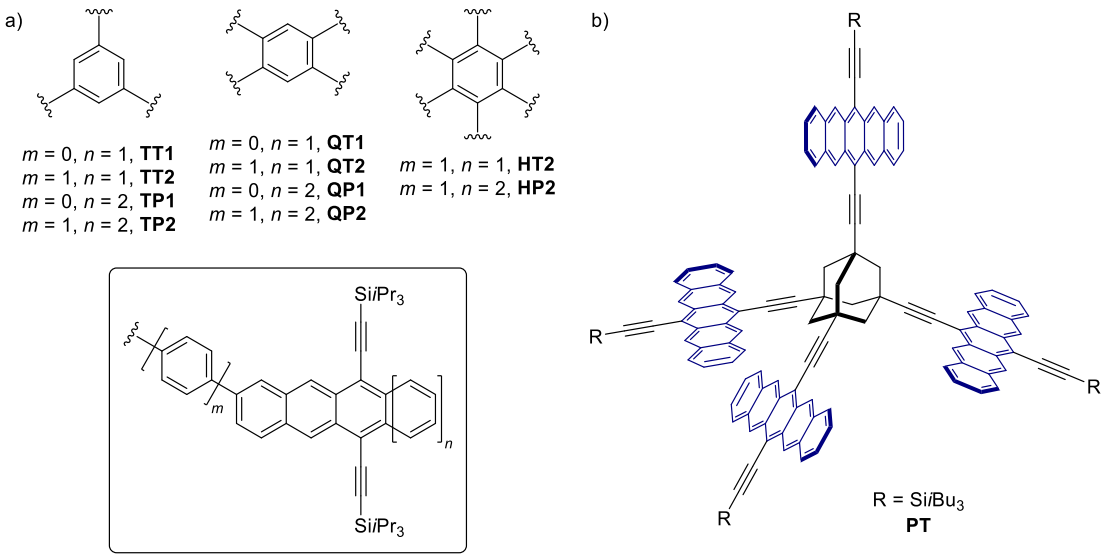

Figure 1.8. Structures of a) oligoacene dendrimers and b) a pentacene tetramer with an adamantyl spacer.

A pentacene tetramer **PT** has been reported in which a non-conjugated adamantyl spacer (Figure 1.8b) provides a system with four spatially equivalent and electronically independent pentacene moieties, designed to support diffusion via chromophore multiplication (i.e., multiple chromophores, covalently linked, with only weak coupling).[155] Although both chromophore multiplication and oligomerization designs contain multiple chromophores, the major difference is that all chromophores in chromophore multiplication remain electronically independent. In this tetrameric assembly, charge-separation experiments show, however, that it is not possible to harvest the free triplets quantitatively following formation of (T_1 + T_1), as harvesting one free triplet comes at the cost of the accelerated decay of the other triplet to the ground state. Thus, harvesting both triplets requires better spatial separation of the triplets than is afforded by the adamantyl spacer.

1.6 Summary

Acenes and their derivatives are used as model compounds for the study of specific hypotheses in photophysical processes. As unsubstituted acenes suffer from poor solubility and stability in common organic solvents, functionalized acenes are necessary. Functionalization of acenes typically has been achieved at either *peri*- or *pro-cata*-positions. The acenes *peri*-alkyne-functionalization are targeted specifically

due to the increased photostability and the ability to tune interaction between chromophores via stepwise modular synthetic method.

The decorrelation of the triplet pair (T_1T_1) to free triplets ($T_1 + T_1$) in SF is focused, as it is the essential step to complete the energy conversion from sunlight to electricity. Two major strategies have been applied to the design of molecules, including HAE and chromophore multiplication. Previous studies on molecules with the heavy atoms selenium, tellurium, and platinum have shown that HAE can impact the decorrelation process. However, the influence of HAE on triplet decorrelation in SF remains unpredictable due to limited examples, and the underlying mechanism of SF in chromophores containing heavy atoms is still unclear. The pentacene tetramer with four spatially equivalent and electronically independent pentacene moieties linked with an adamantyl spacer has been designed to support the triplet diffusion via chromophore multiplication. However, the SF triplets cannot be harvested quantitatively in this tetramer. Other molecules with better spatial separation of the triplets via chromophore multiplication need to be designed and synthesized for further studies.

For both SF and TTA-UC, suitable electronic coupling between the interacting chromophores is crucial to achieve efficient processes. To study the influence of electronic coupling on the competitive processes of SF and TTA-UC, dimeric molecules are preferred compared to monomers, as intramolecular processes can occur. The spatial overlap and degree of coupling between interacting chromophores can be tuned via the synthetic design of the spacers. Previous studies suggest that the electronic coupling can impact the formation of the correlated triplet pair (T_1T_1) strongly, and the following decorrelation step in SF strongly. In principle, intramolecular TTA-UC can occur in the dimers, while the underlying mechanism of iTTA-UC is still not clear. Meanwhile, the studies have been focused on the individual study of either iSF or iTTA-UC, respectively. Therefore, a platform that can provide an insight into the interplay between iSF and iTTA-UC still needs to be explored.

For the iTTA-UC, dimeric and oligomeric sensitizers have been synthesized to study the intramolecular UC. However, molecules that combine intramolecular

sensitization, in addition to intramolecular UC, remain unknown; these could, in principle, achieve fully intramolecular iTTA-UC and have the potential to eliminate the concentration requirements of both photosensitizer and annihilator toward more efficient TTA-UC.

1.7 Motivation and Targets

Motivated by both the questions of how the HAE and chromophore multiplication might influence iSF, a pentacene substituted with a sterically hindered pyridyl group (**L_{pc}**) and its corresponding reference ligand without a pentacene moiety (**L_{ref}**) have been designed and synthesized (Figure 1.9a). The pyridyl group was chosen for these projects due to its known and predictable bonding with metal ions by coordination. It was hypothesized that the presence of the pyridyl ligand could be expoited for the versatile synthesis of pentacene oligomers featuring different metal ions, allowing various processes to be interrogated.[156] Finally, the pyridyl moiety was designed to feature sterically demanding substituents in the 3- and 5-positions[157] that both shield the acene core from reactions[27,31–32,158] and provide solubility.

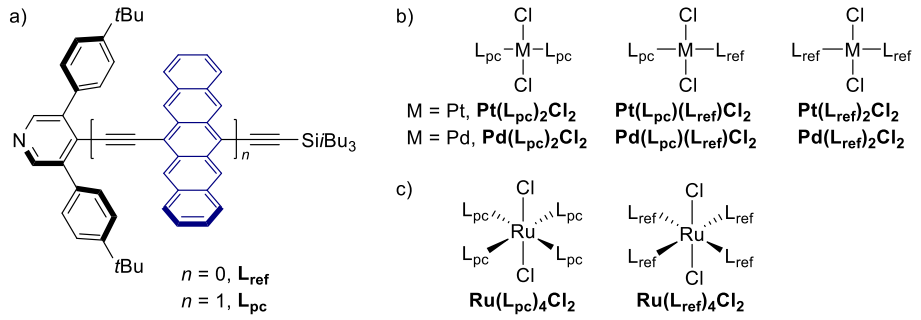

Figure 1.9. Structures of a) ligands, b) dimers, and c) tetramers targeted in this thesis.

Subsequently, the symmetric pentacene dimers (**$Pt(L_{pc})_2Cl_2$** and **$Pd(L_{pc})_2Cl_2$**), reference dimers (**$Pt(L_{ref})_2Cl_2$** and **$Pd(L_{ref})_2Cl_2$**) linked by Pt(II) and Pd(II), and unsymmetric dimers **$Pt(L_{pc})(L_{ref})Cl_2$** and **$Pd(L_{pc})(L_{ref})Cl_2$** bearing both a pentacene ligand and a reference pyridyl ligand have been prepared (Figure 1.9b). It is important to emphasize that, by design, the two dimers, **$Pt(L_{pc})_2Cl_2$** and **$Pd(L_{pc})_2Cl_2$**, are structurally identical, except for the metal ion. As second- and third-row metals, Pd and Pt are congeners, and both **$Pd(L_{pc})_2Cl_2$** and **$Pd(L_{pc})_2Cl_2$** feature a metal in the

+2 oxidation state in the dimers. Thus, while the valence electron structure is the same, the HAE is reduced in Pd compared to Pt, as the effective nuclear charge of Pd is lower than that of Pt.[159–160] In comparison to suitable model compounds that cannot undergo iSF, the electronic influence of the heavy atoms and the impact on the mechanism of SF can be studied carefully.

A pentacene tetramer **Ru(L$_{pc}$)$_4$Cl$_2$** and its corresponding reference compound **Ru(L$_{ref}$)$_4$Cl$_2$** have been designed, based on the well-established structural diversity of hexacoordinate Ru(II) complexes (Figure 1.9c).[161–162] The resulting tetramer is used to document the influence of the HAE in SF, and it offers a unique, coplanar, equatorial relationship between the four pentacene moieties. This arrangement of pentacenes was designed to determine the prospect of triplet diffusion via chromophore multiplication.[155] The influence of HAE and chromophore multiplication on iSF is studied by our collaborators in Germany.

As tetracene dimers have been proved capable for the individual study of both iSF and iTTA-UC,[66,138–139] a series of covalently linked tetracene dimers featuring tunable electronic coupling as well as their corresponding monomers, have been designed and synthesized (Figure 1.10) to unravel the interplay between SF and TTA-UC. In analogy to the previous work on iSF in pentacene dimers, the tetracene dimers are bridged rigidly by either a conjugated *para*-diethynylphenylene (**pPhTc$_2$**), a cross-conjugated *meta*-diethynylphenylene (**mPhTc$_2$**), or a non-conjugated 1,3-diethynyladamantyl spacer (**mAdTc$_2$**).

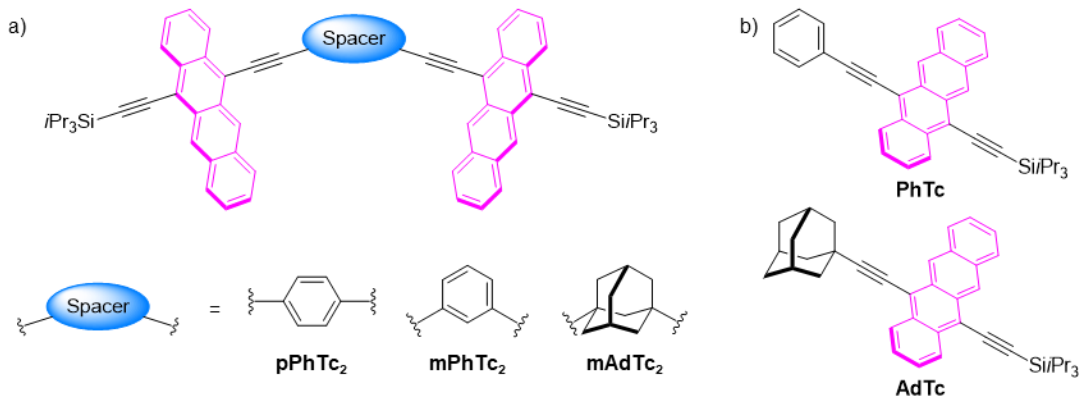

Figure 1.10. Structures of tetracene a) dimers and b) monomers targeted in this thesis.

Intrigued by the results that intramolecular upconversion via oligomers can eliminate the concentration requirements of annihilators,[99,137] we hypothesized that intramolecular sensitization could lead to more efficient TTA-UC, combining the annihilators and photosensitizers into the same molecule. As an initial step to test this premise, compounds **TcPy-1** and **TcPy-2** (Figure 1.11a) have been designed and synthesized. The introduction of the pyridyl group offers a means to coordinate the tetracene annihilator to a Ru-phthalocyanine as a photosensitizer (Figure 1.11b) using **TcPy-1** and **TcPy-2,** which have been tested by our collaborators in Spain through the formation of **Ru-TcPy-1** and **Ru-TcPy-2**. As compounds **Ru-TcPy-1** and **Ru-TcPy-2** are structurally identical, except for the distance between the tetracene moiety and the photosensitizer, the effect of distance between annihilator and photosensitizer on intramolecular sensitization could be studied.

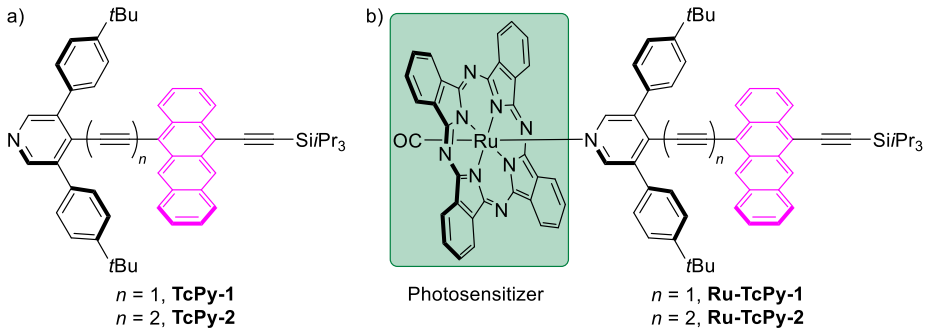

Figure 1.11. a) Structure of **TcPy-1** and **TcPy-2**; b) coordination of tetracene to a photosensitizer to give **Ru-TcPy-1** and **Ru-TcPy-2** targeted in this thesis.

Furthermore, molecules that might achieve intramolecular sensitization, in addition to intramolecular upconversion, have been designed and synthesized (Figure 1.12). These molecules could, in principle, achieve fully intramolecular iTTA-UC, based on both intramolecular photosensitization and upconversion and have the potential to eliminate the concentration requirements of both photosensitizer and annihilator toward more efficient TTA-UC. The *meta*-diethynylphenylene spacer was included in the design, as the **mPhTc2** gave the best performance for TTA-UC among the three dimers with varied electronic coupling (Figure 1.9). The butadiyne spacer was chosen for comparison, as it can be synthesized by well-established coupling reactions,

and the strongly coupled triplet pair shown in butadiyne-linked pentacene dimers[163] may be a benefit for an iTTA-UC system.

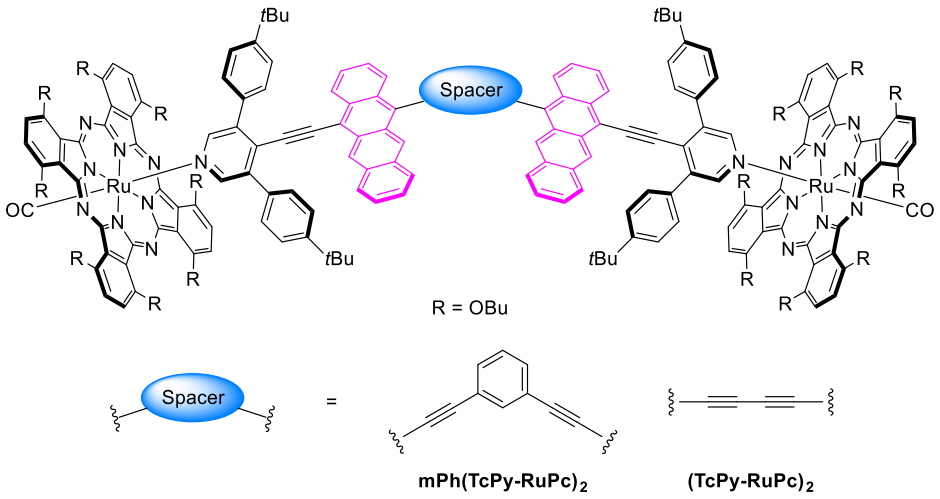

Figure 1.12. Design of iTTA-UC systems **mPh(TcPy-RuPc)$_2$** and **(TcPy-RuPc)$_2$** targeted in this thesis.

Finally, it is important to highlight that the motivation for the targets presented in this thesis has been a dynamic process. Working closely with our collaborators in Germany, the initial design of chromophores has been refined as molecules are characterized via steady-state and time-resolved absorption and fluorescence spectroscopy by our collaborators. Ultimately, the interplay between iSF and iTTA-UC requires critical evaluation of photophysical observations that result from structural change that have been made synthetically. This is, perhaps, the most significant motivation and outcome of my work, namely learning to work closely with our collaborators in Germany to solve important problems.

References

[1] S. Singh, W. J. Jones, W. Siebrand, B. P. Stoicheff, W. G. Schneider, *J. Chem. Phys.* **1965**, *42*, 330–342.

[2] R. P. Groff, P. Avakian, R. E. Merrifield, *Phys. Rev. B* **1970**, *1*, 815–817.

[3] H. Marciniak, M. Fiebig, M. Huth, S. Schiefer, B. Nickel, F. Selmaier, S. Lochbrunner, *Phys. Rev. Lett.* **2007**, *99*, 176402.

[4] J. Gao, F. A. Hegmann, *Appl. Phys. Lett.* **2008**, *93*, 223306.

[5] J. J. Burdett, A. M. Muller, D. Gosztola, C. J. Bardeen, *J. Chem. Phys.* **2010**, *133*, 144506.

[6] C. Gao, W. W. H. Wong, Z. Qin, S. C. Lo, E. B. Namdas, H. Dong, W. Hu, *Adv. Mater.* **2021**, *33*, 2100704.
[7] K. T. Munson, E. R. Kennehan, J. B. Asbury, *J. Mater. Chem. C* **2019**, *7*, 5889–5909.
[8] J. M. Aubry, C. Pierlot, J. Rigaudy, R. Schmidt, *Acc. Chem. Res.* **2003**, *36*, 668–675.
[9] S. Dong, A. Ong, C. Chi, *J. Photochem. Photobiol., C* **2019**, *38*, 27–46.
[10] T. Wang, B. Y. Zhang, H. L. Zhang, *Macromol. Rapid. Commun.* **2022**, *43*, 2200326.
[11] J. Li, H. Cao, Z. Zhang, S. Liu, Y. Xia, *Photonics* **2022**, *9*, 689.
[12] M. J. Dumas, *Ann. Chim. Phys.* **1832**, *50*, 182–197.
[13] X. Qiao, D. Ma, *Mater. Sci. Eng., R* **2020**, *139*, 100519.
[14] A. N. Aleshin, J. Y. Lee, S. W. Chu, J. S. Kim, Y. W. Park, *Appl. Phys. Lett.* **2004**, *84*, 5383–5385.
[15] M. Chen, L. Yan, Y. Zhao, I. Murtaza, H. Meng, W. Huang, *J. Mater. Chem. C* **2018**, *6*, 7416–7444.
[16] L. Jiang, H. Dong, W. Hu, *J. Mater. Chem.* **2010**, *20*, 4994–5007.
[17] T. R. Battersbya, P. Gantzela, K. K. Baldridge, J. S. Siegel, *Tetrahedron Lett.* **1995**, *36*, 845–848.
[18] T. Geiger, A. Haupt, C. Maichle-Mössmer, C. Schrenk, A. Schnepf, H. F. Bettinger, *J. Org. Chem.* **2019**, *84*, 10120–10135.
[19] M. Ehrenberg, *Acta Crystallogr.* **1966**, *20*, 177–182.
[20] O. C. Musgrave, *Chem. Rev.* **2002**, *69*, 499–531.
[21] T. Takahashi, T. Takenobu, J. Takeya, Y. Iwasa, *Adv. Funct. Mater.* **2007**, *17*, 1623–1628.
[22] J. J. Burdett, C. J. Bardeen, *Acc. Chem. Res.* **2013**, *46*, 1312–1320.
[23] R. Lapouyade, A. Nourmamode, H. Bouas-Laurent, *Tetrahedron* **1980**, *36*, 2311–2316.
[24] E. Clar, F. John, *Ber. Dtsch. Chem. Ges.* **1929**, *62*, 3021–3029.
[25] E. Clar, F. John, *Ber. Dtsch. Chem. Ges.* **1930**, *63*, 2967–2977.
[26] N. Vets, M. Smet, W. Dehaen, *Tetrahedron Lett.* **2004**, *45*, 7287–7289.
[27] O. Berg, E. L. Chronister, T. Yamashita, G. W. Scott, R. M. Sweet, J. Calabrese, *J. Phys. Chem. A* **1999**, *103*, 2451–2459.
[28] I. Kaur, G. P. Miller, *New J. Chem.* **2008**, *32*, 459–463.
[29] A. Maliakal, K. Raghavachari, H. Katz, E. Chandross, T. Siegrist, *Chem. Mater.* **2004**, *16*, 4980–4986.
[30] S. S. Zade, M. Bendikov, *J. Phys. Org. Chem.* **2012**, *25*, 452–461.
[31] J. B. Briggs, G. P. Miller, *C. R. Chim.* **2006**, *9*, 916–927.
[32] J. E. Anthony, *Angew. Chem. Int. Ed.* **2008**, *47*, 452–483.
[33] R. E. Blankenship, D. M. Tiede, J. Barber, G. W. Brudvig, G. Fleming, M. Ghirardi, M. R. Gunner, W. Junge, D. M. Kramer, A. Melis, T. A. Moore, C. C. Moser, D. G. Nocera, A. J. Nozik, D. R. Ort, W. W. Parson, R. C. Prince, R. T. Sayre, *Science* **2011**, *332*, 805–809.
[34] J. Hansen, P. Kharecha, M. Sato, V. Masson-Delmotte, F. Ackerman, D. J. Beerling, P. J. Hearty, O. Hoegh-Guldberg, S. L. Hsu, C. Parmesan, J. Rockstrom, E. J. Rohling, J. Sachs, P. Smith, K. Steffen, L. Van Susteren, K. von Schuckmann, J. C. Zachos, *PLoS One* **2013**, *8*, e81648.
[35] L. Tsakalakos, L. C. Hirst, N. J. Ekins-Daukes, in *Next Gener. Photonic Cell Technol. Sol. Energy Convers., Vol. 7772*, **2010**, p. 777211.
[36] R. Rawat, R. Lamba, S. C. Kaushik, *Renewable and Sustainable Energy Rev.* **2017**, *71*, 630–638.
[37] W. Shockley, H. J. Queisser, *J. Appl. Phys.* **1961**, *32*, 510–519.

[38] S. Rühle, *Sol. Energy* **2016**, *130*, 139–147.
[39] A. Rao, R. H. Friend, *Nat. Rev. Mater.* **2017**, *2*, 17063.
[40] J. Xia, S. N. Sanders, W. Cheng, J. Z. Low, J. Liu, L. M. Campos, T. Sun, *Adv. Mater.* **2017**, *29*, 1601652.
[41] M. B. Smith, J. Michl, *Annu. Rev. Phys. Chem.* **2013**, *64*, 361–386.
[42] T. Sharma, P. Mahajan, M. Adil Afroz, A. Singh, Yukta, N. Kumar Tailor, S. Purohit, S. Verma, B. Padha, V. Gupta, S. Arya, S. Satapathi, *ChemSusChem* **2022**, *15*, e202101067.
[43] M. C. Hanna, A. J. Nozik, *J. Appl. Phys.* **2006**, *100*, 074510.
[44] D. Beery, T. W. Schmidt, K. Hanson, *ACS Appl. Mater. Interfaces* **2021**, *13*, 32601–32605.
[45] E. M. Gholizadeh, S. K. K. Prasad, Z. L. Teh, T. Ishwara, S. Norman, A. J. Petty, J. H. Cole, S. Cheong, R. D. Tilley, J. E. Anthony, S. Huang, T. W. Schmidt, *Nat. Photonics* **2020**, *14*, 585–590.
[46] M. Uji, T. J. B. Zahringer, C. Kerzig, N. Yanai, *Angew. Chem. Int. Ed.* **2023**, *62*, e202301506.
[47] M. B. Smith, J. Michl, *Chem. Rev.* **2010**, *110*, 6891–6936.
[48] J. Michl, *Mol. Front. J.* **2019**, *03*, 84–91.
[49] M. K. Gish, N. A. Pace, G. Rumbles, J. C. Johnson, *J. Phys. Chem. C* **2019**, *123*, 3923–3934.
[50] K. Miyata, F. S. Conrad-Burton, F. L. Geyer, X. Y. Zhu, *Chem. Rev.* **2019**, *119*, 4261–4292.
[51] B. S. Basel, J. Zirzlmeier, C. Hetzer, B. T. Phelan, M. D. Krzyaniak, S. R. Reddy, P. B. Coto, N. E. Horwitz, R. M. Young, F. J. White, F. Hampel, T. Clark, M. Thoss, R. R. Tykwinski, M. R. Wasielewski, D. M. Guldi, *Nat. Commun.* **2017**, *8*, 15171.
[52] C. Hetzer, D. M. Guldi, R. R. Tykwinski, *Chem. - Eur. J.* **2018**, *24*, 8245–8257.
[53] H. Sakai, R. Inaya, H. Nagashima, S. Nakamura, Y. Kobori, N. V. Tkachenko, T. Hasobe, *J. Phys. Chem. Lett.* **2018**, *9*, 3354–3360.
[54] R. J. Hudson, A. N. Stuart, D. M. Huang, T. W. Kee, *J. Phys. Chem. C* **2022**, *126*, 5369–5377.
[55] B. S. Basel, J. Zirzlmeier, C. Hetzer, S. R. Reddy, B. T. Phelan, M. D. Krzyaniak, M. K. Volland, P. B. Coto, R. M. Young, T. Clark, M. Thoss, R. R. Tykwinski, M. R. Wasielewski, D. M. Guldi, *Chem* **2018**, *4*, 1092–1111.
[56] M. Chen, M. D. Krzyaniak, J. N. Nelson, Y. J. Bae, S. M. Harvey, R. D. Schaller, R. M. Young, M. R. Wasielewski, *Proc. Natl. Acad. Sci. U. S. A.* **2019**, *116*, 8178–8183.
[57] T. S. C. MacDonald, M. J. Y. Tayebjee, M. I. Collins, E. Kumarasamy, S. N. Sanders, M. Y. Sfeir, L. M. Campos, D. R. McCamey, *J. Am. Chem. Soc.* **2023**, *145*, 15275–15283.
[58] T. Hasobe, *Chem. Lett.* **2021**, *50*, 615–622.
[59] S. N. Sanders, A. B. Pun, K. R. Parenti, E. Kumarasamy, L. M. Yablon, M. Y. Sfeir, L. M. Campos, *Chem* **2019**, *5*, 1988–2005.
[60] T. Minami, S. Ito, M. Nakano, *J. Phys. Chem. Lett.* **2012**, *3*, 2719–2723.
[61] J. Zirzlmeier, D. Lehnherr, P. B. Coto, E. T. Chernick, R. Casillas, B. S. Basel, M. Thoss, R. R. Tykwinski, D. M. Guldi, *Proc. Natl. Acad. Sci. U. S. A.* **2015**, *112*, 5325–5330.
[62] R. Ringstrom, F. Edhborg, Z. W. Schroeder, L. Chen, M. J. Ferguson, R. R. Tykwinski, B. Albinsson, *Chem. Sci.* **2022**, *13*, 4944–4954.
[63] T. Hasobe, S. Nakamura, N. V. Tkachenko, Y. Kobori, *ACS Energy Lett.* **2021**, *7*, 390–400.
[64] R. Casillas, I. Papadopoulos, T. Ullrich, D. Thiel, A. Kunzmann, D. M. Guldi, *Energy Environ. Sci.* **2020**, *13*, 2741–2804.
[65] T. Wang, H. Liu, X. Wang, L. Tang, J. Zhou, X. Song, L. Lv, W. Chen, Y. Chen, X. Li, *J. Mater. Chem. A* **2023**, *11*, 8515–8539.
[66] A. J. Carrod, V. Gray, K. Börjesson, *Energy Environ. Sci.* **2022**, *15*, 4982–5016.
[67] P. Bharmoria, H. Bildirir, K. Moth-Poulsen, *Chem. Soc. Rev.* **2020**, *49*, 6529–6554.

[68] S. E. Seo, H.-S. Choe, H. Cho, H.-i. Kim, J.-H. Kim, O. S. Kwon, *J. Mater. Chem. C* **2022**, *10*, 4483–4496.
[69] L. Zeng, L. Huang, J. Han, G. Han, *Acc. Chem. Res.* **2022**, *55*, 2604–2615.
[70] *Proc. R. Soc. London, Ser. A* **1962**, *269*, 574–584.
[71] T. Trupke, M. A. Green, P. Würfel, *J. Appl. Phys.* **2002**, *92*, 4117–4122.
[72] R. R. Islangulov, J. Lott, C. Weder, F. N. Castellano, *J. Am. Chem. Soc.* **2007**, *129*, 12652–12653.
[73] L. Wei, C. Yang, W. Wu, *Mater. Chem. Front.* **2023**, *7*, 3194–3208.
[74] L. Naimovicius, P. Bharmoria, K. Moth-Poulsen, *Mater. Chem. Front.* **2023**, *7*, 2297–2315.
[75] T. Schloemer, P. Narayanan, Q. Zhou, E. Belliveau, M. Seitz, D. N. Congreve, *ACS Nano* **2023**, *17*, 3259–3288.
[76] J. Feng, J. Alves, D. M. de Clercq, T. W. Schmidt, *Annu. Rev. Phys. Chem.* **2023**, *74*, 145–168.
[77] G. Klein, R. Voltz, M. Schott, *Chem. Phys. Lett.* **1972**, *16*, 340–344.
[78] H. L. Stern, A. Cheminal, S. R. Yost, K. Broch, S. L. Bayliss, K. Chen, M. Tabachnyk, K. Thorley, N. Greenham, J. M. Hodgkiss, J. Anthony, M. Head-Gordon, A. J. Musser, A. Rao, R. H. Friend, *Nat. Chem.* **2017**, *9*, 1205–1212.
[79] F. Edhborg, H. Bildirir, P. Bharmoria, K. Moth-Poulsen, B. Albinsson, *J. Phys. Chem. B* **2021**, *125*, 6255–6263.
[80] A. Olesund, V. Gray, J. Martensson, B. Albinsson, *J. Am. Chem. Soc.* **2021**, *143*, 5745–5754.
[81] R. Ieuji, K. Goushi, C. Adachi, *Nat. Commun.* **2019**, *10*, 5283.
[82] T. Ullrich, D. Munz, D. M. Guldi, *Chem. Soc. Rev.* **2021**, *50*, 3485–3518.
[83] B. J. Walker, A. J. Musser, D. Beljonne, R. H. Friend, *Nat. Chem.* **2013**, *5*, 1019–1024.
[84] S. R. Yost, J. Lee, M. W. B. Wilson, T. Wu, D. P. McMahon, R. R. Parkhurst, N. J. Thompson, D. N. Congreve, A. Rao, K. Johnson, M. Y. Sfeir, M. G. Bawendi, T. M. Swager, R. H. Friend, M. A. Baldo, T. Van Voorhis, *Nat. Chem.* **2014**, *6*, 492–497.
[85] N. V. Korovina, N. F. Pompetti, J. C. Johnson, *J. Chem. Phys.* **2020**, *152*, 040904.
[86] I. Papadopoulos, J. Zirzlmeier, C. Hetzer, Y. J. Bae, M. D. Krzyaniak, M. R. Wasielewski, T. Clark, R. R. Tykwinski, D. M. Guldi, *J. Am. Chem. Soc.* **2019**, *141*, 6191–6203.
[87] A. Kunzmann, M. Gruber, R. Casillas, J. Zirzlmeier, M. Stanzel, W. Peukert, R. R. Tykwinski, D. M. Guldi, *Angew. Chem. Int. Ed.* **2018**, *57*, 10742–10747.
[88] B. S. Basel, I. Papadopoulos, D. Thiel, R. Casillas, J. Zirzlmeier, T. Clark, D. M. Guldi, R. R. Tykwinski, *Trends Chem.* **2019**, *1*, 11–21.
[89] N. V. Korovina, J. Joy, X. Feng, C. Feltenberger, A. I. Krylov, S. E. Bradforth, M. E. Thompson, *J. Am. Chem. Soc.* **2018**, *140*, 10179–10190.
[90] R. S. Mattos, I. Burghardt, A. J. A. Aquino, T. M. Cardozo, H. Lischka, *J. Am. Chem. Soc.* **2022**, *144*, 23492–23504.
[91] S. Mardazad, Y. Xu, X. Yang, M. Grundner, U. Schollwock, H. Ma, S. Paeckel, *J. Chem. Phys.* **2021**, *155*, 194101.
[92] E. A. Buchanan, Z. Havlas, J. Michl, *Bull. Chem. Soc. Jpn.* **2019**, *92*, 1960–1971.
[93] M. W. B. Wilson, A. Rao, K. Johnson, S. Gelinas, R. di Pietro, J. Clark, R. H. Friend, *J. Am. Chem. Soc.* **2013**, *135*, 16680–16688.
[94] D. N. Congreve, J. Y. Lee, N. J. Thompson, E. Hontz, S. R. Yost, P. D. Reusswig, M. E. Bahlke, S. Reineke, T. Van Voorhis, M. A. Baldo, *Science* **2013**, *340*, 334–337.
[95] X. Feng, A. I. Krylov, *Phys. Chem. Chem. Phys.* **2016**, *18*, 7751–7761.
[96] T. C. Wu, N. J. Thompson, D. N. Congreve, E. Hontz, S. R. Yost, T. Van Voorhis, M. A. Baldo, *Appl. Phys. Lett.* **2014**, *104*.

[97] A. B. Pun, S. N. Sanders, E. Kumarasamy, M. Y. Sfeir, D. N. Congreve, L. M. Campos, *Adv. Mater.* **2017**, *29*, 1701416–n/a.

[98] H. Liu, Z. Wang, X. Wang, L. Shen, C. Zhang, M. Xiao, X. Li, *J. Mater. Chem. C* **2018**, *6*, 3245–3253.

[99] A. B. Pun, S. N. Sanders, M. Y. Sfeir, L. M. Campos, D. N. Congreve, *Chem. Sci.* **2019**, *10*, 3969−3975.

[100] K. J. Fallon, E. M. Churchill, S. N. Sanders, J. Shee, J. L. Weber, R. Meir, S. Jockusch, D. R. Reichman, M. Y. Sfeir, D. N. Congreve, L. M. Campos, *J. Am. Chem. Soc.* **2020**, *142*, 19917−19925.

[101] C. J. Imperiale, P. B. Green, E. G. Miller, N. H. Damrauer, M. W. B. Wilson, *J. Phys. Chem. Lett.* **2019**, *10*, 7463–7469.

[102] J. E. Anthony, J. S. Brooks, D. L. Eaton, S. R. Parkin, *J. Am. Chem. Soc.* **2001**, *123*, 9482–9483.

[103] D. Lehnherr, A. H. Murray, R. McDonald, R. R. Tykwinski, *Angew. Chem. Int. Ed.* **2010**, *49*, 6190–6194.

[104] T. Iwanaga, Y. Yamamoto, K. Nishioka, S. Toyota, *Synthesis* **2015**, *47*, 3997–4007.

[105] D. Lehnherr, M. Adam, A. H. Murray, R. McDonald, F. Hampel, R. R. Tykwinski, *Can. J. Chem.* **2016**, *95*, 303–314.

[106] D. R. Maulding, B. G. Roberts, *J. Org. Chem.* **1969**, *34*, 1734–1736.

[107] R. N. Baral, S. W. Thomas, III, *J. Org. Chem.* **2015**, *80*, 11086–11091.

[108] T. Takahashi, K. Kashima, S. Li, K. Nakajima, K.-i. Kanno, *J. Am. Chem. Soc.* **2007**, *129*, 15752–15753.

[109] E. Kumarasamy, S. N. Sanders, A. B. Pun, S. A. Vaselabadi, J. Z. Low, M. Y. Sfeir, M. L. Steigerwald, G. E. Stein, L. M. Campos, *Macromolecules* **2016**, *49*, 1279–1285.

[110] H. Yu, Y. He, Y. Wu, Y. He, C. He, H. Meng, *Org. Electron.* **2020**, *85*.

[111] E. G. Fuemmeler, S. N. Sanders, A. B. Pun, E. Kumarasamy, T. Zeng, K. Miyata, M. L. Steigerwald, X. Y. Zhu, M. Y. Sfeir, L. M. Campos, N. Ananth, *ACS Cent. Sc.* **2016**, *2*, 316–324.

[112] M. J. Y. Tayebjee, S. N. Sanders, E. Kumarasamy, L. M. Campos, M. Y. Sfeir, D. R. McCamey, *Nat. Phys.* **2017**, *13*, 182–188.

[113] D. Casanova, *Chem. Rev.* **2018**, *118*, 7164–7207.

[114] S. Khan, S. Mazumdar, *Phys. Rev. B* **2018**, *98*, 165202.

[115] L. Abu-Sen, J. J. Morrison, A. B. Horn, S. G. Yeates, *Adv. Opt. Mater.* **2014**, *2*, 636–640.

[116] W. Fudickar, T. Linker, *J. Am. Chem. Soc.* **2012**, *134*, 15071–15082.

[117] C. P. Bénard, Z. Geng, M. A. Heuft, K. VanCrey, A. G. Fallis, *J. Org. Chem.* **2007**, *72*, 7229–7236.

[118] P. Coppo, S. G. Yeates, *Adv. Mater.* **2005**, *17*, 3001–3005.

[119] S. Li, Z. Li, K. Nakajima, K.-i. Kanno, T. Takahashi, *Chem. - Asian J.* **2009**, *4*, 294–301.

[120] S. S. Zade, N. Zamoshchik, A. R. Reddy, G. Fridman-Marueli, D. Sheberla, M. Bendikov, *J. Am. Chem. Soc.* **2011**, *133*, 10803–10816.

[121] M. Garcia-Borràs, A. Konishi, A. Waterloo, Y. Liang, Y. Cao, C. Hetzer, D. Lehnherr, F. Hampel, K. N. Houk, R. R. Tykwinski, *Chem. - Eur. J.* **2017**, *23*, 6111–6117.

[122] M. M. Rauhut, B. G. Roberts, D. R. Maulding, W. Bergmark, R. Coleman, *J. Org. Chem.* **1975**, *40*, 330–335.

[123] J. E. Anthony, D. L. Eaton, S. R. Parkin, *Org. Lett.* **2002**, *4*, 15–18.

[124] D. Lehnherr, J. Gao, F. A. Hegmann, R. R. Tykwinski, *Org. Lett.* **2008**, *10*, 4779–4782.

[125] S. A. Odom, S. R. Parkin, J. E. Anthony, *Org. Lett.* **2003**, *5*, 4245–4248.

[126] D. Lehnherr, R. McDonald, M. J. Ferguson, R. R. Tykwinski, *Tetrahedron* **2008**, *64*, 11449–11461.
[127] N. Monahan, X. Y. Zhu, *Annu. Rev. Phys. Chem.* **2015**, *66*, 601–618.
[128] K. M. Felter, F. C. Grozema, *J. Phys. Chem. Lett.* **2019**, *10*, 7208–7214.
[129] R. Casillas, M. Adam, P. B. Coto, A. R. Waterloo, J. Zirzlmeier, S. R. Reddy, F. Hampel, R. McDonald, R. R. Tykwinski, M. Thoss, D. M. Guldi, *Adv. Energy Mater.* **2019**, *9*, 1802221.
[130] M. J. Y. Tayebjee, K. N. Schwarz, R. W. MacQueen, M. Dvořák, A. W. C. Lam, K. P. Ghiggino, D. R. McCamey, T. W. Schmidt, G. J. Conibeer, *J. Phys. Chem. C* **2016**, *120*, 157–165.
[131] A. N. Stuart, P. C. Tapping, E. Schrefl, D. M. Huang, T. W. Kee, *J. Phys. Chem. C* **2019**, *123*, 5813–5825.
[132] C. Gao, S. K. K. Prasad, B. Zhang, M. Dvořák, M. J. Y. Tayebjee, D. R. McCamey, T. W. Schmidt, T. A. Smith, W. W. H. Wong, *J. Phys. Chem. C* **2019**, *123*, 20181–20187.
[133] S. Ito, T. Nagami, M. Nakano, *J. Phys. Chem. A* **2016**, *120*, 6236–6241.
[134] J. Hu, K. Xu, L. Shen, Q. Wu, G. He, J.-Y. Wang, J. Pei, J. Xia, M. Y. Sfeir, *Nat. Commun.* **2018**, *9*, 2999.
[135] E. Busby, J. Xia, Q. Wu, J. Z. Low, R. Song, J. R. Miller, X. Y. Zhu, L. M. Campos, M. Y. Sfeir, *Nat. Mater.* **2015**, *14*, 426–433.
[136] T. Zeng, P. Goel, *J. Phys. Chem. Lett.* **2016**, *7*, 1351–1358.
[137] S. Mattiello, S. Mecca, A. Ronchi, A. Calascibetta, G. Mattioli, F. Pallini, F. Meinardi, L. Beverina, A. Monguzzi, *ACS Energy Lett.* **2022**, *7*, 2435–2442.
[138] A. M. Müller, Y. S. Avlasevich, W. W. Schoeller, K. Müllen, C. J. Bardeen, *J. Am. Chem. Soc.* **2007**, *129*, 14240–14250.
[139] Y. Matsui, S. Kawaoka, H. Nagashima, T. Nakagawa, N. Okamura, T. Ogaki, E. Ohta, S. Akimoto, A. Sato-Tomita, S. Yagi, Y. Kobori, H. Ikeda, *J. Phys. Chem. C* **2019**, *123*, 18813–18823.
[140] J. C. Miller, J. S. Meek, S. J. Strickler, *J. Am. Chem. Soc.* **1977**, *99*, 8175–8179.
[141] L. Lin, J. Zhu, *Inorg. Chem. Front.* **2022**, *9*, 914–924.
[142] D. Lubert-Perquel, E. Salvadori, M. Dyson, P. N. Stavrinou, R. Montis, H. Nagashima, Y. Kobori, S. Heutz, C. W. M. Kay, *Nat. Commun.* **2018**, *9*, 4222.
[143] B. S. Basel, R. M. Young, M. D. Krzyaniak, I. Papadopoulos, C. Hetzer, Y. Gao, N. T. La Porte, B. T. Phelan, T. Clark, R. R. Tykwinski, M. R. Wasielewski, D. M. Guldi, *Chem. Sci.* **2019**, *10*, 11130–11140.
[144] N. Maity, W. Kim, N. A. Panjwani, A. Kundu, K. Majumder, P. Kasetty, D. Mishra, R. Bittl, J. Nagesh, J. Dasgupta, A. J. Musser, S. Patil, *Nat. Commun.* **2022**, *13*, 5244.
[145] D. Sasikumar, A. T. John, J. Sunny, M. Hariharan, *Chem. Soc. Rev.* **2020**, *49*, 6122–6140.
[146] A. J. Musser, M. Al-Hashimi, M. Heeney, J. Clark, *J. Chem. Phys.* **2019**, *151*, 044902.
[147] I. Papadopoulos, Y. Gao, C. Hetzer, R. R. Tykwinski, D. M. Guldi, *Chemphotochem* **2020**, *4*, 5168–5174.
[148] W. L. Chan, J. R. Tritsch, X. Y. Zhu, *J. Am. Chem. Soc.* **2012**, *134*, 18295–18302.
[149] B. Daiber, K. van den Hoven, M. H. Futscher, B. Ehrler, *ACS Energy Lett.* **2021**, *6*, 2800–2808.
[150] S. N. Sanders, E. Kumarasamy, A. B. Pun, M. T. Trinh, B. Choi, J. Xia, E. J. Taffet, J. Z. Low, J. R. Miller, X. Roy, X. Y. Zhu, M. L. Steigerwald, M. Y. Sfeir, L. M. Campos, *J. Am. Chem. Soc.* **2015**, *137*, 8965–8972.
[151] S. N. Sanders, E. Kumarasamy, A. B. Pun, M. L. Steigerwald, M. Y. Sfeir, L. M. Campos, *Chem* **2016**, *1*, 505–511.

[152] G. He, L. M. Yablon, K. R. Parenti, K. J. Fallon, L. M. Campos, M. Y. Sfeir, *J. Am. Chem. Soc.* **2022**, *144*, 3269–3278.
[153] J. Kim, H. T. Teo, Y. Hong, J. Oh, H. Kim, C. Chi, D. Kim, *Angew. Chem. Int. Ed.* **2020**, *59*, 20956–20964.
[154] L. M. Yablon, S. N. Sanders, H. Li, K. R. Parenti, E. Kumarasamy, K. J. Fallon, M. J. A. Hore, A. Cacciuto, M. Y. Sfeir, L. M. Campos, *J. Am. Chem. Soc.* **2019**, *141*, 9564–9569.
[155] C. Hetzer, B. S. Basel, S. M. Kopp, F. Hampel, F. J. White, T. Clark, D. M. Guldi, R. R. Tykwinski, *Angew. Chem. Int. Ed.* **2019**, *58*, 15263–15267.
[156] R. D. Ribson, G. Choi, R. G. Hadt, T. Agapie, *ACS Cent. Sci.* **2020**, *6*, 2088–2096.
[157] Y. Gao, Y. Hou, F. Gordillo Gámez, M. J. Ferguson, J. Casado, R. R. Tykwinski, *Nat. Chem.* **2020**, *12*, 1143–1149.
[158] Y. Li, Y. Wu, P. Liu, Z. Prostran, S. Gardner, B. S. Ong, *Chem. Mater.* **2007**, *19*, 418–423.
[159] T. Theiss, S. Buss, I. Maisuls, R. López-Arteaga, D. Brünink, J. Kösters, A. Hepp, N. L. Doltsinis, E. A. Weiss, C. A. Strassert, *J. Am. Chem. Soc.* **2023**, *145*, 3937–2951.
[160] C. A. Strassert, M. Mauro, L. De Cola, *Adv. Inorg. Chem.* **2011**, *63*, 47–103.
[161] A. K. Pal, G. S. Hanan, *Chem. Soc. Rev.* **2014**, *43*, 6184–6197.
[162] B. Pashaei, H. Shahroosvand, M. Graetzel, M. K. Nazeeruddin, *Chem. Rev.* **2016**, *116*, 9485–9564.
[163] I. Papadopoulos, S. R. Reddy, P. B. Coto, D. Lehnherr, D. Thiel, M. Thoss, R. R. Tykwinski, D. M. Guldi, *J. Phys. Chem. Lett.* **2022**, 5094–5100.

CHAPTER 2

Synthesis of Pentacene Metal Complexes for the Study of the Heavy-atom Effect on Singlet Fission[a]

2.1 Introduction

Pyridyl ligands are ubiquitous in coordination chemistry for their bonding with transition metal ions, which in some cases can form stable metal complexes. Since the sp^2 lone pair on the nitrogen atom is pointing outward from the aromatic ring, it can overlap readily with the vacant orbital on the metal atom to form a σ bond (Figure 2.1a). The π electrons from the metal also can bond to the unoccupied π* orbitals of pyridine through π-back donation (Figure 2.1b).

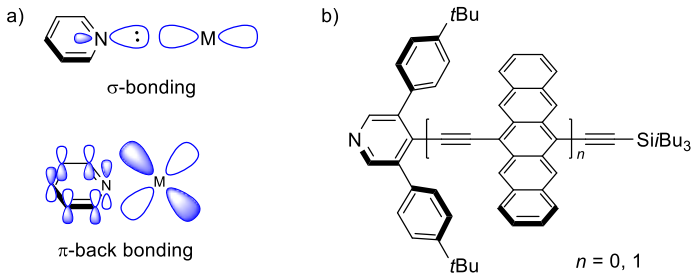

Figure 2.1. a) Schematic illustrations of the formation of σ-bonding and π-back bonding between pyridine and a metal ion; b) structure of pyridyl ligands.

Motivated by both the questions of how the heavy-atom effect (HAE) and oligomers might influence intramolecular singlet fission (iSF, see Chapter 1 for detailed discussions), a pentacene substituted with a sterically hindered pyridyl group and its corresponding model ligand without a pentacene moiety have been designed and synthesized. The pyridyl group is used for bonding with metal ions by coordination and allows the versatile synthesis of pentacene oligomers featuring different metal ions.[1] The pyridyl moiety features sterically demanding substituents in the 3- and 5-positions[2] that both shield the acene core from reactions[3–6] and provide solubility.

[a] The contents of this chapter have been adapted from the following publications:
Y. Hou,† I. Papadopoulos,† Y. Bo, A.-S. Wollny, M. J. Fergusen, L. A. Mai, R. R. Tykwinski, D.M. Guldi, *Precis. Chem.* **2023**, *1*, 555–564.
Y. Hou,† I. Papadopoulos,† M. J. Ferguson, N. Jux, R. R. Tykwinski, D. M. Guldi, *J. Porphyrins Phthalocyanines* **2023**, *27*, 686–693.

Subsequently, the symmetric pentacene dimers and reference dimers linked by Pt(II) and Pd(II) have been synthesized by the reaction of the corresponding ligand with $Pt(PhCN)_2Cl_2$ and $Pd(PhCN)_2Cl_2$, respectively Unsymmetric dimers bearing both a pentacene ligand and a reference pyridyl ligand also have been prepared using the same method. It is important to emphasize that, by design, the two dimers, **$Pt(L_{pc})_2Cl_2$** and **$Pd(L_{pc})_2Cl_2$**, are structurally identical, except for the metal ion. In comparison to suitable model compounds that cannot undergo iSF (**$Pt(L_{pc})(L_{ref})Cl_2$** and **$Pd(L_{pc})(L_{ref})Cl_2$**), the electronic influence of the heavy atoms and the impact on the mechanism of SF can be studied carefully. Photophysical studies performed by our collaborators in Germany show that, despite the presence of heavy-atom Pt or Pd, singlet fission from the pentacene dimers is not inhibited by intersystem crossing. The choice of pyridine coordination reduces decoupling between the pentacenes, while the metal center alters the mechanism of singlet fission. In the presence of Pt in dimer **$Pt(L_{pc})_2Cl_2$** analyses show that $^1(T_1T_1)$ forms directly from iSF. Conversely, the incorporation of Pd in dimer **$Pd(L_{pc})_2Cl_2$** leads to formation of $^1(T_1T_1)$ via a mediating species likely due to the lower spin-orbit coupling.

A pentacene tetramer **$Ru(L_{pc})_4Cl_2$** has been designed based on the well-established structural diversity of hexacoordinate Ru(II) complexes.[7–8] The resulting tetramer is used to document the influence of the HAE in SF, and it offers a unique, coplanar, equatorial relationship between the four pentacene moieties. This arrangement of pentacenes was designed to determine the prospect of triplet diffusion via chromophore multiplication.[9]

2.2 Design and Synthesis of Pyridyl-endcapped Ligands

2.2.1 Synthesis of Pyridyl Group

The synthesis of the desired ligands required a sterically hindered pyridyl group (Scheme 2.1). The preparation of the pyridyl group began with a commercially available 4-pyridone (**2.1**). Bromination of compound **2.1** with bromine in basic conditions gave compound **2.2** in 74% yield. Compound **2.2** was alkylated with methyl iodide, giving *N*-methylated compound (**2.3**) in 89% yield. Compound **2.4** was

synthesized through a Suzuki cross-coupling reaction with compound **2.3** and 2-(4-*tert*-butylphenyl)-4,4,5,5-tetramethyl-1,3,2-dioxaborolane. Then, Compound **2.4** was treated with PBr_3 at 150 °C, giving brominated pyridyl **2.5** in good yield. Compound **2.6** was synthesized through a Sonogashira cross-coupling reaction with compound **2.5** and 2-methyl-3-butyn-2-ol. Subsequently, the desired sterically encumbered 4-ethynylpyridyl group 3,5-bis(4-*tert*-butylphenyl)-4-ethynylpyridine (**2.7**) was obtained by deprotection of compound **2.6** with NaOH in the presence of tris[2-(2-methoxyethoxy)ethyl]amine (TDA-1) in toluene at 110 °C.

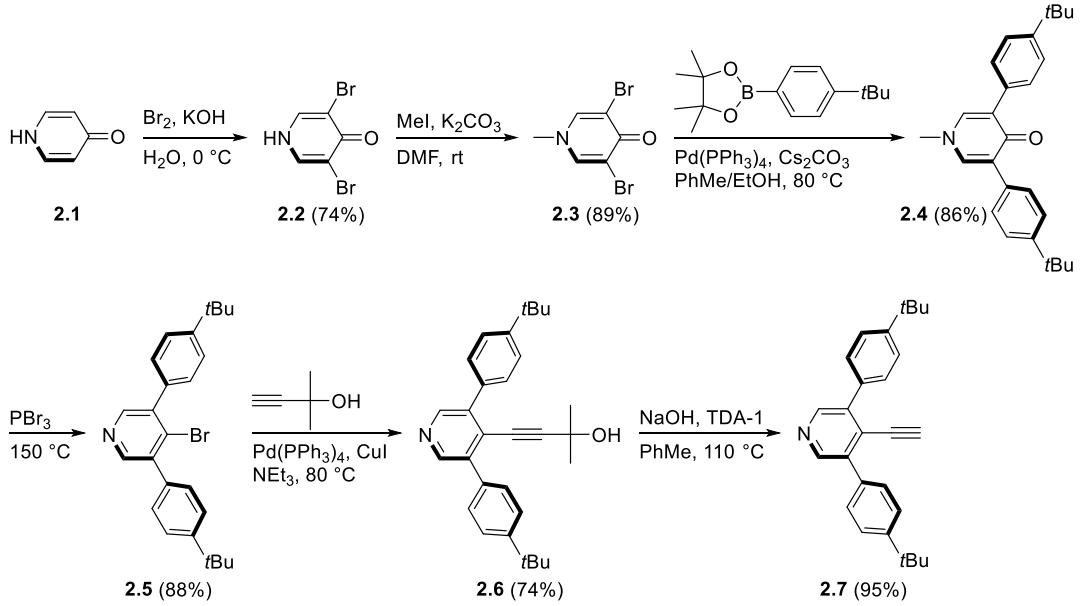

Scheme 2.1. Synthesis of 3,5-bis(4-*tert*-butylphenyl)-4-ethynylpyridine.

2.2.2 Synthesis of Pyridyl-endcapped Pentacene Ligand L_{pc}

The pyridyl-endcapped pentacene ligand (**L_{pc}**) was synthesized using a stepwise nucleophilic substitution of 6,13-pentacenequinone (**2.8**), followed by $SnCl_2$-mediated reductive aromatization (Scheme 2.2). Ketone **2.9** was synthesized as previously reported, by adding lithiated (tri*iso*butylsilyl)acetylene to a suspension of 6,13-pentacenequinone (**2.8**) in dry THF at –78 °C; the resulting alkoxide was quenched by methyl iodide.[10] Surprisingly, lithiation of compound **2.7** with *n*BuLi did not lead to successful addition of the lithiated species to ketone **2.9**. Only starting materials were found and recovered after aqueous workup for all attempts. A test reaction showed that

the peak for the acetylene proton diminished when quenching the lithiation reaction mixture with D_2O rather than adding it to the solution of ketone **2.9** (Figure 2.2). Alternatively, compound **2.7** was lithiated by lithium hexamethyldisilazide (LiHMDS), which was prepared in situ by adding *n*BuLi to a solution of $[(CH_3)_3Si]_2NH$ in dry THF at –78 °C. Then, the reaction mixture was added to a solution of ketone **2.9** in dry THF at –78 °C and stirred for 18 h at rt. Compound **2.10** was formed as a pair of stereoisomers after quenching the reaction with saturated aqueous NH_4Cl solution. The stereoisomers could be separated by recrystallization from a solution of the mixture of two isomers in CH_2Cl_2 by layering with hexanes. Since the two isomers would give rise to the same product following the next reaction step, both isomers were carried on to $SnCl_2$-mediated reductive aromatization to give pyridyl-endcapped pentacene ligand (**L**$_{pc}$) as a dark blue solid in 89% yield.

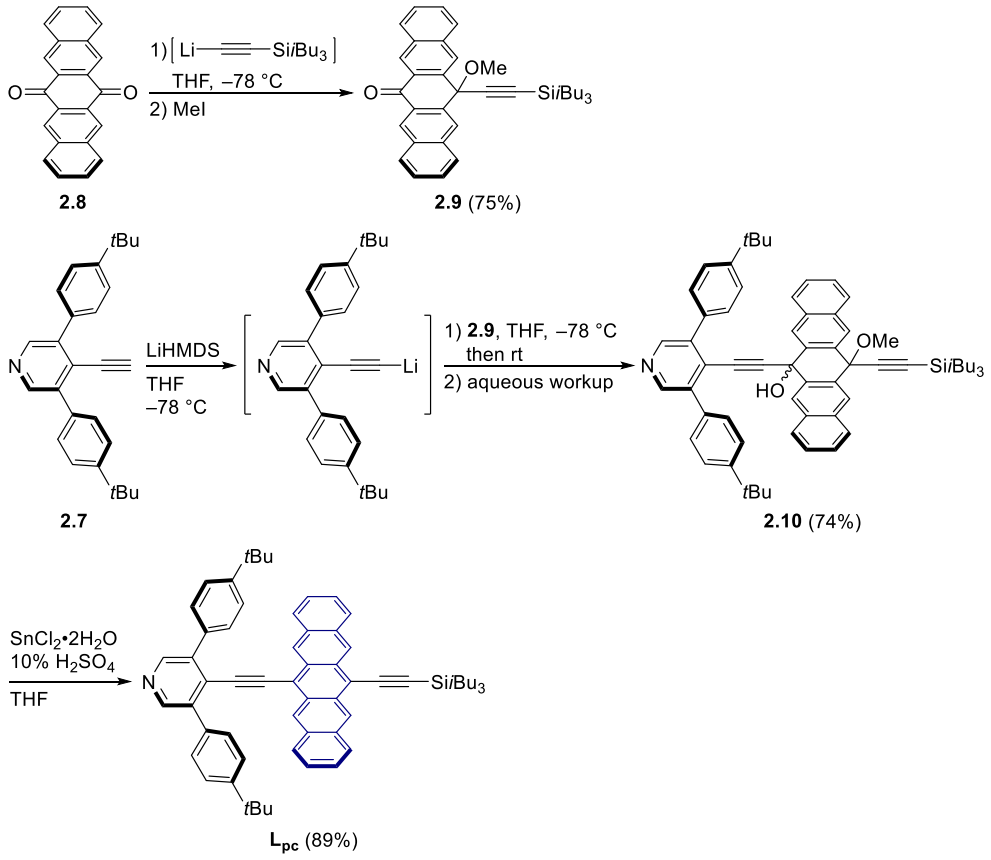

Scheme 2.2. Synthesis of **L**$_{pc}$.

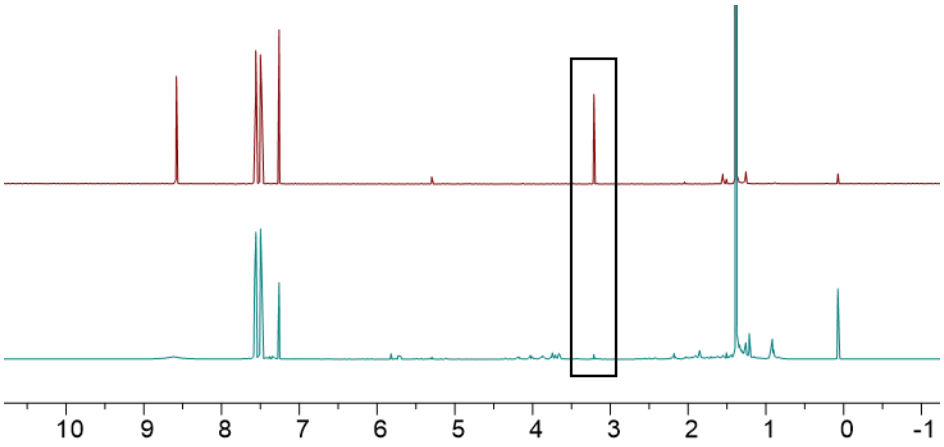

Figure 2.2. ^{1}H NMR spectra (498 MHz) of (top) compound **2.7** and (bottom) compound **2.7** following deprotonation using *n*BuLi and subsequent quenching by addition of D_2O after quenching reaction mixture with D_2O (in $CDCl_3$).

2.2.3 Synthesis of Reference Ligand L_{ref}

The reference ligand without a pentacene moiety **L**$_{ref}$ was synthesized through a Sonogashira cross-coupling reaction with compound **2.5** and (tri*iso*butylsilyl)acetylene using the same conditions as compound **2.6**. The crude product was purified by column chromatography to give **L**$_{ref}$ as a white solid in 77% yield (Scheme 2.3). Notably, the R_f values for the product **L**$_{ref}$ and starting material **2.5** are very similar, leading to difficult separation by chromatography. To solve this problem, 10 equiv of (tri*iso*butylsilyl)acetylene was used in this reaction to exhaust compound **2.5** as much as possible.

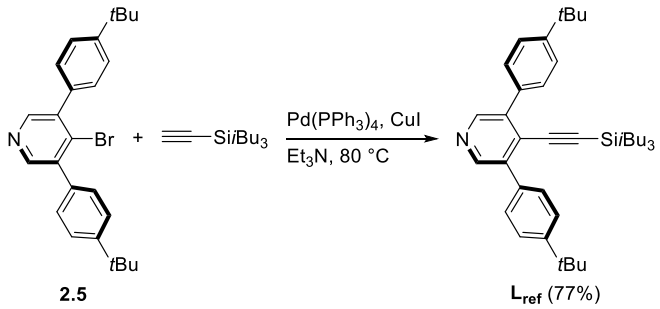

Scheme 2.3. Synthesis of **L**$_{ref}$.

2.3 Synthesis of Platinum- and Palladium-based Dimeric Complexes

With the ligands $\mathbf{L_{pc}}$ and $\mathbf{L_{ref}}$ in hand, a series of dimers linked by Pt(II) and Pd(II) have been synthesized by the ligand exchange reaction of the ligands $\mathbf{L_{pc}}$ and $\mathbf{L_{ref}}$ with $Pt(PhCN)_2Cl_2$ and $Pd(PhCN)_2Cl_2$.

2.3.1 Synthesis of Pentacene Dimers and Reference Compounds

The symmetric dimers with two pentacene moieties ($\mathbf{Pt(L_{pc})_2Cl_2}$ and $\mathbf{Pd(L_{pc})_2Cl_2}$) have been synthesized (Scheme 2.4). The corresponding reference compounds with exactly same geometry but with no pentacene moiety ($\mathbf{Pt(L_{ref})_2Cl_2}$ and $\mathbf{Pd(L_{ref})_2Cl_2}$) in the molecules have been synthesized as well (Scheme 2.4).

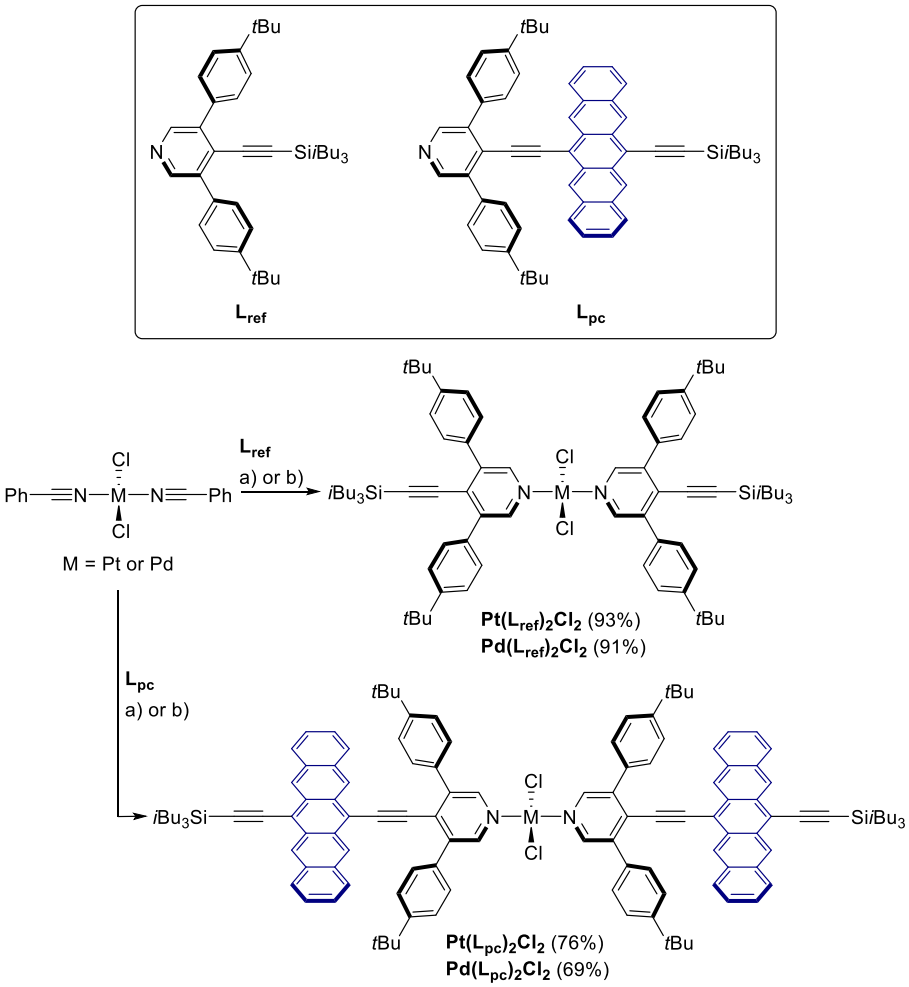

Scheme 2.4. Synthesis of symmetric dimers $\mathbf{Pt(L_{ref})_2Cl_2}$, $\mathbf{Pd(L_{ref})_2Cl_2}$, $\mathbf{Pt(L_{pc})_2Cl_2}$, and $\mathbf{Pd(L_{pc})_2Cl_2}$. Conditions: for Pt dimers a) PhMe, 80 °C; for Pd dimers b) CH_2Cl_2, rt.

Bis(benzonitrile)platinum(II) dichloride ($Pt(PhCN)_2Cl_2$) was prepared with the procedure reported in the literature.[11] The ligand-exchange reactions of $Pt(PhCN)_2Cl_2$ were done in dry toluene at 80 °C. Reacting $Pt(PhCN)_2Cl_2$ with $\mathbf{L_{ref}}$ gave $\mathbf{Pt(L_{ref})_2Cl_2}$ in 93% yield as pale yellow crystals following chromatographic purification (silica gel) and recrystallization (CH_2Cl_2/MeOH). Notably, both *cis*- and *trans*-$Pt(PhCN)_2Cl_2$ were obtained from the preparation and used for the ligand-exchange reaction. But only the trans isomer was obtained for $\mathbf{Pt(L_{ref})_2Cl_2}$, which was confirmed unambiguously by X-ray crystallography and NMR spectroscopy that showed only one compound. Similarly, $\mathbf{Pt(L_{pc})_2Cl_2}$ was synthesized by replacement of benzonitrile in $Pt(PhCN)_2Cl_2$ with $\mathbf{L_{pc}}$. The product was purified by column chromatography (alumina), followed by recrystallization (CH_2Cl_2/hexanes) and isolated in 76% yield as a dark blue solid.

Bis(benzonitrile)palladium(II) dichloride ($Pd(PhCN)_2Cl_2$) was prepared with the procedure reported in the literature as well.[12] Unlike the Pt analogue, only the trans isomer was obtained for $Pd(PhCN)_2Cl_2$.[13] The ligand-exchange reactions of $Pd(PhCN)_2Cl_2$ typically are done at milder conditions, as benzonitrile is lost readily due to a weaker metal-nitrogen interaction.[14–16] $\mathbf{Pd(L_{ref})_2Cl_2}$ and $\mathbf{Pd(L_{pc})_2Cl_2}$ were synthesized from $Pd(PhCN)_2Cl_2$ via the ligand-exchange reaction with $\mathbf{L_{pc}}$ and $\mathbf{L_{ref}}$, respectively. The complexes $\mathbf{Pd(L_{ref})_2Cl_2}$ and $\mathbf{Pd(L_{pc})_2Cl_2}$ were isolated as pale yellow crystals and a dark blue-green solid, respectively.

All products are stable as solids under normal laboratory conditions. However, the compounds containing pentacene moieties ($\mathbf{Pt(L_{pc})_2Cl_2}$ and $\mathbf{Pd(L_{pc})_2Cl_2}$) decompose in solution upon exposure to air (O_2) and light over days.

2.3.2 Synthesis of Unsymmetric Dimers

The unsymmetric Pt dimer $\mathbf{Pt(L_{pc})(L_{ref})Cl_2}$ was made in a stepwise manner from $Pt(PhCN)_2Cl_2$ (Scheme 2.5). Intermediate $\mathbf{Pt(PhCN)(L_{ref})Cl_2}$ was made by dropwise addition of a solution of $\mathbf{L_{ref}}$ in dry toluene to a solution of $Pt(PhCN)_2Cl_2$ (1.5 equiv) in dry toluene at 110 °C. Even though $\mathbf{Pt(PhCN)(L_{ref})Cl_2}$ was the major product, a small amount of $\mathbf{Pt(L_{ref})_2Cl_2}$ was formed during the reaction. The desired compound $\mathbf{Pt(PhCN)(L_{ref})Cl_2}$ was stable on silica gel and isolated by column chromatography. With $\mathbf{Pt(PhCN)(L_{ref})Cl_2}$ in hand, the final product $\mathbf{Pt(L_{pc})(L_{ref})Cl_2}$ was made by

replacing PhCN with the stronger ligand $\mathbf{L_{pc}}$. The compounds $\mathbf{Pt(L_{ref})_2Cl_2}$, $\mathbf{Pt(L_{pc})(L_{ref})Cl_2}$, and $\mathbf{Pt(L_{pc})_2Cl_2}$ were found in the reaction mixture, and the desired unsymmetric dimer $\mathbf{Pt(L_{pc})(L_{ref})Cl_2}$ was the major product. $\mathbf{Pt(L_{pc})_2Cl_2}$ decomposes on silica gel, while the other two dimers ($\mathbf{Pt(L_{ref})_2Cl_2}$ and $\mathbf{Pt(L_{pc})(L_{ref})Cl_2}$) are stable for the duration of the chromatography. Thus, after removal of solvent, the residue was applied to a silica gel column to remove the pentacene dimer $\mathbf{Pt(L_{pc})_2Cl_2}$. However, as these three dimers have very similar R_f values, all attempts to separate $\mathbf{Pt(L_{ref})_2Cl_2}$ and $\mathbf{Pt(L_{pc})(L_{ref})Cl_2}$ were unsuccessful. The mixture was purified by size exclusion column chromatography (Bio-Beads SX3 support) with toluene as eluent, followed by recrystallization, affording $\mathbf{Pt(L_{pc})(L_{ref})Cl_2}$ as dark blue crystals in 58% yield.

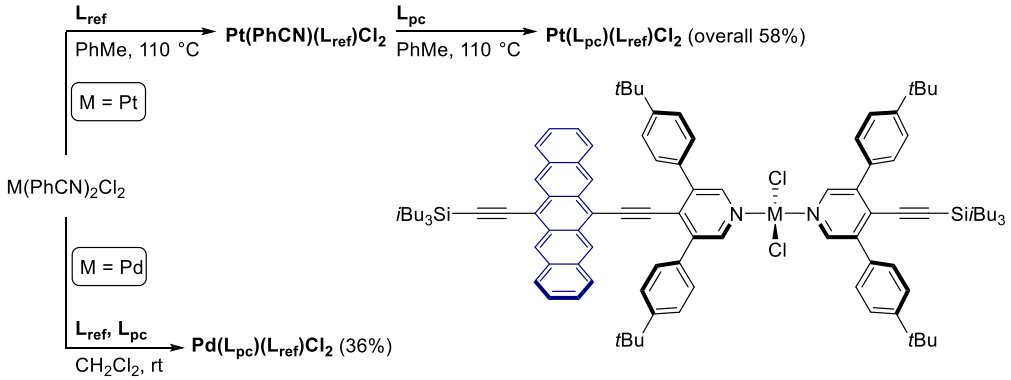

Scheme 2.5. Synthesis of unsymmetric dimers $\mathbf{Pt(L_{pc})(L_{ref})Cl_2}$ and $\mathbf{Pd(L_{pc})(L_{ref})Cl_2}$.

The unsymmetric Pd dimer $\mathbf{Pd(L_{pc})(L_{ref})Cl_2}$ was made using a one-pot protocol instead of stepwise (Scheme 2.5), since the intermediate $\mathbf{Pd(PhCN)(L_{ref})Cl_2}$ could not be isolated by column chromatography (using either silica gel or alumina). While $\mathbf{Pt(L_{pc})(L_{ref})Cl_2}$ could be purified through a sequence of column chromatography and recrystallization, $\mathbf{Pd(L_{pc})(L_{ref})Cl_2}$ was unstable to purification by column chromatography (using either silica gel or alumina). Ultimately, preparative gel permeation chromatography gave the pure product $\mathbf{Pd(L_{pc})(L_{ref})Cl_2}$ as a dark blue-green solid in 36% yield.

2.4 Synthesis of Ruthenium-based Tetrameric Complexes

2.4.1 Synthesis of a Pentacene Tetramer and Its Reference Compound

The tetramer **Ru(L_{ref})$_4$Cl$_2$** was targeted first as a model system without inclusion of the pentacene moiety to confirm the viability of attaching four sterically demanding pyridyl ligands to the Ru(II) metal center. Tetra(benzonitrile)ruthenium(II) dichloride ($Ru(PhCN)_4Cl_2$) was prepared with the procedure reported in the literature.[17] The ligand-exchange reaction of $Ru(PhCN)_4Cl_2$ with **L_{ref}** (4 equiv) gave **Ru(L_{ref})$_4$Cl$_2$** in good yield following chromatographic purification (silica gel) and recrystallization (CH_2Cl_2/MeOH) (Scheme 2.6). MALDI HRMS confirmed the composition of the tetrameric product $C_{156}H_{220}Cl_2N_4RuSi_4$. The proposed structure was ultimately confirmed by X-ray crystallographic analysis (vide infra).

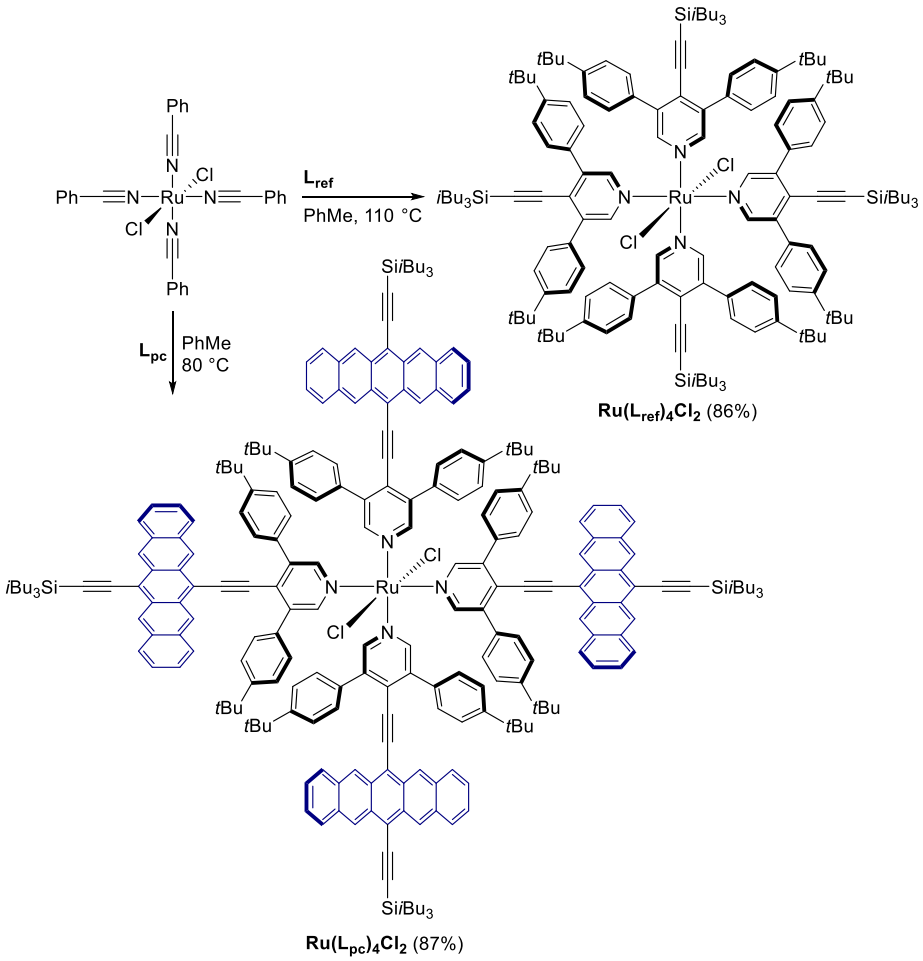

Scheme 2.6. Synthesis of Ru tetramers **Ru(L_{ref})$_4$Cl$_2$** and **Ru(L_{pc})$_4$Cl$_2$**.

The tetramer **Ru(L_{pc})$_4$Cl$_2$** was synthesized from Ru(PhCN)$_4$Cl$_2$ via the ligand exchange reaction with **L_{pc}** (4 equiv). The product was purified by column chromatography (alumina) and recrystallization (CH_2Cl_2/MeOH) and isolated in 87% yield. Similar to the model compound **Ru(L_{ref})$_4$Cl$_2$**, the simplicity of the NMR spectra for **Ru(L_{pc})$_4$Cl$_2$** confirmed the equatorial substitution of the four pentacenyl ligands about the Ru center. MALDI HRMS analysis of **Ru(L_{pc})$_4$Cl$_2$** also was consistent with the proposed structure, showing a strong signal at *m/z* 3633.8646 (M^+, calcd for $C_{252}H_{268}{}^{35}Cl_2N_4{}^{102}RuSi_4$ *m/z* 3633.8645). **Ru(L_{pc})$_4$Cl$_2$** and **Ru(L_{ref})$_4$Cl$_2$** are soluble in common organic solvents such as CH_2Cl_2, $CHCl_3$, tetrahydrofuran (THF), and PhMe, and they are stable as solids under normal laboratory conditions. Pentacenyl tetramer **Ru(L_{pc})$_4$Cl$_2$**, however, slowly decomposes in solution upon exposure to air (O_2) and light over days.

2.4.2 Attempts to Remove Chloride in Ru(L_{pc})$_4$Cl$_2$

In order to study the influence of chloride ligands and replace them in the tetramer **Ru(L_{pc})$_4$Cl$_2$**, attempts were made to remove the chloride with triflate anions and form hexamer **Ru(L_{pc})$_6$(CF_3SO_3)$_2$** (Scheme 2.7). Initial attempts were made by using **L_{pc}** (6 equiv) and an excess amount of $AgCF_3SO_3$ in dry toluene at 80 °C. However, only **Ru(L_{pc})$_4$Cl$_2$** was obtained from the reaction. Alternatively, Ru(PhCN)$_6$(CF_3SO_3)$_2$ was used directly as the starting material. In principle, **L_{pc}** would replace PhCN in Ru(PhCN)$_6$(CF_3SO_3)$_2$ and form the desired product **Ru(L_{pc})$_6$(CF_3SO_3)$_2$** or as a partially substituted product **Ru(L_{pc})$_n$(PhCN)$_{6-n}$(CF_3SO_3)$_2$** (n = 1–6). Surprisingly, all attempts failed; no obvious changes were observed after all reactions.

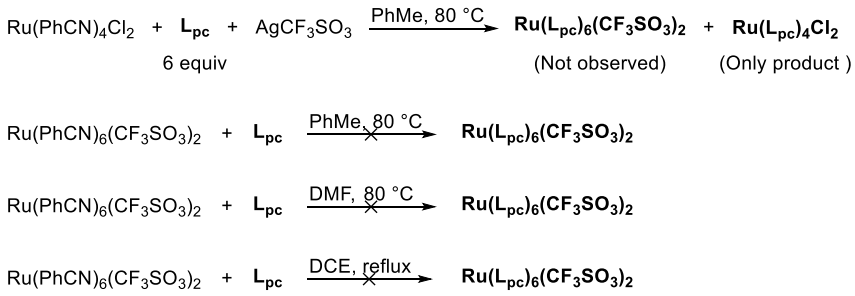

Scheme 2.7. Attempts to replace chloride in **Ru(L_{pc})$_4$Cl$_2$**.

2.5 Characterization of Metal Complexes

The successful formation of the desired metal complexes has been confirmed by mass spectrometry (MS) combined with ^{1}H, ^{13}C NMR, and ^{1}H–^{13}C HSQC NMR spectroscopic analyses. The structures of reference compounds **Pt(L_{ref})$_2$Cl$_2$**, **Pd(L_{ref})$_2$Cl$_2$**, and **Ru(L_{ref})$_4$Cl$_2$,** as well as the unsymmetric dimer **Pt(L_{pc})(L_{ref})Cl$_2$** have been established unambiguously by X-ray crystallography.

2.5.1 ^{1}H Spectroscopic Analysis

2.5.1.1 ^{1}H Spectroscopic Analysis for Platinum- and Palladium-based Dimeric Complexes

^{1}H NMR spectra of **M(L_{ref})$_2$Cl$_2$** and **M(L_{pc})$_2$Cl$_2$** (M = Pt, Pd) mirror the ^{1}H NMR spectra of the ligands **L_{ref}** and **L_{pc}**, as the two organic ligands in the metal complexes are equivalent. It is easy to identify the signal of pyridyl protons (H_a) for **L_{ref}** since there is only one singlet (δ 8.54) in the aromatic region (Figure 2.3). For spectra of **L_{pc}**, **Pt(L_{pc})$_2$Cl$_2$**, and **Pd(L_{pc})$_2$Cl$_2$**, there are three singlet peaks in the range of 8.4–9.1 ppm with integration of 2H, correlating to H_a, H_b, and H_c. ^{1}H–^{13}C HSQC NMR spectra for **L_{pc}**, **Pt(L_{pc})$_2$Cl$_2$**, and **Pd(L_{pc})$_2$Cl$_2$** are used to identify signals of H_a. As shown in Figure 2.3, H_a can be assigned easily through protons correlated to the *ortho*-carbon in the pyridyl ring (~150 ppm).

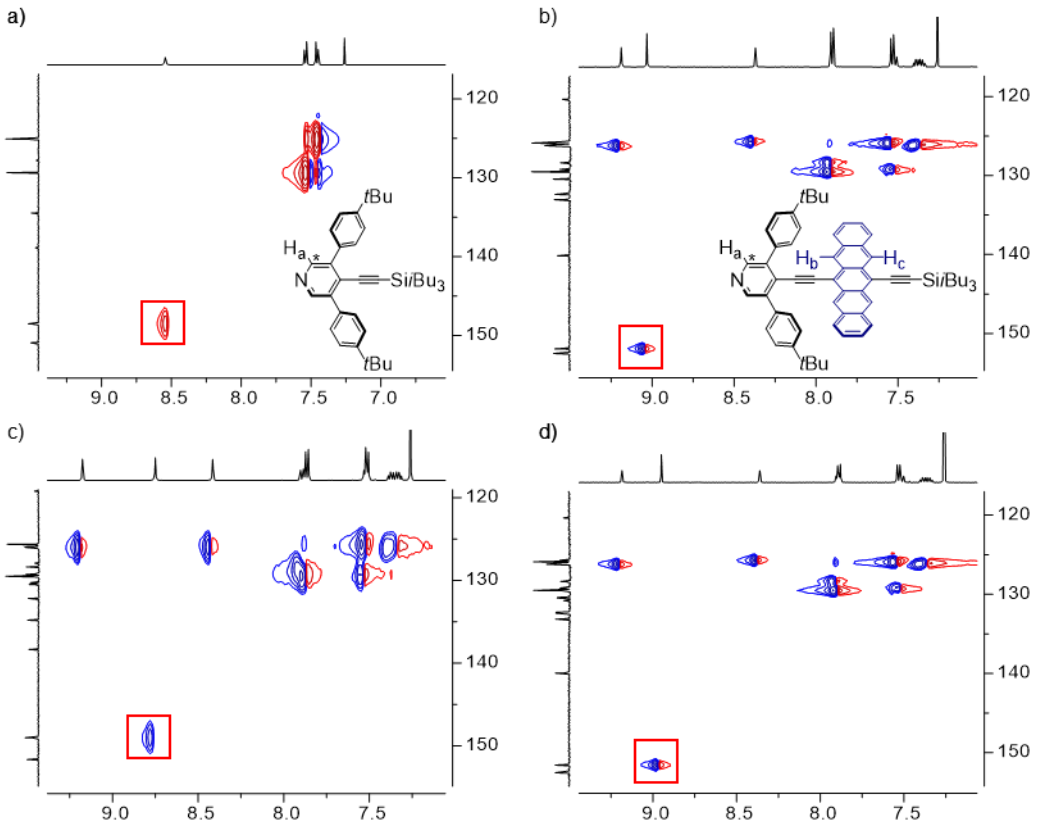

Figure 2.3. Aromatic region of ^{1}H–^{13}C HSQC spectra of a) $\mathbf{L_{ref}}$, b) $\mathbf{L_{pc}}$, c) $\mathbf{Pt(L_{pc})_2Cl_2}$, and d) $\mathbf{Pd(L_{pc})_2Cl_2}$ in $CDCl_3$; red boxes indicate correlation of $H_a \leftrightarrow C^*$.

It is noted, however, that the signals of pyridyl protons in $\mathbf{M(L_{ref})_2Cl_2}$ (Pt: δ8.78 and Pd: δ8.70) and $\mathbf{M(L_{pc})_2Cl_2}$ (Pt: δ9.03 and Pd: δ8.95) are shifted downfield by 0.24–0.28 and 0.16–0.20 ppm for the Pt and Pd complexes (Figure 2.4), respectively, compared to the analogous protons of the free ligands $\mathbf{L_{ref}}$ and $\mathbf{L_{pc}}$ (δ8.54 and δ8.75, respectively). The observed trends in ^{1}H shifts for the pyridyl groups are consistent with literature reports, which indicate a decreased electron density upon metal coordination of a pyridyl ligand.[18–22] The greater deshielding of theses protons when bound to Pt(II) in comparison to Pd(II) corresponds to the lower spin-orbit coupling for Pd due to its nuclear charge.[23–24]

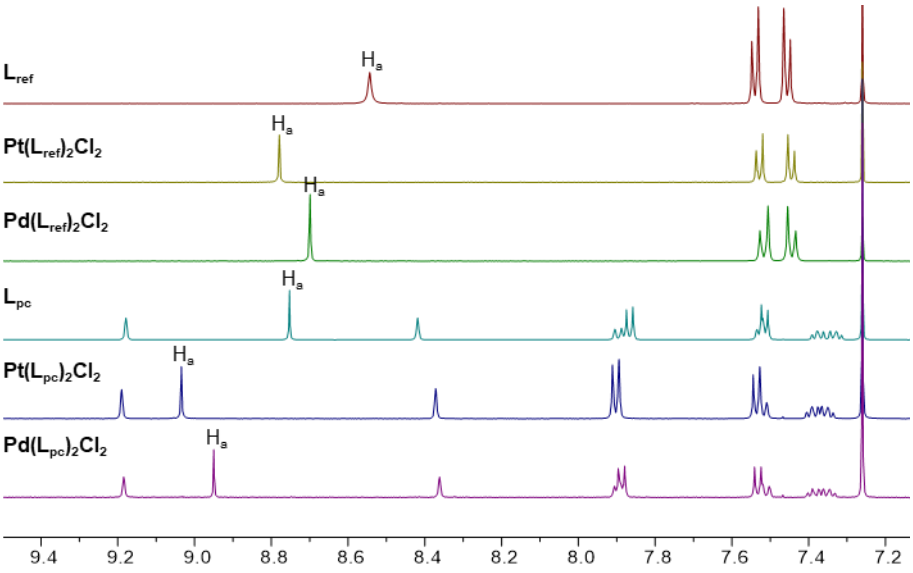

Figure 2.4. Stacked plot of the aromatic region of ^{1}H NMR spectra of **L_{ref}**, **$Pt(L_{ref})_2Cl_2$**, **$Pd(L_{ref})_2Cl_2$**, **L_{pc}**, **$Pt(L_{pc})_2Cl_2$**, and **$Pd(L_{pc})_2Cl_2$** in $CDCl_3$. Signals for protons on pyridyl are labeled with H_a.

2.5.1.2 ^{1}H Spectroscopic Analysis for Ruthenium-based Tetrameric Complexes

The geometry of **$Ru(L_{ref})_4Cl_2$** was substantiated by ^{1}H NMR spectroscopy, which shows a single set of two pseudo-first-order doublets at δ7.30 and 7.38 for the AA'BB' system of the aryl protons and one singlet as δ8.72 arising from the pyridyl protons, confirming the symmetrically equivalent relationship of the four ligands about Ru. As for model compound **$Ru(L_{ref})_4Cl_2$**, the simplicity of the NMR spectra for **$Ru(L_{pc})_4Cl_2$** confirmed the equatorial substitution of the four pentacenyl ligands about the Ru center.

Similar to platinum- and palladium-based dimeric complexes, the signals of pyridyl protons in **$Ru(L_{ref})_2Cl_2$** (δ8.72) and **$Ru(L_{pc})_2Cl_2$** (δ9.16) are shifted downfield by 0.18 and 0.41 ppm, respectively, compared to the analogous protons of the free ligands **L_{ref}** (δ 8.54) and **L_{pc}** (δ 8.75) (Figure 2.5). The results also confirm the decreased electron density after coordination of pyridyl groups. There are signals for a small amount of (<10%) an undefined impurity in the samples of **$Ru(L_{ref})_2Cl_2$** and **$Ru(L_{pc})_2Cl_2$**.

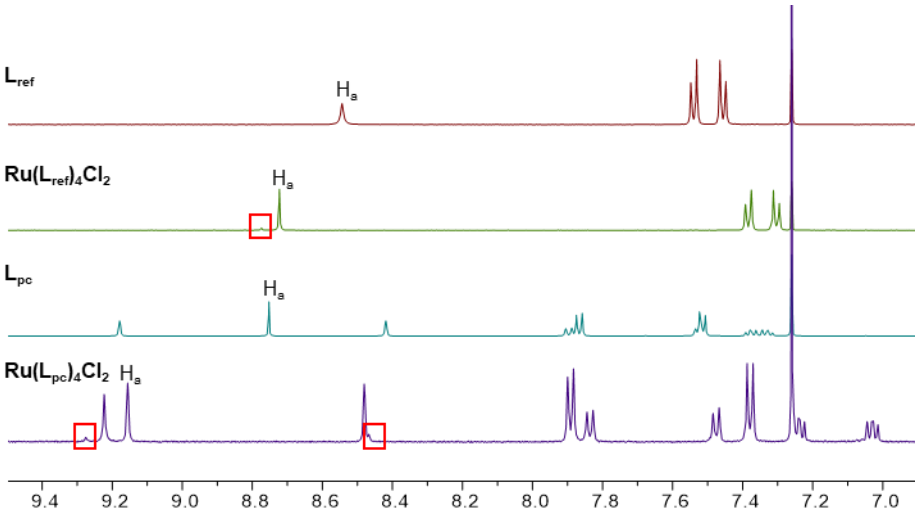

Figure 2.5. Stacked plot of the aromatic region of ^{1}H NMR spectra of $\mathbf{L_{ref}}$, $\mathbf{Ru(L_{ref})_4Cl_2}$, $\mathbf{L_{pc}}$, and $\mathbf{Ru(L_{pc})_4Cl_2}$ in $CDCl_3$. Signals for protons on pyridyl are labeled with H_a. Signals for an undefined impurity are labeled with red boxes.

In order to study if the ruthenium tetramers can undergo thermal trans-cis isomerization, variable temperature ^{1}H NMR spectroscopy was conducted. However, experiments for $\mathbf{Ru(L_{ref})_2Cl_2}$ showed no sign of any changes in the spectra even at 100 °C (Figure 2.6).

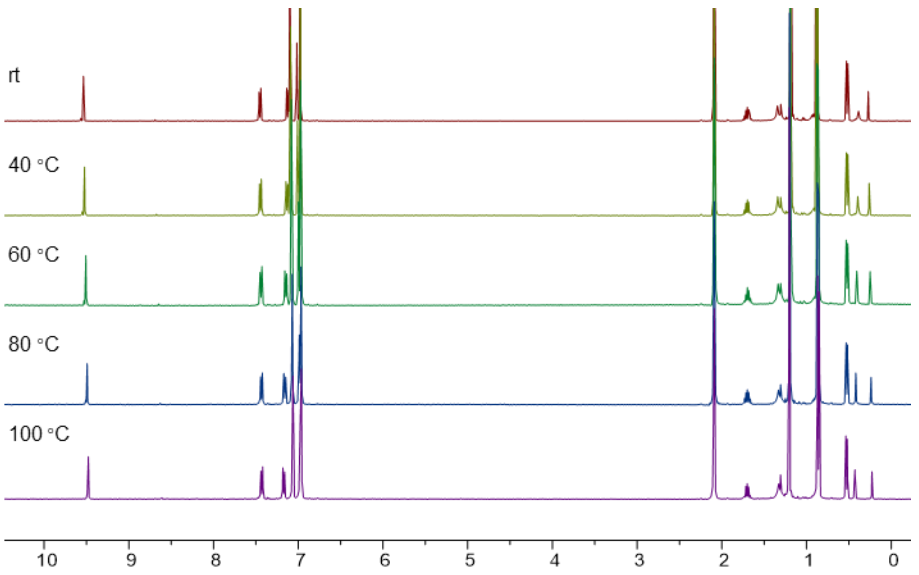

Figure 2.6. Variable temperature NMR spectra of $\mathbf{Ru(L_{ref})_2Cl_2}$ in deuterated toluene.

2.5.2 UV-vis Spectroscopic Analysis

The quantitative UV-vis spectra of metal complexes have been measured in CH_2Cl_2 at room temperature (Figure 2.7). The spectra of reference compounds without pentacenyl groups **L_{ref}**, **$Pt(L_{ref})_2Cl_2$**, and **$Pd(L_{ref})_2Cl_2$** only show absorption bands in the high energy region of the ultraviolet spectrum between 250–400 nm, while **$Ru(L_{ref})_4Cl_2$** has absorption peaks at lower energy between 400–650 nm (Figure 2.7a).

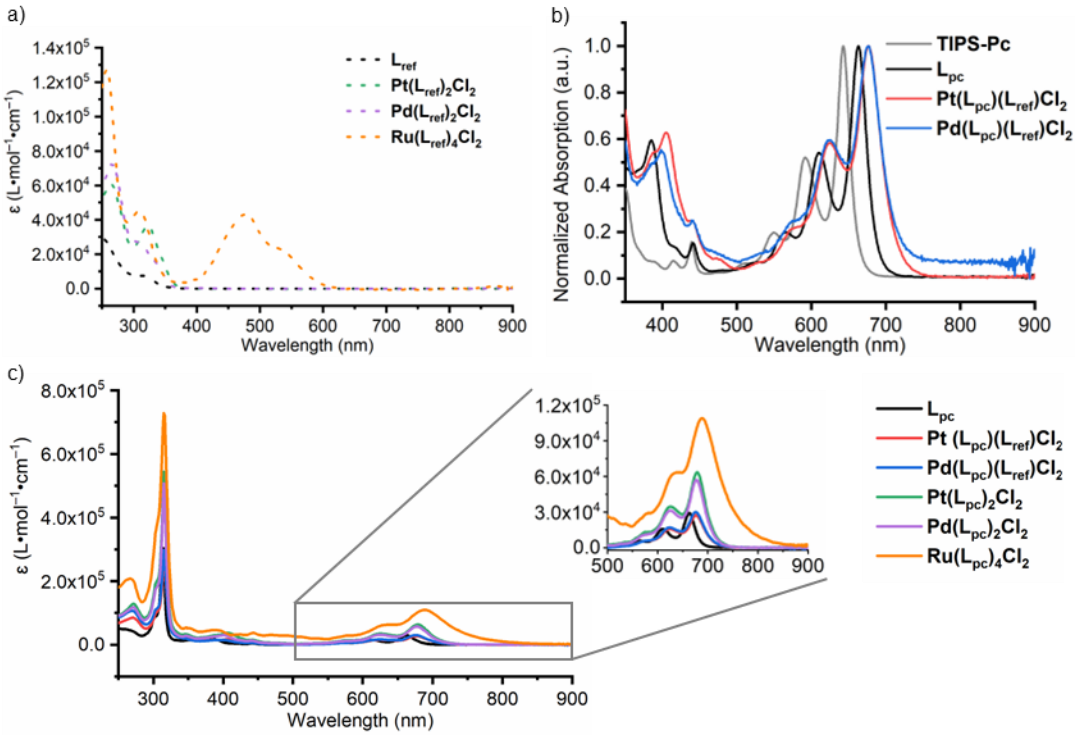

Figure 2.7. a) UV-vis spectra of **L_{ref}**, **$Pt(L_{ref})_2Cl_2$**, **$Pd(L_{ref})_2Cl_2$**, and **$Ru(L_{ref})_4Cl_2$** in CH_2Cl_2; b) normalized UV-vis spectra of **TIPS-Pc**, **L_{pc}**, **$Pt(L_{pc})(L_{ref})Cl_2$**, and **$Pd(L_{pc})(L_{ref})Cl_2$** in CH_2Cl_2; c) UV-vis spectra of **L_{pc}**, **$Pt(L_{pc})(L_{ref})Cl_2$**, **$Pd(L_{pc})(L_{ref})Cl_2$**, **$Pt(L_{pc})_2Cl_2$**, **$Pd(L_{pc})_2Cl_2$**, and **$Ru(L_{pc})_4Cl_2$** in CH_2Cl_2 with expansion of 500–900 nm.

The absorption maximum for **L_{pc}** (λ_{max} = 663 nm) is red-shifted in comparison to 6,13-bis(tri*iso*propylsilylethynyl)pentacene (**TIPS-Pc**, λ_{max} = 643 nm in CH_2Cl_2),[25] presumably due to the increased conjugation length through the pyridyl group (Figure 2.7b). The absorptions for **$Pt(L_{pc})(L_{ref})Cl_2$** (λ_{max} = 677 nm) and **$Pd(L_{pc})(L_{ref})Cl_2$** (λ_{max} = 677 nm) are subtly red-shifted and slightly broadened compared to the free ligand **L_{pc}** (Figure 2.7b, Table 2.1). It is noted that the spectra of **$Pt(L_{pc})(L_{ref})Cl_2$** and **$Pd(L_{pc})(L_{ref})Cl_2$** show well-resolved vibrational fine structure

(Figure 2.7b and 2.7c), in contrast to Pt-acetylide complexes bearing acenes that show broadened features.[26–28] The extinction coefficients of **Pt(L$_{pc}$)(L$_{ref}$)Cl$_2$** (27,200 L mol^{-1} cm^{-1}) and **Pd(L$_{pc}$)(L$_{ref}$)Cl$_2$** (30,100 L mol^{-1} cm^{-1}), which are approximately the same as the ligand **L$_{pc}$** (29,300 L mol^{-1} cm^{-1}) (Figure 2.7c, Table 2.1).

Table 2.1. Relevant UV-vis Data for Metal Complexes Containing Pentacenyl Groups

Metal	Compound	λ_{max} (nm)	ε (L mol^{-1} cm^{-1})
	L$_{pc}$	663	29,300
Pt	**Pt(L$_{pc}$)(L$_{ref}$)Cl$_2$**	677	27,200
	Pt(L$_{pc}$)$_2$Cl$_2$	679	63,500
Pd	**Pd(L$_{pc}$)(L$_{ref}$)Cl$_2$**	677	30,100
	Pd(L$_{pc}$)$_2$Cl$_2$	677	57,100
Ru	**Ru(L$_{pc}$)$_4$Cl$_2$**	689	109,000

The UV-vis spectra of pentacene dimers **Pt(L$_{pc}$)$_2$Cl$_2$** and **Pd(L$_{pc}$)$_2$Cl$_2$** show similar features. The shift in the low-energy absorptions is minimal compared to **Pt(L$_{pc}$)(L$_{ref}$)Cl$_2$** and **Pd(L$_{pc}$)(L$_{ref}$)Cl$_2$**, despite the additional π-conjugation resulting from the second pentacenyl group, pointing towards the presence of an effectively decoupled system in those dimers. The extinction coefficients of **Pt(L$_{pc}$)$_2$Cl$_2$** (63,500 L mol^{-1} cm^{-1}) and **Pd(L$_{pc}$)$_2$Cl$_2$** (57,100 L mol^{-1} cm^{-1}) are nearly twice that of the monomers, further reinforcing this fact (Figure 2.7c, Table 2.1). The absorption spectrum of **Ru(L$_{pc}$)$_4$Cl$_2$** shows broadened absorptions in the range of 550–900 nm when compared to that of the pentacenyl ligand **L$_{pc}$**. The absorption maximum of **Ru(L$_{pc}$)$_4$Cl$_2$** (λ_{max} = 689 nm) shows a further red-shift in comparison to **L$_{pc}$**, suggesting electronic communication across the Ru center. The extinction coefficient of **Ru(L$_{pc}$)$_4$Cl$_2$** is 109,000 L mol^{-1} cm^{-1}, which is approximately quadrupled in comparison to the ligand **L$_{pc}$** (29,300 L mol^{-1} cm^{-1}), as would be expected from its tetrameric nature (Figure 2.7c, Table 2.1).

2.5.3 X-ray Crystallographic Analysis

X-ray crystallographic analysis has been successful in confirming both the proposed structure and geometry for the reference compounds **Pt(L$_{ref}$)$_2$Cl$_2$**, **Pd(L$_{ref}$)$_2$Cl$_2$**, **Ru(L$_{ref}$)$_4$Cl$_2$**, and the unsymmetric dimer **Pt(L$_{pc}$)(L$_{ref}$)Cl$_2$**. The single crystals of **Pt(L$_{ref}$)$_2$Cl$_2$**, **Pd(L$_{ref}$)$_2$Cl$_2$**, and **Pt(L$_{pc}$)(L$_{ref}$)Cl$_2$**•0.5CH_2Cl_2 suitable for

crystallographic analysis were obtained successfully by slow evaporation at room temperature from a CH_2Cl_2 solution layered with MeOH. The structures confirm a trans orientation of the ligands, as well as the expected square-planar geometry (Figure 2.8). The opposing pyridyl ligands are coplanar in all cases. For **Pt(L_{pc})(L_{ref})Cl_2**, the bulky *tert*-butyl substituents on the pyridyl rings prevent coplanarity between the pentacenyl and pyridyl moieties, resulting in a torsion angle of ca. 16° (Figure 2.8c).

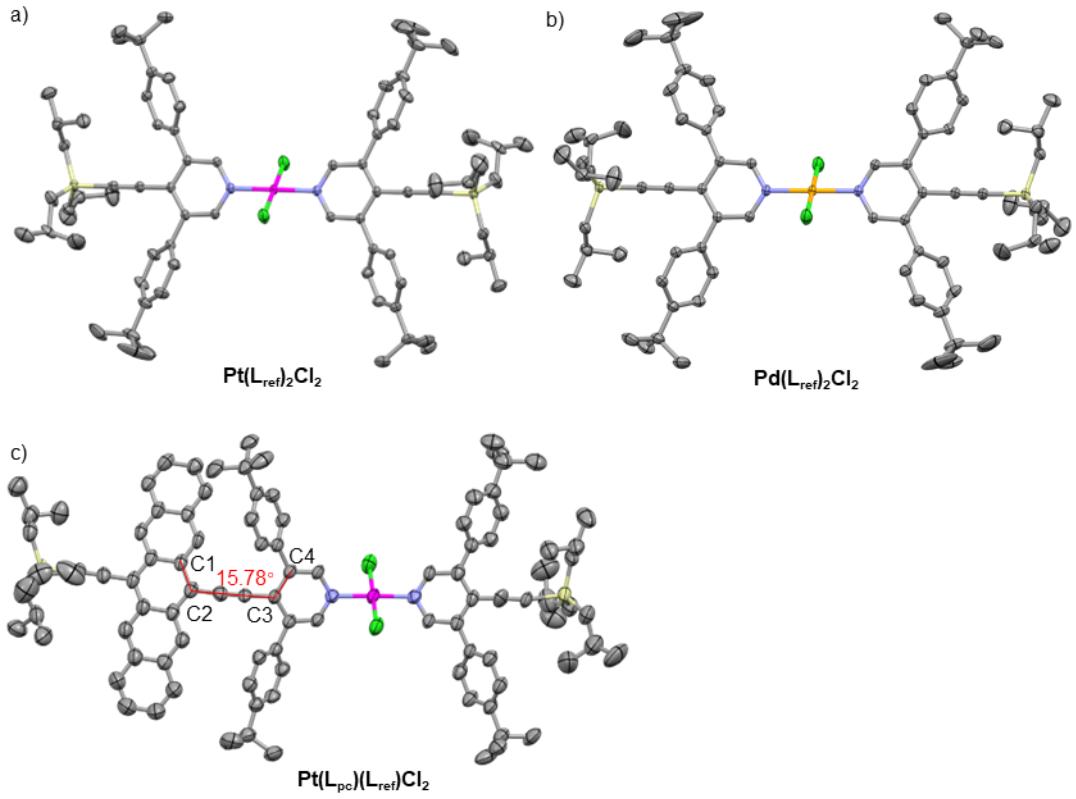

Figure 2.8. ORTEP drawing of a) **Pd(L_{ref})$_2$$Cl_2$**, b) **Pt($L_{ref}$)$_2$$Cl_2$**, and c) **Pt($L_{ref}$)($L_{pc}$)$Cl_2$** with torsion angle of C1–C2–C3–C4. Non-hydrogen atoms are represented by Gaussian ellipsoids at the 30% probability level. For clarity, hydrogen atoms and co-crystalized solvent are omitted.

A single crystal of **Ru(L_{ref})$_4$$Cl_2$**•2.5THF was obtained successfully by slow evaporation at room temperature from a THF solution layered with MeOH. X-ray crystallographic analysis confirms the proposed structure and geometry of the ruthenium tetramer. As shown in Figure 2.9a, **Ru(L_{ref})$_4$$Cl_2$** has a slightly distorted octahedron geometry with four equatorial ligands, **L_{ref}**, and two axial chloro ligands. The Ru center is effectively coplanar within the plane of the four *N*-atoms of the ligands,

with a deviation of only 0.022 Å. The bond lengths of Ru–Cl are 2.4211(6) and 2.4382(6) Å, and the Ru–N bonds are 2.0727(14) and 2.0813(14) Å. These values are in line with previously reported tetra-pyridyl ruthenium complexes bearing either pyridine[29–31] or substituted pyridine groups as ligands in their equatorial positions.[32–34] For example, the four-fold parent system bearing four pyridine rings (**Ru(py)$_4$Cl$_2$**, Figure 2.9b) shows that the Ru atom is coplanar with the plane of the four *N*-atoms of the ligands. The Ru–Cl bond lengths of 2.4083(9) Å and the Ru–N bonds are 2.082(2) Å.[29]

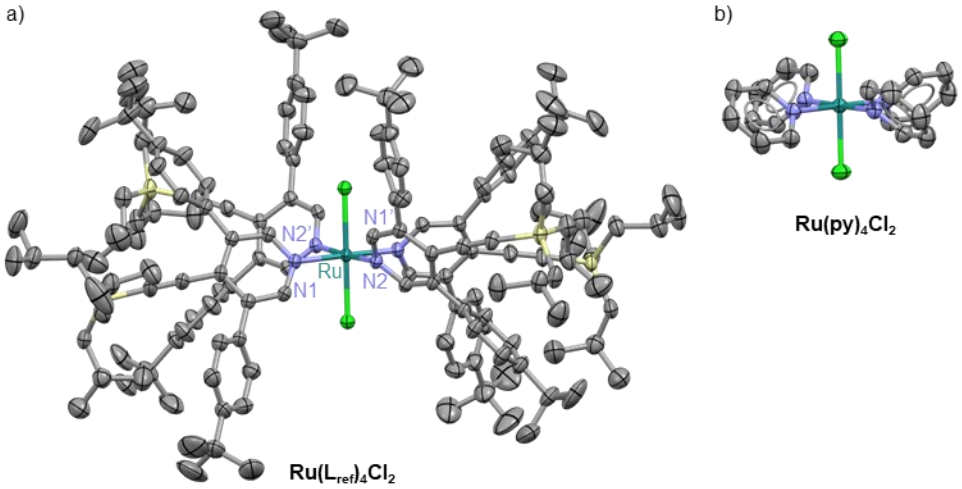

Figure 2.9. Perspective view of a) **Ru(L$_{ref}$)$_4$Cl$_2$** and b) **Ru(py)$_4$Cl$_2$**. Non-hydrogen atoms are represented by Gaussian ellipsoids at the 30% probability level. For clarity, only the major orientation of the disordered *tert*-butyl groups is shown; hydrogen atoms and co-crystalized solvent are omitted.

The arrangement of opposing ligands is nearly linear in **Ru(L$_{ref}$)$_4$Cl$_2$**, with N1–Ru–N1' and N2–Ru–N2' angles 176.35(8)° and 178.84(8)°, respectively. A square planar arrangement is distorted, however, seemingly due to intramolecular CH/π interactions between the phenylene and pyridyl rings. Analysis of the crystal packing also shows a number of intermolecular short contacts between the *iso*-butyl moiety and the pyridyl ring with distances in the range of 2.8–3.4 Å (Figure 2.10).[35] Overall, N1–Ru–N2'/N1'–Ru–N2 angles are contracted slightly to 86°, while the opposing angles N1–Ru–N2/N1'–Ru–N2' are expanded to 94°. The secondary bonding interactions also lead to larger dihedral angles between pyridyl rings and the *N,N,N,N*-plane, which are nearly 60° in **Ru(L$_{ref}$)$_4$Cl$_2$**, versus 49° in **Ru(py)$_4$Cl$_2$**.

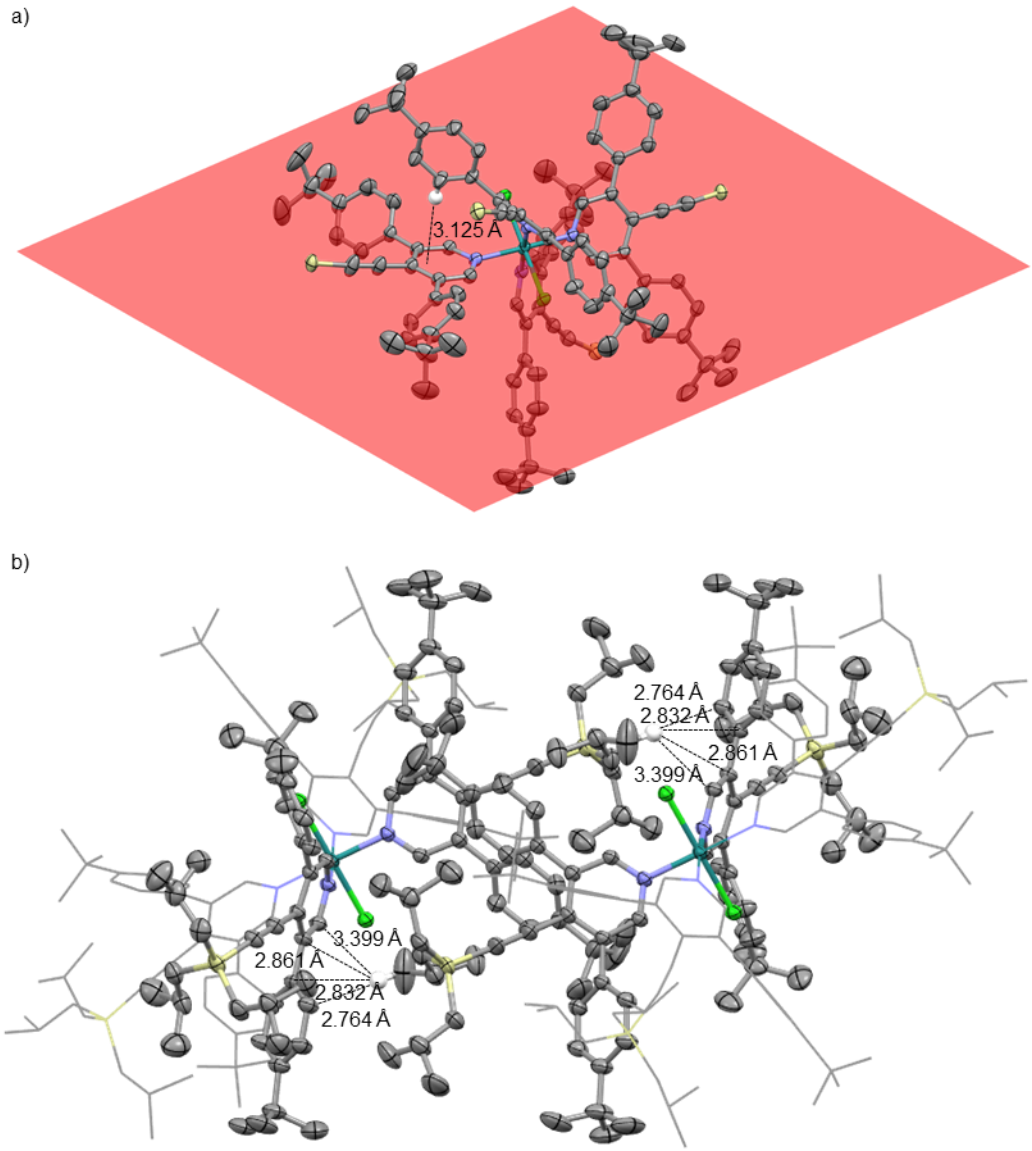

Figure 2.10. X-ray crystal structures with a) CH/π interaction between the phenylene and pyridyl ring (*i*Pr$_3$Si groups are omitted); b) intermolecular short contacts between the *iso*-butyl moiety and the pyridyl ring. Non-hydrogen atoms are represented by Gaussian ellipsoids at the 30% probability level. For clarity, only the major orientation of the disordered *tert*-butyl groups is shown; non-interacting hydrogen atoms and co-crystalized solvent are omitted.

2.6 Brief Results on Singlet Fission

All of the metal complexes have been sent to our collaborators in Germany for the time-resolved transient absorption spectroscopy (TAS) measurements to study the influence of HAE in iSF. The third row transition metal, Pt(II), facilitates inter-pentacene electronic communication that leads to iSF in the dimer **Pt(L$_{pc}$)$_2$Cl$_2$** via a direct mechanism (Figure 2.11a). In the polar solvent benzonitrile, iSF is very efficient and

gives quantum yields of the correlated triplet (T_1T_1) as high as 200%. For the second row transition metal, Pd(II), electronic communication between chromophores is also present, but weaker that for Pt(II). Thus, iSF is observed for **Pd(L$_{pc}$)$_2$Cl$_2$**, but through a mechanism that requires a mediating species in polar solvents (Figure 2.11b). In view of the fact that the dimers are structurally identical, aside from the metal atom, mechanistic changes are attributed to differences in the size and polarizability of the metal species. Furthermore, it is noteworthy that iSF is operative in both **Pt(L$_{pc}$)$_2$Cl$_2$** and **Pd(L$_{pc}$)$_2$Cl$_2$**, despite a rather large inter-pentacene separation in both dimers, as well as enhanced spin-orbit coupling from the presence of heavy atoms. In contrast, SF is not a primary pathway following photoexcitation for **Ru(L$_{pc}$)$_4$Cl$_2$**. Photophysical studies for **Ru(L$_{pc}$)$_4$Cl$_2$** show that the incorporation of Ru as a heavy atom seemingly leads to ultrafast ISC rather than SF (Figure 2.11c).

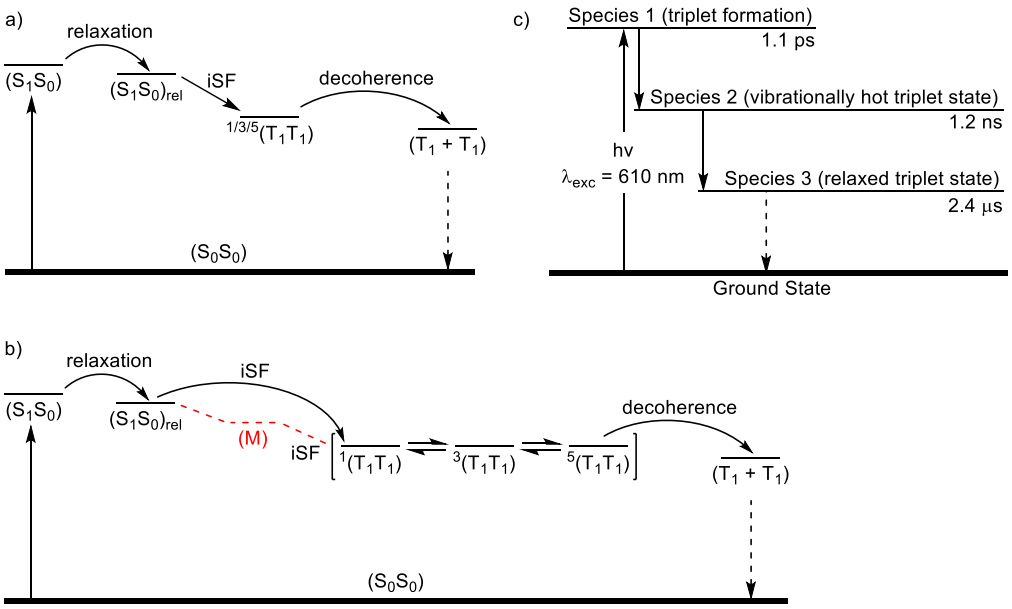

Figure 2.11. Kinetic models used to fit the fs-TAS and ns-TAS data for a) **Pt(L$_{pc}$)$_2$Cl$_2$** via relaxation, iSF, and decoherence, and b) **Pd(L$_{pc}$)$_2$Cl$_2$** via relaxation, iSF, and decoherence in toluene, or via relaxation, an intermediate (M), iSF, and decoherence in THF and benzonitrile; c) qualitative energy diagram depicting the deactivation cascade of **Ru(L$_{pc}$)$_4$Cl$_2$** after photoexcitation at 610 nm, together with representative lifetimes of the involved states in toluene, including the fast triplet formation within 1.1 ps after excitation, subsequent relaxation of the vibrationally hot triplet state within 1.2 ns, and ground state recovery of the relaxed triplet state within 2.4 µs.

2.7 Conclusions

Sterically hindered pyridyl ligands either with or without a pendent pentacene moiety have been designed and synthesized for the formation of complexes with platinum(II), palladium(II), and ruthenium(II). Specifically, the dimeric systems **Pt(L_{pc})$_2$Cl$_2$** and **Pd(L_{pc})$_2$Cl$_2$**, as well as the tetrameric system **Ru(L_{pc})$_4$Cl$_2$**, have been synthesized and the structures established by MS combined with ^{1}H and ^{13}C NMR spectroscopic analyses. All complexes are stable and are suitable to explore the electronic influence of the heavy atoms and the impact on the mechanism of SF.

The UV-vis spectra of the pentacene dimers Pt(L_{pc})$_2$Cl$_2$ (λ_{max} = 679 nm) and **Pd(L_{pc})$_2$Cl$_2$** (λ_{max} = 677 nm) show similar absorptions compared to model compounds **Pt(L_{pc})(L_{ref})Cl$_2$** (λ_{max} = 677 nm) and **Pd(L_{pc})(L_{ref})Cl$_2$** (λ_{max} = 677 nm), and the extinction coefficients of **Pt(L_{pc})$_2$Cl$_2$** (63,500 L mol^{-1} cm^{-1}) and **Pd(L_{pc})$_2$Cl$_2$** (57,100 L mol^{-1} cm^{-1}) are nearly twice that of **Pt(L_{pc})(L_{ref})Cl$_2$** (27,200 L mol^{-1} cm^{-1}) and **Pd(L_{pc})(L_{ref})Cl$_2$** (30,100 L mol^{-1} cm^{-1}). Spectroscopic analysis indicates that the chromophores in the dimers are effectively decoupled, i.e., communication between the two pentacenes via the intervening metal is weak.

The UV-vis analysis of the pentacene tetramer **Ru(L_{pc})$_4$Cl$_2$** (λ_{max} = 689 nm) shows broadened absorptions in the low energy region with a further red-shift of signals in comparison to **L_{pc}** (λ_{max} = 663 nm), suggesting electronic communication across the Ru center. The extinction coefficient of **Ru(L_{pc})$_4$Cl$_2$** (109,000 L mol^{-1} cm^{-1}) is approximately quadrupled compared to the ligand **L_{pc}** (29,300 L mol^{-1} cm^{-1}), which is consistent with its tetrameric structure.

References

[1] R. D. Ribson, G. Choi, R. G. Hadt, T. Agapie, *ACS Cent. Sci.* **2020**, *6*, 2088–2096.

[2] Y. Gao, Y. Hou, F. Gordillo Gámez, M. J. Ferguson, J. Casado, R. R. Tykwinski, *Nat. Chem.* **2020**, *12*, 1143–1149.

[3] O. Berg, E. L. Chronister, T. Yamashita, G. W. Scott, R. M. Sweet, J. Calabrese, *J. Phys. Chem. A* **1999**, *103*, 2451–2459.

[4] J. E. Anthony, *Angew. Chem. Int. Ed.* **2008**, *47*, 452–483.

[5] Y. Li, Y. Wu, P. Liu, Z. Prostran, S. Gardner, B. S. Ong, *Chem. Mater.* **2007**, *19*, 418–423.

[6] J. B. Briggs, G. P. Miller, *C. R. Chim.* **2006**, *9*, 916–927.

[7] A. K. Pal, G. S. Hanan, *Chem. Soc. Rev.* **2014**, *43*, 6184–6197.

[8] B. Pashaei, H. Shahroosvand, M. Graetzel, M. K. Nazeeruddin, *Chem. Rev.* **2016**, *116*, 9485–9564.

[9] C. Hetzer, B. S. Basel, S. M. Kopp, F. Hampel, F. J. White, T. Clark, D. M. Guldi, R. R. Tykwinski, *Angew. Chem. Int. Ed.* **2019**, *58*, 15263–15267.

[10] B. S. Basel, J. Zirzlmeier, C. Hetzer, B. T. Phelan, M. D. Krzyaniak, S. R. Reddy, P. B. Coto, N. E. Horwitz, R. M. Young, F. J. White, F. Hampel, T. Clark, M. Thoss, R. R. Tykwinski, M. R. Wasielewski, D. M. Guldi, *Nat. Commun.* **2017**, *8*, 15171.

[11] J. Sarju, J. Arbour, J. Sayer, B. Rohrmoser, W. Scherer, G. Wagner, *Dalton Trans.* **2008**, 5302–5312.

[12] L. P. Wu, Y. Suenaga, T. KurodaSowa, M. Maekawa, K. Furuichi, M. Munakata, *Inorg. Chim. Acta* **1996**, *248*, 147–152.

[13] M. M. Olmstead, P.-p. Wei, A. S. Ginwalla, A. L. Balch, *Inorg. Chem.* **2000**, *39*, 4555–4559.

[14] T. Nakagawa, H. Danjo, M. Kawahata, K. Yamaguchi, *Tetrahedron* **2019**, *75*, 315–323.

[15] M. J. Mayoral, C. Rest, V. Stepanenko, J. Schellheimer, R. Q. Albuquerque, G. Fernández, *J. Am. Chem. Soc.* **2013**, *135*, 2148–2151.

[16] D. Fujita, A. Takahashi, S. Sato, M. Fujita, *J. Am. Chem. Soc.* **2011**, *133*, 13317–13319.

[17] C. M. Duff, G. A. Heath, *J. Chem. Soc., Dalton Trans.* **1991**, 2401–2411.

[18] C. Tessier, F. D. Rochon, *Inorg. Chim. Acta* **1999**, *295*, 25–38.

[19] L. Pazderski, J. Toušek, J. Sitkowski, K. Maliňáková, L. Kozerski, E. Szłyk, *Magn. Reson. Chem.* **2009**, *47*, 228–238.

[20] L. Pazderski, T. Pawlak, J. Sitkowski, L. Kozerski, E. Szłyk, *Magn. Reson. Chem.* **2010**, *48*, 417–426.

[21] N. A. Lewis, S. Pakhomova, P. A. Marzilli, L. G. Marzilli, *Inorg. Chem.* **2017**, *56*, 9781–9793.

[22] G. Kurpik, A. Walczak, M. Gołdyn, J. Harrowfield, A. R. Stefankiewicz, *Inorg. Chem.* **2022**, *61*, 14019–14029.

[23] C. A. Strassert, M. Mauro, L. De Cola, *Adv. Inorg. Chem.* **2011**, *63*, 47–103.

[24] T. Theiss, S. Buss, I. Maisuls, R. López-Arteaga, D. Brünink, J. Kösters, A. Hepp, N. L. Doltsinis, E. A. Weiss, C. A. Strassert, *J. Am. Chem. Soc.* **2023**, *145*, 3937–2951.

[25] D. Lehnherr, A. H. Murray, R. McDonald, R. R. Tykwinski, *Angew. Chem. Int. Ed.* **2010**, *49*, 6190–6194.

[26] B. S. Basel, R. M. Young, M. D. Krzyaniak, I. Papadopoulos, C. Hetzer, Y. Gao, N. T. La Porte, B. T. Phelan, T. Clark, R. R. Tykwinski, M. R. Wasielewski, D. M. Guldi, *Chem. Sci.* **2019**, *10*, 11130–11140.

[27] I. Papadopoulos, Y. Gao, C. Hetzer, R. R. Tykwinski, D. M. Guldi, *Chemphotochem* **2020**, *4*, 5168–5174.

[28] M.-H. Nguyen, J. H. K. Yip, *Organometallics* **2012**, *31*, 7522–7531.

[29] Z. Bu, Z. Wang, L. Yang, S. Cao, *Appl. Organomet. Chem.* **2010**, *24*, 813–816.

[30] W. T. Wong, T. C. Lau, *Acta Crystallogr. Sect. C: Struct. Chem.* **1994**, *50*, 1406–1407.

[31] M. R. J. Elsegood, D. A. Tocher, *Acta Crystallogr. Sect. C: Struct. Chem.* **1995**, *51*, 40–42.

[32] J. G. Małecki, M. Jaworska, R. Kruszynski, R. Gil-bortnowska, *Polyhedron* **2005**, *24*, 1445–1453.

[33] A. Vertova, I. Cucchi, P. Fermo, F. Porta, D. M. Proserpio, S. Rondinini, *Electrochim. Acta* **2007**, *52*, 2603–2611.

[34] A. Cadranel, J. H. Hodak, *J. Coord. Chem.* **2015**, *68*, 1452–1464.

[35] M. Nishio, *CrystEngComm* **2004**, *6*, 130–158.

CHAPTER 3

Design and Synthesis of Tetracene Dimers for Intramolecular Down- and Up-conversion[b]

3.1 Introduction

Acene dimers allow intramolecular singlet fission (iSF) and intramolecular triplet-triplet annihilation upconversion (iTTA-UC) and are convenient model systems to study these processes in solution. From a synthetic perspective, the major advantage of the dimeric structure is the ability to modify the spacer. The spacer between interacting chromophores is the key to control the geometry, distance, and electronic coupling of acene dimers, which allows detailed investigation of the mechanism of iSF and iTTA-UC (See Chapter 1 for detailed discussions of iSF and iTTA-UC).[1–3]

Tetracene derivatives are capable of both down-conversion (i.e., singlet fission, SF) and upconversion (i.e., triplet-triplet annihilation upconversion, TTA-UC) as the energy of their lowest singlet excited state is about twice of the energy of their triplet excited state. However, previous investigations of tetracene dimers were focused predominantly on the individual study of either iSF or iTTA-UC, respectively. Insight into the interplay between iSF and iTTA-UC remain elusive.[4–6]

To unravel the interplay between SF and TTA-UC, a series of covalently linked tetracene dimers featuring tunable electronic coupling, as well as their corresponding monomers, have been designed and synthesized (Figure 3.1). In analogy to the previous work on iSF in pentacene dimers, the tetracene dimers are bridged rigidly by either a conjugated *para*-diethynylphenylene (**pPhTc$_2$**), a cross-conjugated *meta*-diethynylphenylene (**mPhTc$_2$**) or a non-conjugated 1,3-diethynyladamantyl spacer (**mAdTc$_2$**). The interplay between iSF and iTTA-UC is characterized via steady-state and time-resolved absorption and fluorescence spectroscopy by our collaborators in Germany.

[b] The contents of this chapter have been adapted from the following publication:
Y. Bo,[†] Y. Hou,[†] D. Thiel,[†] R. Weiß, M. J. Fergusen, D. M. Guldi, R. R. Tykwinski, *J. Am. Chem. Soc.* **2023**, *145*, 18260–18275.

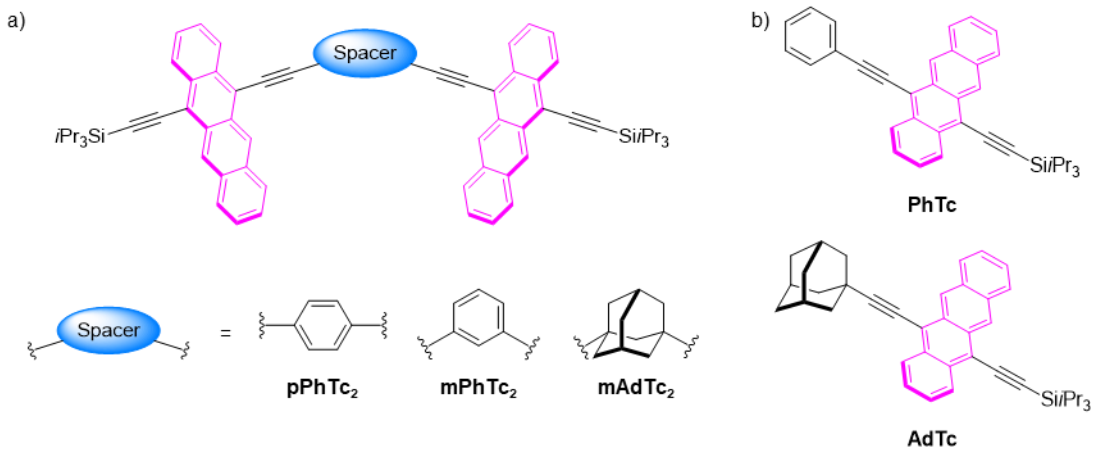

Figure 3.1. Structures of tetracene a) dimers and b) monomers.

3.2 Synthesis of Tetracene Dimers and Corresponding Monomers

The conjugated, cross-conjugated, and non-conjugated tetracene dimers **pPhTc$_2$**, **mPhTc$_2$**, and **mAdTc$_2$** were synthesized through a stepwise substitution of 5,12-naphthacenequinone (**3.1**) by adapting protocols used to form tetracene[7] and pentacene dimers.[2,8] The corresponding tetracene monomers **PhTc** and **AdTc** were synthesized using the same method as well.

3.2.1 Synthesis of Phenylene-linked Tetracene Dimers and Corresponding Monomer

Compound **pPhTc$_2$** was previously synthesized through a one-pot protocol as reported by Toyota and co-workers.[7] As an alternative, we chose a stepwise method a common building block **3.2** (Scheme 3.1). Ketone **3.2** was obtained by addition of lithiated tri*iso*propylsilylacetylene (*i*Pr$_3$Si–C≡C–Li) to a suspension of 5,12-naphthacenequinone (**3.1**) in dry tetrahydrofuran (THF) at –78 °C, followed by in situ trapping of the resulting alkoxide with MeI.[2]

The spacers 1,4-diethynylbenzene (**3.3a**) and 1,3-diethynylbenzene (**3.3b**) were synthesized as previously reported.[9–10] Nucleophilic addition of the lithiated diyne (**3.4a** or **3.4b**) to ketone **3.2**, followed by passing crude product through a pad of silica gel with CH_2Cl_2, gave the diols **3.5a** and **3.5b**. It is noted that the crude product contained a mixture of diastereomers, and the resulting diol products were not isolated individually because all isomers would give rise to the desired final products. The crude

products **3.5a** and **3.5b** were subjected to $SnCl_2$-mediated reductive aromatization and produced the desired products **pPhTc2** and **mPhTc2**. The dimeric were purified by column chromatography and were isolated in 85% yield as a reddish purple solid and in 72% yield as a scarlet solid, respectively.

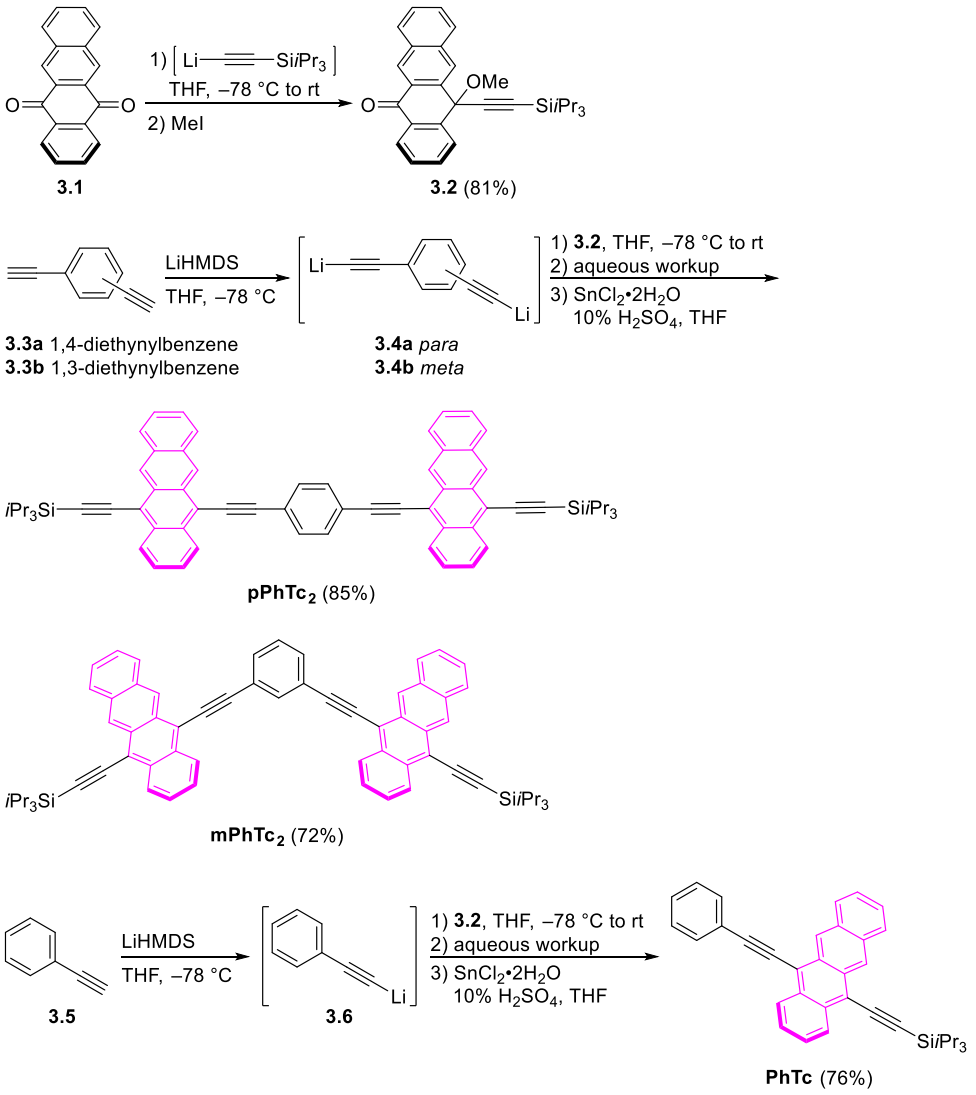

Scheme 3.1. Synthesis of **pPhTc2**, **mPhTc2**, and **PhTc**.

The corresponding monomer **PhTc** was synthesized by the same method (Scheme 3.1). 1-Ethynylbenzene (**3.5**) was lithiated by LiHMDS forming lithium phenylacetylide (**3.6**), which was added to ketone **3.2**. Reductive aromatization with

$SnCl_2$ gave the desired product **PhTc** in 76% yield as a scarlet solid. The structures of **PhTc** and **mPhTc2** were confirmed by X-ray crystallography.

3.2.2 Synthesis of Adamantyl-linked Tetracene Dimer and Corresponding Monomer

The non-conjugated tetracene dimer **mAdTc2** was synthesized using the same stepwise method through the common building block **3.2** (Scheme 3.2). The spacer 1,3-diethynyladamantane (**3.7**) was synthesized as previously reported.[11] The desired product **mAdTc2** was obtained by nucleophilic addition of the lithiated diyne (**3.8**) to ketone **3.2**, followed by $SnCl_2$-mediated reductive aromatization to give **mAdTc2** in 57% yield as a scarlet solid.

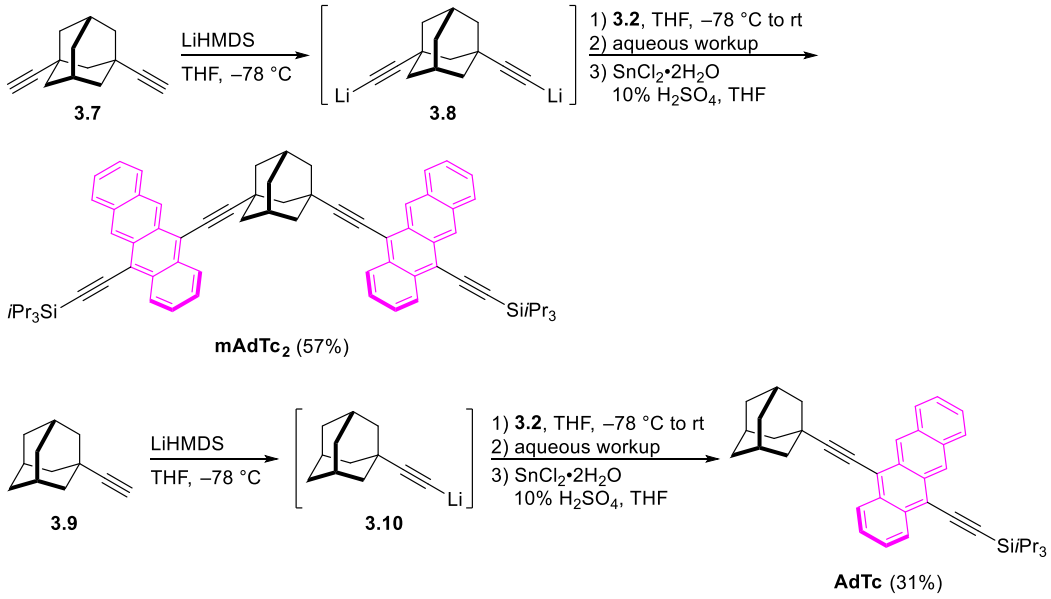

Scheme 3.2. Synthesis of **mAdTc2** and **AdTc**.

For the synthesis of the corresponding monomer, 1-ethynyladamantane (**3.9**) was synthesized as previously reported.[12] The monomer **AdTc** was obtained by nucleophilic addition of the lithiated monoyne (**3.10**) to ketone **3.2**, followed by reductive aromatization.

After the initial column chromatography, both **mAdTc2** and **AdTc** showed a single spot by TLC analysis, indicating successful purification. However, there were signals in the ^1H NMR spectra of **mAdTc2** and **AdTc** for a small amount of (<10%)

impurities in the samples (Figure 3.2). TLC analysis was conducted for the NMR samples. Additional spots with higher R_f values were shown on the TLC plate, indicating the impurities were formed after column chromatography.

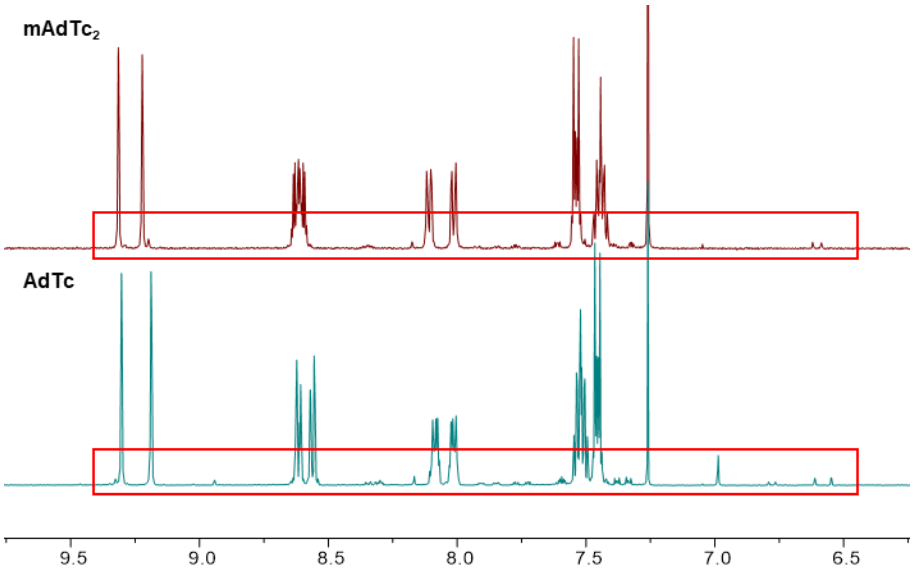

Figure 3.2. Stacked plot of the aromatic region of ^{1}H NMR spectra of **mAdTc$_2$** and **AdTc** in $CDCl_3$. The range of signals for impurities are labeled with red boxes.

All attempts to remove the impurities by recrystallization with different conditions were unsuccessful. It was noticed that the bright orange color of the solutions of **mAdTc$_2$** and **AdTc** in CH_2Cl_2 diminished after keeping them under ambient light for several hours (Figure 3.3, insert). ^{1}H NMR spectroscopic analysis was performed for the transparent, colorless decomposed sample of **AdTc** (Figure 3.3a). The signals for this sample are consistent with the photooxidation products **3.11** and **3.12** (Scheme 3.3)[13] and are consistent with those for the impurities in the original sample of **AdTc** (Figure 3.3b). Moreover, the ratio of the two photooxidation products **3.11** and **3.12** is approximately 1:1. Pure samples of **mAdTc$_2$** and **AdTc** were obtained successfully by column chromatography, followed by immediate removal of solvents in the dark. The tetracene derivatives are stable as solids under normal laboratory conditions for weeks, although they decompose quickly in solution upon exposure to air (O_2) and light (minutes to hours). Adamantyl-linked dimer (**mAdTc$_2$**) and its corresponding monomer (**AdTc**) are more vulnerable to photooxidation compared to

phenylene-linked dimers (**pPhTc2** and **mPhTc2**) and the corresponding monomer (**PhTc**). This leads to lower yields of the adamantyl derivatives due to losses during the purification processes.

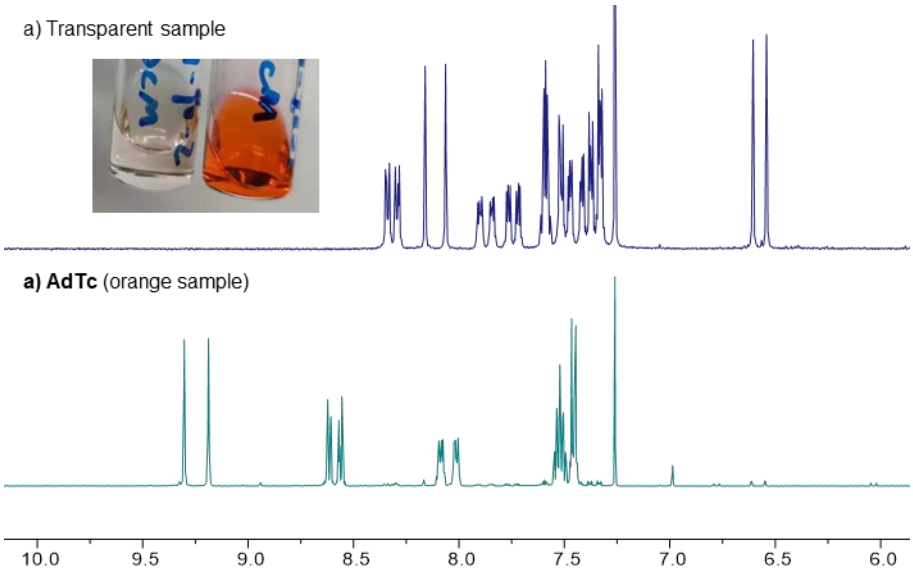

Figure 3.3. Stacked plot of the aromatic region of ^{1}H NMR spectra of a) the transparent decomposed sample and b) **AdTc** in $CDCl_3$. Inset: Picture of the transparent decomposed sample (left) and original orange sample of **AdTc** (right).

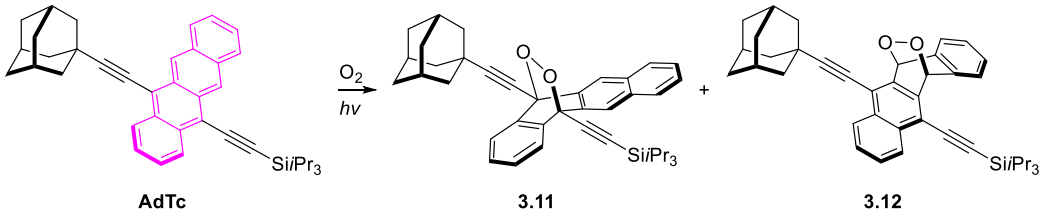

Scheme 3.3. Photooxidation of **AdTc**.

3.3 Synthesis of a Palladium Porphyrin

As part of this collaborative project, a palladium porphyrin Pd(II) 5,10,15,20-tetrakis(4-*tert*butylphenyl)porphyrin (**Pd-por**) was synthesized and intended to serve as a photosensitizer for TTA-UC. **Pd-por** was synthesized by stirring **H2-por** (1 equiv) and $PdCl_2$ (2 equiv) in PhCN at reflux for 3 h (Scheme 3.4). Even though the similar compound Pd(II) 5,10,15,20-tetrakis(3,5-di-*tert*butylphenyl)porphyrin was reported in the literature to be purified by column chromatography with silica gel,[14] **Pd-por** was found to be unstable on silica gel. The TLC analysis showed one major spot with red

color with R_f = 0.54 (CH_2Cl_2/hexanes 1:2) indicating the desired product and one spot on the baseline indicating side product. However, when using the same eluent system as TLC analysis for column chromatography, only trace amounts of the product were obtained. The majority of the red band remained on the baseline. When switching to more polar solvents such as CH_2Cl_2 or EtOAc as eluent, the red band did not move on the column. Alternatively, filtering the crude product through a pad of alumina with CH_2Cl_2 followed by recrystallization (CH_2Cl_2/MeOH) gave **Pd-por** as a dark red solid in 78% yield.

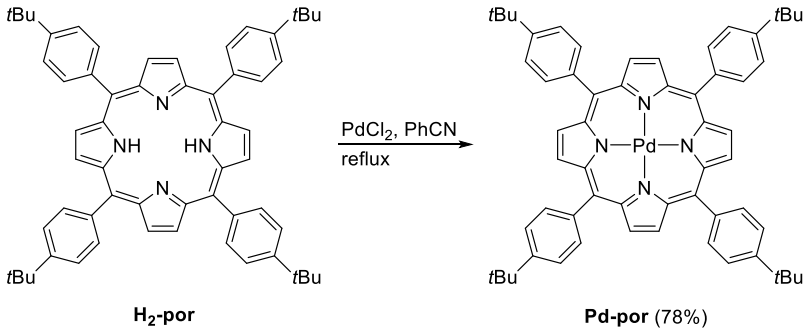

Scheme 3.4. Synthesis of **Pd-por**.

3.4 Characterization

3.4.1 UV-vis Spectroscopic Analysis

The quantitative UV-vis spectra of the tetracene dimers (**pPhTc2**, **mPhTc2**, and **mAdTc2**), their corresponding monomer (**PhTc** and **AdTc**), and the photosensitizer **Pd-por** have been measured in CH_2Cl_2 at room temperature (Figure 3.4, Table 3.1). All of the tetracene derivatives show absorption bands in both high energy region (250–400 nm) and low energy region (450–600 nm). The palladium porphyrin **Pd-por** has a major absorption at 418 nm (the Soret band) and a λ_{max} absorption at 524 nm (the Q band). However, the λ_{max} of **Pd-por** is not lower energy than λ_{max} of all tetracene derivatives, which means tetracene annihilators will be excited directly when irradiating **Pd-por**. For optimal TTA-UC to occur, the photosensitizer should be selectively excited with a low-energy incident light. Therefore, **Pd-por** is not suitable to serve as a photosensitizer for the tetracene derivatives.

The absorption maximum for **PhTc** (λ_{max} = 545 nm) is red shifted compared to **AdTc** (λ_{max} = 533 nm) as a result of extended π-conjugation and better electronic delocalization. The extinction coefficient of **PhTc** (33,100 L mol^{-1} cm^{-1}) is also slightly higher compared to **AdTc** (29,500 L mol^{-1} cm^{-1}).

More significant differences are observed when comparing the UV-vis spectra of the dimers **pPhTc2**, **mPhTc2**, and **mAdTc2**. The spectrum of **mAdTc2** (λ_{max} = 534 nm, 64,600 L mol^{-1} cm^{-1}) represents effectively a linear sum of two **AdTc** monomers (λ_{max} = 533 nm, 29,500 L mol^{-1} cm^{-1}), both in terms of absorption maxima and extinction coefficients. For **pPhTc2** (λ_{max} = 571 nm, 76,500 L mol^{-1} cm^{-1}) and **mPhTc2** (λ_{max} = 550 nm, 66,500 L mol^{-1} cm^{-1}) the absorption maxima are red shifted in comparison to **PhTc** (λ_{max} = 545 nm, 33,100 L mol^{-1} cm^{-1}), and the spectra of **pPhTc2** and **mPhTc2** are not simply a linear sum of two **PhTc** monomers. Especially for **pPhTc2**, the λ_{max} value is red shifted for 26 nm (0.1 eV) compared to the corresponding monomer **PhTc**. The conjugated dimer **pPhTc2** also shows broadened spectral features, while the spectrum of non-conjugated dimer **mAdTc2** shows more distinct vibrational fine structure. These observations confirm that the π-conjugation is extended between two tetracene moieties in **pPhTc2**, and, thus, the intramolecular electronic coupling is appreciably stronger in **pPhTc2** than in **mPhTc2** and **mAdTc2**.[3,15–16]

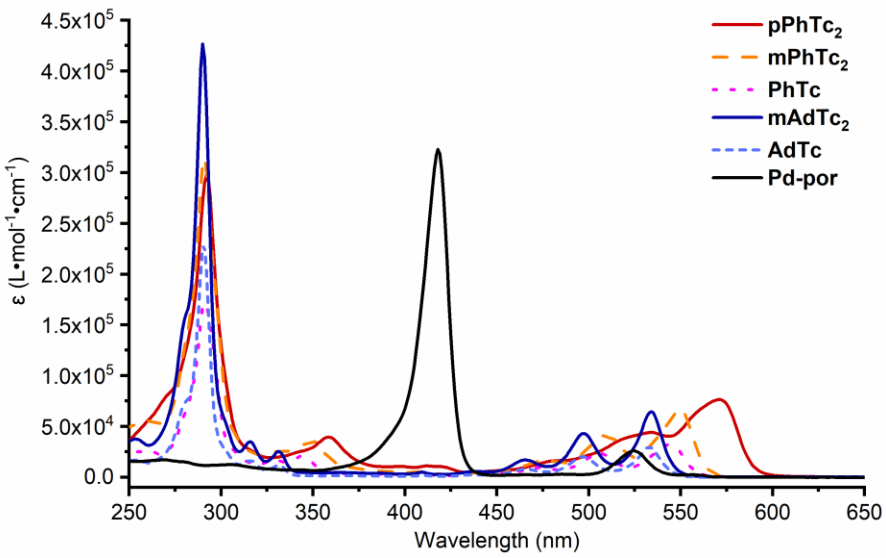

Figure 3.4. UV-vis spectra of **pPhTc2**, **mPhTc2**, **PhTc**, **mAdTc2**, **AdTc**, and **Pd-por** in CH_2Cl.

Table 3.1. Relevant UV-vis Data for Tetracene Derivatives and **Pd-por**

Spacer	Compound	λ_{max} (nm)	ε (L mol^{-1} cm^{-1})
Ph	**pPhTc$_2$**	571	76,500
	mPhTc$_2$	550	66,500
	PhTc	545	33,100
Ad	**mAdTc$_2$**	534	64,600
	AdTc	533	29,500
	Pd-por	524	25,900

3.4.2 X-ray Crystallographic Analysis

X-ray crystallographic analysis has been successful in confirming the proposed structure for the *meta*-diethynylphenylene-linked tetracene dimer **mPhTc$_2$** and its corresponding monomer **PhTc**. A single crystal of **mPhTc$_2$** suitable for crystallographic analysis has been grown at room temperature by slow evaporation of a CH_2Cl_2/THF solution layered with MeOH. As shown in Figure 3.5a, the phenylene ring and the tetracene moieties are not coplanar in **mPhTc$_2$**, with a torsion angle of ~17°. Face-to-face interactions are observed in the crystal packing for **mPhTc$_2$** (Figure 3.5b). The distance between the planes formed from two neighboring tetracenes is 3.367 Å.

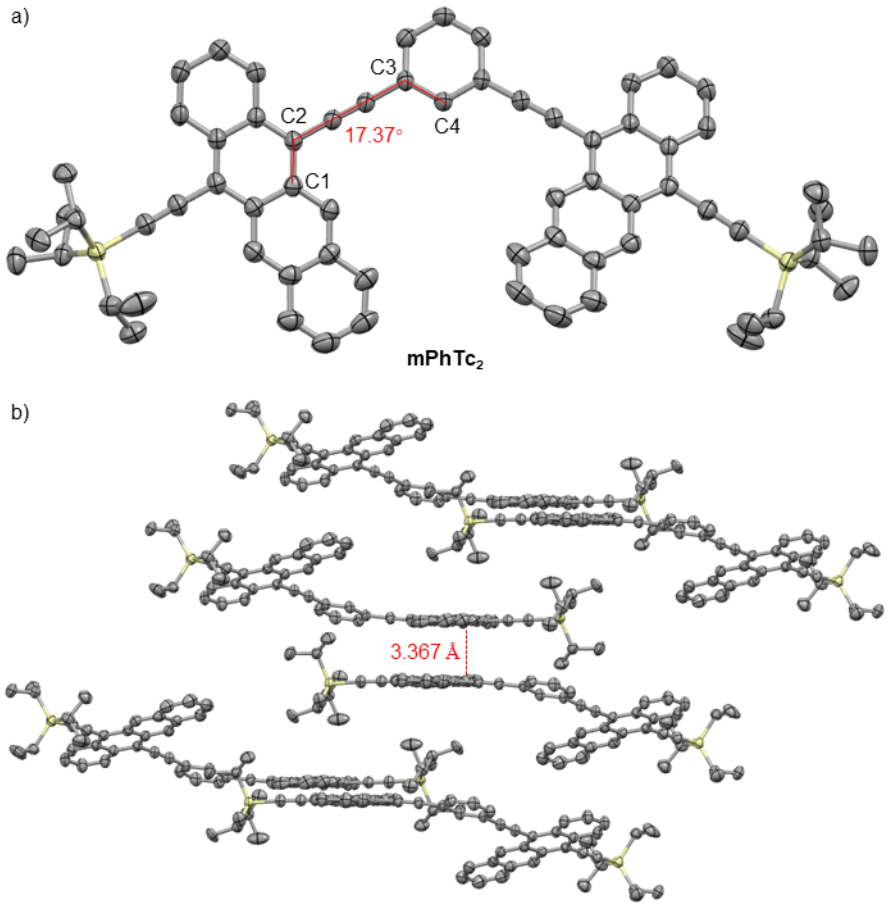

Figure 3.5. ORTEP drawing of a) **mPhTc₂** with torsion angle of C1–C2–C3–C4; b) crystal packing diagram of compound **mPhTc₂** with face-to-face interactions. Non-hydrogen atoms are represented by Gaussian ellipsoids at the 30% probability level. For clarity, only the major orientation of the disordered *iso*-butyl groups is shown; hydrogen atoms are omitted.

A single crystal of **PhTc** suitable for crystallographic analysis has been obtained by slow evaporation at room temperature from a CH_2Cl_2 solution layered with MeOH. As shown in Figure 3.6a, four independent molecules are observed in the crystal structure. The phenyl ring and the tetracene moiety are not coplanar in all four molecules of **PhTc**, with torsion angles of 2.8–14.3°. Selected intermolecular interactions are shown in Figure 3.6b. The shortest intermolecular carbon-to-carbon distance between the two tetracene moieties is 3.367 Å and 3.398 Å, respectively. The distance between alkyne C_{sp} and the tetracene plane (generated using 6 atoms of the benzene ring connected with alkynes in the tetracene moiety) is 3.379–3.427 Å. Furthermore, the carbon-to-carbon distance between two phenyl groups is 3.361 Å.

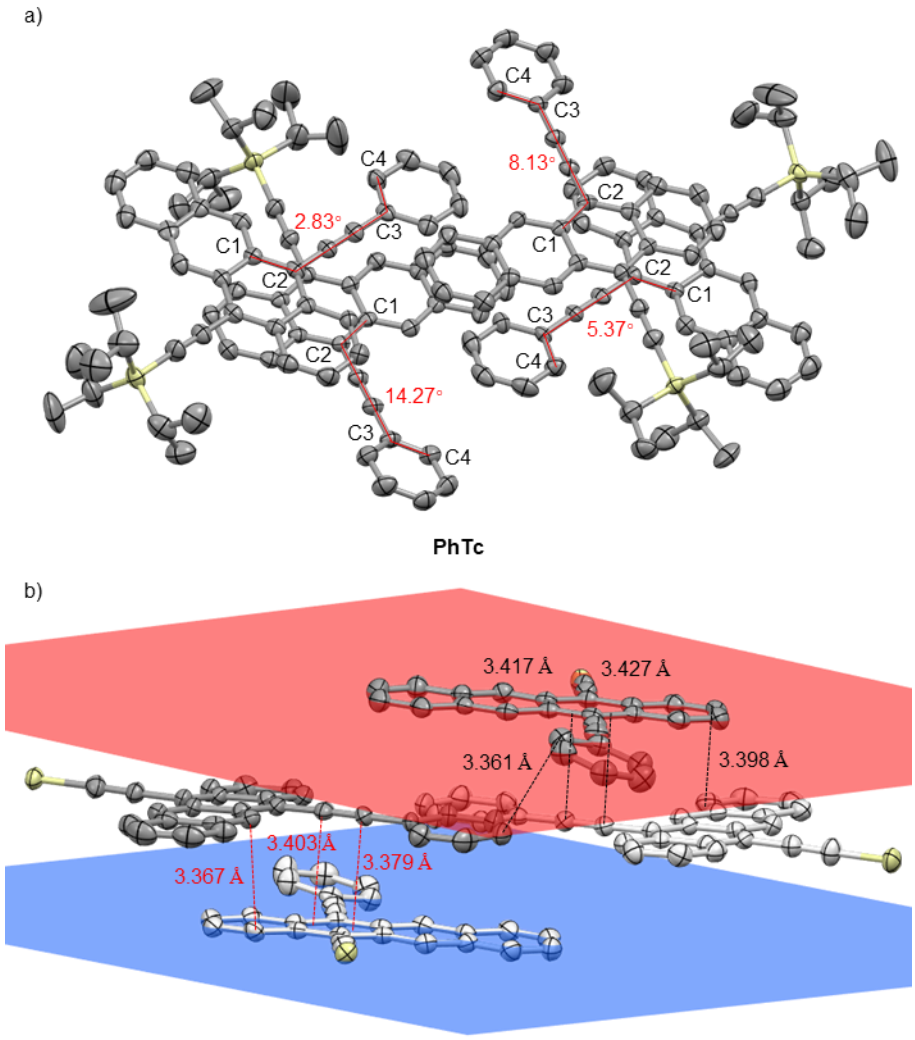

Figure 3.6. ORTEP drawing of a) **PhTc** with torsion angle of C1–C2–C3–C4; b) crystal packing diagram of compound **PhTc** with intermolecular interaction. Non-hydrogen atoms are represented by Gaussian ellipsoids at the 30% probability level. For clarity, hydrogen atoms are omitted.

3.5 Summary of Results from Studies of SF and TTA-UC

Both iSF and iTTA-UC are demonstrated unequivocally for **mPhTc$_2$** and **mAdTc$_2$** through a combination of steady-state and time-resolved measurements. In the conjugated dimer linked by the para-phenylene spacer, **pPhTc$_2$**, however, SF is too fast and TTA-UC is deactivated by a fast ground-state recovery that is driven by triplet-triplet annihilation due to strong electronic coupling between two tetracene moieties.

In dimers **mAdTc$_2$** and **mPhTc$_2$**, following photoexcitation, iSF operates efficiently with over 100% triplet quantum yields. The mechanism in these two dimers

is mediated by a superposition of the initial excited state (S_1S_0), an intermediate charge transfer state, and the resultant correlated triplet state $^1(T_1T_1)$. Using Pd(II) 1,4,8,11,15,18,22,25-octabutoxyphthalocyanine (**PdPc**, Figure 3.7a) as the photosensitizer, both **mPhTc2** and **mAdTc2** give rise to more efficient TTA-UC than the corresponding monomers **PhTc** and **AdTc**, confirming the intramolecular nature of TTA-UC (Figure 3.7b). The cross-conjugated dimer **mPhTc2** exhibits a better upconversion performance due to more efficient iTTA-UC that results from stronger inter-tetracene coupling compared to non-conjugated dimer **mAdTc2**.

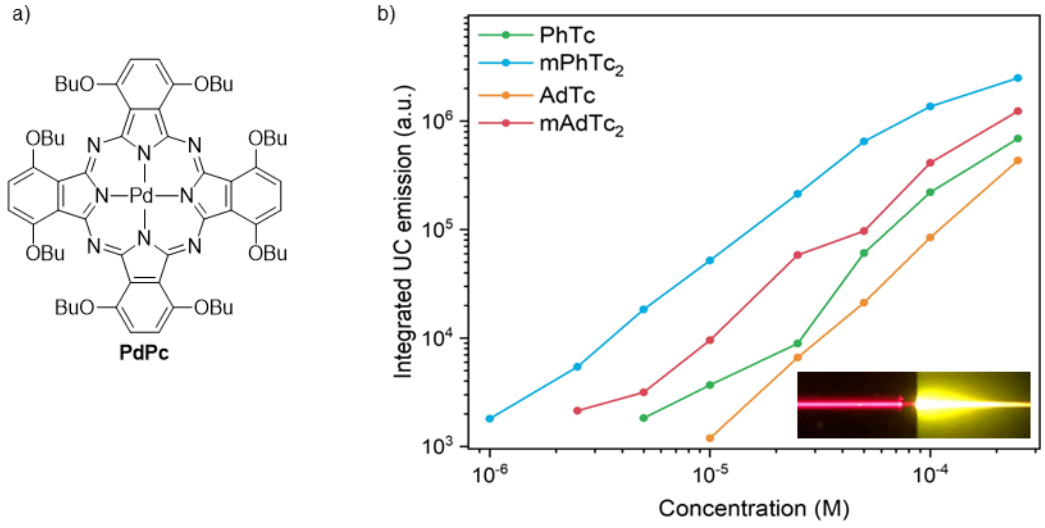

Figure 3.7. a) Structure of the photosensitizer **PdPc**; b) Log-log plots of integrated up-converted fluorescence as a function of the concentrations of the tetracene molecules at a constant concentration of **PdPc** (4×10^{-5} M). Inset: Picture of the up-converted **mPhTc2** fluorescence via photoexcitation of **PdPc** at 730 nm.

As illustrated in Figure 3.8, inter-tetracene coupling is the decisive factor that governs the fate of the correlated triplet pair (T_1T_1). On the one hand, the more strongly coupled, cross-conjugated dimer **mPhTc2** favors TTA-UC from (T_1T_1) annihilation. On the other hand, the more weakly coupled, non-conjugated 1,3-diethynyladamantyl spacer of **mAdTc2** supports efficient (T_1T_1) decorrelation, which is vital for efficient iSF.

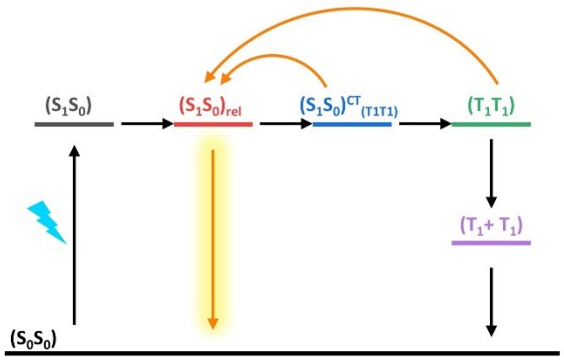

Figure 3.8. Schematic representations of iSF (black arrows) and iTTA-UC (orange arrows) after photoexcitation of **mPhTc2** and **mAdTc2 at** 480 nm in argon-saturated toluene and benzonitrile.

3.6 Conclusions

In summary, a stepwise method, through a common building block, has been developed to provide a series of tetracene dimers (**pPhTc2**, **mPhTc2**, and **mAdTc2**) featuring variable electronic coupling between two interacting tetracene moieties. Their corresponding monomers (**PhTc** and **AdTc**) have been synthesized using the same method with the common building block. A palladium porphyrin **Pd-por** has been synthesized as well. The successful synthesis of these compounds has been confirmed by mass spectrometry combined with ^{1}H and ^{13}C NMR spectroscopic analyses. The structures of **mPhTc2** and **PhTc** have been proved by X-ray crystallography. The electronic coupling of tetracene derivatives has been examined with UV-vis spectroscopy analysis.

The π-conjugation is extended between two tetracene moieties across the 1,4-diethynylbenzene in **pPhTc2** in comparison to the monomer **PhTc** indicated by significant red shifted absorption maximum in UV-vis spectrum leading to strongest electronic coupling. As is well established in the field, strong coupling leads to SF is too rapid, and, furthermore, TTA-UC is not observed in **pPhTc2**. The electronic coupling between tetracenes is greatly diminished in non-conjugated dimer **mAdTc2** with 1,3-diethynyladamantane as the spacer. The weakened coupling in **mAdTc2** is beneficial for (T_1T_1) decorrelation towards efficient iSF. The cross-conjugated dimer **mPhTc2** has stronger electronic coupling between two interacting tetracenes compared to non-conjugated dimer **mAdTc2** and shows a better upconversion performance from

(T_1T_1) annihilation towards efficient TTA-UC. The results underpin the significance of inter-chromophore electronic coupling in competitive process SF and TTA-UC as we highlight the opposing dependencies of iSF and iTTA-UC on the inter-chromophore coupling.

References

[1] J. Zirzlmeier, D. Lehnherr, P. B. Coto, E. T. Chernick, R. Casillas, B. S. Basel, M. Thoss, R. R. Tykwinski, D. M. Guldi, *Proc. Natl. Acad. Sci. U. S. A.* **2015**, *112*, 5325–5330.

[2] B. S. Basel, J. Zirzlmeier, C. Hetzer, B. T. Phelan, M. D. Krzyaniak, S. R. Reddy, P. B. Coto, N. E. Horwitz, R. M. Young, F. J. White, F. Hampel, T. Clark, M. Thoss, R. R. Tykwinski, M. R. Wasielewski, D. M. Guldi, *Nat. Commun.* **2017**, *8*, 15171.

[3] C. Hetzer, D. M. Guldi, R. R. Tykwinski, *Chem. - Eur. J.* **2018**, *24*, 8245–8257.

[4] A. M. Müller, Y. S. Avlasevich, W. W. Schoeller, K. Müllen, C. J. Bardeen, *J. Am. Chem. Soc.* **2007**, *129*, 14240–14250.

[5] Y. Matsui, S. Kawaoka, H. Nagashima, T. Nakagawa, N. Okamura, T. Ogaki, E. Ohta, S. Akimoto, A. Sato-Tomita, S. Yagi, Y. Kobori, H. Ikeda, *J. Phys. Chem. C* **2019**, *123*, 18813–18823.

[6] A. J. Carrod, V. Gray, K. Börjesson, *Energy Environ. Sci.* **2022**, *15*, 4982–5016.

[7] T. Iwanaga, Y. Yamamoto, K. Nishioka, S. Toyota, *Synthesis* **2015**, *47*, 3997–4007.

[8] D. Lehnherr, R. McDonald, R. R. Tykwinski, *Org. Lett.* **2008**, *10*, 4163–4166.

[9] T. X. Neenan, G. M. Whitesides, *J. Org. Chem.* **1988**, *53*, 2489–2496.

[10] D. W. Price, S. M. Dirk, F. Maya, J. M. Tour, *Tetrahedron* **2003**, *59*, 2497–2518.

[11] T. G. Archibald, A. A. Malik, K. Baum, M. R. Unroe, *Macromolecules* **1991**, *24*, 5261–5265.

[12] M. Bregnhoj, M. Westberg, F. Jensen, P. R. Ogilby, *Phys. Chem. Chem. Phys.* **2016**, *18*, 22946–22961.

[13] Z. Liang, W. Zhao, S. Wang, Q. Tang, S.-C. Lam, Q. Miao, *Org. Lett.* **2008**, *10*, 2007–2010.

[14] K. T. Weber, K. Karikis, M. D. Weber, P. B. Coto, A. Charisiadis, D. Charitaki, G. Charalambidis, P. Angaridis, A. G. Coutsolelos, R. D. Costa, *Dalton Trans.* **2016**, *45*, 13284–13288.

[15] N. V. Korovina, J. Joy, X. Feng, C. Feltenberger, A. I. Krylov, S. E. Bradforth, M. E. Thompson, *J. Am. Chem. Soc.* **2018**, *140*, 10179–10190.

[16] M. Lippitz, C. G. Hübner, T. Christ, H. Eichner, P. Bordat, A. Herrmann, K. Müllen, T. Basché, *Phys. Rev. Lett.* **2004**, *92*, 103001.

CHAPTER 4

Synthesis of Tetracene-Ruthenium Phthalocyanine Complexes for Intramolecular Upconversion

4.1 Introduction

Triplet-triplet annihilation upconversion (TTA-UC) refers to the formation of one high-energy photon from two lower-energy photons. By utilizing the lower-energy sub-band-gap photons that normally cannot be absorbed by the light absorbing materials (i.e., silicon), TTA-UC potentially could benefit organic solar cells.[1–3] During the process of TTA-UC, the low-energy incident light selectively excites a ground state photosensitizer to its singlet excited state, which then undergoes intersystem crossing to form a triplet exciton. Intermolecular triplet energy transfer from the sensitizer to another molecule, the annihilator, then occurs. Finally, combination of two annihilator triplet excitons (T_1) results in generation of one higher energy singlet exciton (S_1). Tetracene derivatives are one of the widely used annihilators for the study of TTA-UA, as they fulfill the energy requirement of $E(S_1) \leq 2E(T_1)$, and their high $E(T_1)$ allows for utilization of visible and near-infrared light.[4–6]

TTA-UC is typically a bimolecular process, thus high concentrations of both photosensitizer and annihilator are needed for an efficient process. As discussed in Chapter 3, tetracene dimers linked by an adamantyl (**mAdTc$_2$**) or a *meta*-phenylene (**mPhTc$_2$**) spacer give rise to more efficient TTA-UC than the corresponding monomers, which demonstrates that intramolecular upconversion can eliminate the concentration requirements of annihilators. The results with **mAdTc$_2$** and **mPhTc$_2$** are consistent with other studies using oligomeric annihilators.[4,7] We hypothesized that intramolecular sensitization could lead to more efficient TTA-UC, combining the annihilators and photosensitizers into the same molecule. As an initial step to test this premise, compounds **TcPy-1** and **TcPy-2** (Figure 4.1a) have been designed and synthesized. The introduction of the pyridyl group offers a means to coordinate the tetracene annihilator to a Ru-phthalocyanine as a photosensitizer (Figure 4.1b) using **TcPy-1** and **TcPy-2** which have been tested by our collaborators in Spain through the

formation of **Ru-TcPy-1** and **Ru-TcPy-2**. As compounds **Ru-TcPy-1** and **Ru-TcPy-2** are structurally identical, except for the distance between the tetracene moiety and the photosensitizer, the effect of distance between annihilator and photosensitizer on intramolecular sensitization could be studied. The complexes **Ru-TcPy-1** and **Ru-TcPy-2** show good stability both as a solid and in solution under dark, which confirms the potential to assemble a photosensitizer with an annihilator. The promising results with **Ru-TcPy-1** and **Ru-TcPy-2** suggest fully intramolecular TTA-UC (iTTA-UC) that combines intramolecular sensitization and intramolecular upconversion could be possible.

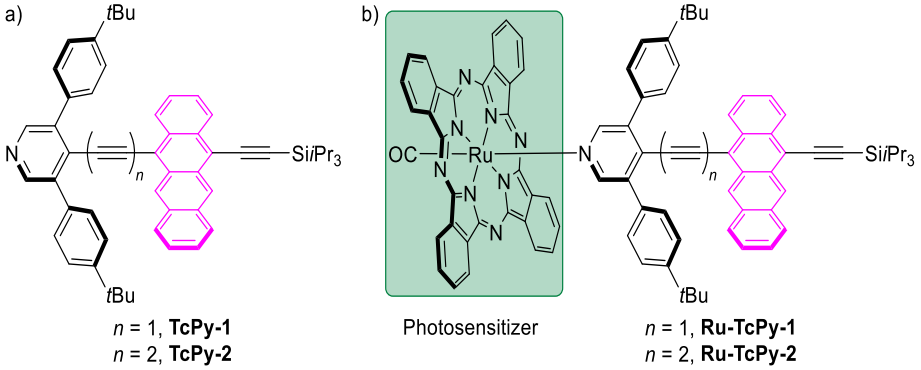

Figure 4.1. a) Structure of **TcPy-1** and **TcPy-2**; b) coordination of tetracene to a photosensitizer to give **Ru-TcPy-1** and **Ru-TcPy-2**.

Thus, molecules that might achieve intramolecular sensitization in addition to intramolecular upconversion have been designed and synthesized (Figure 4.2). These molecules could, in principle, achieve fully iTTA-UC based on both intramolecular photosensitization and upconversion and have the potential to eliminate the concentration requirements of both photosensitizer and annihilator toward more efficient TTA-UC. The *meta*-diethynylphenylene spacer was included in the design, as the **mPhTc2** gave the best performance for TTA-UC among the three dimers with varied electronic coupling, as described in Chapter 3. The butadiyne spacer was chosen for comparison, as it can be synthesized easily by well-established coupling reactions, and the strong coupled triplet pair shown in butadiyne-linked pentacene dimers[8] may be a benefit for an iTTA-UC system.

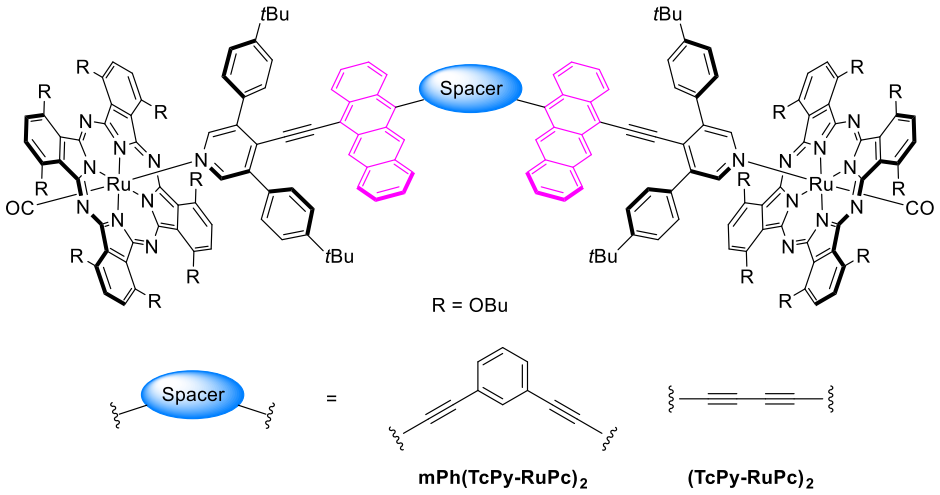

Figure 4.2. Design of iTTA-UC systems **mPh(TcPy-RuPc)$_2$** and **(TcPy-RuPc)$_2$**.

4.2 Synthesis of Pyridyl-endcapped Tetracenes

The pyridyl-endcapped terminal diyne **4.1** was synthesized, as reported in the literature,[9] through a Cadiot–Chodkiewicz cross-coupling reaction with monoyne **2.7** and Br–C≡C–C(CH$_3$)$_2$OH (4-bromo-2-methyl-3-butyn-2-ol). The resulting diyne product **4.2** was deprotected in the presence of NaOH and tris[2-(2-methoxyethoxy)ethyl]amine (TDA-1) in toluene at rt to give **4.1** as a white solid in 82% yield (Scheme 4.1). TDA-1 was used as a phase transfer catalyst to avoid high temperature (usually heating under reflux in toluene) for the deprotection reaction.[10]

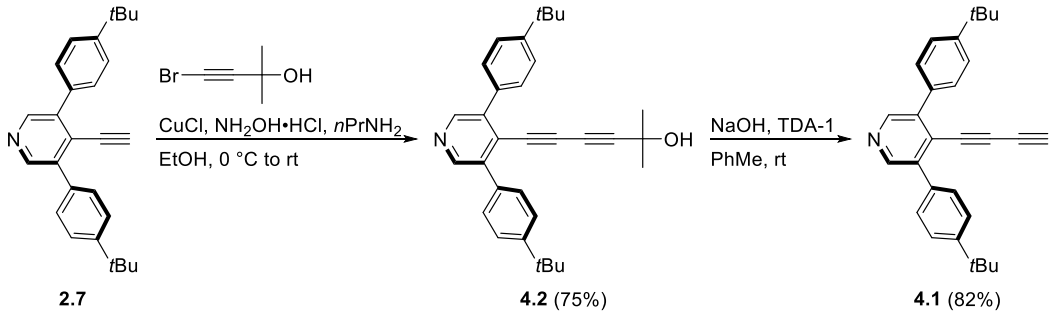

Scheme 4.1. Synthesis of compound **4.1**.

Two tetracenes linked with a sterically hindered pyridyl group via one (**TcPy-1**) or two alkynyl units (**TcPy-2**) were synthesized using the stepwise route through the common building block **3.2** (Scheme 4.2), which was described in Chapter 3. The

monoyne **2.7** was lithiated by lithium hexamethyldisilazide (LiHMDS) in dry THF at –78 °C. The reaction mixture of the resulting acetylide was added to a solution of ketone **3.2** in dry THF at –78 °C. The reaction mixture was warmed to rt slowly and stirred for 16 h at rt. Compound **4.3** was obtained in 64% yield as a white solid after quenching the reaction with saturated aqueous NH_4Cl solution, followed by purification with column chromatography. Reductive aromatization of compound **4.3** with $SnCl_2•2H_2O$ in the presence of acid gave the pyridyl-endcapped tetracene linked via one alkynyl unite **TcPy-1** as a red solid in 89% yield.

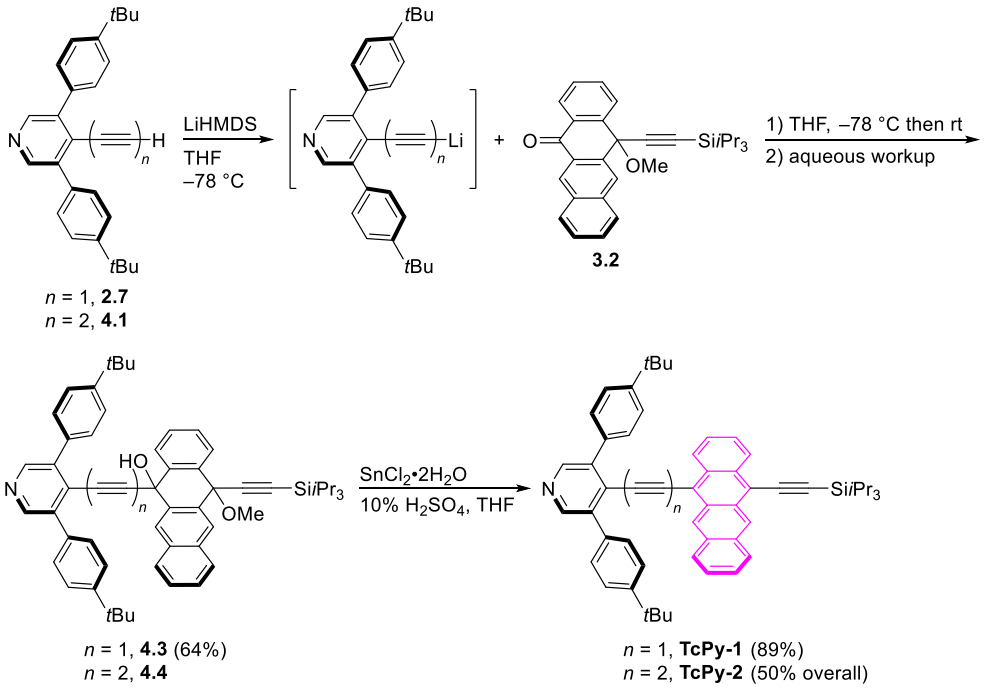

Scheme 4.2. Synthesis of **TcPy-1** and **TcPy-2**.

The diyne **4.1** was lithiated by LiHMDS in dry THF at –78 °C as well (Scheme 4.2). Then, the reaction mixture of the resulting acetylide was added to a solution of ketone **3.2** in dry THF at –78 °C and stirred for 16 h at rt. Compound **4.4** was not isolated, and the crude product was subjected directly to reductive aromatization after passing through a pad of silica gel with THF. The desired pyridyl-endcapped tetracene linked via two alkynyl unites **TcPy-2** was obtained as a purple red solid in 50% yield overall via purification by column chromatography and recrystallization.

4.3 Synthesis of Pyridyl-endcapped Tetracene Dimers and Corresponding Monomer

4.3.1 Synthesis of Pyridyl-endcapped Tetracene Dimers

The sterically hindered pyridyl-endcapped tetracene dimers **mPh(TcPy)$_2$** and **(TcPy)$_2$** were synthesized, as outlined in Scheme 4.3. Compound **4.5** was obtained by desilylation of compound **4.3** with tetrabutylammonium fluoride (TBAF) in wet THF. With compounds **4.5** in hand, the *meta*-diethynylphenylene-linked dimer **mPh(TcPy)$_2$** was synthesized through a Sonogashira cross-coupling reaction with 1,3-diiodobenzene with the presence of $Pd(PPh_3)_4$, CuI, and di*iso*propylamine in THF. Subsequently, the desired product was obtained as a dark purple solid in 66% yield by tin-mediated reductive aromatization with the presence of acid. The budadiyne-linked dimer **(TcPy)$_2$** was synthesized by subjecting precursor **4.5** to standard Hay homocoupling conditions (CuI, TMEDA)[11] at rt, followed by reductive aromatization with $SnCl_2 \bullet 2H_2O$, to give the product as a dark blue solid in 72% yield via purification by column chromatography and recrystallization.

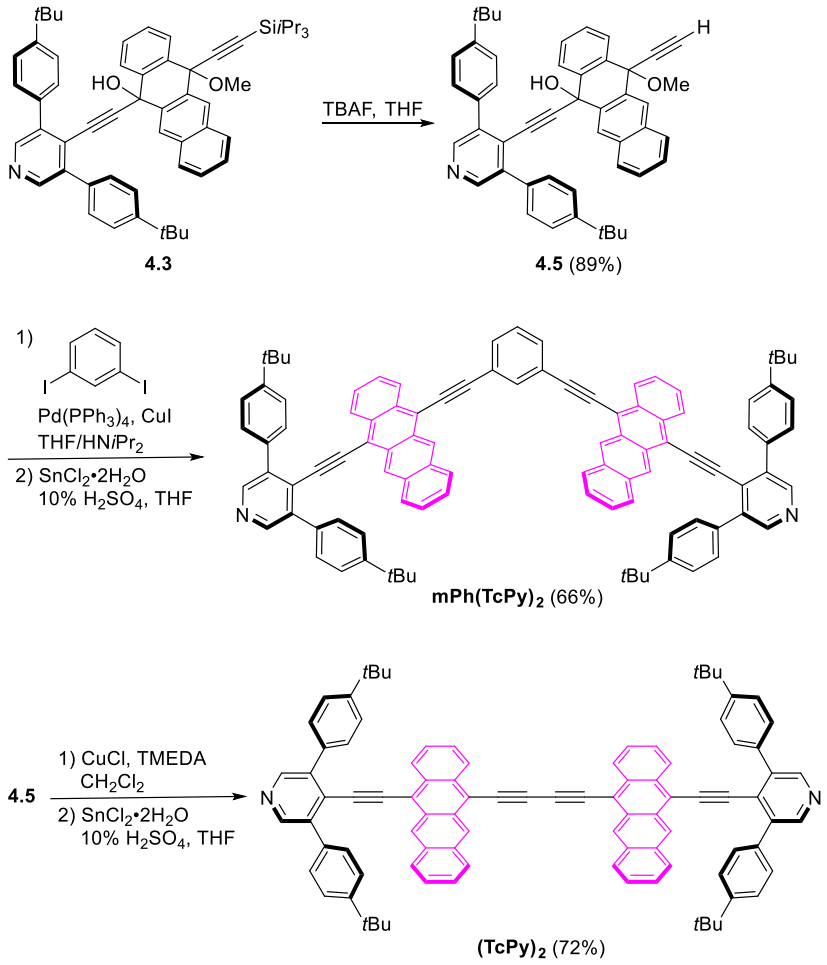

Scheme 4.3. Synthesis of **mPh(TcPy)2** and **(TcPy)2**.

When synthesizing the *meta*-diethynylphenylene-linked dimer **mPh(TcPy)2** via the Sonogashira cross-coupling reaction, a small amount of homocoupling dimer **(TcPy)2** was produced as a side product. These compounds have very similar polarity on silica gel, resulting in difficult separation by column chromatography. Alternatively, **mPh(TcPy)2** was synthesized by the desymmetrization of 5,12-naphthacenequinone (**3.1**) via stepwise nucleophilic acetylide addition (Scheme 4.4).[12–13] Lithiated pyridyl acetylide **4.6** was added to a solution of **3.1** in dry THF at –78 °C and stirred for 4 h at rt. Then, the lithiated diyne **3.4a** was added to the solution at –78 °C and stirred for an additional 16 h at rt. The reaction mixture was quenched by addition of a saturated aqueous NH_4Cl solution at 0 °C, followed by extraction with CH_2Cl_2 and solvent removal under vacuum. The residue was passed through a pad of silica gel with THF

before conducting to a $SnCl_2$-mediated reductive aromatization. The product **mPh(TcPy)$_2$** was purified by column chromatography with silica gel and obtained in 59% yield, which was significantly higher compared to Sonogashira cross-coupling route (overall 30% from **3.1**) shown in Scheme 4.3.

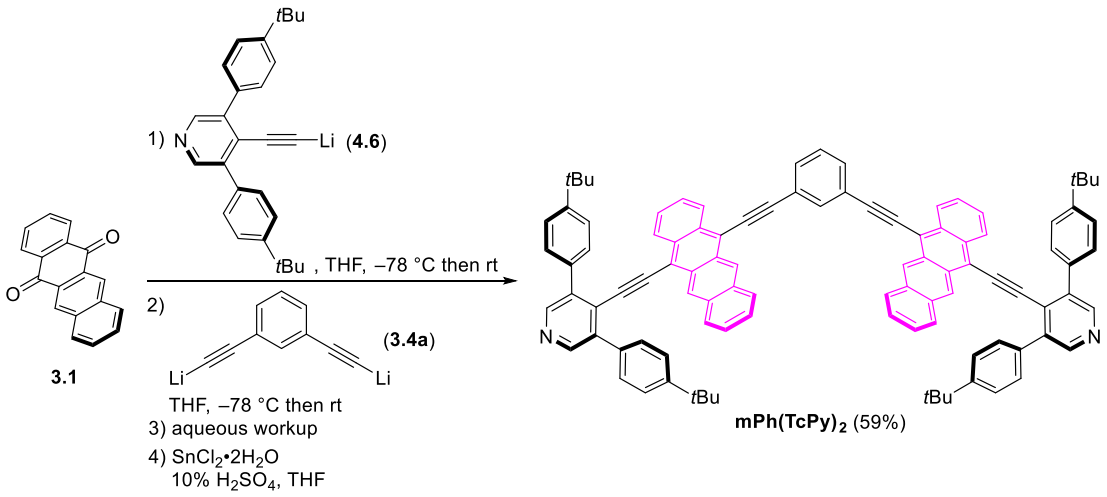

Scheme 4.4. Alternative synthesis of **mPh(TcPy)$_2$**.

4.3.2 Synthesis of Corresponding Monomer

The monomer **PhTcPy** was synthesized through both a Sonogashira cross-coupling reaction and a stepwise nucleophilic addition reaction (Scheme 4.5). Sonogashira cross-coupling reaction with compound **4.5** and iodobenzene, followed by $SnCl_2$-mediated reductive aromatization gave **PhTcPy** as a scarlet solid in 59% yield. Alternatively, **PhTcPy** was synthesized by a stepwise addition protocol that began with addition of lithiated pyridyl acetylide **4.6** to tetracene quinone **3.1**, followed by addition lithiated ethynylbenzene (**3.6**). Reductive aromatization with $SnCl_2$•$2H_2O$ and purification by column chromatography and recrystallization gave **PhTcPy** in 76% yield. Similar to the synthesis of **mPh(TcPy)$_2$**, the yield of the stepwise nucleophilic reaction to obtain **PhTcPy** was significantly higher compared to the Sonogashira cross-coupling route.

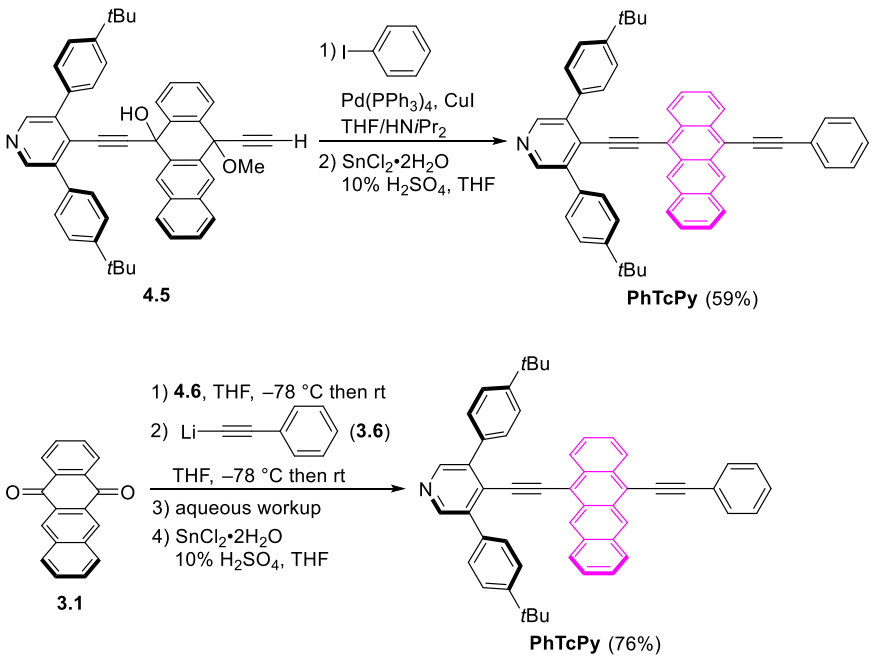

Scheme 4.5. Synthesis of **PhTcPy**.

4.4 Coordination of Tetracenes to RuPc

4.4.1 Synthesis of Ruthenium Phthalocyanine RuPc

Ru(II) 1,4,8,11,15,18,22,25-octabutoxyphthalocyanine (**RuPc**) was synthesized by metalation of the phthalocyanine free base (**H_2-Pc**) using $Ru_3(CO)_{12}$ in heated benzonitrile (Scheme 4.6), using a procedure adapted from the literature.[14] As shown in Figure 4.3, the reaction was monitored by UV-vis analysis until deemed complete after 30 min, as indicated by the appearance of the Q-band of **RuPc** (λ = 708 nm) and disappearance of that of **H_2-Pc** (λ = 769 nm). Even though the compound **RuPc** was purified by column chromatography with silica gel followed by further purification with size exclusion chromatography in the literature, I found that it was not stable on silica gel. The spot stayed on the baseline when using $CHCl_3$ or $CHCl_3$/MeOH 1:1 as eluent and it turned to brown from dark green in several minutes in TLC analysis. Alternatively, the reaction solvent was removed under vacuum, and the crude product was dissolved in $CHCl_3$ followed by filtration through a small amount of cotton wool inside a Pasteur pipette before applying it to size exclusion chromatography with Bio-

Beads SX-1 with $CHCl_3$. The desired product **RuPc** was obtained as a dark green solid in 54% yield.

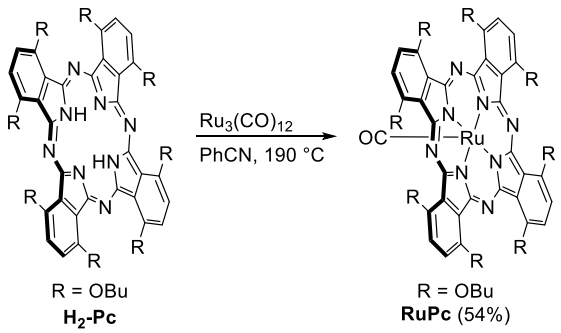

Scheme 4.6. Synthesis of **RuPc**.

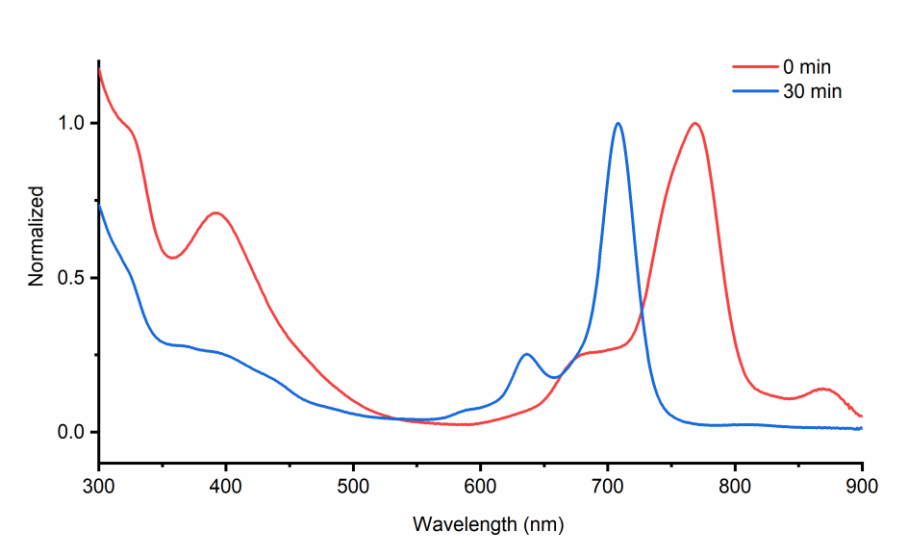

Figure 4.3. UV-vis spectrum of reaction mixture forming **RuPc** before and after heating for 30 min in CH_2Cl_2.

4.4.2 Synthesis of PhTcPy-RuPc Complex

The monomer **PhTcPy** was used to study the reaction condition and purification process for coordination of tetracene derivatives with **RuPc**. The complex **PhTcPy-RuPc** was obtained by stirring **PhTcPy** and **RuPc** (1.2 equiv) in $CHCl_3$ at rt for 5 min (Scheme 4.7). The product, **PhTcPy-RuPc**, was found to be unstable on alumina as a support for chromatography. Searching for an alternative, TLC analysis of the product mixture on silica gel showed three spots corresponding to the product **PhTcPy-RuPc** and the two starting materials **PhTcPy** and **RuPc**. Attempts to purify

the complex **PhTcPy-RuPc** by column chromatography with silica gel failed. **PhTcPy** was obtained primarily, indicating that the complex was decomposing into starting materials on the silica gel support. Next, size exclusion chromatography was the then explored due to the size difference between the complex and starting materials. However, all attempts to purify the complex **PhTcPy-RuPc** by size exclusion chromatography on Bio-Beads S-X3 with THF, toluene, $CHCl_3$ or CH_2Cl_2 were unsuccessful, even though the size of the complex (MW = 1912.41) is within the molecular weight limit of S-X3 gel (≤ 2,000), and only impure product mixtures were obtained. Using THF as the eluent led to decomposition of the complex, as indicated by the color change of the band of the complex on the column from the original purple to dark green. Finally, it was determined that purification could be achieved by size exclusion chromatography using Bio-Beads SX-1 and $CHCl_3$ as the eluent, which gave **PhTcPy-RuPc** as a dark purple solid in a quantitative yield.

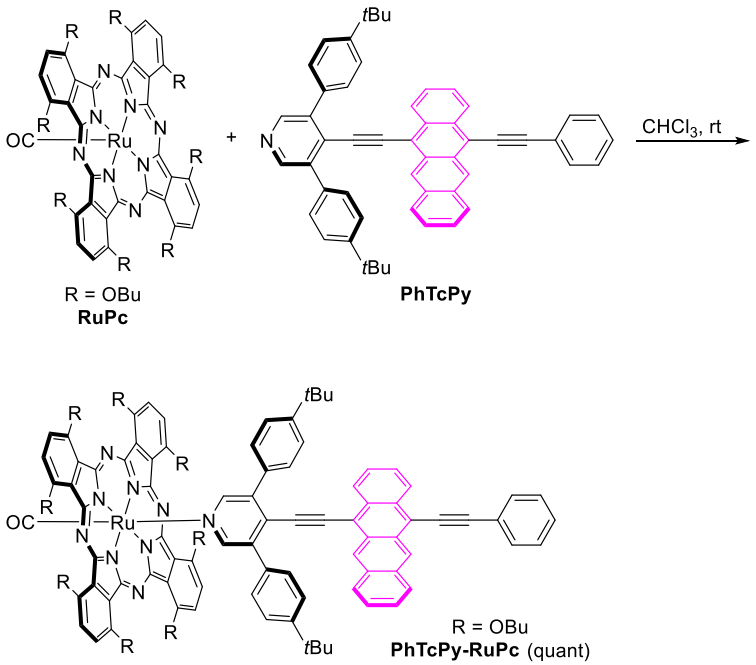

Scheme 4.7. Synthesis of **PhTcPy-RuPc**.

The successful formation of the desired complex **PhTcPy-RuPc** has been confirmed by mass spectrometry (MS) combined with ^{1}H, ^{13}C NMR, and ^{1}H–^{13}C HSQC NMR spectroscopic analyses. MALDI HRMS analysis confirms the

composition of **PhTcPy-RuPc**, showing a strong signal at *m/z* 1911.8488 (M^+, calcd for $C_{118}H_{123}N_9O_9{}^{102}Ru$ *m/z* 1911.8482). ^1H NMR spectra of **PhTcPy** and **PhTcPy-RuPc** are shown in Figure 4.4a. The pyridyl protons (H_a) for **PhTcPy** can be easily identified as there is only one singlet with integration of 2H (δ 8.72) in the aromatic region. The other two singlets in the range of 8.4–9.2 ppm with integration of 1H correlating to H_b and H_c. For the ^1H NMR spectrum of **PhTcPy-RuPc**, there is one singlet with integration of 2H as well, which should be correlated to H_a. However, it is very upfield (δ 2.40) compared to the analogous protons in **PhTcPy** (δ 8.72). ^1H–^{13}C HSQC NMR spectra for **PhTcPy** (Figure 4.4b) and **PhTcPy-RuPc** (Figure 4.4c) are used to confirm the identification of H_a, which can be assigned through the protons correlated to the *ortho*-carbon in the pyridyl ring (140–150 ppm). The significant upfield of the pyridyl protons in **PhTcPy-RuPc** results from shielding by the diamagnetic ring current of the phthalocyanine which is consistent with other ruthenium phthalocyanine complexes with axial ligands reported in the literature.[15–18]

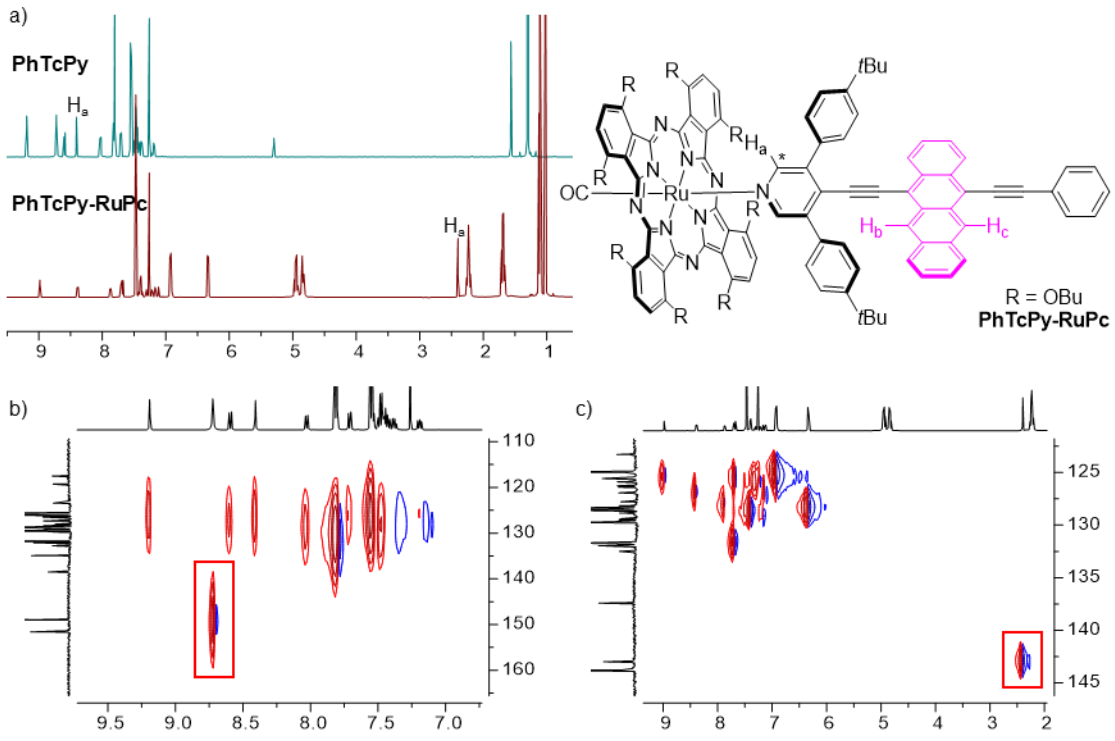

Figure 4.4. a) Plots of the ^1H NMR spectra of **PhTcPy** and **PhTcPy-RuPc** in $CDCl_3$; signals for protons on the pyridyl moiety are labeled as H_a; b) ^1H–^{13}C HSQC spectrum of **PhTcPy**, and c) ^1H–^{13}C HSQC spectrum of **PhTcPy-RuPc** in $CDCl_3$ (in $CDCl_3$, red boxes indicate correlation of $H_a \leftrightarrow C^*$).

4.4.3 Synthesis of Tetracene Dimers Complexes

With competent reaction conditions and a purification process established through formation of the monomer **PhTcPy-RuPc**, the formation of dimeric complexes **mPh(TcPy-RuPc)$_2$** and **(TcPy-RuPc)$_2$** were explored (Scheme 4.8). Combining the corresponding tetracene dimers **mPh(TcPy)$_2$** and **(TcPy)$_2$** with **RuPc** (2.4 equiv) in $CHCl_3$, stirring at rt for 5 min, and purification by size exclusion chromatography on Bio-Beads SX-1 with $CHCl_3$ gave **mPh(TcPy-RuPc)$_2$** as a dark purple solid in a quantitative yield and **(TcPy-RuPc)$_2$** as a dark blue solid in 56% yield. It is noted that the dimer **(TcPy-RuPc)$_2$** deposed slowly on Bio-Beads SX-1. The decomposed products remained on Bio-Beads SX-1, however, and did not move with $CHCl_3$ or other solvents (CH_2Cl_2, THF, toluene), which greatly simplified purification.

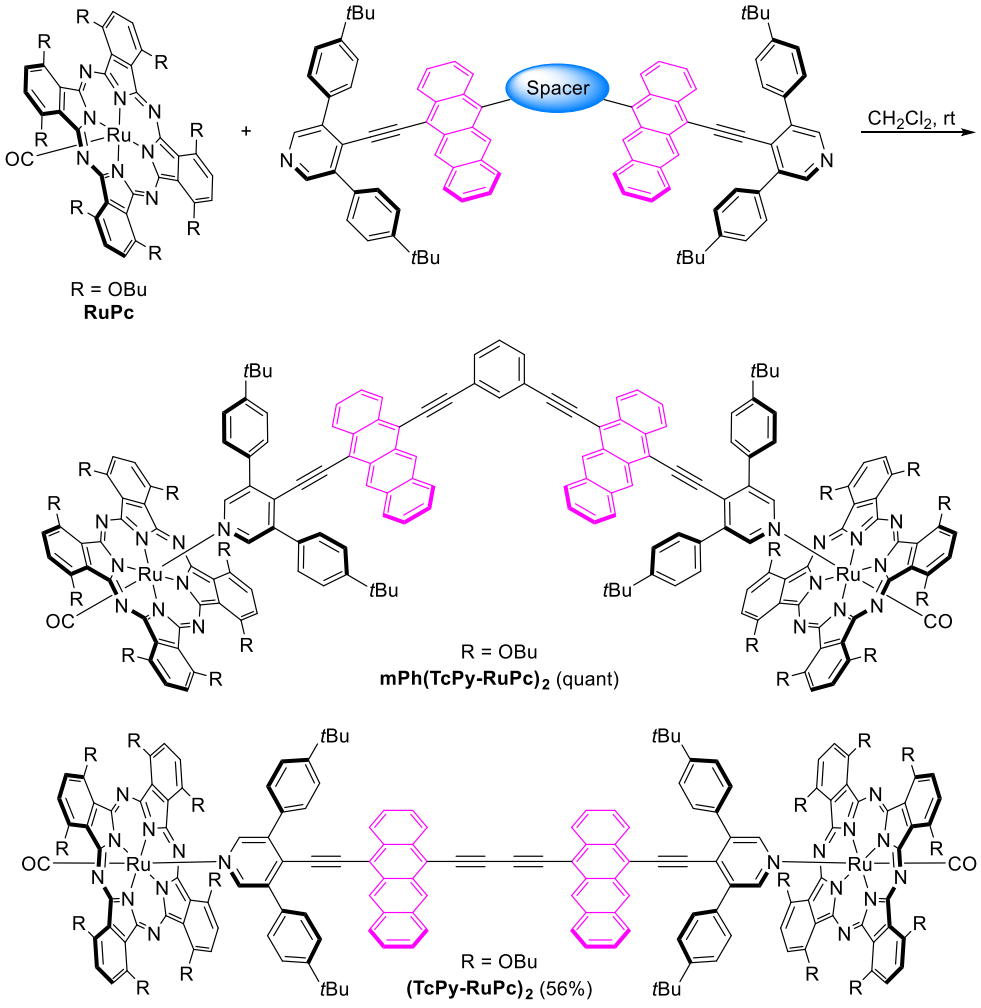

Scheme 4.8. Synthesis of **mPh(TcPy)$_2$-RuPc** and **(TcPy)$_2$-RuPc**.

The successful formation of the dimeric complexes **mPh(TcPy-RuPc)$_2$** and **(TcPy-RuPc)$_2$** has been confirmed primarily by ^{1}H NMR spectroscopic analyses, which shows similar features as **PhTcPy-RuPc** (Figure 4.5). The pyridyl protons (H$_a$) are identified easily as there is only one singlet with integration of 4H in the spectra of **mPh(TcPy)$_2$** (δ 8.73), **mPh(TcPy-RuPc)$_2$** (δ 2.39), **TcPy)$_2$** (δ 8.74), **(TcPy-RuPc)$_2$** (δ 2.39). The significant upfield of the pyridyl protons in the dimeric complexes **mPh(TcPy-RuPc)$_2$** and **(TcPy-RuPc)$_2$** is consistent with the monomeric complex **PhTcPy-RuPc**, which confirms the successful axial coordination with **RuPc**.

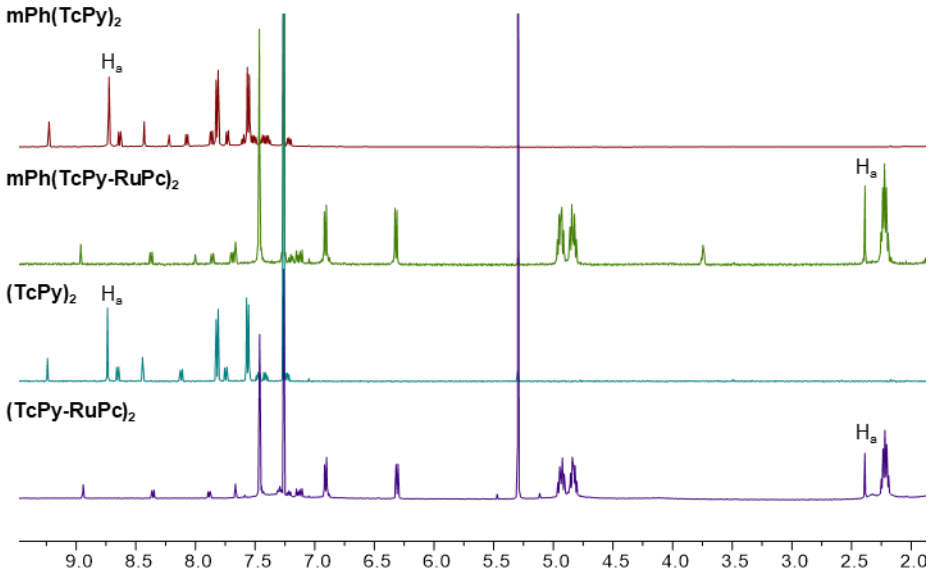

Figure 4.5. a) Plots of ^{1}H NMR spectra of **mPh(TcPy)$_2$**, **mPh(TcPy-RuPc)$_2$**, **(TcPy)$_2$**, and **(TcPy-RuPc)$_2$** in $CDCl_3$; signals for protons on the pyridyl moiety are labeled as H$_a$.

4.5 UV-vis Spectroscopy Analysis

The quantitative UV-vis spectra of the pyridyl-endcapped tetracenes **TcPy-1** and **TcPy-2** have been measured in CH_2Cl_2 at room temperature (Figure 4.6, Table 4.1). The absorption maximum for **TcPy-1** (λ_{max} = 555 nm) is red shifted compared to **PhTc** (λ_{max} = 545 nm, Chapter 3) as the replacement of the phenyl group in **PhTc** with the pyridyl group in **TcPy-1**. The absorption maximum for **TcPy-2** (λ_{max} = 560 nm) is red shifted further. The extinction coefficients of the pyridyl-endcapped tetracenes **TcPy-1** and **TcPy-2** (36,300 L mol^{-1} cm^{-1} and 33,600 L mol^{-1} cm^{-1}, respectively) are quite similar to that of **PhTc** (33,100 L mol^{-1} cm^{-1}).

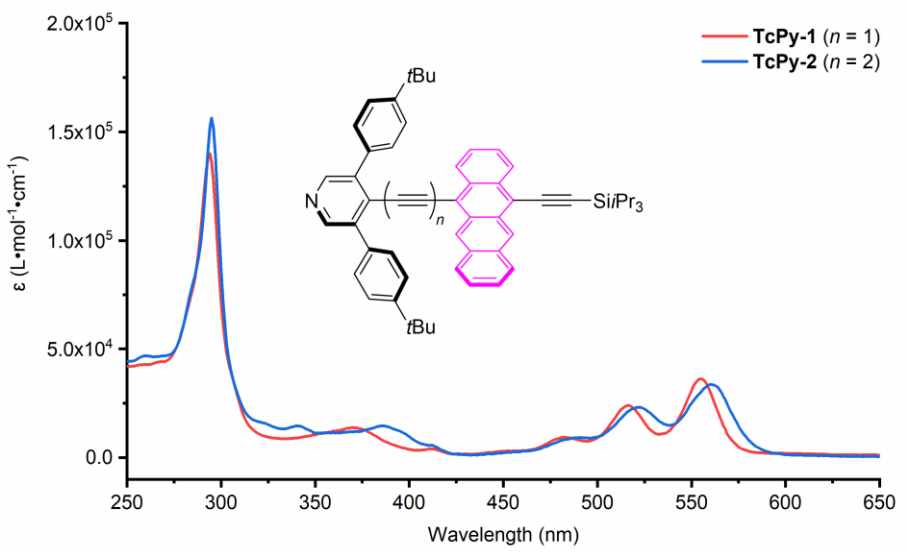

Figure 4.6. UV-vis spectra of **TcPy-1** and **TcPy-2** in CH_2Cl_2.

The UV-vis spectra of the tetracene dimers **mPh(TcPy)$_2$** and **(TcPy)$_2$**, their corresponding monomer **PhTcPy,** as well as the ruthenium phthalocyanine RuPc have been measured in CH_2Cl_2 at room temperature (Figure 4.7a, Table 4.1). The absorption maximum for **PhTcPy** (λ_{max} = 564 nm) is red shifted compared to **TcPy-1** (λ_{max} = 555 nm) as a result of extended π-conjugation from the additional phenyl group. The absorption maximum for **mPh(TcPy)$_2$** (λ_{max} = 569 nm) is slightly red shifted compared to the monomer **PhTcPy** (λ_{max} = 564 nm). The λ_{max} of butadiyne-linked dimer **(TcPy)$_2$** is red shifted further to 642 nm and the spectrum shows broadened features. The result features of **(TcPy)$_2$** are similar to the pentacene analogue.[12] Moreover, the λ_{max} of **RuPc** is lower energy than λ_{max} of the tetracene derivatives, which means it can be selectively excited with a low-energy incident light and serve as a photosensitizer for these tetracene derivatives.

The UV-Vis spectra for tetracene ruthenium phthalocyanine complexes **PhTcPy-RuPc**, **mPh(TcPy-RuPc)$_2$**, and **(TcPy-RuPc)$_2$** have been measured in CH_2Cl_2 at room temperature (Figure 4.7b–d, Table 4.1). The spectra of these complexes show features from both the tetracene and the ruthenium phthalocyanine groups. As shown in Figure 4.7b, the absorption of **PhTcPy-RuPc** is effectively a linear combination of **PhTcPy** and **RuPc**. The absorption maximum for **PhTcPy-RuPc** (λ_{max} = 704 nm) is similar to **RuPc** (λ_{max} = 708 nm), while the absorption from the tetracene

moiety is red shifted by 11 nm (0.04 eV). The UV-vis spectra of the dimeric complexes **mPh(TcPy-RuPc)$_2$** and **(TcPy-RuPc)$_2$** show similar features. While the absorptions derived from the phthalocyanine groups of (**mPh(TcPy-RuPc)$_2$** (λ_{max} = 704 nm) and **(TcPy-RuPc)$_2$** (λ_{max} = 710 nm) are similar to **RuPc** (λ_{max} = 708 nm), the absorptions from the tetracene moiety are red shifted. These spectroscopic features are consistent with other systems that have a pyridyl ligand coordinated with ruthenium phthalocyanine.[15,17–18]

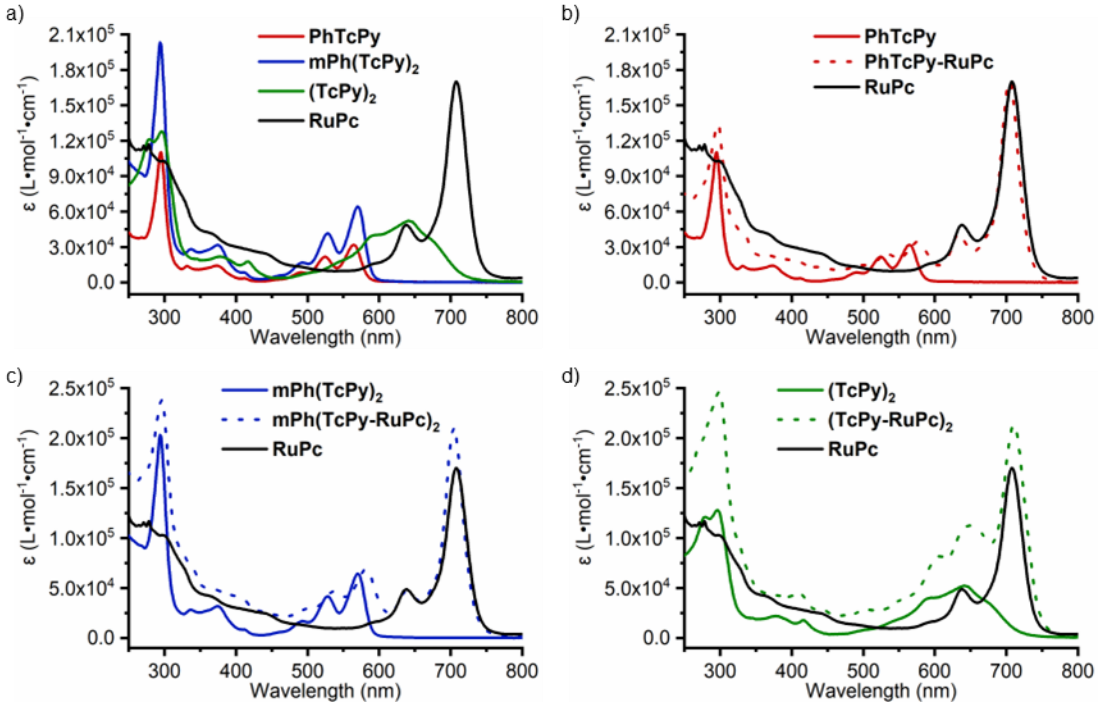

Figure 4.7. UV-vis spectra of a) **PhTcPy**, **mPh(TcPy)$_2$**, **(TcPy)$_2$**, and **RuPc**; b) **PhTcPy**, **RuPc**, and **PhTcPy-RuPc**; c) **mPh(TcPy)$_2$**, **RuPc**, and **mPh(TcPy-RuPc)$_2$**; d) **(TcPy)$_2$**, **RuPc**, and **(TcPy-RuPc)$_2$** in CH_2Cl_2.

Table 4.1. Relevant UV-vis Data for Tetracene Derivatives and **RuPc**

Compound	λ_{max} (nm)	ε (L mol^{-1} cm^{-1})
TcPy-1	555	36,300
TcPy-2	560	33,600
RuPc	708	170,000
PhTcPy	565	31,900
PhTcPy-RuPc	704	170,000
mPh(TcPy)$_2$	570	64,300
mPh(TcPy-RuPc)$_2$	704	209,000
(TcPy)$_2$	642	53,100
(TcPy-RuPc)$_2$	710	213,000

4.6 Conclusions

In summary, two sterically hindered pyridyl-endcapped tetracenes **TcPy-1** and **TcPy-2** with identical structures, except for the distance between the tetracene moiety and the photosensitizer have been synthesized through the stepwise method via the common building block **3.2** developed in Chapter 3. These two compounds have been sent to our collaborators in Spain to coordinate with ruthenium phthalocyanine for the primary study of the process of intramolecular sensitizing in TTA-UC.

The butadiyne-linked dimer **(TcPy)$_2$** has been obtained through a Hay homocoupling reaction of **4.5**. The *meta*-diethynylphenylene-linked dimer **mPh(TcPy)$_2$** and the corresponding monomer **PhTcPy** have been synthesized through both a Sonogashira cross-coupling reaction and a stepwise nucleophilic addition desymmetrization of 5,12-naphthacenequinone. The results show that the stepwise nucleophilic addition reaction gives both the dimer **mPh(TcPy)$_2$** and the monomer **PhTcPy** in better yields.

The monomer **PhTcPy** has been coordinated to a ruthenium phthalocyanine **RuPc** to form a complex **PhTcPy-RuPc**, which can achieve intramolecular sensitization in principle. The dimers **mPh(TcPy)$_2$** and **(TcPy)$_2$** have been coordinated to **RuPc** as well. The complexes **mPh(TcPy-RuPc)$_2$** and **(TcPy-RuPc)$_2$** have the potential to achieve intramolecular sensitization in addition to intramolecular upconversion. These molecules have been sent to our collaborators in Germany to study the process of iTTA-UC.

The successful synthesis of these compounds has been confirmed by mass spectrometry combined with ^{1}H and ^{13}C NMR spectroscopic analyses. The UV-vis spectrum of **(TcPy)$_2$** (λ_{max} = 642 nm) shows a red shift of the absorption wavelengths compared to **mPh(TcPy)$_2$** (λ_{max} = 569 nm) and **PhTcPy** (λ_{max} = 564 nm) as a result of extended π-conjugation. Moreover, the UV-vis spectra of the complexes show absorption peaks from both tetracene parts and **RuPc**.

References

[1] E. M. Gholizadeh, S. K. K. Prasad, Z. L. Teh, T. Ishwara, S. Norman, A. J. Petty, J. H. Cole, S. Cheong, R. D. Tilley, J. E. Anthony, S. Huang, T. W. Schmidt, *Nat. Photonics* **2020**, *14*, 585–590.

[2] T. Trupke, M. A. Green, P. Würfel, *J. Appl. Phys.* **2002**, *92*, 4117–4122.

[3] R. R. Islangulov, J. Lott, C. Weder, F. N. Castellano, *J. Am. Chem. Soc.* **2007**, *129*, 12652–12653.

[4] A. B. Pun, S. N. Sanders, M. Y. Sfeir, L. M. Campos, D. N. Congreve, *Chem. Sci.* **2019**, *10*, 3969−3975.

[5] K. J. Fallon, E. M. Churchill, S. N. Sanders, J. Shee, J. L. Weber, R. Meir, S. Jockusch, D. R. Reichman, M. Y. Sfeir, D. N. Congreve, L. M. Campos, *J. Am. Chem. Soc.* **2020**, *142*, 19917−19925.

[6] C. J. Imperiale, P. B. Green, E. G. Miller, N. H. Damrauer, M. W. B. Wilson, *J. Phys. Chem. Lett.* **2019**, *10*, 7463–7469.

[7] S. Mattiello, S. Mecca, A. Ronchi, A. Calascibetta, G. Mattioli, F. Pallini, F. Meinardi, L. Beverina, A. Monguzzi, *ACS Energy Lett.* **2022**, *7*, 2435–2442.

[8] I. Papadopoulos, S. R. Reddy, P. B. Coto, D. Lehnherr, D. Thiel, M. Thoss, R. R. Tykwinski, D. M. Guldi, *J. Phys. Chem. Lett.* **2022**, 5094–5100.

[9] Y. Gao, Y. Hou, F. Gordillo Gámez, M. J. Ferguson, J. Casado, R. R. Tykwinski, *Nat. Chem.* **2020**, *12*, 1143–1149.

[10] S. J. Havens, P. M. Hergenrother, *J. Org. Chem.* **1985**, *50*, 1763–1765.

[11] A. S. Hay, *J. Org. Chem.* **1962**, *27*, 3320–3321.

[12] D. Lehnherr, A. H. Murray, R. McDonald, R. R. Tykwinski, *Angew. Chem. Int. Ed.* **2010**, *49*, 6190–6194.

[13] T. Iwanaga, Y. Yamamoto, K. Nishioka, S. Toyota, *Synthesis* **2015**, *47*, 3997–4007.

[14] A. P. Kroitor, A. A. Dmitrienko, A. G. Martynov, Y. G. Gorbunova, A. B. Sorokin, *Org. Biomol. Chem.* **2023**, *21*, 69–74.

[15] M. Hanack, Y. G. Kang, *Chem. Ber.* **1991**, *124*, 1607–1612.

[16] M. Hanack, S. Knecht, R. Polley, *Chem. Ber.* **1995**, *128*, 929–933.

[17] T. Rawling, A. McDonagh, *Coord. Chem. Rev.* **2007**, *251*, 1128–1157.

[18] A. N. Cammidge, G. Berber, I. Chambrier, P. W. Hough, M. J. Cook, *Tetrahedron* **2005**, *61*, 4067–4074.

CHAPTER 5

Miscellaneous Projects

As presented in previous chapters, photophysical processes, such as singlet fission (SF) and triplet-triplet annihilation upconversion (TTA-UC) are strategies that have been proposed to improve the performance of organic solar cells (OSCs). Despite extensive studies on the photophysical concepts of SF over the past decades, the underlying molecular mechanisms are not well defined yet, and the application of organic SF materials to OSCs remains to be achieved. One of the key aspects of my PhD work has been to design and synthesize acene oligomers with controlled distance, geometry, and electronic coupling between interacting chromophores using molecular spacers. These molecules provide models for our collaborators to answer specific hypotheses regarding the detailed mechanism of these photophysical processes and help establish the structure-properties relationships for future design. During collaboration, some side projects have been initiated but not finished completely for multiple reasons. Anticipating that others might continue with these projects, more details have been included here in comparison to other chapters.

5.1 Design and Attempts to Synthesize a Twisted Pentacene Dimer

5.1.1 Introduction

Pentacene derivatives have been one of the most extensively studied organic systems for the process of SF, which allows the generation of two triplet excitons from one excited singlet exciton and provides a possibility to increase the power conversion efficiency limit in conventional photovoltaics to over 45% (See Chapter 1 for detailed discussion).[1] Pentacene oligomers are preferred for SF in comparison to monomers, as intramolecular SF (iSF) can occur in dilute solution, which provide an opportunity to study the impacts of chemical structure on the mechanism of iSF in dilute solution.[2–5] Even though extensive studies have been conducted in recent years on iSF, the fundamental relationship between the structure of molecules and the process of iSF still is lacking. One question remaining is how rotation of the chromophores effect the

mechanism of iSF. Previous research on different systems showed that the twist angle between two interacting chromophores could impact the rates of iSF and the recombination of the triplets drastically.[6–8] However, a general understanding about the rotational effect on iSF is not achieved yet.

Pentacene dimers linked by butadiyne has been used frequently to study the mechanism of iSF, as they can be synthesized easily by well-established coupling reactions of terminal acetylenes.[9] The molecules favor a planar conformation when there are no substitutions on pentacene units (Figure 5.1).[10–11] In principle, by adding sterically bulky groups, twisted conformers with a dihedral angle between the planes of the two pentacene moieties can be achieved. Then, the rotational effect on the process of iSF can be studied.

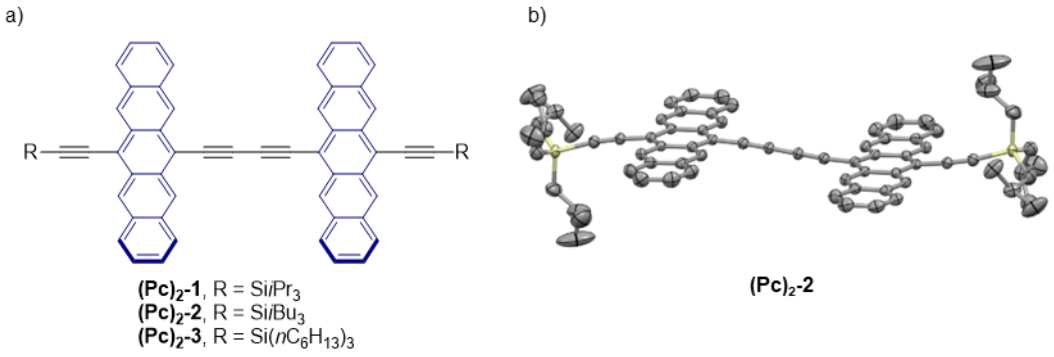

Figure 5.1. a) Structure of butadiyne linked pentacene dimers; b) X-ray crystal structure of **(Pc)$_2$-2**.

The synthesis of a sterically hindered pentacene dimer linked by butadiyne, in which rotation is restricted between the two pentacene moieties, was targeted. This molecule could serve as a model compound to compare with the unsubstituted dimer **(Pc)$_2$-2** and be used to study the rotational effect on iSF. For the formation of the twisted pentacene dimer, the sterically demanding substituents can be, in principle, installed either at the inner ring of the molecule (5,7,12,14-substituted, Figure 5.2a) or at the outer ring of the molecule (1,4,8,11-substituted, Figure 5.2b).

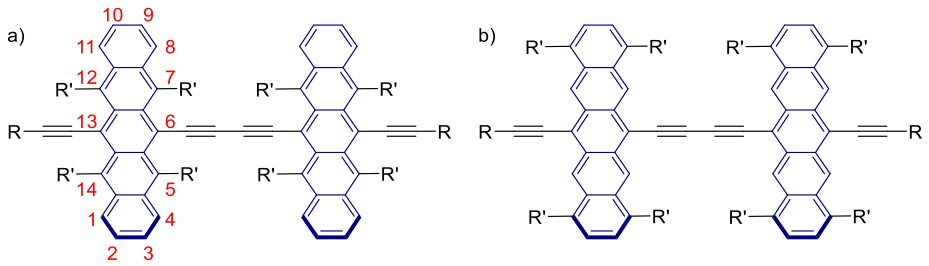

Figure 5.2. Structures of a) 5,7,12,14-substituted and b) 1,4,8,11-substituted pentacene dimers.

5.1.2 Attempts to Synthesize a Twisted Pentacene Dimer

The first molecule I designed was **tetraPh-(Pc)$_2$** (Figure 5.3) as the starting material 5,7,12,14-tetraphenyl-6,13-pentacenequinone (**5.1**) is known in the literature.[12–13] The tri*iso*butylsilyl group was chosen to make it as consistent as possible with **(Pc)$_2$-2** and provide solubility. The calculation results from our collaborators show that there is a potential energy minimum for rotation for **tetraPh-(Pc)$_2$** about the central single bond when the two pentacene moieties are perpendicular, and the potential energy increases as the dihedral angle between the planes of the two pentacene moieties decreases. As this molecule could serve as the model compound to study the rotational effect on iSF, my work was devoted to synthesizing this twisted pentacene dimer **tetraPh-(Pc)$_2$**.

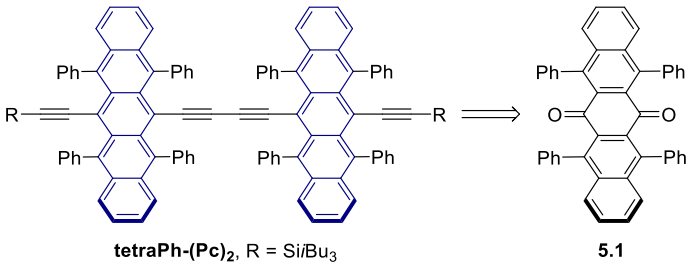

Figure 5.3. Structures of the target molecule **tetraPh-(Pc)$_2$** and its precursor **5.1**.

5.1.2.1 Attempts to Synthesize the Tetraphenyl-Pentacene Dimer [5]tetraPh

As shown in Scheme 5.1, 5,7,12,14-tetraphenyl-6,13-pentacenequinone (**5.1**) was synthesized, as reported in the literatures.[12–13] A Diels–Alder cycloaddition of the commercially available 1,3-diphenyl*iso*benzofuran (**5.2**) and *p*-benzoquinone (**5.3**) under reflux in EtOH gave compound **5.4** as a white solid in 95% yield. Two dehydration methods presented in the literature were attempted. The dehydration with concentrated H_2SO_4[12] gave purer product (**5.1**), based on ^{1}H NMR analysis, but the

yield was lower (~5% yield) compared to dehydration with anhydrous *p*-toluenesulfonic acid[13]. A Dean–Stark apparatus was used in this step to remove the water from the reaction system.

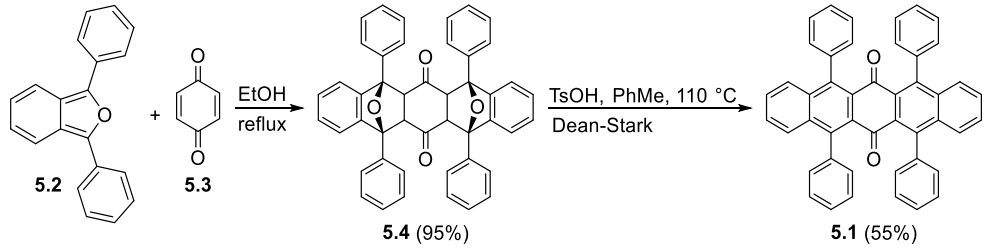

Scheme 5.1. Synthesis of **5.1**.

With 5,7,12,14-tetraphenyl-6,13-pentacenequinone (**5.1**) in hand, a stepwise nucleophilic substitution protocol was intended to be used for the synthesis of **tetraPh-(Pc)$_2$**. The route started with the synthesis of the monosubstituted pentacenequinone **5.5** (Scheme 5.2). Different conditions were attempted to synthesize **5.5** (Table 5.1). In the first experiment, 0.9 equivalents of lithiated (tri*iso*butylsilyl)acetylene (Li–C≡C–Si*i*Bu$_3$), which was prepared in situ by adding nBuLi to a solution of (tri*iso*butylsilyl)acetylene in dry THF at –78 °C, were added to a suspension of **5.1** in dry THF at –78 °C. Less than 1 equiv of the lithiated acetylide was used to avoid possible di-substitution of **5.1**. The reaction mixture was warmed to rt slowly and stirred at rt for 16 h. However, after aqueous workup, no new compound was observed in the reaction mixture (by TLC analysis), and only the starting material **5.1** was recovered. Then, I switched the lithiated acetylide with a sterically demanding tri*iso*butylsilyl group to a triethylsilyl and trimethylsilyl group. No reaction was observed in either cased. Alternatively, ethynylmagnesium bromide was used in either THF or Et$_2$O at 0 °C. Only **5.1** was found in these reactions and recovered after aqueous workup.

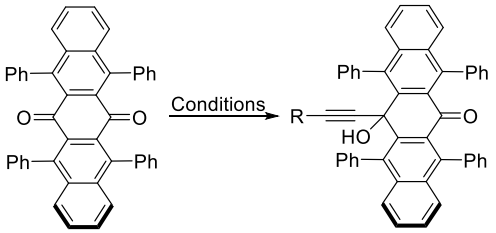

5.1

5.5a R = Si*i*Bu$_3$
5.5b R = SiEt$_3$
5.5c R = SiMe$_3$
5.5d R = H

Scheme 5.2. Attempts to synthesize **5.5a–d**.

Table 5.1. Conditions Attempted for the Synthesis of **5.5**

Entry	Reagent	Equivalent	Solvent	Temperature	Result
1	*i*Bu$_3$Si–C≡C–Li	0.9 equiv	THF	–78 °C then rt	No reaction
2	Et$_3$Si–C≡C–Li	0.9 equiv	THF	–78 °C then rt	No reaction
3	Me$_3$Si–C≡C–Li	0.9 equiv	THF	–78 °C then rt	No reaction
4	H–C≡C–MgBr	1 equiv	THF	0 °C then rt	No reaction
5	H–C≡C–MgBr	1 equiv	Et$_2$O	0 °C then rt	No reaction
6	H–C≡C–MgBr	2 equiv	THF	0 °C then rt	No reaction
7	Me$_3$Si–C≡C–Li	20 equiv	Et$_2$O	–78 °C then rt	**5.5c**, R = SiMe$_3$
8	*i*Bu$_3$Si–C≡C–Li	20 equiv	Et$_2$O	–78 °C then rt	**5.5a**, R = Si*i*Bu$_3$

As all attempts with less than 2 equivalents of nucleophile failed, a large excess of lithiated acetylide was used to test the feasibility of this reaction. Compound **5.5c** was obtained successfully by adding 20 equivalents of lithiated (trimethylsilyl)acetylene (Li–C≡C–SiMe$_3$) to a suspension of **5.1** in dry Et$_2$O at –78 °C. The reaction mixture was warmed to rt slowly and stirred at rt for 16 h before quenching with saturated aqueous NH$_4$Cl solution. However, the solubility of **5.5c** was poor in common organic solvents, like THF, Et$_2$O, CH$_2$Cl$_2$, EtOAc, which led to difficult purification. Therefore, the reaction using a tri*iso*butylsilyl analogue was attempted with the analogous method. Compound **5.5a** was obtained as a white solid in 73% yield. It was noticed that even though an excess amount of lithiated acetylide was used for the formation of **5.5c** and **5.5a**, a di-substituted side product was not observed, presumably due to the sterically demanding phenyl groups of **5.1**.

Only compound **5.5a** was carried on to the next step due to better solubility compared to **5.5c** (Scheme 5.3). The unsymmetrical pentacene **5.6**, however, could not be obtained from the tri*iso*butylsilylacetylene intermediate **5.5a** in all attempts (Table 5.2). Even in the presence of an excess amount of lithiated

(trimethylsilyl)acetylene, ethynylmagnesium bromide, or lithiated (trimethylsilyl)butadiyne (Li–C≡C–C≡C–$SiMe_3$), the desired product could not be detected.

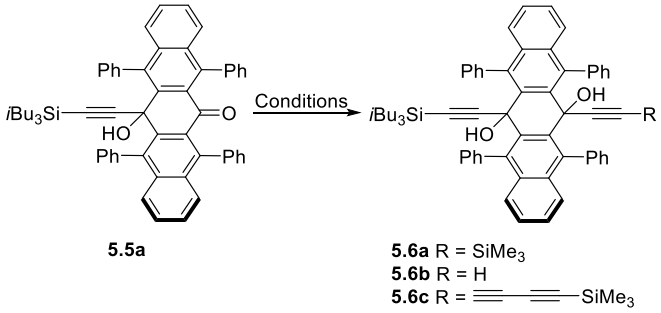

Scheme 5.3. Attempts to synthesize **5.6a–c**.

Table 5.2. Conditions Attempted for the Synthesis of **5.6a–c**

Entry	Reagent	Equivalent	Solvent	Temperature	Result
1	Li–C≡C–$SiMe_3$	30 equiv	Et_2O	–78 °C then rt	No reaction
2	Li–C≡C–$SiMe_3$ (Lithiated by *n*BuLi)	30 equiv	THF	–78 °C then rt	No reaction
3	Li–C≡C–$SiMe_3$ (Lithiated by LiHMDS)	30 equiv	THF	–78 °C then rt	No reaction
4	BrMg–C≡C–H	50 equiv	THF	0 °C then rt	No reaction
5	BrMg–C≡C–H	50 equiv	Et_2O	0 °C then rt	No reaction
6	Li–C≡C–C≡C–$SiMe_3$	10 equiv	Et_2O	–78 °C then rt	No reaction

An alternative route to achieve **5.6b** is shown in Scheme 5.4. The diethynyl-substituted pentacenequinone **5.7** was obtained successfully by adding ethynylmagnesium bromide to a suspension of **5.1** in dry THF at 0 °C. The reaction mixture was heated to reflux and stirred at reflux for 16 h. Heating was necessary, as the attempt with same conditions at rt failed to give the desired product. However, the unsymmetrical pentacene **5.6b** could not be obtained from the diethynyl intermediate **5.7**. The synthesis of **5.6b** from **5.5a** was attempted again under the refluxing conditions, but after aqueous workup no new compound was observed in the reaction mixture and only the starting material **5.5a** was recovered.

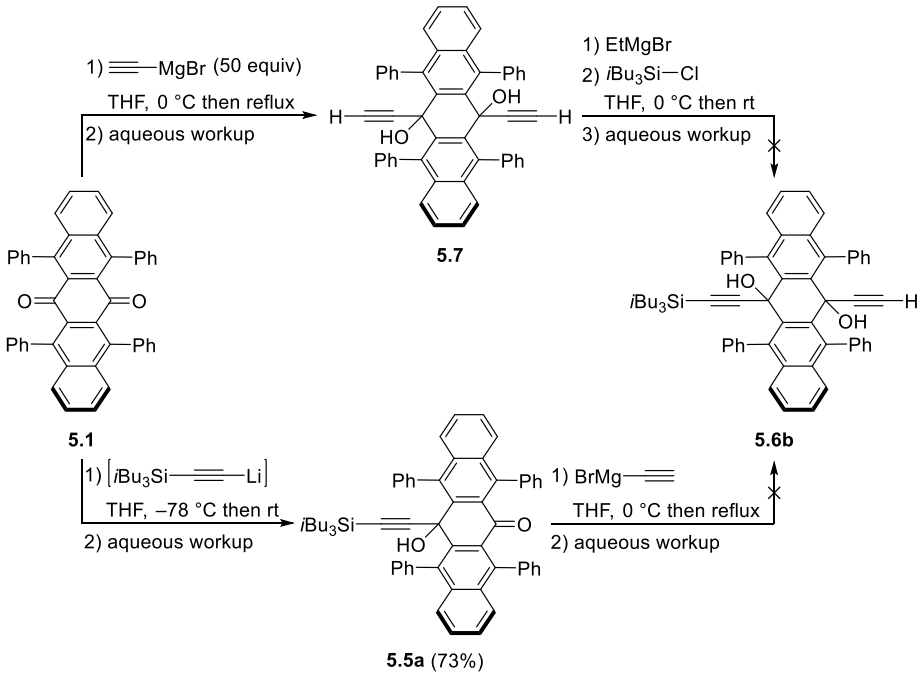

Scheme 5.4. Attempts to synthesize **5.6b**.

As **5.6b** could not be obtained, a homocoupling reaction of **5.8** was attempted first to form the butadiyne linker (Scheme 5.5). Desilylation of the mono-substituted product **5.5a** with tetrabutylammonium fluoride (TBAF) gave the ethynyl substituted product **5.8** cleanly as a white solid. Then, **5.8** was subjected to a standard Hay homocoupling reaction condition with CuI and TMEDA at rt.[14] The starting material **5.8** was consumed and a product with slightly lower R_f value was observed during the reaction, based on TLC analysis. However, instead of the desired product **5.9**, the pentacenequinone **5.1** was isolated after the reaction, based on ^{1}H NMR spectroscopic analysis, indicating that the acetylide was lost during the reaction. The loss of acetylide has been observed in other systems with sterically hindered endgroups.[15]

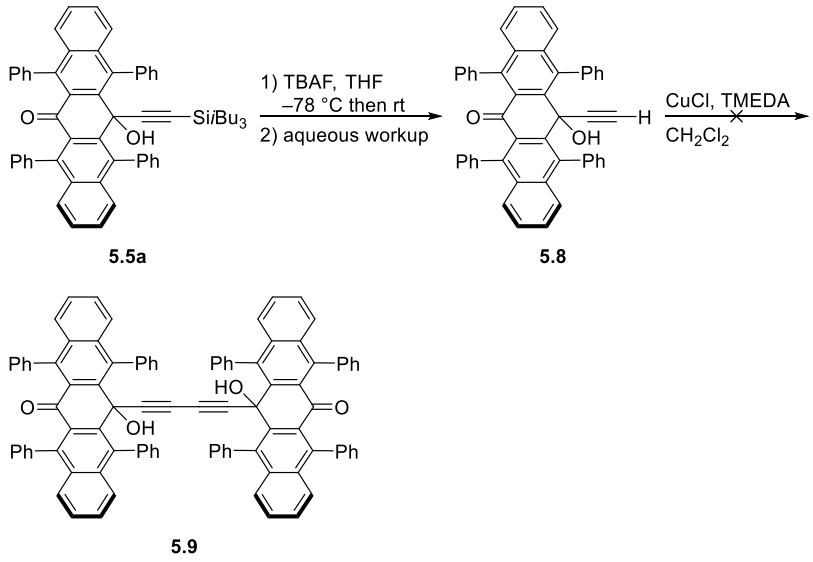

Scheme 5.5. Attempts to synthesize **5.9**.

In order to avoid the loss of acetylide, the hydroxy group in **5.5a** and **5.8** was replaced by a methoxy group. Ketone **5.10** was synthesized by adding lithiated (tri*iso*butylsilyl)acetylene to a suspension of 5,7,12,14-tetraphenyl-6,13-pentacenequinone (**5.1**) in dry THF at –78 °C; the resulting alkoxide was quenched by dimethyl sulfate. It is noted that dimethyl sulfate cannot be replaced by the other common methylation reagent methyl iodide. Quenching the reaction mixture with methyl iodide, followed by aqueous workup, gave **5.5a** instead of **5.10**. The terminal alkyne **5.11** was obtained by desilylation of the **5.10** with TBAF in wet THF (The crude product was dissolved in a small amount of CH_2Cl_2, and the solution was layered with MeOH. The product **5.10** was obtained after filtration as a white solid in 78% yield. In principle, the homocoupling reaction could be done successfully for **5.1,** as the methoxy group prevents the formation of pentacenequinone that was encountered in analogous reactions with the hydroxy analogue **5.8**. Hay homocoupling conditions were tried but without any success. Alternatively, Eglinton homocoupling conditions were attempted using $Cu(OAc)_2$, CuCl, and pyridine, which have been successful for the formation of other diynes bearing sterically hindered endgroups.[16] The homocoupled product **5.12** (Scheme 5.6) was obtained as a white solid in 92% yield via purification by column chromatography.

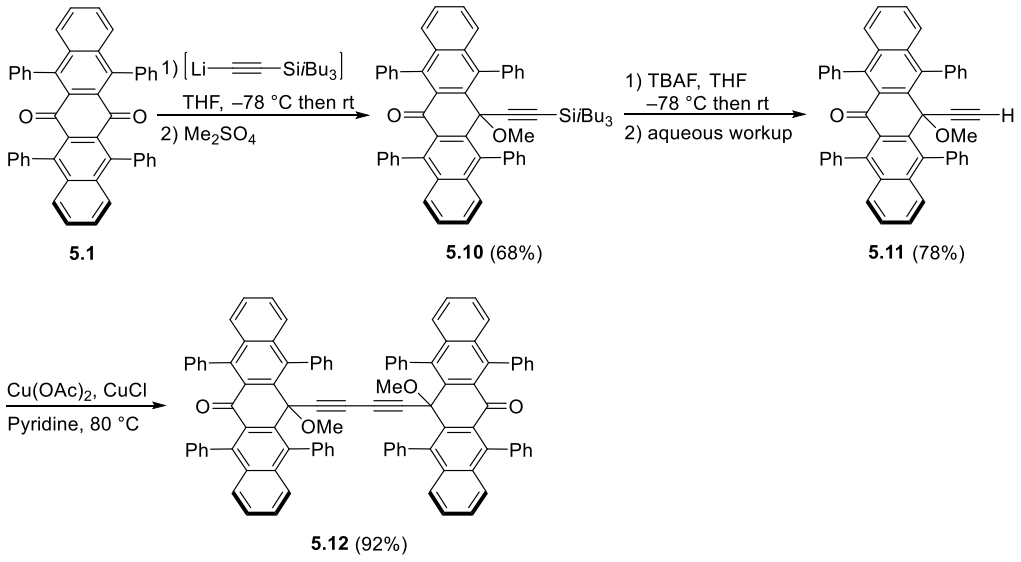

Scheme 5.6. Synthesis of **5.12**.

In principle, the two methoxy groups in the diyne intermediate **5.12** could be removed formally by a $SnCl_2$-mediated reductive elimination reaction with tin chloride, leading to the formation of a corresponding [5]cumulene **[5]tetraPh**. Thus, **[5]tetraPh** was synthesized by adding $SnCl_2$ and HCl (1.0 M in Et_2O) into a solution of **5.12** in CH_2Cl_2, followed by stirring at rt for 16 h (Scheme 5.7). The reaction mixture was passed through a pad of basic alumina with CH_2Cl_2. The desired product **[5]tetraPh** was purified by recrystallization (CH_2Cl_2/MeOH) and isolated in 70% yield as purple red crystals. Cumulene **[5]tetraPh** is soluble in common organic solvents, such as CH_2Cl_2, $CHCl_3$, THF, and toluene, and it is stable both as a solid and in solution under normal laboratory conditions.

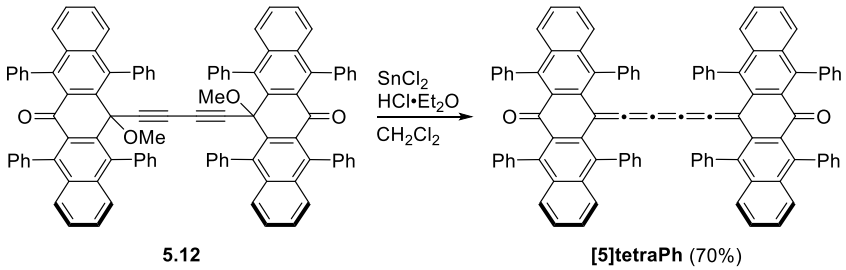

Scheme 5.7. Synthesis of **[5]tetraPh**.

The successful formation of **[5]tetraPh** has been confirmed by mass spectrometry (MS) combined with ^{1}H and ^{13}C NMR NMR spectroscopic analyses. MALDI HRMS analysis of **[5]tetraPh** is consistent with the proposed structure, showing a strong signal at *m/z* 1240.4281 (M^{+}, calcd for $C_{96}H_{56}O_2$ *m/z* 1240.4275). The ^{1}H NMR spectrum shows multiplets in the aromatic region, with a total integration of 14, and the disappearance of the signal of methoxy protons at ~3 ppm substantiates the successful reduction elimination reaction. The formation of [5]cumulene **[5]tetraPh** also has been confirmed by ^{13}C NMR spectroscopic analyses, which show peaks at δ 159.6, 133.3, and 116.8 arising from the cumulenic core.[17–18] Furthermore, the structure of **[5]tetraPh** is established unambiguously by X-ray crystallography (See Section 5.1.3 for detailed discussions).

Assembling a pentacene dimer bearing alkyne groups on both sides (**5.13**) was attempted with the diyne **5.12** (Scheme 5.8) under different conditions (Table 5.3). In all attempts, a large excess amount of nucleophile was used, and different solvents and reaction temperatures were tested. However, all experiments failed to give a detectable product, and only the starting material **5.12** was found and recovered after aqueous workup.

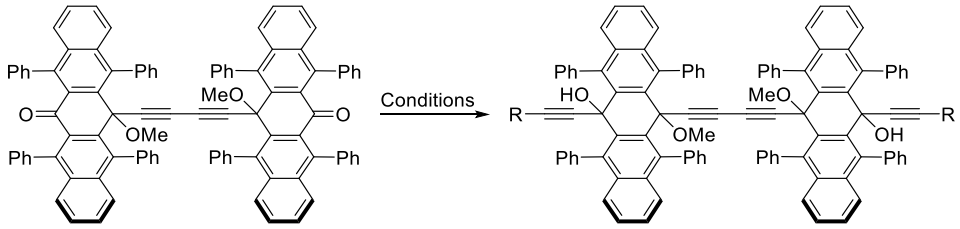

5.12

5.13a R = Si*i*Bu$_3$
5.13b R = Si*i*Pr$_3$
5.13c R = H

Scheme 5.8. Attempts to synthesize **5.13a–c**.

Table 5.3. Conditions Attempted for the Synthesis of **5.13a–c**

Entry	Reagent	Equivalent	Solvent	Temperature	Result
1	Li–C≡C–Si*i*Bu$_3$	30 equiv	Et_2O	–78 °C then rt	No reaction
2	Li–C≡C–Si*i*Bu$_3$	50 equiv	THF	–78 °C then reflux	No reaction
3	Li–C≡C–Si*i*Pr$_3$	100 equiv	Hexanes	–78 °C then reflux	No reaction
4	BrMg–C≡C–Si*i*Pr$_3$	100 equiv	THF	0 °C then reflux	No reaction
5	BrMg–C≡C–H	100 equiv	THF	0 °C then reflux	No reaction
6	Li–C≡C–SiMe$_3$ (Lithiated by LiHMDS)	200 equiv	Hexanes	0 °C then rt	No reaction

Alternatively, attempts were made to install an aryl group to the ketone **5.10** to form the unsymmetrically substituted pentacene **5.1,** as shown in Scheme 5.9. The successful use of phenyl lithium for reaction of the ketone between two phenyl groups in a similar system under reflux in benzene has been reported.[19] Thus, 4-*tert*-butylphenyl lithium was tested, in which the *tert*-butyl group was expected to improve the solubility of the product. Compound **5.14** was synthesized by adding 4-*tert*-butylphenyl lithium, which was formed in situ via a halogen-lithium exchange reaction with 4-*tert*-butylbromobenzene with *n*BuLi to a solution of **5.10** in dry THF at –78 °C. The reaction mixture was warmed to rt slowly and stirred at rt for 30 min. Compound **5.14** was obtained successfully after quenching the reaction with a saturated aqueous NH_4Cl solution. Desilylation of the **5.14** with TBAF gave the ethynyl substituted product **5.15** as a white solid via purification by column chromatography with silica gel. Then, **5.15** was subjected to Eglinton homocoupling reaction conditions with $Cu(OAc)_2$ and CuI in pyridine at 80 °C. The butadiyne linked dimer **5.16** was synthesized successfully. The crude product **5.16** was carried on directly to the next step without further purification. Subsequently, the diethynyl intermediate **5.16** was dissolved in THF and treated with $SnCl_2•2H_2O$ and 10% H_2SO_4 solution. The reaction was stirred at rt for 16 h, but there was no indication that the desired product was formed; i.e., the diagnostic blue or red colored of pentacene or cumulene did not appear. TLC analyses confirmed that only starting material **5.16** was present in the reaction mixture. Then, the reaction mixture was heated and stirred under reflux for another 24 h. However, the desired twisted pentacene dimer **5.17** did not form, and only the starting material **5.16** was found and recovered.

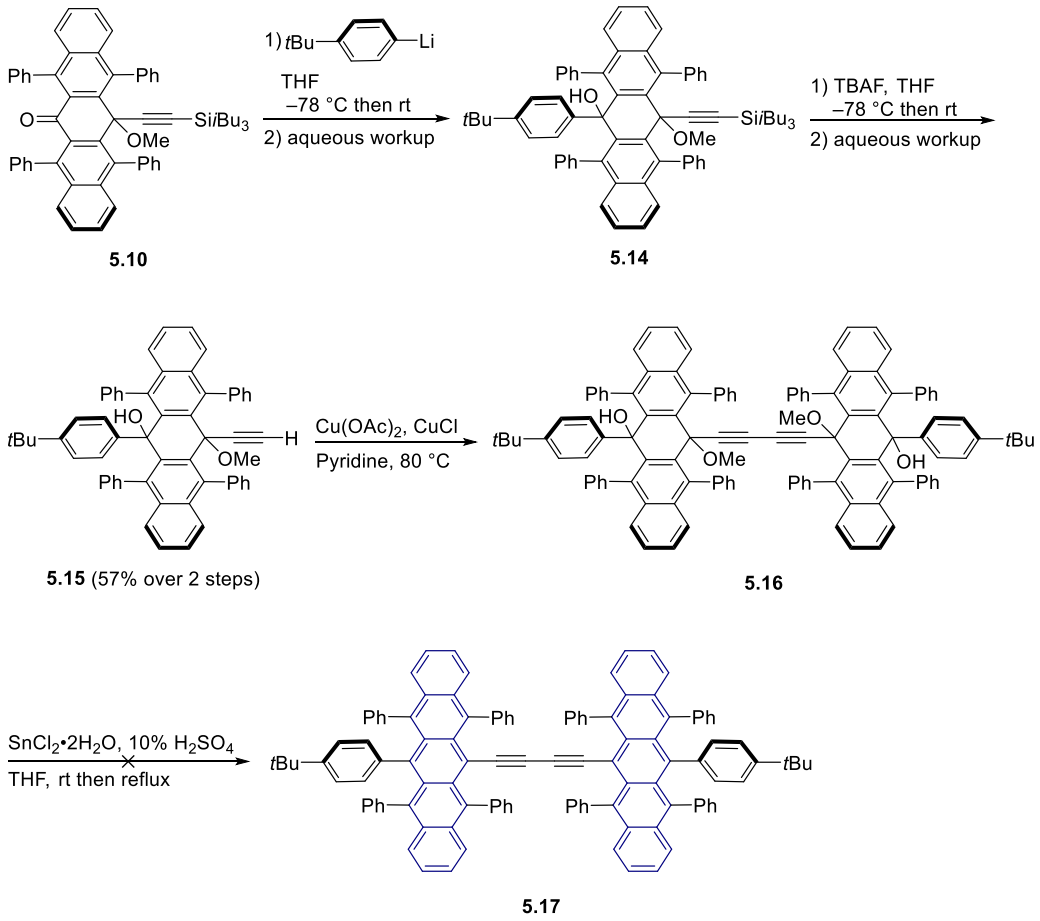

5.10 **5.14** **5.15** (57% over 2 steps) **5.16** **5.17**

Scheme 5.9. Attempts to synthesize **5.17**.

Interestingly, upon treatment of the solution of diethynyl intermediate **5.16** in CH_2Cl_2 with $SnCl_2$ and HCl (1.0 M in Et_2O), a [5]cumulene **5.18**, (Figure 5.4a) presumably was formed instead of pentacene, which was indicated by the red color of the reaction mixture (Figure 5.4b). The TLC analyses showed four spots. The top two red spots might correspond to two stereoisomers of **5.18**, while the bottom two yellow spots likely correspond to decomposition products. After stirring at rt for 2 h, the reaction mixture was passed through a pad of basic alumina with CH_2Cl_2. The resulting solution was concentrated under a flow of nitrogen and layered with MeOH for recrystallization. However, the possible [5]cumulene **5.18** presumably decomposed under these conditions, as no red compound was isolated, and the solution turned to brown from red. No further studies were conducted on this reaction due to time limitations.

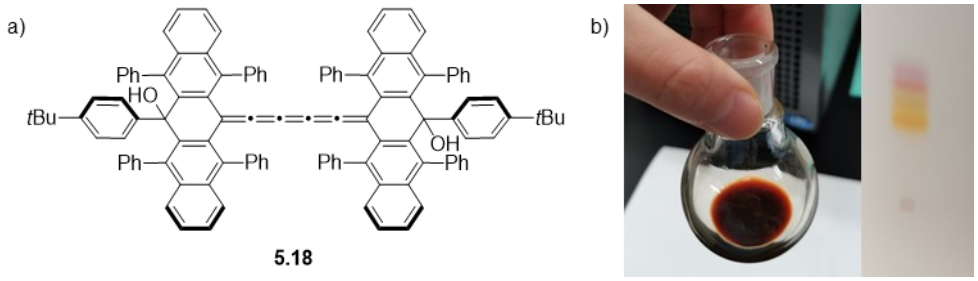

Figure 5.4. a) Structure of **5.18**; b) photo of the reaction mixture and TLC plate.

5.1.2.2 Attempts to Synthesize the Octaphenyl-Pentacene Dimer octaPh-(Pc)$_2$

As shown in Figure 5.2, the alternative design was to substitute the molecule at the outer ring (1,4,8,11-substituted) instead of the inner ring (5,7,12,14-substituted). In principle, the two carbonyl groups should be more accessible for nucleophilic addition in 1,4,8,11-substituted-pentacenequinone, which makes the formation of pentacene bearing alkyne groups on both sides possible. For the simplicity of the synthesis, **octaPh-(Pc)$_2$** was targeted, which started with 1,2,3,4,8,9,10,11-octaphenyl-pentacenequinone (**5.19**, Figure 5.5).

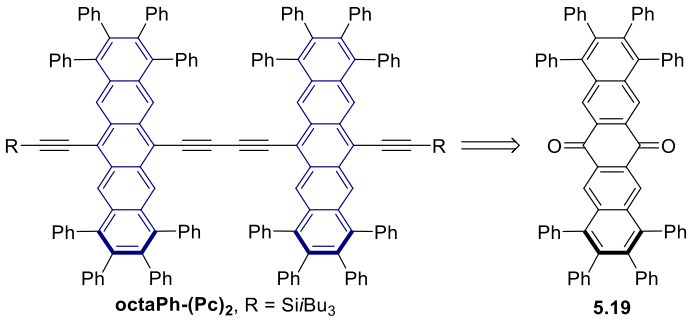

Figure 5.5. Structures of the target molecule **octaPh-(Pc)$_2$** and its precursor **5.19**.

The synthesis of the 1,4,8,11-octaphenyl-pentacenequinone (**5.19**) was carried out by adapting the procedure of Llorente et al, (Scheme 5.10).[20] A Diels–Alder reaction between tetraphenylcyclopentadienone (**5.20**) and dimethyl acetylenedicarboxylate (**5.21**) in 1,2-dichlorobenzene at reflux for 13 h gave compound **5.22**, which was formed via thermal decomposition of the bicyclic Diels–Alder product via loss of carbon monoxide.[21] Compound **5.22** was reduced to the diol **5.23** by reaction with $LiAlH_4$, followed by aqueous workup.[22] Bromination of **5.23** with PBr_3 in toluene gave **5.24** in 54% yield.[22] Reaction of **5.24** with *p*-benzenequinone (**5.25**)

with the presence of NaI in anhydrous DMF at 90 °C for 19 h gave the desired pentacenequinone **5.19**, which precipitated out of the reaction mixture after the reaction and was collected by filtration and washed with water and then acetone.

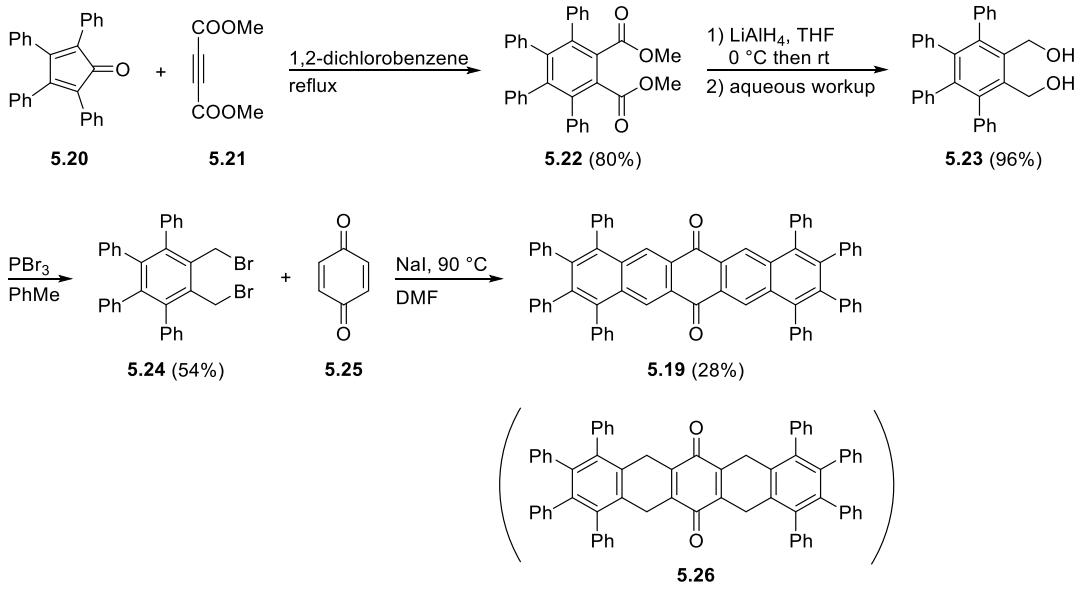

Scheme 5.10. Synthesis of **5.19**.

However, the solubility of **5.19** was extremely poor in common organic solvents, such as CH_2Cl_2, $CHCl_3$, THF, EtOAc, MeOH, 1,2-dibromoethane, acetonitrile, and toluene. The solution was not sufficiently soluble for meaningful ^1H NMR spectroscopic analyses. The composition of **5.19** was, however, confirmed by MS analysis (Figure 5.6). MALDI HRMS analysis of **5.19** was consistent with the proposed structure, showing signals at *m/z* 916.3328 and 917.3410 for M^+ and $[M + H]^+$, respectively, calcd for $C_{70}H_{44}O_2$ *m/z* 916.3336 and $C_{70}H_{45}O_2$ *m/z* 917.3419). Besides the desired compound **5.19**, additional signals correlated to $C_{70}H_{46}O_2$ (*m/z* 918.3431), $C_{70}H_{48}O_2$ (*m/z* 920.3643), $C_{70}H_{50}O_2$ (*m/z* 922.3801), and $C_{70}H_{52}O_2$ (*m/z* 9224.3863, **5.26**), indicating that the reaction presumably did not go to completion.

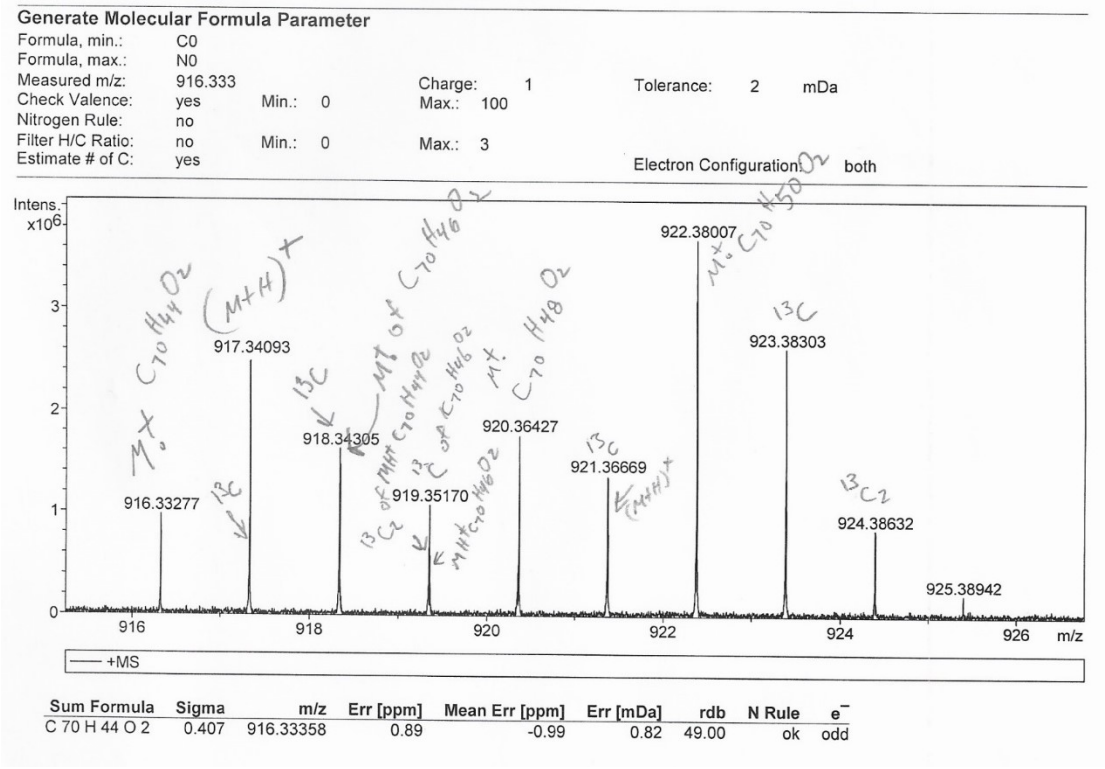

Figure 5.6. HRMS of compound **5.19**.

Despite the poor solubility of pentacenequinone **5.19**, a standard nucleophilic addition reaction was attempted to form the mono-substituted product **5.27** by adding lithiated trimethylsilylacetylene to a suspension of **5.19** in dry THF at –78 °C (Scheme 5.11). The reaction mixture was warmed up to rt and stirred at rt for 16 h. However, only the starting material **5.19** was observed from the reaction, and it was recovered after the aqueous workup.

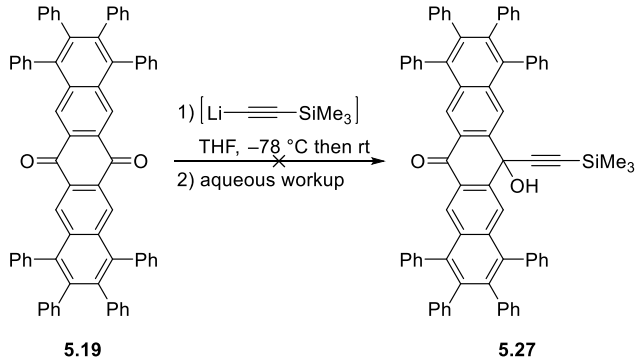

Scheme 5.11. Attempts to synthesize **5.27**.

5.1.2.3 Attempts to Synthesize the Octa*tert*-Butylphenyl-Pentacene Dimer octa*t*BuPh-(Pc)$_2$

As the failure of formation of **5.27** is presumably due to the poor solubility of **5.19**, 5,7,12,14-tetra*tert*-butylphenyl-pentacene dimer **octa*t*BuPh-(Pc)$_2$** was designed (Figure 5.7). The *tert*-butyl group on the phenyl could improve the solubility of the molecule.

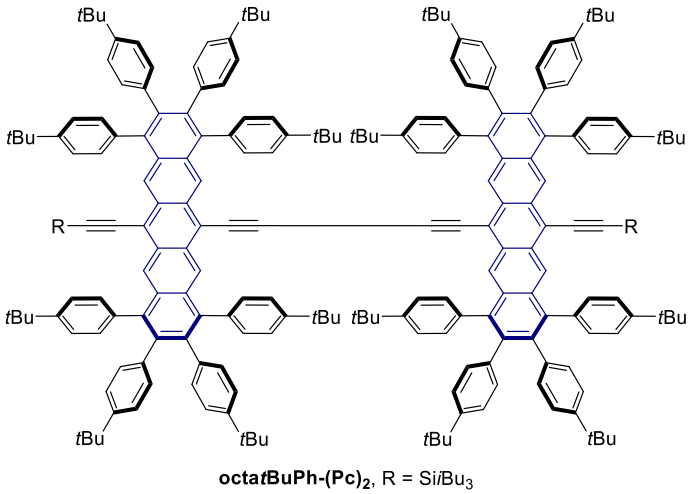

Figure 5.7. Structure of **octa*t*BuPh-(Pc)$_2$**.

In order to synthesize the **octa*t*BuPh-(Pc)$_2$**, the corresponding pentacenequinone must be obtained first, which started with **5.28**, the *tert*-butylpheneyl analogue of **5.22**. With compound **5.28** in hand, the desired pentacenequinone could be formed following the synthetic routine shown in Scheme 5.10. As outlined in Scheme 5.12, commercially available tetrabromophthalic anhydride (**5.29**) was heated to reflux in potassium hydroxide solution for 30 min, followed by acidic workup. The diacid **5.30** precipitated out from the reaction mixture and was isolated by filtration. The white solid was dried under vacuum and carried on to the next step without further purification. Compound **5.31** was formed by adding Me_2SO_4 and di*iso*propylethylamine to a solution of **5.30** in DMF. The reaction mixture was heated to 85 °C and stirred for 1 h. Then, compound **5.28** was obtained by a Suzuki cross-coupling reaction with compound **5.31** and 2-(4-*tert*-butylphenyl)-4,4,5,5-tetramethyl-1,3,2-dioxaborolane in the presence of $Pd(PPh_3)_4$ and K_2CO_3 in 1,4-dioxane, followed by purification with column chromatography and recrystallization. As shown in Figure

5.8, the successful formation of **5.28** has been confirmed by ^{1}H NMR spectroscopy, which shows two sets of two pseudo-first-order doublets with integration of 2H for the two AA'BB' systems of the aryl protons, one singlet with integration of 3H for the methoxy group, and two singlets with integration of 9H arising from the *tert*-butyl groups.

In principle, **5.28** could be carried on for the synthesis of 1,2,3,4,8,9,10,11-octa*tert*buylphenyl-pentacenequinone and then the desired twisted pentacene dimer. However, this project was discontinued due to a lack of time.

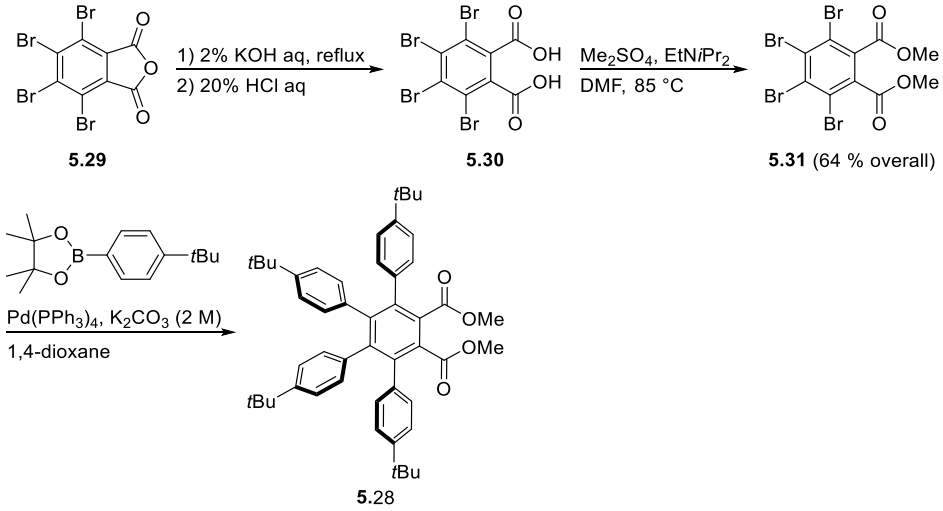

Scheme 5.12. Synthesis of **5.31**.

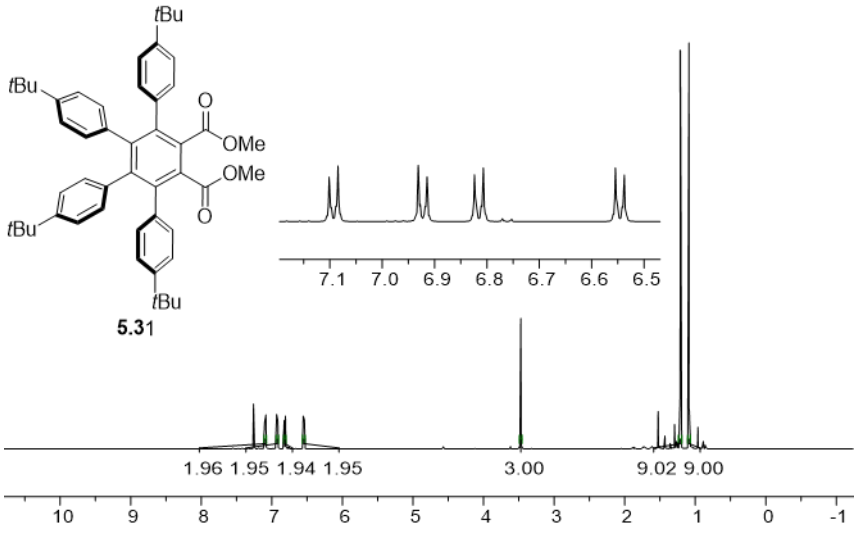

Figure 5.8. ^{1}H NMR spectrum of **5.31** in $CDCl_3$.

5.1.3 X-ray Crystallographic Analysis of [5]tetraPh

X-ray crystallographic analysis has been successful in confirming the proposed structure for the [5]cumulene **[5]tetraPh**. The single crystal of **[5]tetraPh** suitable for crystallographic analysis was obtained successfully by slow evaporation at room temperature from a CH_2Cl_2 solution layered with MeOH. As shown in Figure 5.9, the core is not planar (~150° between two naphthalene planes), adopting a "so-called" butterfly conformation.[18] This is contrary to the conformation of [3]cumulenes bearing unsubstituted pentacenequinonone groups, which are planar. The no planar structure of **[5]tetraPh** presumably results from steric interactions from the pendent phenyl groups. The eight phenyl substituents on **[5]tetraPh** are not coplanar with the naphthalene cores, with a large torsion angle in the range of 59–83°.

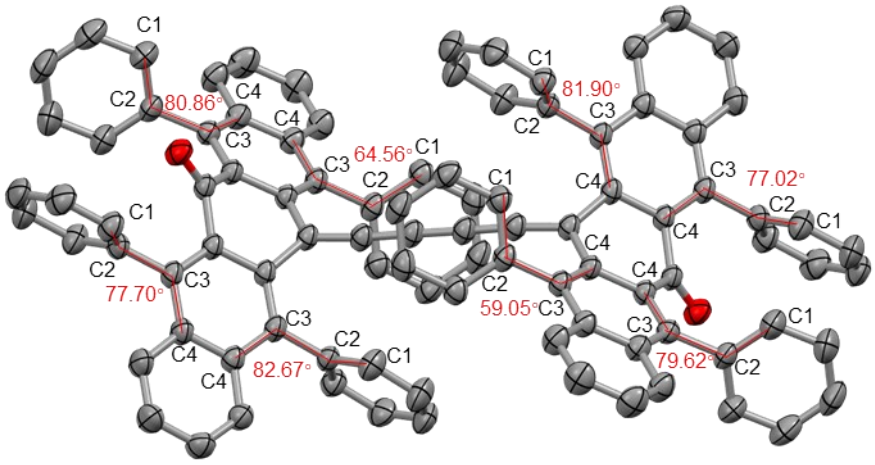

Figure 5.9. ORTEP drawing of **[5]tetraPh** with torsion angle of C1–C2–C3–C4. Non-hydrogen atoms are represented by Gaussian ellipsoids at the 30% probability level. For clarity, hydrogen atoms are omitted.

As shown in Figure 5.10a, H-bonds are observed between the oxygen atoms and hydrogens of the phenyl rings in the crystal packing for **[5]tetraPh** with a distance of 2.556 Å. Analysis of the crystal packing also shows intermolecular short contacts between the phenyl ring and naphthalene. [23] The distance between the naphthalene hydrogen and the phenyl carbon is 2.897 Å (Figure 5.10b).

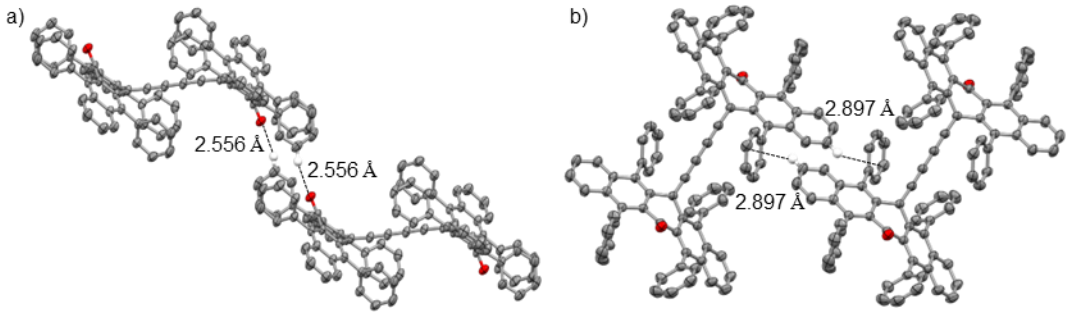

Figure 5.10. X-ray crystal structures with a) H-bonds; b) intermolecular short contacts between the. phenyl ring and naphthalene. Non-hydrogen atoms are represented by Gaussian ellipsoids at the 30% probability level. For clarity, non-interacting hydrogen atoms are omitted.

5.1.4 UV-vis Spectroscopic Analysis of [5]tetraPh

The qualitative UV-vis spectrum of the [5]cumulene **[5]tetraPh** has been measured in CH_2Cl_2 at room temperature (Figure 5.11). The spectrum shows absorption bands in both the high energy region between 250–400 nm, which corresponds to the pentacenequinone moieties, and the lower energy region between 400–650 nm, corresponding to cumulene core. The absorption maximum for **[5]tetraPh** (λ_{max} = 566 nm) is red-shifted in comparison to tetraphenyl [5]cumulene (**[5]Ph**, λ_{max} = 488 nm in benzene)[24], presumably due to the increased conjugation length through the pentacenequinone.

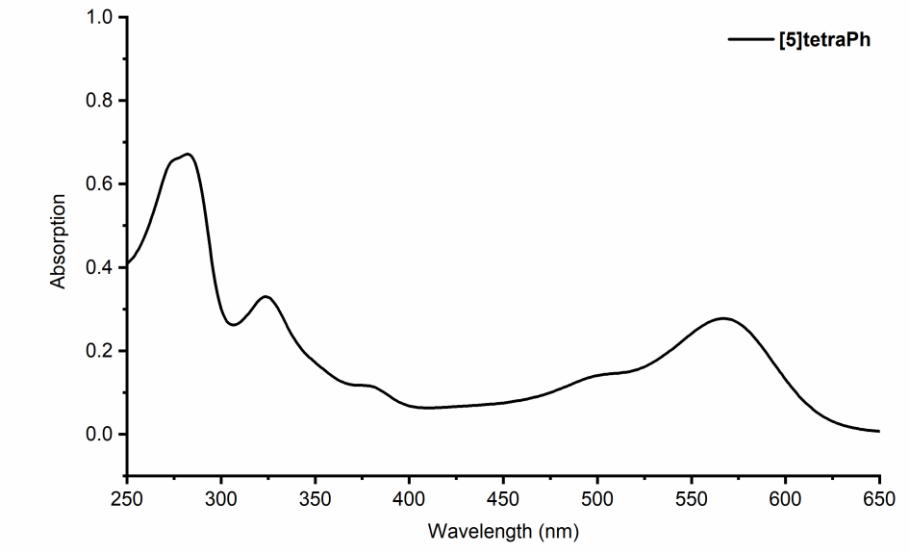

Figure 5.11. UV-vis spectrum of **[5]tetraPh** in CH_2Cl_2.

5.1.4 Summary

In summary, three rotationally restricted pentacene dimers linked by a butadiynyl group **tetraPh-(Pc)$_2$**, **octaPh-(Pc)$_2$**, and **octa*t*BuPh-(Pc)$_2$** have been designed and their synthesis attempted. In principle, these cumulenes could serve as model compounds for the study of rotational effect on the process of iSF

The corresponding 5,7,12,14-tetraphenyl-6,13-pentacenequinone (**5.1**) for the synthesis of the pentacene dimer **tetraPh-(Pc)$_2$** has been obtained successfully through a Diels–Alder reaction, followed by dehydration. However, the unsymmetrical pentacene (**5.6b**) cannot be formed from either the monoethynyl intermediate (**5.8**), obtained by desilylation of **5.5a** with TBAF, or the diethynyl intermediate (**5.7**). Under conditions that were attempted, the homo-coupling reaction of **5.8** to form the dimer **5.9** was unsuccessful. When replacing the hydroxy group in **5.8** with methoxy group (**5.11**), the homo-coupling reaction can be done successfully. The methoxy group in **5.11** prevents the reversion to pentacenequinone **5.1** by based catalyzed extrusion of the acetylide, which is encountered in analogous reactions with the hydroxy analogue **5.8**. In the final step, the diethynyl intermediate **5.12** can be reduced to the [5]cumulene **[5]tetraPh** by reaction with tin chloride.

The successful synthesis of **[5]tetraPh** has been confirmed by mass spectrometry combined with ^{1}H and ^{13}C NMR spectroscopic analyses. The structure of **[5]tetraPh** also has been established by X-ray crystallographic analysis.

Alternatively, 1,2,3,4,8,9,10,11-octaphenyl-pentacenequinone (**5.19**) with less sterically hindered ketones was targeted for the synthesis of **octaPh-(Pc)$_2$**. The successful synthesis of **5.19** has been confirmed by mass spectrometry. However, due to the extremely poor solubility of **5.19**, the mono-substituted intermediate **5.27** has not been reached.

In order to improve the solubility of the pentacenequinone **5.19**, *tert*butyl had been installed on the phenyl, leading to the synthesis of **octa*t*BuPh-(Pc)$_2$**. The precursor **5.28** for the synthesis of pentacenequinone has been obtained by a Suzuki cross-coupling reaction. The successful formation of **5.28** was confirmed by ^{1}H NMR spectroscopy. However, the synthesis of 1,2,3,4,8,9,10,11-octa*tert*buylphenylene-

pentacenequinone and then **octa*t*BuPh-(Pc)$_2$** has not been attempted due to time limitations.

5.2 Synthesis of an Azobenzene-linked Pentacene Dimer

5.2.1 Introduction

The spacer between two pentacene moieties in pentacene dimer is critical to tune the geometry, distance, and electronic coupling of pentacene dimers, which allows studies of the underlying mechanism of iSF (See Chapter 1 for detailed discussion). Azobenzene and its derivatives are known as molecular photoswitches. The switchable nature of azo group in photoisomerization reactions allows tuning the configuration of molecules and, thus, the spatial arrangement between substituents on azo group.[25–27] In order to incorporate this photoswitchable feature into a pentacene dimer for iSF, a pentacenes linked by azobenzene **azo-Pc$_2$** has been proposed. Upon irradiation with light, this dimer could, in principle, isomerize between the cis- and trans-isomers (Figure 5.12). In these two isomers, the through bond interaction between two pentacene moieties is the same, while the through space interaction is different, which could result in different processes of iSF. As well, the symmetry and dipole moment changes significantly as a function of geometry, which also could influence iSF. Therefore, this system has a potential to serve as a photoswitch for iSF.

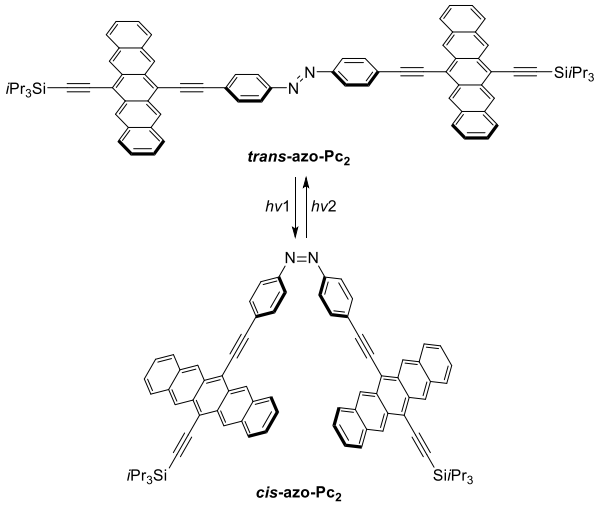

Figure 5.12. Structures of azobenzene-linked pentacene dimers ***trans*-azo-Pc$_2$** and ***cis*-azo-Pc$_2$**.

5.2.2 Synthesis of the Azobenzene-linked Pentacene Dimer

As shown is Scheme 5.13, a Sonogashira cross-coupling reaction with compound **5.32**[10] and **5.33**[28] with the presence of $Pd(PPh_3)_4$, CuI, and di*iso*propylamine in THF gave the intermediate **5.34**. As all diastereoisomers of **5.34** produced in this reaction would give rise to the same product following the next reaction step, the crude product was passed through a pad of silica gel with THF and carried on without separation to a $SnCl_2$-mediated reductive aromatization. The ***trans*-azo-Pc$_2$** was purified by column chromatography with silica gel and recrystallization (CH_2Cl_2/MeOH) and isolated as a dark blue solid in 62% yield. The formation of ***trans*-azo-Pc$_2$** was confirmed by ^{1}H NMR spectroscopy (Figure 5.13). It is noticed that two singlets in the aromatic region arising from pentacene are distinguishable. However, the AA'BB' systems of pentacene protons and phenylene protons are overlapping, leading to challenging assignments.

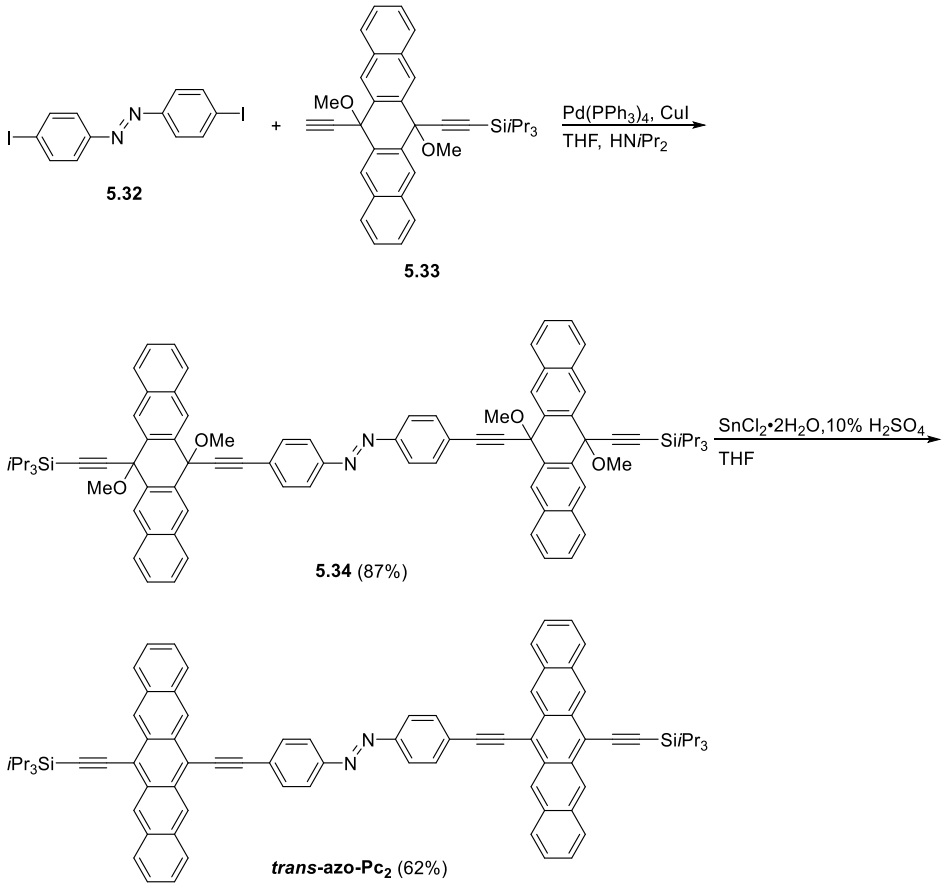

Scheme 5.13. Synthesis of ***trans*-azo-Pc$_2$**.

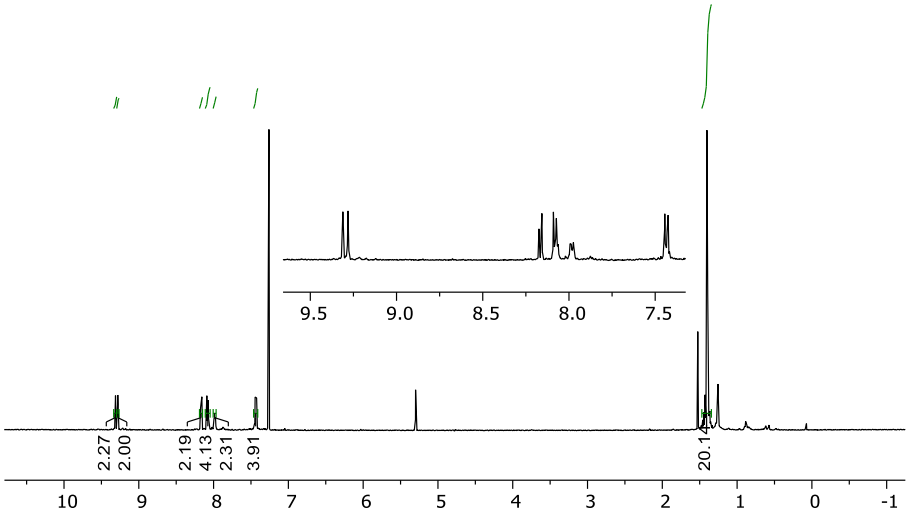

Figure 5.13. ^{1}H NMR spectrum of ***trans*-azo-Pc$_2$** in $CDCl_3$.

5.2.3 Photoswitching Studies of azo-Pc$_2$ and Its Precursor 5.34

Several preliminary studies of photoswitching of ***trans*-azo-Pc$_2$** and **5.34** have been performed. However, they were discontinued because of a lack of time. The unaromatized pentacene precursor **5.34** served as a reference compound for the evaluating the photoswitching. When irradiated at 365 nm, the absorptions at 246 nm and 372 nm for **5.34** diminished, while an absorption at 309 nm increased, indicating trans-cis switching.[29–30] Meanwhile, a shoulder peak above 425 nm was appearing upon irradiation (Figure 5.14).

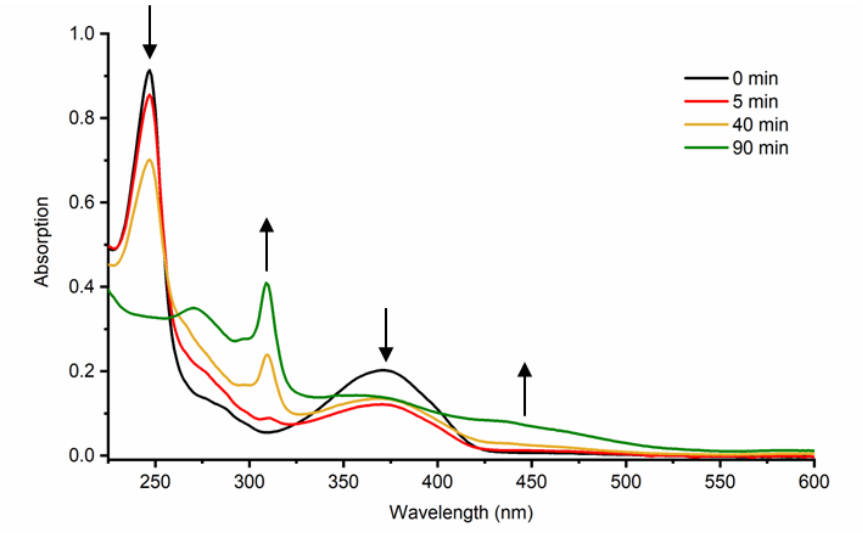

Figure 5.14. UV-vis spectral changes of **5.34** in CH_2Cl_2 upon irradiation at 365 nm.

As the precursor **5.34** showed photoswitching, the azobenzene-linked pentacene dimer ***trans*-azo-Pc2** was tested. Initially, ***trans*-azo-Pc2** was irradiated at 365 as well. However, in this case the ***trans*-azo-Pc2** decomposed immediately, as indicated by disappearance of the blue color of pentacene from the solution. Alternatively, lower energy light at 450 nm was tested. As shown in Figure 5.15, when irradiating at 450 nm, no obvious changes were observed.

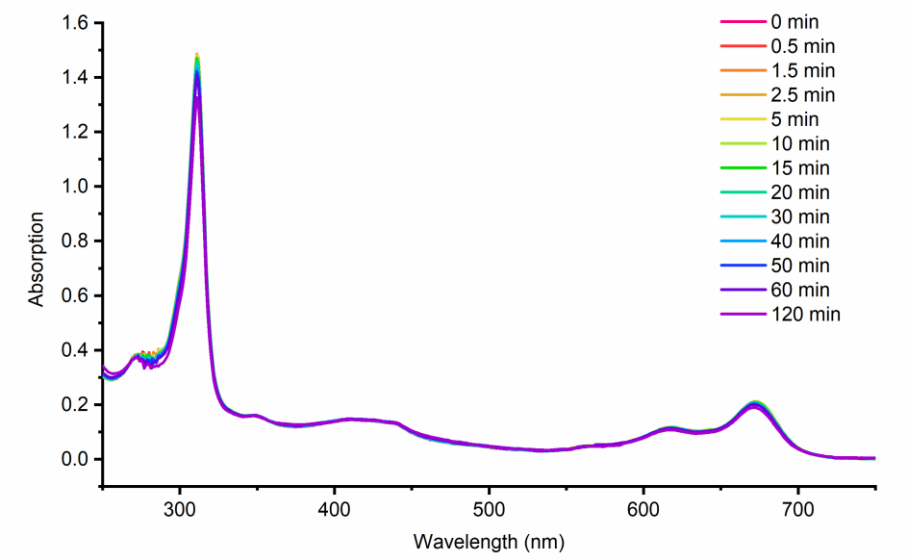

Figure 5.15. UV-vis spectral changes of ***trans*-azo-Pc2** in CH_2Cl_2 upon irradiation at 450 nm.

When irradiating of ***trans*-azo-Pc2** at 400 nm, the peaks at 373 nm and 450 nm increased while the peaks at 311 nm and 405 nm decreased, which might correlate to photoswitch of azo group. However, the lower energy peaks at 566, 614, 673 nm also diminished, consistent with the decomposition of the pentacene chomophore(s) (Figure 5.16).

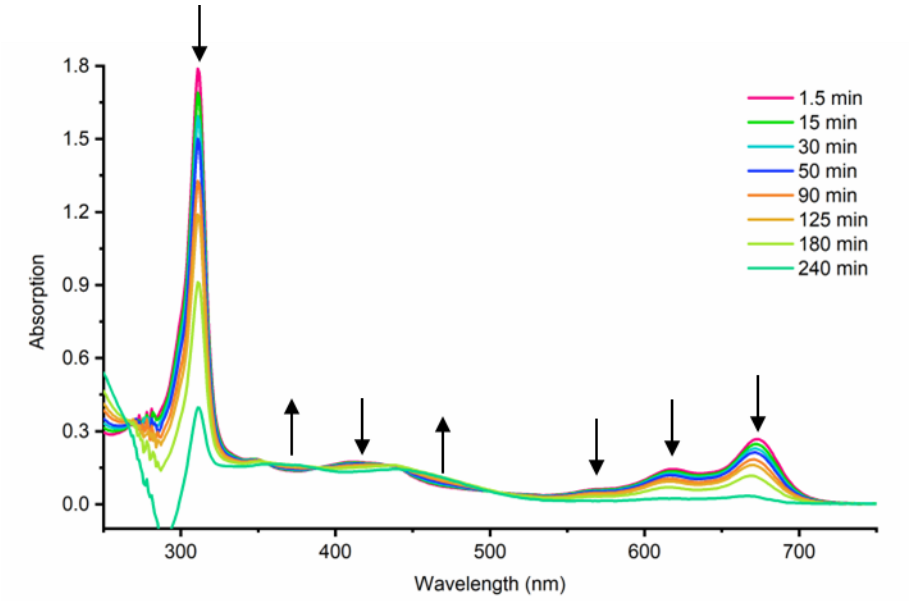

Figure 5.16. UV-vis spectral changes of ***trans*-azo-Pc$_2$** in CH_2Cl_2 upon irradiation at 400 nm.

5.2.4 Summary

In summary, a pentacene dimer linked by azobenzene ***trans*-azo-Pc$_2$** has been synthesized successfully through a Sonogashira reaction with the bis(4-iodophenyl)diazene (**5.32**) and the unsymmetrically substituted pentacenequinone **5.33.** The successful formation of ***trans*-azo-Pc$_2$** is confirmed by ^{1}H NMR spectroscopy. Preliminary studies of photoswitching of the unaromatized precursor **5.34** with irradiation at 365 nm shows trans to cis isomerization. However, preliminary studies of photoswitching of ***trans*-azo-Pc$_2$** with irradiation at 365, 400, and 450 nm indicates that decomposition of the pentacene moieties effectively competes with switching.

5.3 Synthesis of Tetracene Metal Complexes‡

5.3.1 Introduction

The results in Chapter 2 show that iSF is operative in both pentacene dimers **Pt(L$_{pc}$)$_2$Cl$_2$** and **Pd(L$_{pc}$)$_2$Cl$_2$**, despite a rather large inter-pentacene separation as well as enhanced spin-orbit coupling from the presence of heavy atoms. The third row transition metal Pt(II) facilitates inter-pentacene electronic communication that leads to iSF in the dimer **Pt(L$_{pc}$)$_2$Cl$_2$** via a direct mechanism. On the other hand, in the second

‡ This work was done in collaboration with Melchor Matabuena, an undergraduate under my supervision for his CHEM 401/403 project during the 2021–2022 academic year.

row transition metal Pd(II) with weaker electronic communication, iSF is through a mechanism that requires a mediating species in polar solvents. Unlike pentacenes, the energy of lowest singlet excited state of tetracenes is about twice the energy of their triplet excited state, which makes these acenes capable for both SF and triplet-triplet annihilation upconversion (TTA-UC), as described in Chapter 3. To study the heavy-atom effect (HAE) in tetracene dimers in both SF and TTA-UC, the tetracene analogues of the pentacene dimers (**Pt(L_{tc})$_2$Cl$_2$** and **Pd(L_{tc})$_2$Cl$_2$**) have been synthesized.

5.3.2 Synthesis of Platinum- and Palladium-based Tetracene Dimers

As shown in Scheme 5.14, the pyridyl-endcapped tetracene ligand (**L_{tc}**) was synthesized using a stepwise nucleophilic substitution of 5,12-napthacenequinone (**5.35**). Ketone **5.36** was synthesized using the analogous procedure as the pentacenequinone derivative **2.9**.[31] The addition of lithiated tri*iso*butylsilylacetylene to a suspension of 5,12-tetracenequinone (**5.35**) in dry THF at –78 °C, followed by quenching the resulting alkoxide with methyl iodide, gave **5.36** in 75% yield. The acetylide form compound **2.7** was formed by reaction with lithium hexamethyldisilazide (LiHMDS), which was prepared in situ by adding *n*BuLi to a solution of $[(CH_3)_3Si]_2NH$ in dry THF at –78 °C. Then, the acetylide mixture was added to a solution of ketone **5.36** in dry THF at –78 °C and stirred for 16 h at rt. Compound **5.37** was formed as a pair of diastereoisomers after quenching the reaction with a saturated aqueous NH_4Cl solution. The crude product was passed through a pad with silica gel with THF before conducting reductive aromatization. The $SnCl_2$-mediated reductive aromatization gave the pyridyl-endcapped tetracene ligand (**L_{tc}**) as a red solid in 63% yield.

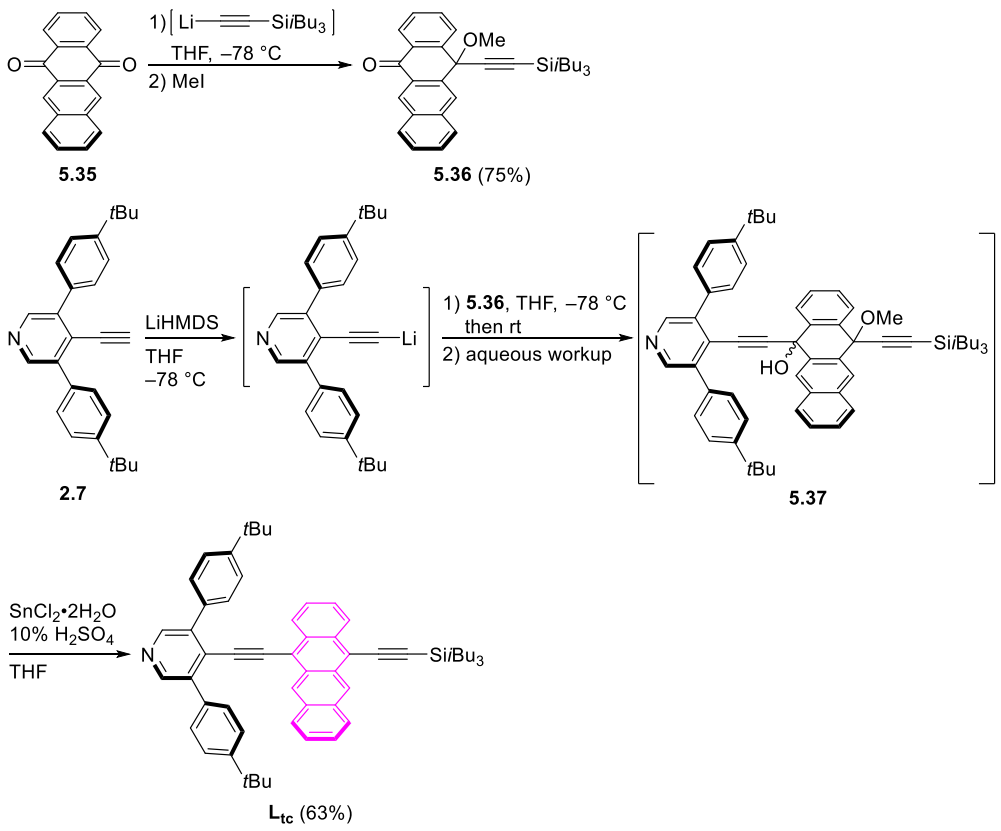

Scheme 5.14. Synthesis of $\mathbf{L_{tc}}$.

With the ligand $\mathbf{L_{tc}}$ in hand, the desired tetracene dimers were synthesized by the ligand exchange reaction of the ligands $\mathbf{L_{tc}}$ with $Pt(PhCN)_2Cl_2$ and $Pd(PhCN)_2Cl_2$ (Scheme 5.15). Bis(benzonitrile)platinum(II) dichloride ($Pt(PhCN)_2Cl_2$)[32] and bis(benzonitrile)palladium(II) dichloride ($Pd(PhCN)_2Cl_2$)[33] were prepared by the procedures reported in the literature. Reaction of $Pt(PhCN)_2Cl_2$ with $\mathbf{L_{tc}}$ in dry toluene at 80 °C gave $\mathbf{Pt(L_{tc})_2Cl_2}$ in 82% yield as purple crystals following chromatographic purification (alumina) and recrystallization (CH_2Cl_2/MeOH). $\mathbf{Pd(L_{tc})_2Cl_2}$ was synthesized from $Pd(PhCN)_2Cl_2$ via the ligand-exchange reaction with $\mathbf{L_{tc}}$ in CH_2Cl_2 at rt. The complex $\mathbf{Pd(L_{tc})_2Cl_2}$ was purified by column chromatography on alumina, followed by recrystallization, and it was isolated as purple crystals in 79% yield.

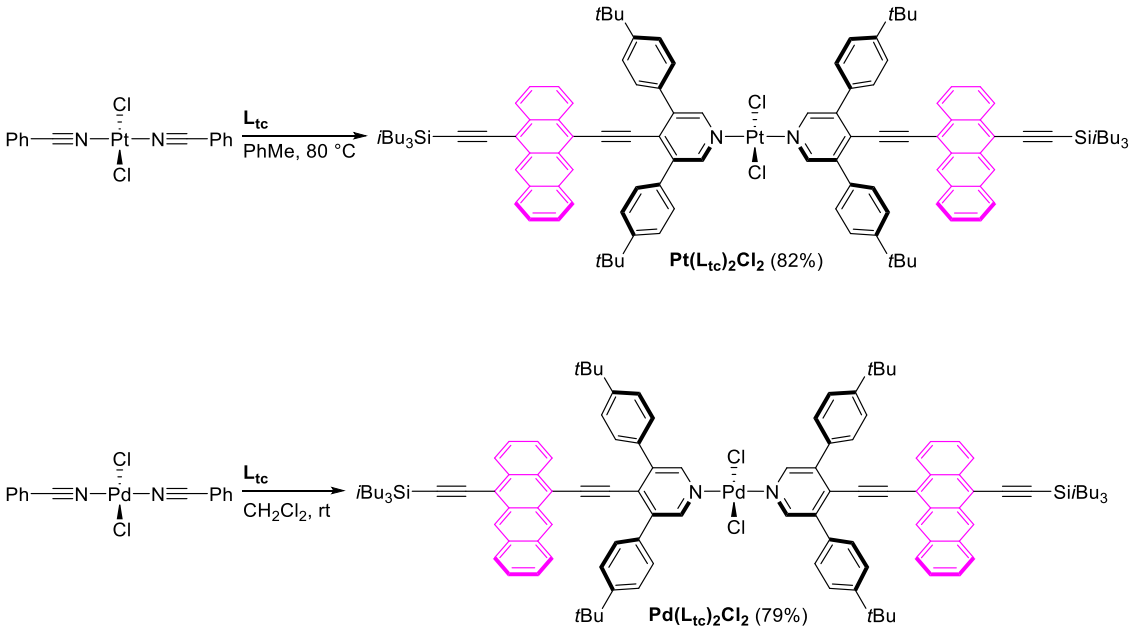

Scheme 5.15. Synthesis of symmetric dimers $\mathbf{Pt(L_{tc})_2Cl_2}$ and $\mathbf{Pd(L_{tc})_2Cl_2}$.

The successful formation of the pyridyl-tetracene ligand $\mathbf{L_{tc}}$ and the desired metal complexes $\mathbf{Pt(L_{tc})_2Cl_2}$ and $\mathbf{Pd(L_{tc})_2Cl_2}$ has been confirmed by mass spectrometry (MS) combined with ^{1}H and ^{13}C NMR spectroscopic analyses. All products are stable as solids under normal laboratory conditions, but they decompose in solution upon exposure to air (O_2) and light over days, as is typical for tetracene derivatives.

5.3.3 Characterization

5.3.3.1 ^{1}H Spectroscopic Analysis

Similar to the pentacene dimers $\mathbf{Pt(L_{pc})_2Cl_2}$ and $\mathbf{Pd(L_{pc})_2Cl_2}$, ^{1}H NMR spectra of $\mathbf{Pt(L_{tc})_2Cl_2}$ and $\mathbf{Pd(L_{tc})_2Cl_2}$ mirror the ^{1}H NMR spectrum of the ligand $\mathbf{L_{tc}}$, as the two organic ligands in the metal complexes are equivalent. It is easy to identify the signal of pyridyl protons (H_a) for the tetracene series since there is only one singlet with integration of 2H in the aromatic region (Figure 5.17). The signals of pyridyl protons in $\mathbf{Pt(L_{tc})_2Cl_2}$ (δ 8.98) and $\mathbf{Pd(L_{tc})_2Cl_2}$ (δ 8.90) are shifted downfield by 0.27 and 0.19 ppm for the Pt and Pd complexes, respectively, compared to the analogous protons of the free ligand $\mathbf{L_{tc}}$ (δ 8.71). The observed trends in ^{1}H shifts for the pyridyl groups are consistent with the pentacene analogues $\mathbf{Pt(L_{pc})_2Cl_2}$ and $\mathbf{Pd(L_{pc})_2Cl_2}$, which

indicate a decreased electron density upon metal coordination of a pyridyl ligand.[34–38] The greater deshielding of protons H_a when bound to Pt(II) in comparison to Pd(II) corresponds to the lower spin-orbit coupling for Pd due to its nuclear charge.[39–40]

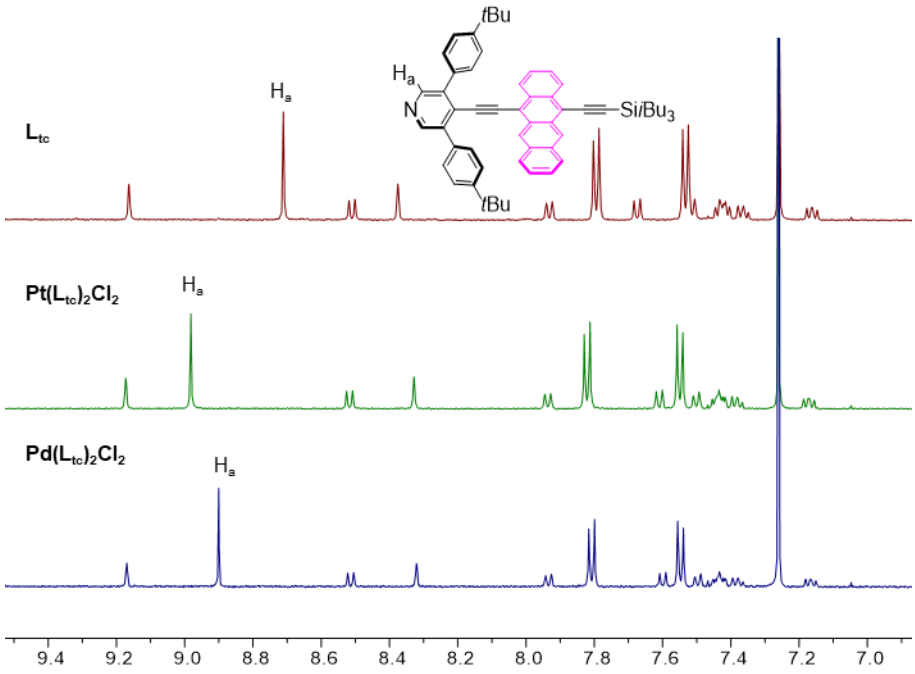

Figure 5.17. Stacked plot of the aromatic region of ^{1}H NMR spectra of **L$_{tc}$**, **Pt(L$_{tc}$)$_2$Cl$_2$**, and **Pd(L$_{tc}$)$_2$Cl$_2$** in $CDCl_3$. Signals for protons on pyridyl are labeled with H_a.

5.3.3.2 UV-vis Spectroscopic Analysis

The quantitative UV-vis spectra of **L$_{tc}$**, **Pt(L$_{tc}$)$_2$Cl$_2$**, and **Pd(L$_{tc}$)$_2$Cl$_2$** have been measured in CH_2Cl_2 at room temperature (Figure 5.18). The absorptions profiles for **Pt(L$_{tc}$)$_2$Cl$_2$** (λ_{max} = 573 nm) and **Pd(L$_{tc}$)$_2$Cl$_2$** (λ_{max} = 571 nm) are similar, show reasonably well-resolved vibrational fine structure, and are slightly broadened compared to the free ligand **L$_{tc}$**. The λ_{max} absorption maximum for **Pt(L$_{tc}$)$_2$Cl$_2$** (λ_{max} = 573 nm) and **Pd(L$_{tc}$)$_2$Cl$_2$** (λ_{max} = 571 nm) are red-shifted in comparison to **L$_{tc}$** (λ_{max} = 555 nm), indicating a reasonably strong interaction with the metal center. The extinction coefficients of **Pt(L$_{tc}$)$_2$Cl$_2$** (75,200 L mol^{-1} cm^{-1}) and **Pd(L$_{tc}$)$_2$Cl$_2$** (71,800 L mol^{-1} cm^{-1}) (Table 5.4), which are approximately double the extinction coefficient of the ligand **L$_{pc}$** (34,600 L mol^{-1} cm^{-1}).

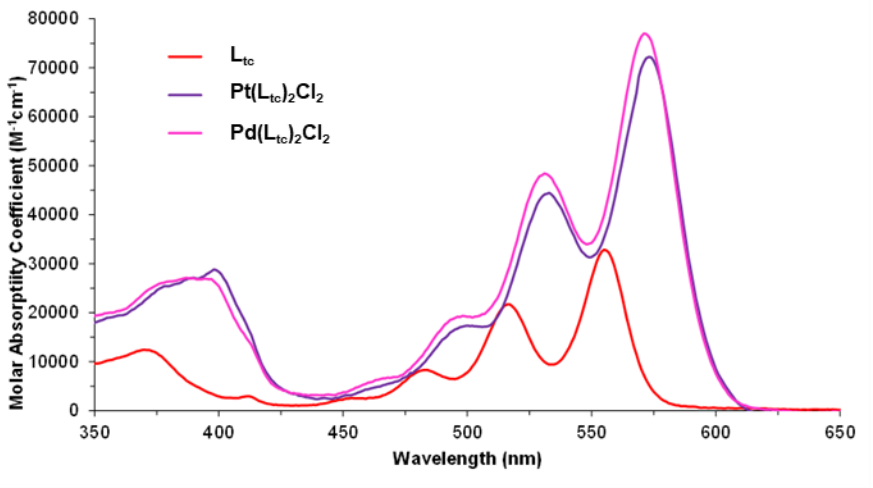

Figure 5.18. UV-vis spectra of **L_{tc}**, **$Pt(L_{tc})_2Cl_2$**, and **$Pd(L_{tc})_2Cl_2$** in CH_2Cl_2.

Table 5.4. Relevant UV-vis Data for **L_{tc}**, **$Pt(L_{tc})_2Cl_2$**,and **$Pd(L_{tc})_2Cl_2$**, as well as **L_{pc}**, **$Pt(L_{pc})_2Cl_2$**,and **$Pd(L_{pc})_2Cl_2$**

Metal	Compound	λ_{max} (nm)	ε (L mol^{-1} cm^{-1})
	L_{tc}	555	34,600
	L_{pc}	663	29,300
Pt	**$Pt(L_{tc})_2Cl_2$**	573	75,200
	$Pt(L_{pc})_2Cl_2$	679	63,500
Pd	**$Pd(L_{tc})_2Cl_2$**	571	71,800
	$Pd(L_{pc})_2Cl_2$	677	57,100

5.3.4 Summary

In summary, a pyridyl group has been appended to the tetracenyl chromophore, providing a ligand for the formation of complexes with platinum(II) and palladium(II). The dimeric systems **$Pt(L_{tc})_2Cl_2$** and **$Pd(L_{tc})_2Cl_2$** have been synthesized and characterized by mass spectrometry (MS) combined with ^{1}H and ^{13}C NMR spectroscopic analyses. The UV-vis spectra of tetracene dimers **$Pt(L_{tc})_2Cl_2$** (λ_{max} = 573 nm) and **$Pd(L_{tc})_2Cl_2$** (λ_{max} = 571 nm) show red-shift absorptions compared to the ligand **L_{tc}** (λ_{max} = 555 nm), and the extinction coefficients of **$Pt(L_{tc})_2Cl_2$** (75,200 L mol^{-1} cm^{-1}) and **$Pd(L_{tc})_2Cl_2$** (71,800 L mol^{-1} cm^{-1}) are nearly twice that of the ligand (34,600 L mol^{-1} cm^{-1}), indicating the two tetracene moieties are reasonably decoupled in those dimers.

References

[1] M. B. Smith, J. Michl, *Chem. Rev.* **2010**, *110*, 6891–6936.

[2] T. Wang, H. Liu, X. Wang, L. Tang, J. Zhou, X. Song, L. Lv, W. Chen, Y. Chen, X. Li, *J. Mater. Chem. A* **2023**, *11*, 8515–8539.

[3] N. V. Korovina, N. F. Pompetti, J. C. Johnson, *J. Chem. Phys.* **2020**, *152*, 040904.
[4] R. Casillas, M. Adam, P. B. Coto, A. R. Waterloo, J. Zirzlmeier, S. R. Reddy, F. Hampel, R. McDonald, R. R. Tykwinski, M. Thoss, D. M. Guldi, *Adv. Energy Mater.* **2019**, *9*, 1802221.
[5] C. Hetzer, D. M. Guldi, R. R. Tykwinski, *Chem. - Eur. J.* **2018**, *24*, 8245–8257.
[6] A. M. Alvertis, S. Lukman, T. J. H. Hele, E. G. Fuemmeler, J. Feng, J. Wu, N. C. Greenham, A. W. Chin, A. J. Musser, *J. Am. Chem. Soc.* **2019**, *141*, 17558–17570.
[7] L. M. Yablon, S. N. Sanders, K. Miyazaki, E. Kumarasamy, G. He, B. Choi, N. Ananth, M. Y. Sfeir, L. M. Campos, *Mater. Horiz.* **2022**, *9*, 462–470.
[8] R. Ringstrom, F. Edhborg, Z. W. Schroeder, L. Chen, M. J. Ferguson, R. R. Tykwinski, B. Albinsson, *Chem. Sci.* **2022**, *13*, 4944–4954.
[9] P. Siemsen, R. C. Livingston, F. Diederich, *Angew. Chem. Int. Ed.* **2000**, *39*, 2632–2657.
[10] D. Lehnherr, A. H. Murray, R. McDonald, R. R. Tykwinski, *Angew. Chem. Int. Ed.* **2010**, *49*, 6190–6194.
[11] I. Papadopoulos, S. R. Reddy, P. B. Coto, D. Lehnherr, D. Thiel, M. Thoss, R. R. Tykwinski, D. M. Guldi, *J. Phys. Chem. Lett.* **2022**, 5094–5100.
[12] C. F. H. Allen, J. W. Gates, *J. Am. Chem. Soc.* **1943**, *65*, 1502–1503.
[13] G. P. Miller, J. Briggs, in *Fullerenes--Volume 12: The Exciting World of Nanocages and Nanotubes, Vol. 12* (Eds.: P. V. Kamat, D. M. Guldi, K. M. Kadish), Electrochemical Society, New Jersey, **2002**, pp. 279–284.
[14] A. S. Hay, *J. Org. Chem.* **1962**, *27*, 3320–3321.
[15] B. Sun, PhD Thesis, University of Alberta (Edmonton), **2022**.
[16] Y. Gao, Y. Hou, F. Gordillo Gámez, M. J. Ferguson, J. Casado, R. R. Tykwinski, *Nat. Chem.* **2020**, *12*, 1143–1149.
[17] J. P. C. M. van Dongen, M. J. A. de Bie, R. Steur, *Tetrahedron Lett.* **1973**, *14*, 1371–1374.
[18] M. Gruber, K. Padberg, J. Min, A. R. Waterloo, F. Hampel, H. Maid, T. Ameri, C. J. Brabec, R. R. Tykwinsk, *Chem. - Eur. J.* **2017**, *23*, 17829–17835.
[19] R. G. Clevenger, B. Kumar, E. M. Menuey, G. H. Lee, D. Patterson, K. V. Kilway, *Chem. - Eur. J.* **2018**, *24*, 243–250.
[20] G. R. Llorente, M. B. Dufourg-Madec, D. J. Crouch, R. G. Pritchard, S. Ogier, S. G. Yeates, *Chem. Commun.* **2009**, 3059–3061.
[21] H. Matsubara, S. Yasuda, H. Sugiyama, I. Ryu, Y. Fujii, K. Kita, *Tetrahedron* **2002**, *58*, 4071–4076.
[22] R. P. Kopreski, J. B. Briggs, W. Lin, M. Jazdzyk, G. P. Miller, *J. Org. Chem.* **2012**, *77*, 1308–1315.
[23] M. Nishio, *CrystEngComm* **2004**, *6*, 130–158.
[24] H. Fischer, *The chemistry of alkenes*, John Wiley & Sons Ltd., New York, **1964**.
[25] C. Zong, Y. Zhao, H. Ji, X. Han, J. Xie, J. Wang, Y. Cao, S. Jiang, C. Lu, *Angew. Chem. Int. Ed.* **2016**, *55*, 3931–3935.
[26] Y. Dong, P. E. S. Silva, J. V. I. Timonen, J. Vapaavuori, *Chemphyschem* **2023**, *24*, e202300153.
[27] I. C. D. Merritt, D. Jacquemin, M. Vacher, *Phys. Chem. Chem. Phys.* **2021**, *23*, 19155–19165.
[28] J. Strueben, P. J. Gates, A. Staubitz, *J. Org. Chem.* **2014**, *79*, 1719–1728.
[29] J. M. Mativetsky, G. Pace, M. Elbing, M. A. Rampi, M. Mayor, P. Samori, *J. Am. Chem. Soc.* **2008**, *130*, 9192–9193.
[30] A. N. Oldacre, C. A. Pointer, S. M. Martin, A. Kemmerer, E. R. Young, *Chem. Commun.* **2019**, *55*, 5874–5877.

[31] B. S. Basel, J. Zirzlmeier, C. Hetzer, B. T. Phelan, M. D. Krzyaniak, S. R. Reddy, P. B. Coto, N. E. Horwitz, R. M. Young, F. J. White, F. Hampel, T. Clark, M. Thoss, R. R. Tykwinski, M. R. Wasielewski, D. M. Guldi, *Nat. Commun.* **2017**, *8*, 15171.

[32] J. Sarju, J. Arbour, J. Sayer, B. Rohrmoser, W. Scherer, G. Wagner, *Dalton Trans.* **2008**, 5302–5312.

[33] L. P. Wu, Y. Suenaga, T. KurodaSowa, M. Maekawa, K. Furuichi, M. Munakata, *Inorg. Chim. Acta* **1996**, *248*, 147–152.

[34] C. Tessier, F. D. Rochon, *Inorg. Chim. Acta* **1999**, *295*, 25–38.

[35] L. Pazderski, J. Toušek, J. Sitkowski, K. Maliňáková, L. Kozerski, E. Szłyk, *Magn. Reson. Chem.* **2009**, *47*, 228–238.

[36] L. Pazderski, T. Pawlak, J. Sitkowski, L. Kozerski, E. Szłyk, *Magn. Reson. Chem.* **2010**, *48*, 417–426.

[37] N. A. Lewis, S. Pakhomova, P. A. Marzilli, L. G. Marzilli, *Inorg. Chem.* **2017**, *56*, 9781–9793.

[38] G. Kurpik, A. Walczak, M. Gołdyn, J. Harrowfield, A. R. Stefankiewicz, *Inorg. Chem.* **2022**, *61*, 14019–14029.

[39] C. A. Strassert, M. Mauro, L. De Cola, *Adv. Inorg. Chem.* **2011**, *63*, 47–103.

[40] T. Theiss, S. Buss, I. Maisuls, R. López-Arteaga, D. Brünink, J. Kösters, A. Hepp, N. L. Doltsinis, E. A. Weiss, C. A. Strassert, *J. Am. Chem. Soc.* **2023**, *145*, 3937–2951.

CHAPTER 6

Summary and Outlook

6.1 Polymeric System

6.1.1 Pentacene Polymeric Systems Toward Triplets Harvesting in SF

The successful synthesis of the pyridyl-endcapped pentacene ligand **L_{pc}** allows the versatile formation of pentacene dimers with platinum(II) and palladium(II), as well as a tetramer with ruthenium(II). These complexes are used to study the heavy-atom effect on singlet fission (SF). The results show that SF is efficient in both **$Pt(L_{pc})_2Cl_2$** and **$Pd(L_{pc})_2Cl_2$** despite a rather large inter-pentacene separation and enhanced spin-orbit coupling from the presence of heavy atoms Pt and Pd. However, one of the problems of these molecular systems is that the diffusion of excitons is not sufficient thus the triplets formed from SF cannot be harvested (i.e., collected at electrodes to form a current).[1–6] One proposed strategy to facilitate harvesting is the development of polymeric systems via a pentacene linker with pyridyl groups on both ends (**PyPcPy**, Scheme 6.1).

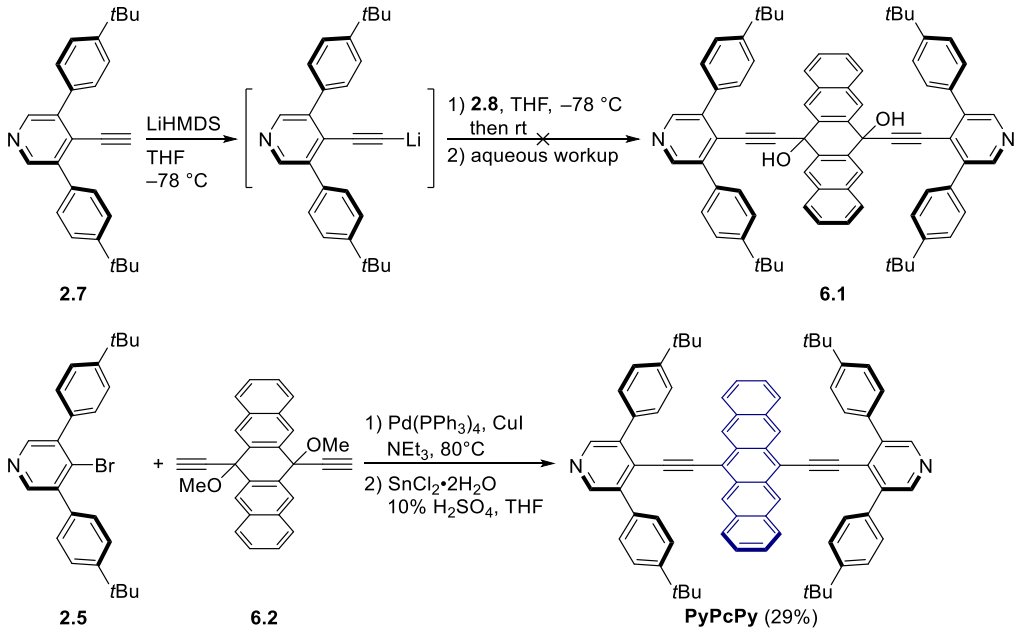

Scheme 6.1. Synthesis of **PyPcPy**.

The synthesis of pentacene linker **PyPcPy** was attempted first by adding 3 equivalents lithiated compound **2.7** to a suspension of 6,13-pentacenequinone (**2.8**) in dry THF at –78 °C. However, the desired diol **6.1** could not be obtained, and only mono-substituted product was observed after the reaction based on ^{1}H NMR spectroscopic analysis. Alternatively, a preliminary synthesis of **PyPcPy** was achieved through a Sonogashira cross-coupling reaction with compounds **2.5** and **6.2** in the presence of $Pd(PPh_3)_4$ and CuI in NEt_3 at 80 °C. Compound **6.2** was synthesized as previously reported.[7] The crude product was purified by column chromatography to give **PyPcPy** as a dark blue-green solid in 29% yield.

The successful synthesis of **PyPcPy** is supported by ^{1}H NMR spectroscopy (Figure 6.1), which shows characteristic singlets at δ 8.74 and δ 8.32 arising from the two central rings of pentacene moiety and pyridyl groups, respectively, as well as a singlet at δ 1.15 arising from the *tert*-butyl protons. Finally, the expected set of two pseudo-first-order doublets for the AA'BB' system of the aryl protons, as well as second-order resonances for the terminal rings of pentacene moiety are clearly seen. The simplicity of the NMR spectrum confirms the symmetry of **PyPcPy**.

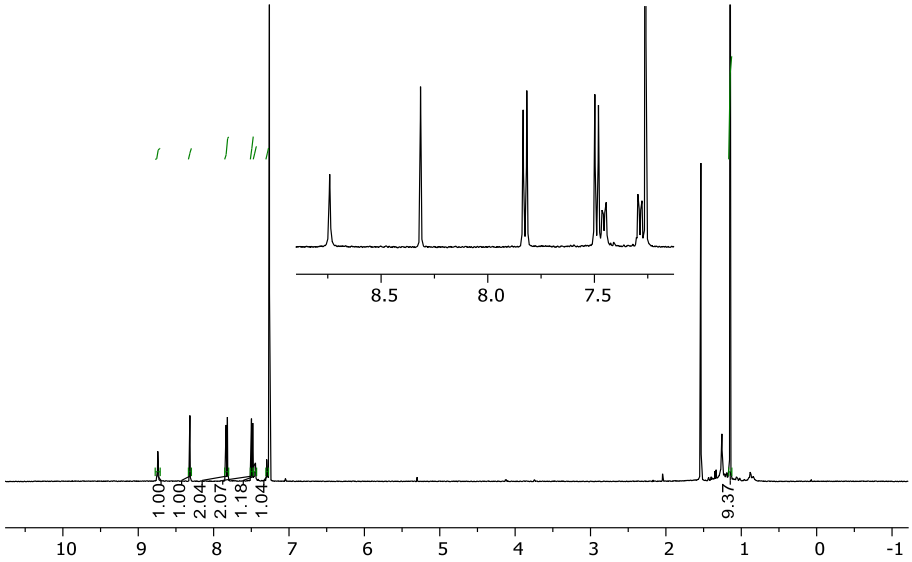

Figure 6.1. ^{1}H NMR spectra (498 MHz) of compound **PyPcPy** (in $CDCl_3$).

It is hypothesized that the formation of polymeric systems by coordinating **PyPcPy** with metal ions could be a strategy to mimic a solid, in which triplets could

diffuse apart. Such systems would facilitate the study of the diffusion process in SF. As shown in Figure 6.2, linear polymers and two-dimensional networks might be obtained by ligand exchange reactions of **PyPcPy** with $M(PhCN)_2Cl_2$ (M = Pt or Pd) and $Ru(PhCN)_4Cl_2$, respectively. These use of Pt(II), Pd(II), and Ru(II) would allow studies to build from our established knowledge for these systems in the corresponding di- and tetramers. Beyond Pt(II), Pd(II), and Ru(II), three-dimensional metal-organic frameworks could targeted as well using other metals like Cu.[8–13]

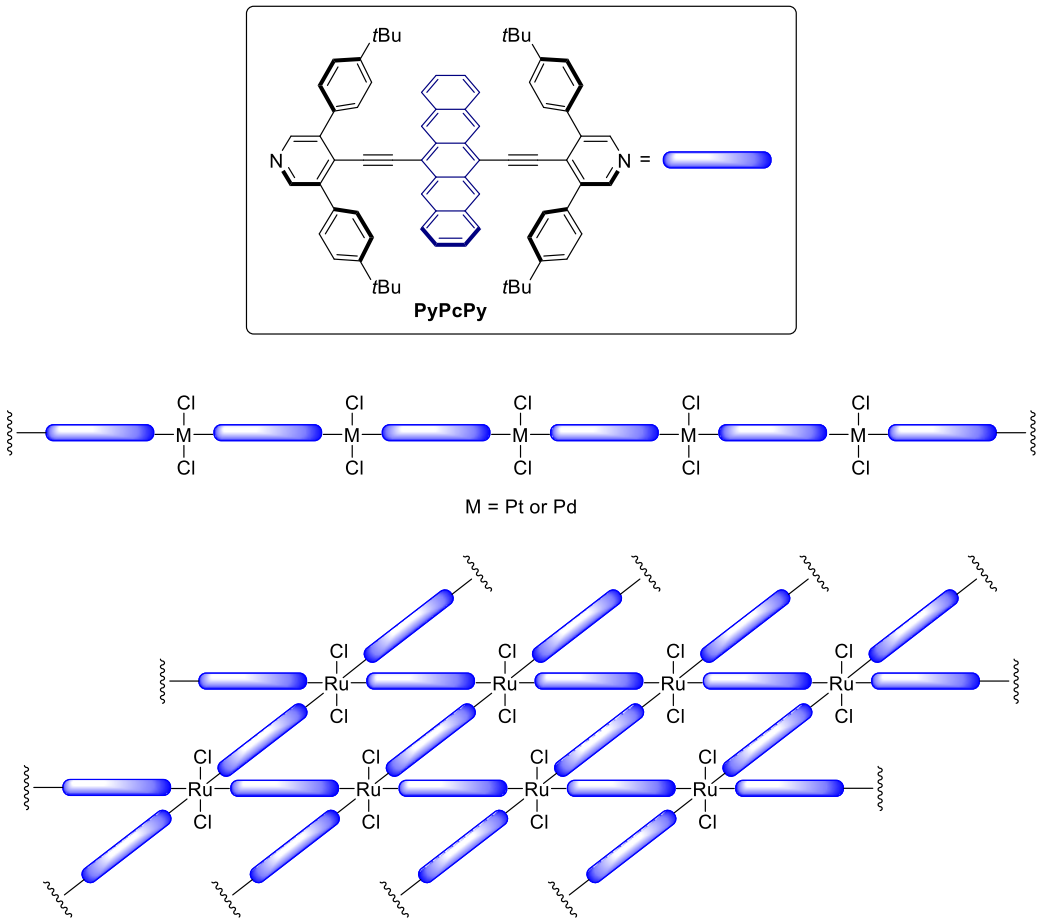

Figure 6.2. Illustration of polymeric systems using **PyPcPy**.

6.1.2 Tetracene Polymeric Systems Toward Efficient iTTA-UC

A system that can achieve fully intramolecular triplet-triplet annihilation upconversion (iTTA-UC) has been, in principle, successfully designed and synthesized through coordinating pyridyl-endcapped tetracene dimer annihilators with ruthenium

phthalocyanine sensitizers. However, the major concern for this system is that the two ruthenium phthalocyanine moieties in the same molecule cannot been irradiated concurrently Thus, the efficiency of TTA-UC would be compromised even though the high concentration requirements for both annihilator and sensitizer could be eliminated. One proposed strategy is the development of polymeric assemblies for iTTA-UC (Figure 6.3). In the polymeric systems, multiple annihilators could be irradiated at the same time, which should increase the efficiency of TTA-UC.[14–17]

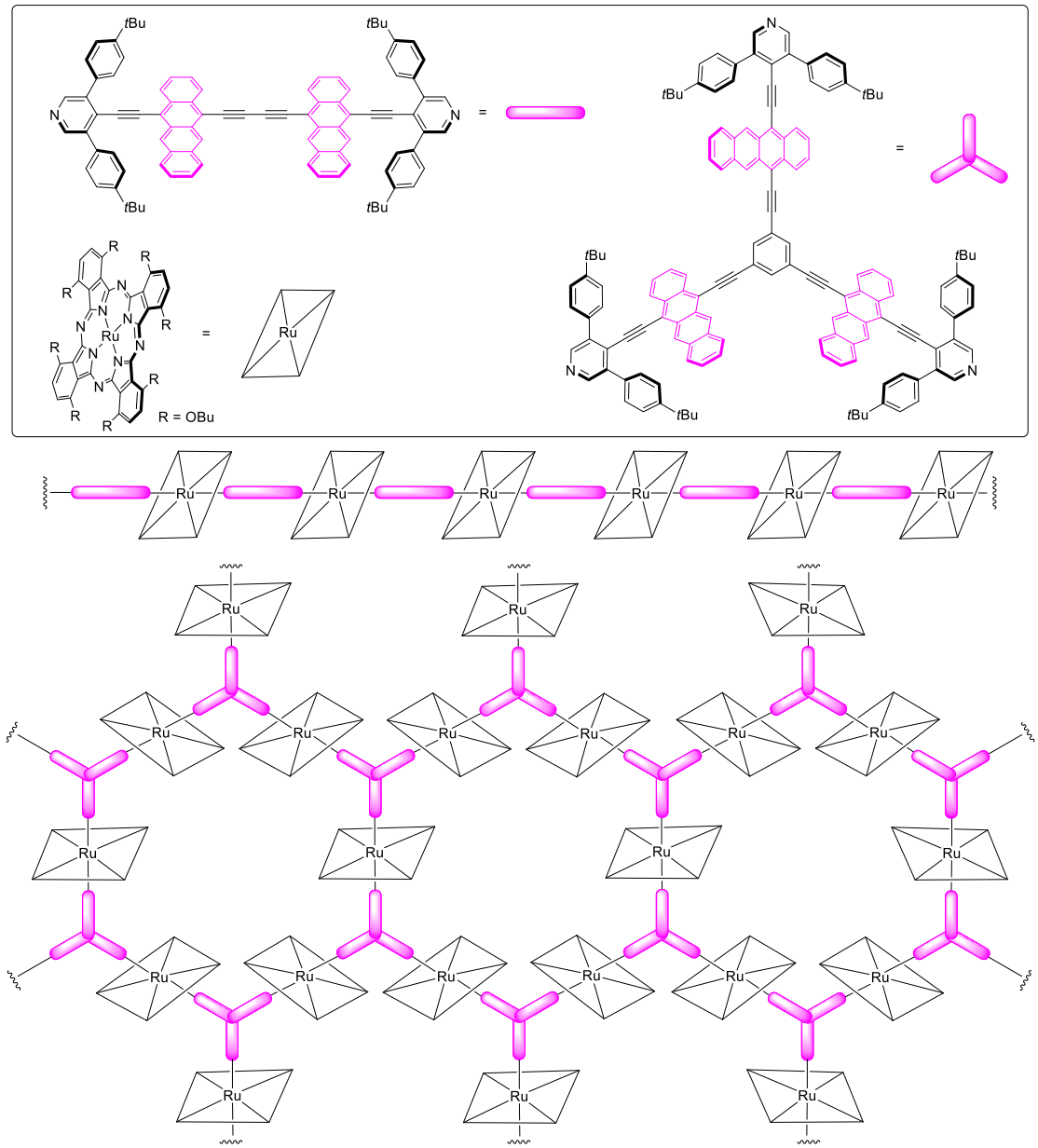

Figure 6.3. Illustration of polymeric systems for iTTA-UC.

6.2 Sensitizing TTA-UC with Nanocrystals

A proposed strategy to improve the efficiency of TTA-UC is through developing systems for iTTA-UC that use semiconductor nanocrystals (NCs), which could allow broadband absorption and less energy loss during sensitization due to the small exchange splitting.[18–22] As shown in Figure 6.4, the pyridyl groups on tetracene dimer is replaced with carboxylic groups for better coordination to the semiconductor NCs. It is important that the NCs designed for this system must be carefully selected so that their energy levels (e.g., the singlet and triplet state energies) fulfill the necessary energy requirements to achieve efficient TTA-UC. The energy levels of semiconductor NCs are readily tunable via the quantum confinement effect, which is a great advantage to use as a photosensitizer in iTTA-UC systems.[20,23–24] For example, the tunability of the silicon NCs spans from the ultraviolet (UV) to near-infrared (NIR) range (355–1130 nm).[25]

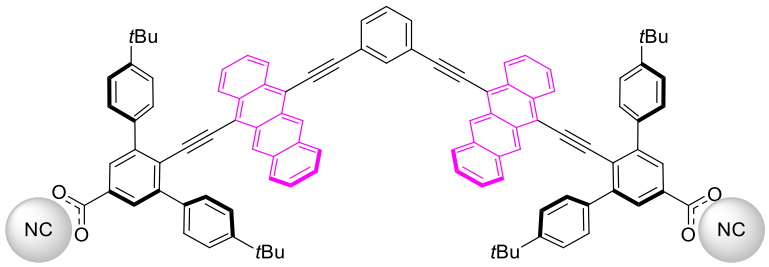

Figure 6.4. Illustration of an iTTA-UC system with NCs.

References

[1] N. V. Korovina, N. F. Pompetti, J. C. Johnson, *J. Chem. Phys.* **2020**, *152*, 040904.

[2] D. Sasikumar, A. T. John, J. Sunny, M. Hariharan, *Chem. Soc. Rev.* **2020**, *49*, 6122–6140.

[3] B. Daiber, K. van den Hoven, M. H. Futscher, B. Ehrler, *ACS Energy Lett.* **2021**, *6*, 2800–2808.

[4] E. Zojer, C. Winkler, *J, Phys. Chem. Lett.* **2021**, *12*, 7002–7009.

[5] R. J. Hudson, A. N. Stuart, D. M. Huang, T. W. Kee, *J. Phys. Chem. C* **2022**, *126*, 5369–5377.

[6] T. Wang, H. Liu, X. Wang, L. Tang, J. Zhou, X. Song, L. Lv, W. Chen, Y. Chen, X. Li, *J. Mater. Chem. A* **2023**, *11*, 8515–8539.

[7] D. Lehnherr, A. H. Murray, R. McDonald, R. R. Tykwinski, *Angew. Chem. Int. Ed.* **2010**, *49*, 6190–6194.

[8] O. Alduhaish, R. B. Lin, H. L. Wang, B. Li, H. D. Arman, T. L. Hu, B. L. Chen, *Cryst. Growth Des.* **2018**, *18*, 4522–4527.

[9] A. V. Desai, S. Sharma, S. Let, S. K. Ghosh, *Coord. Chem. Rev.* **2019**, *395*, 146–192.

[10] M. Mostaghimi, C. R. C. Rêgo, R. Haldar, C. Wöll, W. Wenzel, M. Kozlowska, *Front. Mater.* **2022**, *9*, 840644.
[11] S. S. Rajasree, J. Yu, F. Fajardo-Rojas, H. C. Fry, R. Anderson, X. Li, W. Xu, J. Duan, S. Goswami, K. Maindan, D. A. Gomez-Gualdron, P. Deria, *J. Am. Chem. Soc.* **2023**, *145*, 17678–17688.
[12] R. Haldar, M. Kozlowska, M. Ganschow, S. Ghosh, M. Jakoby, H. Chen, F. Ghalami, W. Xie, S. Heidrich, Y. Tsutsui, J. Freudenberg, S. Seki, I. A. Howard, B. S. Richards, U. H. F. Bunz, M. Elstner, W. Wenzel, C. Woll, *Chem. Sci.* **2021**, *12*, 4477–4483.
[13] E. Zojer, C. Winkler, *J. Phys. Chem. Lett.* **2021**, *12*, 7002–7009.
[14] L. Naimovicius, P. Bharmoria, K. Moth-Poulsen, *Mater. Chem. Front.* **2023**, *7*, 2297–2315.
[15] T. Schloemer, P. Narayanan, Q. Zhou, E. Belliveau, M. Seitz, D. N. Congreve, *ACS Nano* **2023**, *17*, 3259–3288.
[16] M. Uji, T. J. B. Zahringer, C. Kerzig, N. Yanai, *Angew. Chem. Int. Ed.* **2023**, *62*, e202301506.
[17] L. Wei, C. Yang, W. Wu, *Mater. Chem. Front.* **2023**, *7*, 3194–3208.
[18] M. Wu, D. N. Congreve, M. W. B. Wilson, J. Jean, N. Geva, M. Welborn, T. Van Voorhis, V. Bulović, M. G. Bawendi, M. A. Baldo, *Nat. Photonics* **2015**, *10*, 31–34.
[19] E. M. Gholizadeh, S. K. K. Prasad, Z. L. Teh, T. Ishwara, S. Norman, A. J. Petty, J. H. Cole, S. Cheong, R. D. Tilley, J. E. Anthony, S. Huang, T. W. Schmidt, *Nat. Photonics* **2020**, *14*, 585–590.
[20] M. W. Brett, C. K. Gordon, J. Hardy, N. Davis, *ACS Phys. Chem. Au* **2022**, *2*, 364–387.
[21] V. Gray, W. Drake, J. R. Allardice, Z. Zhang, J. Xiao, D. G. Congrave, J. Royakkers, W. Zeng, S. Dowland, N. C. Greenham, H. Bronstein, J. E. Anthony, A. Rao, *J. Mater. Chem. C Mater.* **2022**, *10*, 16321–16329.
[22] L. Zeng, L. Huang, J. Han, G. Han, *Acc. Chem. Res.* **2022**, *55*, 2604–2615.
[23] V. Gray, J. R. Allardice, Z. Zhang, A. Rao, *Chem. Phys. Rev.* **2021**, *2*, 031305.
[24] C. Ye, D.-S. Zhang, B. Chen, C.-H. Tung, L.-Z. Wu, *Chem. Phys. Rev.* **2023**, *4*, 011304.
[25] C. C. Huang, Y. Tang, M. van der Laan, J. van de Groep, A. F. Koenderink, K. Dohnalova, *ACS Appl. Nano Mater.* **2021**, *4*, 288–296.

CHAPTER 7

Experimental Section

7.1 General Procedures and Methods

Reagents were purchased reagent grade from commercial suppliers and used without further purification. Dry tetrahydrofuran (THF), CH_2Cl_2, and PhMe were obtained from a commercial solvent purification system (LC Technology Solutions INC). $MgSO_4$ was used as the drying reagent after aqueous work-up.

^1H and ^{13}C NMR spectra were recorded on an Agilent/Varian DD2 MR two-channel 400 MHz spectrometer (^1H: 400 MHz), an Agilent/Varian Inova four-channel 500 MHz spectrometer (^1H: 498 MHz), an Agilent VNMRS four-channel, dual receiver 700 MHz spectrometer (^{13}C: 176 MHz), or an Agilent/Varian VNMRS two-channel 500 MHz spectrometer equipped with a $^{13}C/^1H$ dual cold probe (^1H: 498 MHz, ^{13}C: 126 MHz). NMR spectra were recorded at ambient probe temperature and referenced to the residual solvent signal (^1H: $CDCl_3$: 7.26 ppm, ^{13}C: $CDCl_3$: 77.06 ppm). The coupling constants of protons in ^1H spectra have been reported as pseudo first-order when possible, even though they can be higher-order (ABC, ABX, AA'BB') spin systems; coupling constants are reported as observed.

Routine, steady-state UV-vis measurements were carried out on a Cary-400 spectrophotometer at room temperature. The wavelength λ is recorded in nm, the molar extinction ε is reported in L mol^{-1} cm^{-1}.

High resolution mass spectra were obtained at the University of Alberta mass spectrometry facility, using from an Agilent Technologies 6220 oaTOF instrument (ESI) or a Bruker 9.4T Apex-Qe FTICR instrument (MALDI).

IR spectra were recorded on a Thermo Nicolet 8700 FTIR spectrometer and continuum FTIR microscope as films.

Differential scanning calorimetry (DSC) measurements were made on a Mettler Toledo DSC or Perkin Elmer Pyris 1 DSC. All DSC measurements were carried out under a flow of nitrogen with a heating rate of 10 °C/min.

Melting points were measured with 6406-K Thomas-Hoover melting point apparatus with a periscopic thermometer reader.

X-ray crystallographic analysis was performed using a Bruker Platform diffractometer at the Department of Chemistry, University of Alberta.

Thin layer chromatography (TLC) analyses were carried out on TLC glass plates from Merck KGaA and visualized via UV-light (254/364 nm). Column chromatography used Supelco™ silica gel (SiO_2, 60 Å, 40−63 μm). Size exclusion column chromatography was performed using Bio-Beads™ SX1 or SX3 supports (Bio-Rad). Preparative GPC was carried out on a Shimadzu recycling GPC system equipped with a LC-20AR pump, SPD-M20A UV detector, and a set of PSS SDV (20 × 300 mm) columns in chloroform as eluent at a flow rate of 6.25 mL/min.

7.2 Experimental Data for Chapter 2

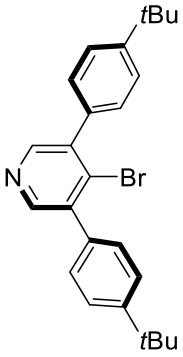

2.5 (88%)

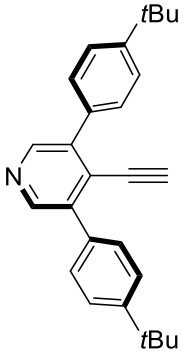

2.7 (95%)

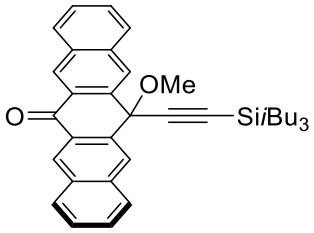

2.9 (75%)

Compounds **2.5**,[1] **2.7**,[1] and **2.9**[2] were synthesized as described in the literature.

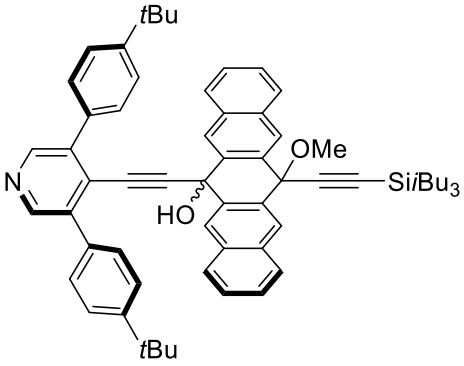

Compound 2.10. A solution of lithium hexamethyldisilazide (LiHMDS) was prepared by adding *n*BuLi (2.5 M in hexanes, 3.26 mL, 8.15 mmol) to a solution of $[(CH_3)_3Si]_2NH$ (1.82 mL, 2.36 g, 8.68 mmol) in dry THF (10 mL) at –78 °C. After stirring at –78 °C for 30 min, the solution of LiHMDS was added to a mixture of **2.7** (200 mg, 0.544 mmol) and **2.9** (327 mg, 0.598 mmol) in dry THF (15 mL) at –78 °C via a cannula. The solution was

warmed to rt and stirred for 18 h under an atmosphere of N_2. After cooling to 0 °C, satd aq NH_4Cl (10 mL) was added, followed by H_2O (50 mL), the layers were separated, and the aqueous phase was extracted with CH_2Cl_2 (3 × 50 mL). The organic phases were combined, dried ($MgSO_4$), and filtered. After removing the solvent under reduced pressure, the residue was purified by column chromatography (silica gel, EtOAc/hexanes 1:6) to afford a mixture of two diastereomers of **2.10** (368 mg, 74%) as a white solid. The stereoisomers were separated by recrystallization from a solution of the mixture of two isomers in CH_2Cl_2 (1 mL) by layering with hexanes (20 mL). The major isomer was characterized. Mp 264 °C (decomp). R_f = 0.25 or 0.36 (EtOAc/hexanes 1:3). IR (CH_2Cl_2, cast) 3055 (w), 3029 (w), 2953 (s), 2930 (m), 2901 (m), 2867 (m), 2817 (w), 2167 (w), 1604 (w), 1579 (w) cm^{-1}. ^1H NMR (498 MHz, $CDCl_3$) δ 8.58 (s, 2H), 8.48 (s, 2H), 8.34 (s, 2H), 7.96–7.87 (m, 4H), 7.60–7.53 (m, 4H), 7.38 (d, J = 8.4 Hz, 4H), 6.97 (d, J = 8.4 Hz, 4H), 3.10 (s, 1H), 2.42 (s, 3H), 2.09 (nonet, J = 6.7 Hz, 3H), 1.12 (s, 18H), 1.11 (d, J = 7.6 Hz, 18H), 0.86 (d, J = 7.0 Hz, 6H). ^{13}C NMR (126 MHz, $CDCl_3$) δ 151.0, 148.4, 138.2, 137.4, 133.8, 133.5, 132.62, 132.58, 129.2, 128.3, 128.2, 127.9, 127.0, 126.8, 126.3, 125.0, 124.7, 103.9, 102.1, 95.9, 80.4, 67.7, 51.1, 34.4, 31.2, 26.5, 25.4, 25.3 (one signal coincident or not observed). ESI HRMS calcd for $C_{64}H_{72}NO_2Si$ ($[M + H]^+$) 914.5327, found 914.5339.

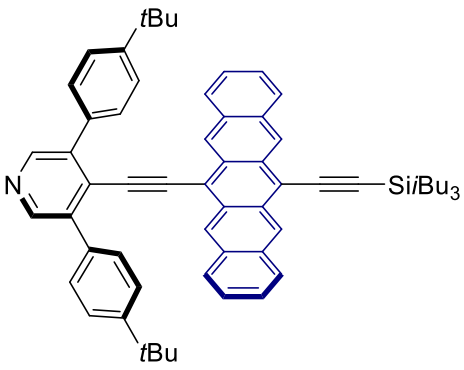

Compound L_{pc}. To a solution of a mixture of isomers of **2.10** (200 mg, 0.219 mmol) in dry, deoxygenated THF (10 mL) was added $SnCl_2$•$2H_2O$ (148 mg, 0.656 mmol) and 10% H_2SO_4 (0.1 mL) at rt. The flask was wrapped in aluminum foil during the reaction to limit light exposure. The reaction mixture was stirred for 6 h under an atmosphere of N_2 and then neutralized by the addition of 1 M aq NaOH (1 mL). The mixture was poured into H_2O (20 mL). The suspension was filtered, and the residue was washed with MeOH (3 × 5 mL). Recrystallization from a solution of crude product in CH_2Cl_2 (2 mL) by the

addition of MeOH (30 mL) afforded **L$_{pc}$** as a dark blue solid (168 mg, 89%). Mp 180 °C (decomp). R_f = 0.44 (EtOAc/hexanes 1:3). UV-vis (CH_2Cl_2) λ_{max} (ε) 304 (sh, 89,600), 314 (304,000), 386 (17,300),442 (4,360), 565 (5,730), 610 (15,800), 663 nm (29,300). IR (CH_2Cl_2, cast) 3049 (w), 2953 (s), 2928 (m), 2902 (m), 2867 (m), 2180 (w), 2122 (w), 1568 (w), 1462 (m) cm^{-1}. ^{1}H NMR (498 MHz, $CDCl_3$) δ 9.18 (s, 2H), 8.75 (s, 2H), 8.42 (s, 2H), 7.92–7.84 (m, 6H), 7.55–7.49 (m, 6H), 7.40–7.30 (m, 4H), 2.18 (nonet, J = 6.7 Hz, 3H), 1.18 (d, J = 6.1 Hz, 18H), 1.18 (s, 18H), 0.95 (d, J = 7.0 Hz, 6H). ^{13}C NMR (126 MHz, $CDCl_3$) δ 151.7, 149.0, 138.4, 134.8, 132.24, 132.18, 130.5, 130.3, 129.5, 129.3, 128.4, 127.9, 126.1, 126.01, 125.96, 125.8, 125.6, 119.2, 117.3, 110.4, 104.7, 101.3, 98.4, 34.7, 31.2, 26.6, 25.49, 25.46. ESI HRMS calcd for $C_{63}H_{68}NSi$ ($[M + H]^+$) 866.5116, found 866.5122. DSC: Decomposition, 189 °C (onset), 194 °C (peak).

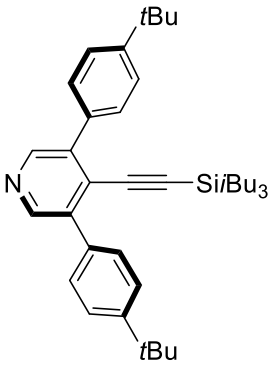

Compound L$_{ref}$. The synthesis of **L$_{ref}$** was carried out by adapting the procedure of Gao et al.[1] A solution of (tri*iso*butylsilyl)acetylene (1.06 g, 4.72 mmol) in Et_3N (5 mL) was deoxygenated under a flow of N_2 for 20 min. To this solution was added **2.5** (200 mg, 0.47 mmol), $Pd(PPh_3)_4$ (55 mg, 0.048 mmol), and CuI (14 mg, 0.074 mmol). The mixture was stirred for 2 d at 80 °C under an atmosphere of N_2. The reaction mixture was cooled to rt, H_2O (50 mL) and CH_2Cl_2 (50 mL) were added, the layers were separated, and the aqueous phase was extracted with CH_2Cl_2 (2 × 50 mL). The organic phases were combined, washed with satd aq NH_4Cl (50 mL), dried ($MgSO_4$), and filtered. Solvent removal and purification by column chromatography (silica gel, EtOAc/hexanes 1:10) afforded **L$_{ref}$** (207 mg, 77%) as a white solid. Mp 89–90 °C. R_f = 0.61 (EtOAc/hexanes 1:4). UV-vis (CH_2Cl_2) λ_{max} (ε) 251 (29,300), 315 nm (sh, 7,480). IR (CH_2Cl_2, cast) 3029 (w), 2954 (s), 2903 (m), 2867 (m), 2156 (w), 1570 (w), 1463 (m) cm^{-1}. ^{1}H NMR (498 MHz, $CDCl_3$) δ 8.54 (s, 2H), 7.54 (d, J = 8.4 Hz, 4H), 7.46 (d, J = 8.4 Hz, 4H), 1.61 (nonet, J = 6.6 Hz, 3H), 1.38 (s, 18H), 0.78 (d, J = 6.6 Hz, 18H), 0.47 (d, J = 6.9 Hz, 6H). ^{13}C NMR (126 MHz, $CDCl_3$)

δ 150.9, 148.5, 138.9, 134.5, 129.3, 127.8, 125.1, 105.9, 102.6, 34.7, 31.4, 26.2, 24.9, 24.6. ESI HRMS calcd for $C_{39}H_{56}NSi$ ($[M + H]^+$) 566.4177, found 566.4172. DSC: Mp = 92 °C.

Bis(benzonitrile)platinum(II) dichloride ($Pt(PhCN)_2Cl_2$) was prepared via the procedure reported in the literature.[3]

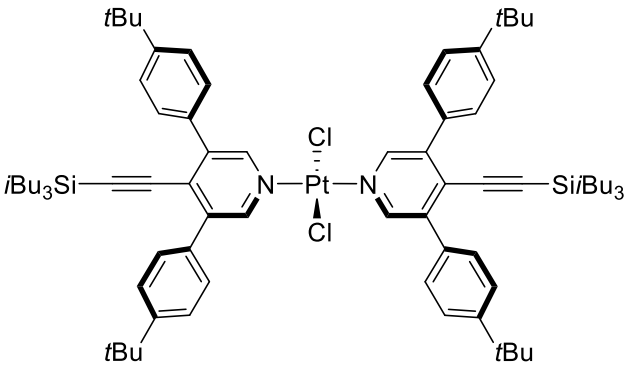

Compound $Pt(L_{ref})_2Cl_2$. A mixture of $\mathbf{L_{ref}}$ (25 mg, 0.044 mmol) and $Pt(PhCN)_2Cl_2$ (10 mg, 0.021 mmol) in dry PhMe (10 mL) was stirred at 80 °C for 16 h under an atmosphere of argon. The reaction mixture was cooled to rt, and then the solvent was removed under reduced pressure. The residue was purified by column chromatography (silica gel, CH_2Cl_2/hexanes 1:4). Solvent was removed, and the residue was dissolved in CH_2Cl_2 (2 mL), followed by the addition of MeOH (15 mL). The resulting suspension was filtered, and the residue was washed with MeOH (3 × 2 mL), affording **$Pt(L_{ref})_2Cl_2$** as a pale yellow crystal (28 mg, 93%). Mp 276 °C (decomp). R_f = 0.66 (EtOAc/hexanes 1:6). UV-vis (CH_2Cl_2) λ_{max} (ε) 265 (60,700), 323 nm (36,700). IR (CH_2Cl_2, cast) 3089 (w), 3032 (w), 2954 (s), 2927 (m), 2902 (m), 2867 (m), 2155 (m), 1595 (w), 1462 (m) cm^{-1}. ^1H NMR (498 MHz, $CDCl_3$) δ 8.78 (s, 4H), 7.53 (d, J = 8.5 Hz, 8H), 7.45 (d, J = 8.5 Hz, 8H), 1.58 (nonet, J = 6.6 Hz, 6H), 1.37 (s, 36H), 0.76 (d, J = 6.5 Hz, 36H), 0.46 (d, J = 7.0 Hz, 12H). ^{13}C NMR (126 MHz, $CDCl_3$) δ 151.7, 151.4, 140.7, 132.5, 130.4, 129.3, 125.3, 110.4, 101.4, 34.7, 31.4, 26.2, 24.8, 24.3. ESI HRMS calcd for $C_{78}H_{110}{}^{35}Cl_2N_2Na^{195}PtSi_2$ ($[M + Na]^+$) 1418.7125, found 1418.7151. DSC: Decomposition, 283 °C (onset), 285 °C (peak).

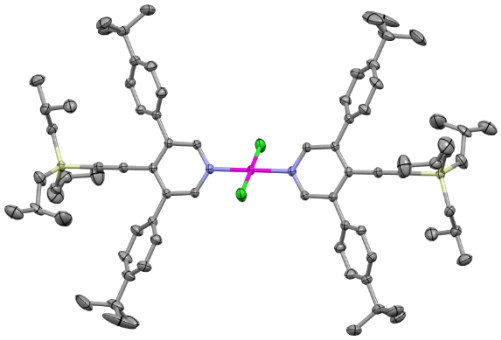

A crystal of **Pt(L$_{ref}$)$_2$Cl$_2$** suitable for crystallographic analysis has been grown at rt by slow evaporation of a CH_2Cl_2 solution layered with MeOH. X-ray data for **Pt(L$_{ref}$)$_2$Cl$_2$** ($C_{78}H_{110}Cl_2N_2PtSi_2$), F_w = 1397.84; crystal dimensions 0.29 × 0.23 × 0.21 mm, monoclinic crystal system; space group *C*2/*c* (No. 15); a = 23.7356(18) Å, b = 13.9543(10) Å, c = 24.4208(18) Å; β = 111.9341(10)°; V = 7503.0(10) Å^3; Z = 4; ρ_{calcd} = 1.237 g/cm^3; $2\theta_{max}$ = 66.84°; μ = 2.014 mm^{-1}; T = 173 K; total data collected = 145582; R_1 = 0.0216 [11655 observed reflections with $F_o^2 \geq 2\sigma(F_o^2)$]; ωR_2 = 0.0566 for 14311 data, 426 variables, and 22 restraints; largest difference, peak and hole = 0.740 and –0.765 e Å^{-3}. The C39–C40A and C39–C40B distances were restrained to be approximately the same by use of the *SHELXL* **SADI** instruction. Additionally, the anisotropic displacement parameters of the atoms within the disordered isobutyl group were restrained by the rigid-bond restraint **RIGU**. CCDC 2288684.

Bis(benzonitrile)palladium(II) dichloride ($Pd(PhCN)_2Cl_2$) was prepared with the procedure reported in the literature.[4]

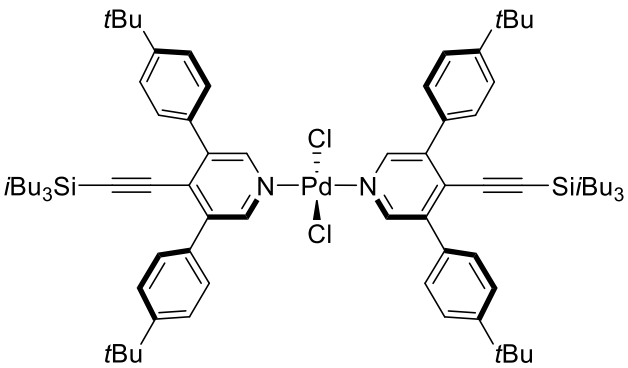

Compound Pd(L$_{ref}$)$_2$Cl$_2$. A mixture of **L$_{ref}$** (30 mg, 0.052 mmol) and $Pd(PhCN)_2Cl_2$ (10 mg, 0.026 mmol) in dry CH_2Cl_2 (5 mL) was stirred at rt for 15 h under an atmosphere of argon. The solvent was removed under reduced pressure, and the residue was purified by column chromatography (silica gel, CH_2Cl_2/hexanes 1:1). The solvent was removed, and the residue was dissolved in CH_2Cl_2 (2 mL), followed by the addition of MeOH (15 mL). The resulting suspension

was filtered, and the residue was washed with MeOH (3 × 2 mL), affording **Pd(L$_{ref}$)$_2$Cl$_2$** as a pale yellow crystal (31 mg, 91%). Mp 280 °C (decomp). R_f = 0.27 (CH_2Cl_2/hexanes 1:2). UV-vis (CH_2Cl_2) λ_{max} (ε) 266 (72,400), 307 nm (sh, 26,900). IR (CH_2Cl_2, cast) 3086 (w), 3032 (w), 2954 (s), 2902 (m), 2867 (m), 2158 (m), 1593 (m), 1463 (m) cm^{-1}. ^{1}H NMR (498 MHz, $CDCl_3$) δ 8.70 (s, 4H), 7.52 (d, J = 8.4 Hz, 8H), 7.44 (d, J = 8.4 Hz, 8H), 1.57 (nonet, J = 6.7 Hz, 6H), 1.37 (s, 36H), 0.76 (d, J = 6.5 Hz, 36H), 0.45 (d, J = 6.9 Hz, 12H). ^{13}C NMR (126 MHz, $CDCl_3$) δ 151.8, 151.1, 140.6, 132.6, 130.7, 129.3, 125.3, 110.3, 101.4, 34.8, 31.4, 26.2, 24.8, 24.4. ESI HRMS calcd for $C_{78}H_{110}{}^{35}Cl_2N_2Na^{106}PdSi_2$ ([M + Na]$^+$) 1329.6512, found 1329.6529. DSC: Decomposition, 300 °C (onset), 300 °C (peak).

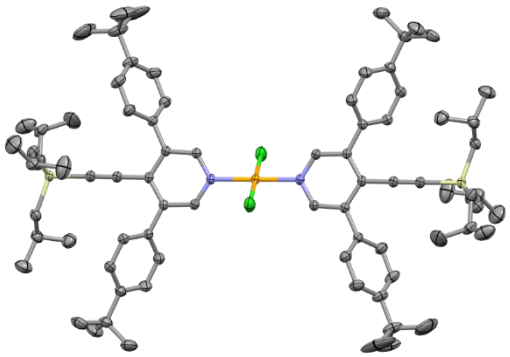

A crystal of **Pd(L$_{ref}$)$_2$Cl$_2$** suitable for crystallographic analysis has been grown at rt by slow evaporation of a CH_2Cl_2 solution layered with MeOH. X-ray data for **Pd(L$_{ref}$)$_2$Cl$_2$** ($C_{78}H_{110}Cl_2N_2PdSi_2$), F_w = 1309.15; crystal dimensions 0.39 × 0.21 × 0.14 mm, monoclinic crystal system; space group $C2/c$ (No. 15); a = 23.7115(11) Å, b = 13.9570(6) Å, c = 24.3980(11) Å; β = 111.7864(6)°; V = 7497.6(6) Å^3; Z = 4; ρ_{calcd} = 1.160 g/cm^3; $2\theta_{max}$ = 63.18°; μ = 0.392 mm^{-1}; T = 173 K; total data collected = 137336; R_1 = 0.0310 [10516 observed reflections with $F_o{}^2 \geq 2\sigma(F_o{}^2)$]; ωR_2 = 0.0878 for 12572 data, 426 variables, and 1 restraint; largest difference, peak and hole = 0.455 and –0.364 e Å^{-3}. The C39–C40A and C39–C40B distances were restrained to be approximately the same by use of the *SHELXL* **SADI** instruction. CCDC: 2288685.

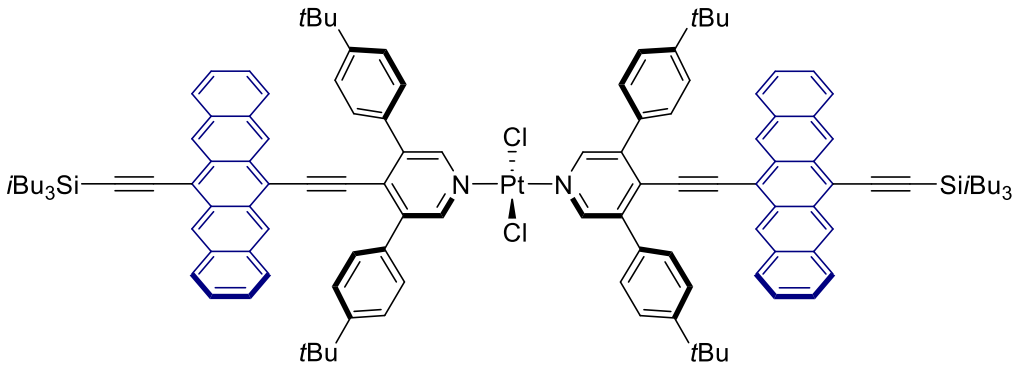

Compound $Pt(L_{pc})_2Cl_2$. A mixture of $\mathbf{L_{pc}}$ (36 mg, 0.042 mmol) and $Pt(PhCN)_2Cl_2$ (10 mg, 0.021 mmol) in dry PhMe (5 mL) was stirred at 80 °C for 16 h under an atmosphere of argon. The flask was wrapped in aluminum foil during the reaction to limit light exposure. The reaction mixture was cooled to rt, and then the solvent was removed under reduced pressure. The residue was purified by column chromatography (alumina, CH_2Cl_2). The eluent volume was reduced in vacuo to ~1 mL, followed by the addition of hexanes (15 mL). The resulting suspension was filtered, and the residue was washed with hexanes (3 × 2 mL), affording **$Pt(L_{pc})_2Cl_2$** as a dark blue solid (32 mg, 76%). Mp 322 °C (decomp). R_f = 0.50 (CH_2Cl_2/hexanes 1:2). UV-vis (CH_2Cl_2) λ_{max} (ε) 271 (128,000), 306 (sh, 202,000), 315 (544,000), 347 (33,200), 407 (36,700), 441 (15,600), 577 (sh, 13,200), 626 (34,700), 679 nm (63,500). IR (CH_2Cl_2, cast) 3086 (w), 3050 (w), 2953 (s), 2927 (m), 2901 (m), 2867 (m), 2168 (m), 2122 (w), 1590 (m), 1461 (m) cm^{-1}. ^1H NMR (498 MHz, $CDCl_3$) δ 9.19 (s, 4H), 9.03 (s, 4H), 8.37 (s, 4H), 7.94–7.86 (m, 12H), 7.56–7.50 (m, 12H), 7.41–7.33 (m, 8H), 2.18 (nonet, J = 6.6 Hz, 6H), 1.20 (s, 36H), 1.19 (d, J = 6.6 Hz, 36H), 0.96 (d, J = 7.0 Hz, 12H). ^{13}C NMR (126 MHz, $CDCl_3$) δ 152.5, 151.9, 140.2, 133.0, 132.4, 132.3, 130.5, 130.4, 129.5, 129.2, 128.4, 126.2, 126.1, 125.9, 125.7, 120.3, 116.4, 111.2, 104.6, 102.0, 100.4, 34.8, 31.2, 26.6, 25.5, 25.4 (two signals coincident or not observed). MALDI HRMS (DCTB) calcd for $C_{126}H_{134}{}^{35}Cl_2N_2{}^{195}PtSi_2$ (M^+) 1995.9105, found 1995.9082. DSC: Decomposition, 347 °C (onset), 353 °C (peak).

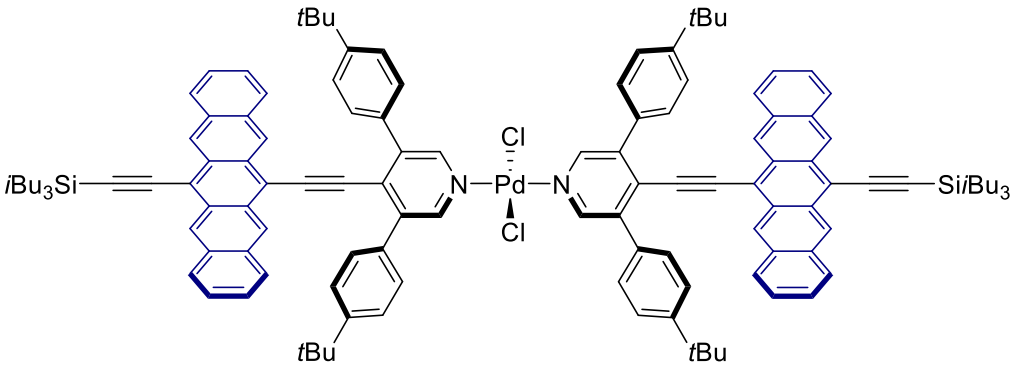

Compound Pd($\mathbf{L_{pc}}$)$_2$Cl$_2$. A mixture of $\mathbf{L_{pc}}$ (45 mg, 0.052 mmol) and $Pd(PhCN)_2Cl_2$ (10 mg, 0.026 mmol) in dry CH_2Cl_2 (5 mL) was stirred at rt for 15 h under an atmosphere of argon. The flask was wrapped in aluminum foil during the reaction to limit light exposure. The reaction mixture was plugged through a pad of alumina (CH_2Cl_2). The eluent volume was reduced in vacuo to ~1 mL, followed by the addition of hexanes (15 mL). The resulting suspension was filtered, and the residue was washed with hexanes (3 × 2 mL), affording **Pd($\mathbf{L_{pc}}$)$_2$Cl$_2$** as a dark blue-green solid (34 mg, 69%). Mp 309 °C (decomp). R_f = 0.75 (CH_2Cl_2/hexanes 1:1). UV-vis (CH_2Cl_2) λ_{max} (ε) 271 (118,000), 306 (sh, 183,000), 315 (507,000), 348 (28,000), 400 (29,600), 441 (12,400), 573 (sh, 10,700), 625 (31,300), 677 nm (57,100). IR (CH_2Cl_2, cast) 3080 (w), 3050 (w), 2953 (s), 2927 (m), 2902 (m), 2867 (m), 2166 (m), 2120 (w), 1588 (m), 1461 (m) cm^{-1}. ^{1}H NMR (498 MHz, $CDCl_3$) δ 9.18 (s, 4H), 8.95 (s, 4H), 8.36 (s, 4H), 7.92–7.87 (m, 12H), 7.56–7.50 (m, 12H), 7.41–7.33 (m, 8H), 2.18 (nonet, J = 6.7 Hz, 6H), 1.20 (s, 36H), 1.18 (d, J = 6.7 Hz, 36H), 0.96 (d, J = 7.0 Hz, 12H). ^{13}C NMR (126 MHz, $CDCl_3$) δ 152.5, 151.6, 140.0, 133.1, 132.4, 132.3, 130.8, 130.5, 130.4, 129.5, 129.2, 128.4, 126.2, 126.1, 125.9, 125.7, 120.4, 116.3, 111.2, 104.5, 101.9, 100.3, 34.8, 31.2, 26.6, 25.5, 25.4 (one signal coincident or not observed). MALDI HRMS (DCTB) calcd for $C_{126}H_{134}{}^{35}Cl_2N_2{}^{106}PdSi_2$ (M^+) 1906.8492, found 1906.8510. DSC: Decomposition, 321 °C (onset), 330 °C (peak).

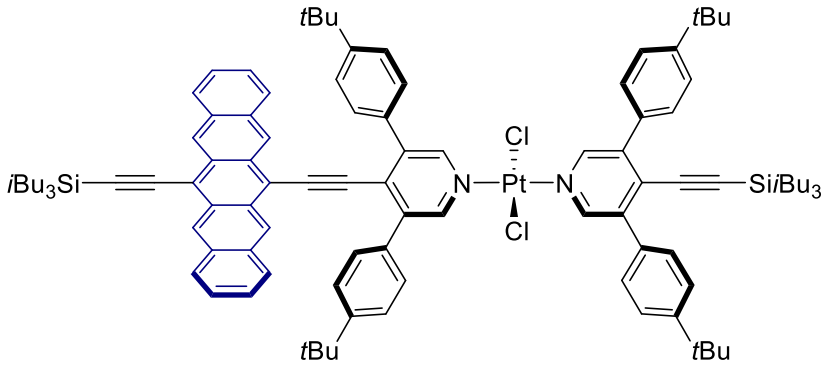

Compound Pt(L_{pc})(L_{ref})Cl_2. A solution of $Pt(PhCN)_2Cl_2$ (31 mg, 0.066 mmol) in dry PhMe (2 mL) was stirred at 110 °C, followed by adding a solution of L_{ref} (25 mg, 0.044 mmol) in dry PhMe (7 mL) dropwise over 5 min. This reaction mixture was stirred at 110 °C for 20 min under an atmosphere of argon. The reaction mixture was cooled to rt, and then the solvent was removed under reduced pressure. Purification by column chromatography (silica gel, EtOAc/hexanes 1:4) afforded **Pt(L_{ref})(PhCN)Cl_2** as a pale yellow solid (40 mg, 97%). A solution of **Pt(L_{ref})(PhCN)Cl_2** (40 mg, 0.043 mmol) in dry PhMe (3 mL) was stirred at 110 °C, followed by adding a solution of L_{pc} (34 mg, 0.039 mmol) in dry PhMe (10 mL) dropwise over 5 min. The reaction mixture was stirred at 110 °C for 14 h under an atmosphere of argon. The flask was wrapped in aluminum foil during the reaction to limit light exposure. The reaction mixture was cooled to rt, and then the solvent was removed under reduced pressure. The residue was purified by column chromatography (silica gel, EtOAc/hexanes 1:50), followed by size exclusion column chromatography (Bio-Beads SX3 support, PhMe). Solvent was removed, and the residue was dissolved in CH_2Cl_2 (2 mL), followed by the addition of MeOH (20 mL). The resulting suspension was filtered, and the residue was washed with MeOH (3 × 2 mL), affording **Pt(L_{pc})(L_{ref})Cl_2** as a dark blue crystal (39 mg, 60%, 58% over 2 steps). Mp 270 °C (decomp). R_f = 0.59 (EtOAc/hexanes 1:6). UV-vis (CH_2Cl_2) λ_{max} (ε) 271 (85,400), 306 (sh, 104,000), 316 (265,000), 344 (23,400), 391 (sh, 14,800), 406 (17,000), 440 (660), 580 (sh, 5,890), 626 (15,800), 677 nm (27,200). IR (CH_2Cl_2, cast) 3089 (w), 3051 (w), 2954 (s), 2902 (m), 2867 (m), 2175 (w), 2100 (w), 1592 (w), 1462 (m) cm^{-1}. ^1H NMR (498 MHz, $CDCl_3$) δ 9.18 (s, 2H), 8.97 (s, 2H), 8.85 (s, 2H), 8.35 (s, 2H), 7.91–7.85 (m, 6H), 7.59–7.55 (m, 4H), 7.53–7.45 (m, 10H), 7.41–7.32 (m, 4H), 2.18 (nonet, J = 6.6 Hz, 3H), 1.59 (nonet, J = 6.6 Hz, 3H), 1.38 (s,

18H), 1.18 (s, 18H), 1.18 (d, J = 6.6 Hz, 18H), 0.95 (d, J = 7.0 Hz, 6H), 0.78 (d, J = 6.6 Hz, 18H), 0.47 (d, J = 7.0 Hz, 6H). ^{13}C NMR (126 MHz, $CDCl_3$) 152.5, 151.9, 151.8, 151.5, 140.8, 140.1, 133.0, 132.6, 132.4, 132.3, 130.43, 130.40, 129.5, 129.3, 129.2, 128.4, 126.2, 126.1, 125.9, 125.7, 125.3, 120.3, 116.4, 111.1, 110.5, 104.5, 102.0, 101.5, 100.3, 34.77, 34.76, 31.4, 31.1, 26.6, 26.2, 25.5, 25.4, 24.9, 24.4 (three signals coincident or not observed). MALDI HRMS (DCTB) calcd for $C_{102}H_{122}{}^{35}Cl_2N_2{}^{195}PtSi_2$ (M^+) 1695.1866, found 1696.8143. DSC: Decomposition, 251°C (onset), 268 °C (peak).

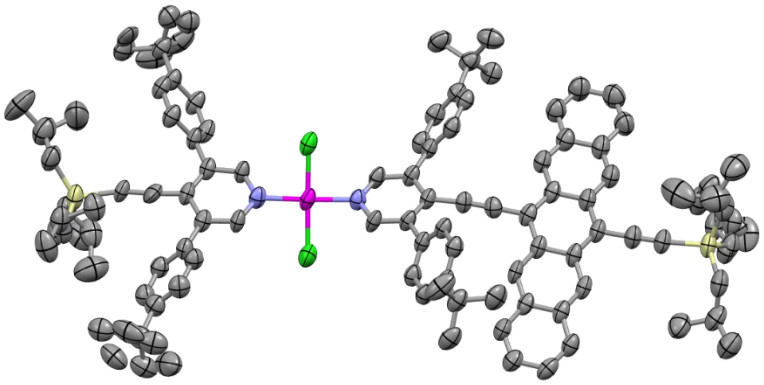

A crystal of **Pt(L$_{pc}$)(L$_{ref}$)Cl$_2$** suitable for crystallographic analysis has been grown at rt by slow evaporation of a CH_2Cl_2 solution layered with MeOH. X-ray data for **Pt(L$_{pc}$)(L$_{ref}$)Cl$_2$**•0.5CH_2Cl_2 ($C_{102.50}H_{123}Cl_3N_2PtSi_2$), F_w = 1740.64; crystal dimensions 0.22 × 0.10 × 0.02 mm, triclinic crystal system; space group $P\bar{1}$ (No. 2); a = 13.7003(4) Å, b = 16.5954(6) Å, c = 21.1156(9) Å; α= 91.722(3)°, β= 97.447(3)°, γ = 99.825(2)°; V = 4683.9(3) Å^3; Z = 2; ρ_{calcd} = 1.234 g/cm^3; $2\theta_{max}$ = 143.39°; μ = 4.172 mm^{-1}; T = 173 K; total data collected = 90605; R_1 = 0.0755 [12723 observed reflections with $F_o{}^2 \geq 2\sigma(F_o{}^2)$]; ωR_2 = 0.2031 for 17182 data, 1083 variables, and 91 restraints; largest difference, peak and hole = 2.884 and –1.296 e Å^{-3}. The C–C distances within the disordered *tert*-butyl groups were restrained by use of the *SHELXL* **SADI** instruction to be approximately the same. Likewise, the C–C and the C…C distances within the disordered isobutyl groups also were restrained. The Si2–C95 and Si2–C95A distances were restrained to be approximately the same. The rigid-bond restraint (**RIGU**) was applied to the following atoms to improve the quality of their anisotropic displacement parameters: C60 to C63A; C75, C76A to C78A; and C95 to C98. Finally, the following pairs of atoms were constrained to have equivalent anisotropic displacement parameters: C60 and C60A; C95 and C95A. CCDC: 2288686.

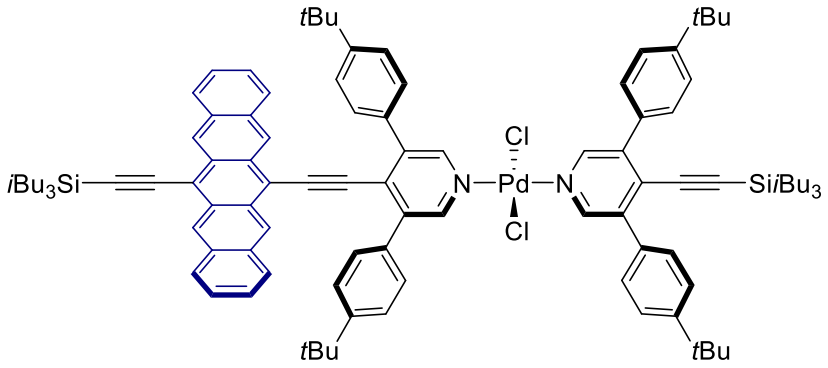

Compound Pd(L_{pc})(L_{ref})Cl_2. A solution of $Pd(PhCN)_2Cl_2$ (20 mg, 0.052 mmol) in dry CH_2Cl_2 (1 mL) was stirred at rt, followed by dropwise addition (~1 drop/s) of a solution of $\mathbf{L_{ref}}$ (35 mg, 0.062 mmol) in dry CH_2Cl_2 (2 mL) and then a solution of $\mathbf{L_{pc}}$ (45 mg, 0.052 mmol) in dry CH_2Cl_2 (2 mL) under an atmosphere of argon. The flask was wrapped in aluminum foil during the reaction to limit light exposure. After addition, the reaction mixture was plugged through a pad of alumina (CH_2Cl_2), and the solvent was then removed under reduced pressure. The residue was purified by recycling GPC ($CHCl_3$), followed by solvent removed under reduced pressure affording **Pd(L_{pc})(L_{ref})Cl_2** as a dark blue-green solid (30 mg, 36%). Mp 256 °C (decomp). R_f = 0.72 (CH_2Cl_2/hexanes 1:1). UV-vis (CH_2Cl_2) λ_{max} (ε) 270 (106,000), 306 (sh, 115,000), 315 (297,000), 346 (sh, 20,000), 401(15,400), 442 (5,890), 584 (sh, 5,890), 625 (17,000), 677 (30,100). IR (CH_2Cl_2, cast) 3084 (w), 3050 (w), 2954 (s), 2903 (m), 2867 (m), 2175 (m), 2124 (w), 1589 (m), 1506 (w), 1462 (m) cm^{-1}. ^1H NMR (498 MHz, $CDCl_3$) δ 9.18 (s, 2H), 8.89 (s, 2H), 8.76 (s, 2H), 8.34 (s, 2H), 7.90–7.85 (m, 6H), 7.56–7.54 (m, 4H), 7.52–7.46 (m, 10H), 7.38–7.34 (m, 4H), 2.17 (nonet, J = 6.7 Hz, 3H), 1.59 (nonet, J = 6.7 Hz, 3H), 1.38 (s, 18H), 1.178 (s, 18H), 1.177 (d, J = 6.6 Hz, 18H), 0.95 (d, J = 6.9 Hz, 6H), 0.77 (d, J = 6.6 Hz, 18H), 0.47 (d, J = 6.6 Hz, 6H). ^{13}C NMR (126 MHz, $CDCl_3$) 152.5, 151.89, 151.5, 151.1, 140.6, 139.9, 133.1, 132.6, 132.4, 132.3, 130.74, 130.70, 130.5, 130.4, 129.5, 129.3, 129.2, 128.4, 126.2, 126.1, 125.9, 125.7, 125.3, 120.3, 116.2, 111.1, 110.4, 104.5, 101.9, 101.4, 100.2, 34.77, 34.76, 31.4, 31.1, 26.6, 26.2, 25.5, 25.4, 24.9, 24.4 (one signal coincident or not observed). MALDI HRMS (DCTB) calcd for $C_{102}H_{122}{}^{35}Cl_2N_2{}^{106}PdSi_2$ (M^+) 1606.7553, found 1606.7539.

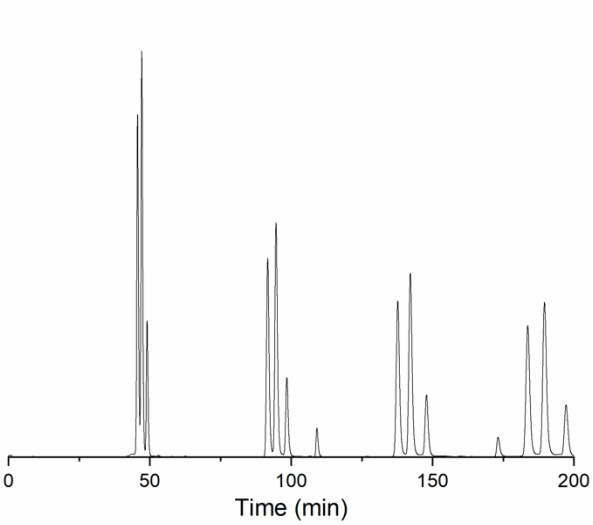

A typical recycling GPC trace of the residue for **Pd(L$_{pc}$)(L$_{ref}$)Cl$_2$** (eluting with $CHCl_3$, λ = 250 nm).

Tetra(benzonitrile)ruthenium(II) dichloride ($Ru(PhCN)_4Cl_2$) was prepared with the procedure reported in the literature.[5]

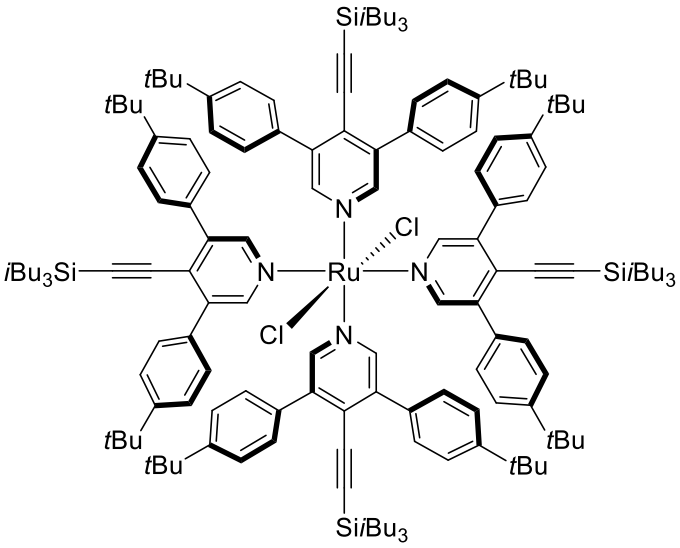

Compound Ru(L$_{ref}$)$_4$Cl$_2$. A mixture of **L$_{ref}$** (40 mg, 0.070 mmol) and $Ru(PhCN)_4Cl_2$ (10 mg, 0.017 mmol) in dry PhMe (5 mL) was stirred at 110 °C for 1 h under an atmosphere of argon. The reaction mixture was cooled to rt, and then the solvent was removed under reduced pressure. The residue was purified by column chromatography (silica gel, CH_2Cl_2/hexanes 1:2). The solvent was removed, and the residue was dissolved in CH_2Cl_2 (2 mL), followed by the addition of MeOH (15 mL). The resulting suspension was filtered, and the residue was washed with MeOH (3 × 2 mL), affording **Ru(L$_{ref}$)$_4$Cl$_2$** as a dark red solid (36 mg, 86%). Mp

288 °C (decomp). R_f = 0.34 (CH_2Cl_2/hexanes 1:3). UV-vis (CH_2Cl_2) λ_{max} (ε) 257 (127,000), 309 (45,000), 478 (43,500), 525 (sh, 23,900), 606 nm (sh, 1,670). IR (CH_2Cl_2, cast) 3063 (w), 3030 (w), 2954 (s), 2903 (m), 2867 (m), 2620 (w), 2153 (m), 1739 (w), 1503 (w), 1463 (m) cm^{-1}. ^1H NMR (498 MHz, $CDCl_3$) δ 8.72 (s, 8H), 7.38 (d, J = 8.3 Hz, 16H), 7.30 (d, J = 8.5 Hz, 16H), 1.61 (nonet, J = 6.6 Hz, 12H), 1.31 (s, 72H), 0.77 (d, J = 6.6 Hz, 72H), 0.47 (d, J = 6.9 Hz, 24H). ^{13}C NMR (126 MHz, $CDCl_3$) δ 156.1, 150.6, 138.1, 133.9, 133.8, 129.7, 126.1, 124.8, 106.9, 103.3, 34.6, 31.4, 26.2, 24.8, 24.5. MALDI HRMS (DCTB) calcd for $C_{156}H_{220}{}^{35}Cl_2N_4{}^{102}RuSi_4$ (M^+) 2435.4817, found 2435.4817. DSC: Mp = 208 °C, decomposition, 377 °C (onset), 383 °C (peak).

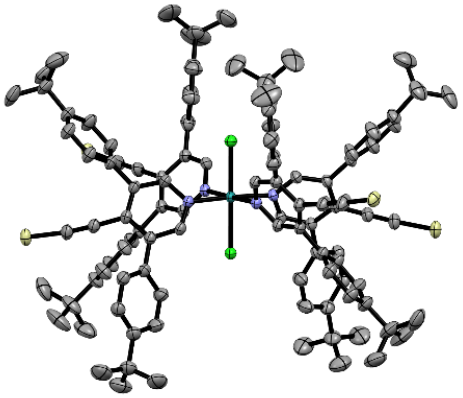

A crystal of **Ru(L$_{ref}$)$_4$Cl$_2$** suitable for crystallographic analysis has been grown at rt by slow evaporation of a THF solution layered with MeOH. X-ray data for **Ru(L$_{ref}$)$_4$Cl$_2$** ($C_{156}H_{220}Cl_2N_4RuSi_4$•2.5$C_4H_8O$), F_w = 2615.94; crystal dimensions 0.20 × 0.12 × 0.09 mm, monoclinic crystal system; space group $C2/c$ (No. 15); a = 42.4557(10) Å, b = 14.6682(4) Å, c = 27.1780(7) Å; β = 104.1601(13)°; V = 16410.8(7) $Å^3$; Z = 4; ρ_{calcd} = 1.059 g/cm^3; $2\theta_{max}$ = 144.61°; μ = 1.716 mm^{-1}; T = 173 K; total data collected = 353694; R_1 = 0.0375 [14382 observed reflections with $F_o{}^2 \geq 2\sigma(F_o{}^2)$]; ωR_2 = 0.1034 for 16185 data, 856 variables, and 242 restraints; largest difference, peak and hole = 0.480 and –0.590 e $Å^{-3}$. Attempts to refine peaks of residual electron density as disordered or partial-occupancy solvent tetrahydrofuran oxygen or carbon atoms were unsuccessful. The data were corrected for disordered electron density through use of the SQUEEZE procedure as implemented in *PLATON*.[6] A total solvent-accessible void volume of 2256 $Å^3$ with a total electron count of 402 (consistent with 10 molecules of solvent tetrahydrofuran, or 2.5 molecules per formula unit of the Ru complex) was found in the unit cell. The disordered *iso*-butyl group described by atoms C34, C35A/B, C36A/B, C37A/B had the following sets of C–C distances restrained to be approximately equal (**SADI**): C34–C35A and C34–C35B; C35A–C36A, C35A–C37A, C35B–C36B,

C35B–C37B. The C–C distances within the disordered *tert*-butyl group (C76, C77A/B, C78A/B, C79A/B) were restrained to be approximately the same. The disordered tri(*iso*-butyl)silyl group (Si2A/B, C80A/B to C83A/B and C88A/B to C91A/B had distance restraints applied to the Si–C and C–C distances to ensure that the equivalent types of bonds had approximately the same bond length. Finally, the anisotropic displacement parameters for Si and C atoms of this group were restrained to be similar by use of the *SHELXL* instruction **SIMU** and the ADPs for C83A and C83B were constrained to be equal. CCDC: 2234601.

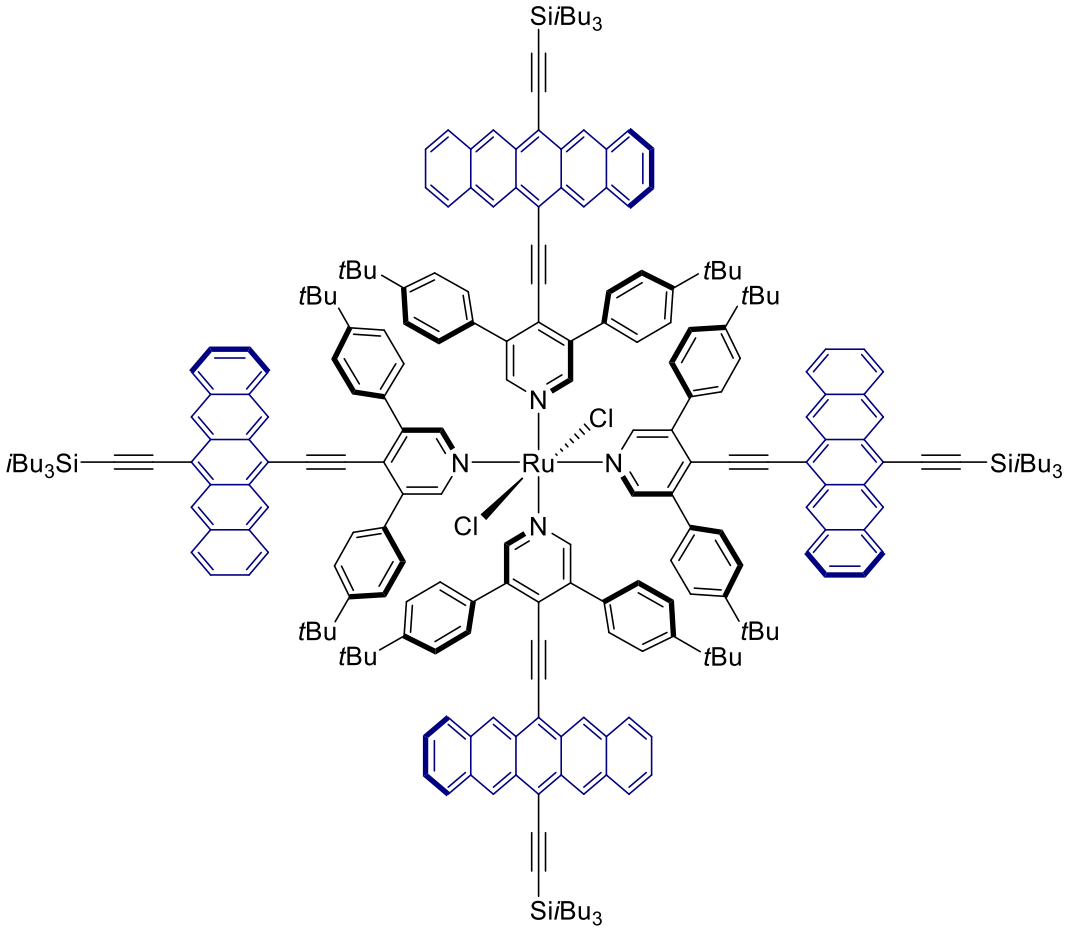

Compound Ru(L_{pc})$_4$Cl$_2$. A mixture of **L_{pc}** (59 mg, 0.068 mmol) and Ru(PhCN)$_4$Cl$_2$ (10 mg, 0.017 mmol) in dry PhMe (5 mL) was stirred at 80 °C for 16 h under an atmosphere of argon. The flask was wrapped in aluminum foil during the reaction to limit light exposure. The reaction mixture was cooled to rt, and the solvent was then removed under reduced pressure. The residue was purified by column chromatography

(alumina, CH_2Cl_2). The eluent volume was reduced in vacuo to ~1 mL, followed by the addition of MeOH (20 mL). The resulting suspension was filtered, and the residue was washed with MeOH (3 × 2 mL), affording **Ru(L$_{pc}$)$_4$Cl$_2$** as a dark blue solid (54 mg, 87%). Mp 224 °C (decomp). R_f = 0.74 (CH_2Cl_2/hexanes 1:2). UV-vis (CH_2Cl_2) λ_{max} (ε) 267 (208,000), 307 (sh, 396,000), 315 (729,000), 347 (54,200), 390 (45,200), 443 (37,200), 578 (sh, 28,700), 639 (63,300), 689 nm (109,000). IR (CH_2Cl_2, cast) 3050 (w), 2953 (s), 2924 (m), 2903 (m), 2867 (m), 2172 (m), 2122 (w), 1909 (w), 1738 (w), 1501 (w), 1462 (m) cm^{-1}. ^1H NMR (498 MHz, $CDCl_3$) δ 9.22 (s, 8H), 9.16 (s, 8H), 8.48 (s, 8H), 7.89 (d, J = 8.2 Hz, 16H), 7.84 (d, J = 8.7 Hz, 8H), 7.48 (d, J = 8.7 Hz, 8H), 7.38 (d, J = 8.4 Hz, 16H), 7.27–7.20 (m, 8H), 7.09–6.99 (m, 8H), 2.18 (nonet, J = 6.7 Hz, 12Hz), 1.18 (d, J = 6.6 Hz, 24H), 0.95 (d, J = 7.0 Hz, 72H), 1.87 (s, 72H). ^{13}C NMR (126 MHz, $CDCl_3$) δ 156.7, 151.6, 137.9, 134.3, 132.3, 132.2, 130.6, 130.3, 129.9, 129.3, 128.1, 126.6, 126.0, 125.9, 125.6, 119.0, 117.5, 110.3, 104.9, 102.8, 99.5, 34.4, 30.9, 26.6, 25.49, 25.46. MALDI HRMS (DCTB) calcd for $C_{252}H_{268}{}^{35}Cl_2N_4{}^{102}RuSi_4$ (M^+) 3633.8645, found 3633.8646. DSC: Decomposition, 338 °C (onset), 344 °C (peak).

7.3 Experimental Data for Chapter 3

General Procedure A. A solution of LiHMDS was prepared by adding *n*BuLi (9.5 equiv per acetylene moiety) to a solution of $[(CH_3)_3Si]_2NH$ (10 equiv per acetylene moiety) in dry THF (5 mL) at –78 °C. The solution was stirred at –78 °C for 30 min before the solution of appropriate terminal acetylene (1 equiv) in dry THF (10 mL) was added at –78 °C. After stirring at –78 °C for 30 min, the solution was added to a solution of **3.2** (1.1 equiv per acetylene moiety) in dry THF (10 mL) at –78 °C via a cannula. The solution was warmed to rt and stirred for 16 h under an atmosphere of N_2. After cooling to 0 °C, satd aq NH_4Cl (10 mL) was added, followed by H_2O (50 mL), the layers were separated, and the aqueous phase was extracted with CH_2Cl_2 (3 × 50 mL). The organic phases were combined, dried ($MgSO_4$), and filtered. After removing the solvent under reduced pressure, the residue was dissolved in CH_2Cl_2, passed through a pad of silica gel (CH_2Cl_2), and the solvent removal in vacuo. The crude product, presumably as a mixture of diastereomers, was dissolved in dry, deoxygenated THF

(20 mL), to which $SnCl_2 \cdot 2H_2O$ (3 equiv per tetracene moiety) and 10% H_2SO_4 (0.1 mL) were added at rt. The flask was wrapped in aluminum foil during the reaction to limit light exposure. The reaction mixture was stirred for 16 h under an atmosphere of N_2 and then poured into MeOH (100 mL). The suspension was filtered, and the residue was washed with MeOH (3 × 5 mL). Column chromatography (silica gel) or recrystallization, if necessary, provided the desired products.

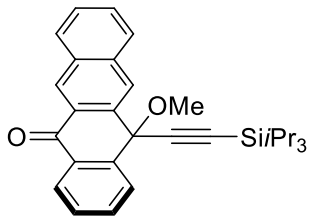

Compound 3.2. To a solution of (tri*iso*propylsilyl)acetylene (847 mg, 4.64 mmol) in dry THF (5 mL), *n*BuLi (2.5 M in hexanes, 1.78 mL, 4.45 mmol) was added at –78 °C dropwise. The solution was stirred at –78 °C for 30 min and then added via a cannula to a suspension of 5,12-naphthacenequinone (1.00 g, 3.87 mmol) in dry THF (15 mL) at –78 °C. The solution was warmed to rt and stirred for 5 h under an atmosphere of N_2. After cooling to –78 °C, MeI (2.41 mL, 38.7 mmol) was added. The solution was warmed to rt and stirred for 16 h. After cooling to 0 °C, satd aq NH_4Cl (10 mL) was added, followed by H_2O (50 mL). The layers were separated, and the aqueous phase was extracted with CH_2Cl_2 (3 × 50 mL). The organic phases were combined, dried ($MgSO_4$), and filtered. After removing the solvent, the residue was dissolved in boiling CH_2Cl_2 (5 mL), followed by addition of hexanes (40 mL) and cooling to –78 °C for 1 h. The resulting pale-yellow solid was collected by vacuum filtration and washed with hexanes (3 × 5 mL), affording **3.2** as a white solid (1.42 g, 81%). Mp 99–100 °C. R_f = 0.38 (CH_2Cl_2). IR (CH_2Cl_2, cast) 3059 (w), 2943 (s), 2891 (m), 2865 (s), 2818 (w), 2171 (w), 1675 (s), 1628 (m), 1600 (m) cm^{-1}. ^1H NMR (498 MHz, $CDCl_3$) δ 8.80 (s, 1H), 8.60 (s, 1H), 8.29 (dd, J = 7.7, 1.1 Hz, 1H), 8.18 (dd, J = 7.8, 0.8 Hz, 1H), 8.05 (dd, J = 7.5 Hz, 1H), 7.93 (dd, J = 7.6 Hz, 1H), 7.70 (dt, J = 7.6, 1.4 Hz, 1H), 7.64 (dt, J = 8.2, 6.9, 1.3 Hz, 1H), 7.61–7.56 (m, 2H), 3.07 (s, 3H), 1.22–1.14 (m, 21H). ^{13}C NMR (126 MHz, $CDCl_3$) δ 184.4, 141.1, 135.7, 135.1, 133.4, 132.9, 132.1, 129.8, 129.41, 129.38, 129.1, 128.9, 128.7, 128.6, 128.4, 127.7, 127.5, 105.1, 92.0, 74.0, 52.0, 18.8, 11.4. ESI HRMS calcd for $C_{30}H_{34}NaO_2Si$ ($[M + Na]^+$) 477.2220, found 477.2227.

1,4-Diethynylbenzene (**3.3a**) and 1,3-diethynylbenzene (**3.3b**) were synthesized as previously reported.[7–8]

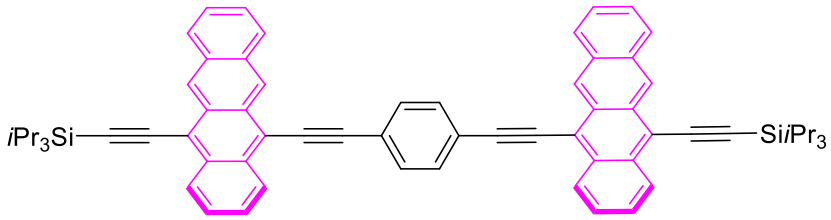

Compound pPhTc2. The acetylene 1,4-diethynylbenzene (**3.3a**, 100 mg, 0.79 mmol), *n*BuLi (2.5 M in hexanes, 6.0 mL, 15.0 mmol), $[(CH_3)_3Si]_2NH$ (3.2 mL, 15.9 mmol), compound **3.2** (793 mg, 1.74 mmol), and $SnCl_2{\bullet}2H_2O$ (1.18 g, 5.22 mmol) were used according to **General Procedure A**. The residue was purified by column chromatography (silica gel, CH_2Cl_2/hexanes 1:8), followed by solvent removal in vacuo. The solid was dissolved in minimal amount of CH_2Cl_2 (~5 mL), followed by the addition of MeOH (45 mL). The resulting suspension was filtered, and the residue was washed with MeOH (3 × 5 mL), affording **pPhTc2** as a reddish-purple solid (633 mg, 85%). Mp >350 °C (no obvious change). R_f = 0.63 (CH_2Cl_2/hexanes 1:4). UV-vis (CH_2Cl_2) λ_{max} (ε) 273 (sh, 83,000), 292 (297,000), 344 (sh, 26,800), 359 (40,500), 396 (10,600), 412 (11,100), 419 (11,800), 457 (sh, 7,000), 481 (16,500), 522 (sh, 39,700), 534 (44,000), 571 nm (76,500). IR (CH_2Cl_2, cast) 3052 (w), 2942 (s), 2890 (m), 2864 (s), 2128 (m), 1510 (m) cm^{-1}. ^1H NMR (498 MHz, $CDCl_3$) δ 9.36 (s, 2H), 9.32 (s, 2H), 8.72–8.67 (m, 4H), 8.17–8.15 (m, 2H), 8.06–8.04 (m, 2H), 7.96 (s, 4H), 7.62–7.59 (m, 4H), 7.52–7.50 (m, 4H), 1.41–1.32 (m, 42H). ^{13}C NMR (126 MHz, $CDCl_3$) δ 132.7, 132.4, 132.3, 132.2, 131.9, 130.4, 129.9, 128.7, 128.6, 127.6, 127.3, 126.8, 126.6, 126.2, 126.1, 125.9, 123.8, 119.1, 118.0, 106.2, 104.0, 103.1, 89.6, 19.0, 11.7 (one signal coincident or not observed). MALDI HRMS calcd for $C_{68}H_{66}Si_2$ (M^+) 938.4698, found 938.4691. DSC: Decomposition, 233 °C (onset), 240 °C (peak). Spectral and physical data for **pPhTc2** were consistent with that reported, see: Iwanaga T, Yamamoto Y, Nishioka K, Toyota S. *Synthesis* **2015**, *47*, 3997–4007.

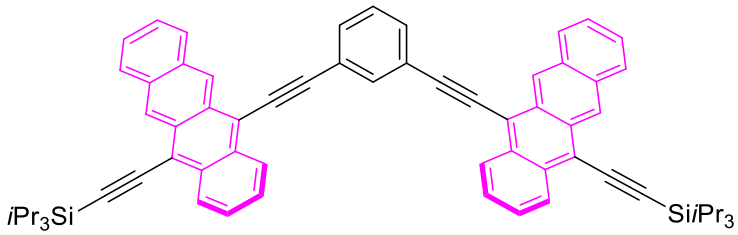

Compound mPhTc2. The acetylene 1,3-diethynylbenzene (**3.3b**, 20 mg, 0.16 mmol), *n*BuLi (2.5 M in hexanes, 1.20 mL, 3.0 mmol), $[(CH_3)_3Si]_2NH$ (0.66 mL, 3.2 mmol), compound **3.2** (159 mg, 0.35 mmol), and $SnCl_2•2H_2O$ (237 mg, 1.05 mmol) were used according to **General Procedure A**. The residue was purified by column chromatography (silica gel, CH_2Cl_2/hexanes 1:4), followed by solvent removal in vacuo. The solid was dissolved in minimal amount of CH_2Cl_2 (~1 mL), followed by the addition of MeOH (20 mL). The resulting suspension was filtered, and the residue was washed with MeOH (3 × 5 mL), affording **mPhTc2** as a scarlet solid (108 mg, 72%). Mp >350 °C (no obvious change). R_f = 0.54 (CH_2Cl_2/hexanes 1:2). UV-vis (CH_2Cl_2) λ_{max} (ε) 263 (56,700), 291 (314,000), 333 (26,200), 349 (36,300), 410 (5,760), 451 (sh, 5,870), 476 (16,600), 510 (42,200), 550 nm (66,500). IR (CH_2Cl_2, cast) 3055 (w), 2942 (s), 2891 (m), 2864 (s), 2130 (m), 1591 (m) cm^{-1}. ^1H NMR (498 MHz, $CDCl_3$) δ 9.36 (s, 2H), 9.34 (s, 2H), 8.73 (d, J = 8.0 Hz, 2H), 8.67 (d, J = 8.3 Hz, 2H), 8.30 (s, 1H), 8.17–8.16 (m, 2H), 8.05–8.04 (m, 2H), 7.91 (dd, J = 7.7, 1.5 Hz, 2H), 7.63–7.60 (m, 5H), 7.59–7.48 (m, 4H), 1.40–1.27 (m, 42H). ^{13}C NMR (126 MHz, $CDCl_3$) δ 134.7, 132.7, 132.5, 132.3, 131.9, 130.5, 130.0, 129.1, 128.7, 128.6, 127.6, 127.4, 126.87, 126.85, 126.6, 126.2, 126.1, 125.9, 124.2, 119.1, 117.9, 106.3, 104.0, 102.3, 88.1, 19.0, 11.7 (one signal coincident or not observed). MALDI HRMS calcd for $C_{68}H_{66}Si_2$ (M^+) 938.4698, found 938.4689. DSC: Decomposition, 231 °C (onset), 236 °C (peak).

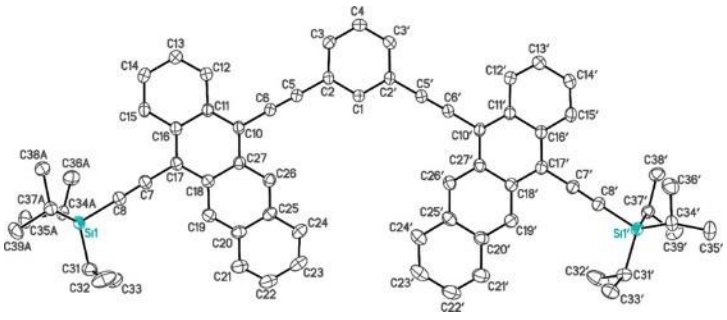

A crystal of **mPhTc2** suitable for crystallographic analysis has been grown at rt by slow evaporation of a CH_2Cl_2/THF solution layered with MeOH. X-ray data for **mPhTc2** ($C_{68}H_{66}Si_2$), F_w = 939.38; crystal dimensions 0.29 × 0.18 × 0.03 mm, monoclinic crystal

system; space group $C2/c$ (No. 15); a = 21.4979(4) Å, b = 11.6467(2) Å, c = 22.1342(4) Å; β = 96.0588(10)°; V = 5511.00(17) Å^3; Z = 4; ρ_{calcd} = 1.132 g/cm^3; $2\theta_{max}$ = 145.35°; μ = 0.878 mm^{-1}; T = 173 K; total data collected = 127036; R_1 = 0.0476 [4667 observed reflections with $F_o{}^2 \geq 2\sigma(F_o{}^2)$]; ωR_2 = 0.1378 for 5368 data, 343 variables, and 12 restraints; largest difference, peak and hole = 0.448 and –0.251 e Å^{-3}. The Si1–C34A/B and Si1–C37A/B distances were restrained to be approximately the same by use of the *SHELXL* **SADI** instruction. Additionally, the C34A/B–C35A/B and C34A/B–C36A/B distances within one of the disordered isopropyl groups were restrained to be approximately the same. CCDC: 2213852.

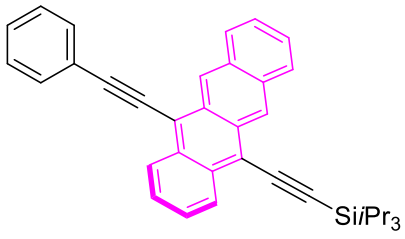

Compound PhTc. To a solution of 1-ethynylbenzene (68 mg, 0.67 mmol) in dry THF (5 mL), *n*BuLi (2.5 M in hexanes, 0.25 mL, 0.63 mmol) was added dropwise at –78 °C. After stirring at –78 °C for 30 min, the solution was added to a solution of **3.2** (205 mg, 0.45 mmol) in dry THF (15 mL) at –78 °C via a cannula. The solution was warmed to rt and stirred for 16 h under an atmosphere of N_2. After cooling to 0 °C, satd aq NH_4Cl (10 mL) was added, followed by H_2O (50 mL). The layers were separated, and the aqueous phase was extracted with CH_2Cl_2 (3 × 50 mL). The organic phases were combined, dried ($MgSO_4$), filtered. After removing the solvent, the residue was dissolved in CH_2Cl_2 and passed through a pad of silica gel (CH_2Cl_2), followed by solvent removal in vacuo. The crude product, presumably as a mixture of diastereomers, was dissolved in dry, deoxygenated THF (20 mL), to which $SnCl_2$•$2H_2O$ (305 mg, 1.35 mmol) and 10% H_2SO_4 (0.1 mL) were added at rt. The flask was wrapped in aluminum foil during the reaction to limit light exposure. The reaction mixture was stirred for 16 h under an atmosphere of N_2 and then poured into MeOH (100 mL). The suspension was filtered, and the residue was washed with MeOH (3 × 5 mL). The residue was purified by column chromatography (silica gel, CH_2Cl_2/hexanes 1:6), followed by solvent removal in vacuo. The resulting solid was dissolved in minimal amount of CH_2Cl_2 (~2 mL), followed by the addition of MeOH

(20 mL). The resulting suspension was filtered, and the residue was washed with MeOH (3 × 5 mL), affording **PhTc** as a scarlet solid (174 mg, 76%). Mp 140–142 °C. R_f = 0.62 (CH_2Cl_2/hexanes 1:2). UV-vis (CH_2Cl_2) λ_{max} (ε) 260 (26,800), 291 (172,000), 329 (17,800), 345 (22,300), 411 (3,790), 449 (sh, 3,430), 473 (9,730), 506 (23,300), 545 nm (33,100). IR (CH_2Cl_2, cast) 3054 (w), 2942 (s), 2890 (m), 2864 (s), 2129 (m), 1597 (w) cm^{-1}. ^1H NMR (498 MHz, $CDCl_3$) δ 9.34 (s, 1H), 9.29 (s, 1H), 8.69–8.64 (m, 2H), 8.12–8.10 (m, 1H), 8.04–8.02 (m, 1H), 7.86–7.84 (m, 2H), 7.58–7.56 (m, 2H), 7.52–7.46 (m, 5H), 1.40–1.31 (m, 21H). ^{13}C NMR (126 MHz, $CDCl_3$) δ 132.7, 132.35, 132.28, 132.2, 131.8, 130.5, 130.0, 128.8, 128.69, 128.66, 128.6, 127.5, 127.4, 126.8, 126.7, 126.5, 126.1, 126.0, 123.6, 118.7, 118.4, 106.0, 104.0, 103.3, 87.1, 19.0, 11.7 (one signal coincident or not observed). MALDI HRMS calcd for $C_{37}H_{36}Si$ (M^+) 508.2581, found 508.2581. DSC: Mp = 140 °C.

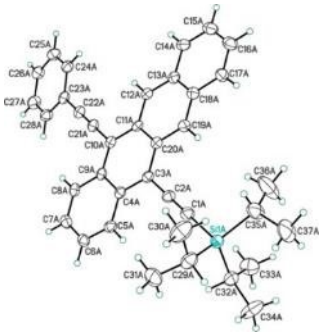

A crystal of **PhTc** suitable for crystallographic analysis has been grown at rt by slow evaporation of a CH_2Cl_2 solution layered with MeOH. X-ray data for **PhTc** ($C_{37}H_{36}Si$), F_w = 508.75; crystal dimensions 0.20 × 0.08 × 0.07 mm, orthorhombic crystal system; space group *Pna*21 (No. 33); a = 34.9449(10) Å, b = 8.5384(3) Å, c = 39.2234(12) Å; V = 11703.2(6) $Å^3$; Z = 16; ρ_{calcd} = 1.155 g/cm^3; $2\theta_{max}$ = 144.84°; μ = 0.864 mm^{-1}; T = 173 K; total data collected = 167627; R_1 = 0.0742 [19731 observed reflections with $F_o^2 \geq 2\sigma(F_o^2)$]; ωR_2 = 0.2067 for 23102 data, 1392 variables, and 0 restraints; largest difference, peak and hole = 0.511 and –0.321 e $Å^{-3}$. CCDC: 2213851.

1,3-Diethynyladamantane (**3.7**) was synthesized as previously reported.[9]

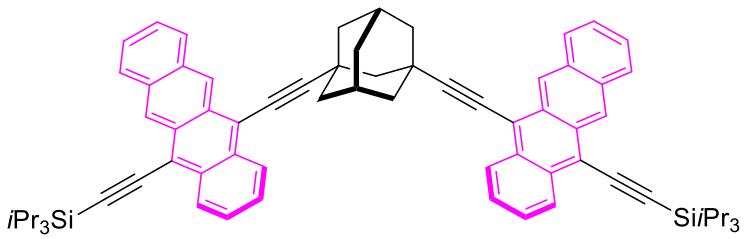

Compound mAdTc2. The acetylene 1,3-diethynyl-adamantane (**3.7**, 50 mg, 0.27 mmol), *n*BuLi (2.5 M in hexanes, 2.06 mL, 5.13 mmol), $[(CH_3)_3Si]_2NH$ (1.14 mL, 5.4 mmol), compound **3.2** (271 mg, 0.60 mmol), and $SnCl_2•2H_2O$ (406 mg, 1.8 mmol) were used according to **General Procedure A**. The residue was purified by column chromatography (silica gel, CH_2Cl_2/hexanes 1:6), followed by solvent removal in vacuo. The solid was dissolved in minimal amount of CH_2Cl_2 (~1 mL), followed by the addition of MeOH (20 mL). The resulting suspension was filtered, and the residue was washed with MeOH (3 × 5 mL), affording **mAdTc2** as a red solid (154 mg, 57%). Mp 183–184 °C. R_f = 0.46 (CH_2Cl_2/hexanes 1:4). UV-vis (CH_2Cl_2) λ_{max} (ε) 254 (39,300), 282 (sh, 165,000), 290 (427,000), 299 (sh, 71,400), 316 (34,800), 331 (27,100), 409 (4,940), 438 (5,870), 466 (17,100), 497 (43,100), 534 nm (64,600). IR (CH_2Cl_2, cast) 3053 (w), 2940 (s), 2864 (s), 2206 (W), 2136 (m) cm^{-1}. ^1H NMR (498 MHz, $CDCl_3$) δ 9.31 (s, 2H), 9.22 (s, 2H), 8.63–8.59 (m, 4H), 8.11 (d, J = 7.7 Hz, 2H), 8.06 (d, J = 8.1 Hz, 2H), 7.56–7.52 (m, 4H), 7.47–7.42 (m, 4H), 2.79 (s, 2H), 2.43–2.36 (m, 10H), 1.97 (s, 2H), 1.40–1.30 (m, 42H). ^{13}C NMR (126 MHz, $CDCl_3$) δ 132.8, 132.2, 132.1, 132.0, 130.5, 130.0, 128.7, 128.6, 127.5, 127.4, 126.7, 126.4, 126.3, 126.1, 126.0, 125.9, 119.2, 117.8, 111.3, 105.3, 104.1, 77.7, 47.9, 42.3, 35.4, 31.8, 28.3, 19.0, 11.7. MALDI HRMS calcd for $C_{72}H_{76}Si_2$ (M^+) 996.5480, found 996.5480. DSC: Mp = 254 °C, decomposition, 308 °C (onset), 309 °C (peak).

1-Ethynyladamantane (**3.9**) was synthesized as previously reported.[10]

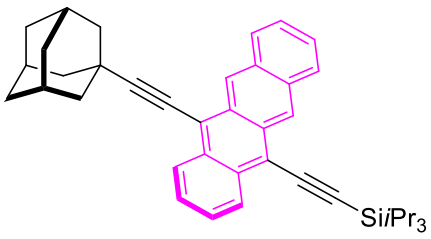

Compound AdTc. The acetylene 1-ethynyladamantane (**3.9**, 59 mg, 0.37 mmol), *n*BuLi (2.5 M in hexanes, 1.40 mL, 3.5 mmol), $[(CH_3)_3Si]_2NH$ (0.78 mL, 3.7 mmol), compound **3.2** (159 mg, 0.407 mmol), and $SnCl_2•2H_2O$ (275mg, 1.22 mmol) were used according to **General Procedure A**. The residue was purified by column chromatography (silica gel, CH_2Cl_2/hexanes 1:8), followed by solvent removal in vacuo. The solid was dissolved in minimal amount of CH_2Cl_2

(~1 mL), followed by the addition of MeOH (20 mL). The resulting suspension was filtered, and the residue was washed with MeOH (3 × 5 mL), affording **AdTc** as a red solid (65 mg, 31%). Mp 114–116 °C. R_f = 0.62 (CH_2Cl_2/hexanes 1:4). UV-vis (CH_2Cl_2) λ_{max} (ε) 253 (18,100), 283 (sh, 76,800), 291 (228,000), 300 (sh, 335,000), 316 (16,600), 331 (12,500), 409 (2,130), 438 (2,600), 465 (8,260), 497 (20,500), 533 nm (29,500). IR (CH_2Cl_2, cast) 3056 (w), 2906 (s), 2863 (s), 2205 (w), 2130 (m) cm^{-1}. ^1H NMR (498 MHz, $CDCl_3$) δ 9.30 (s, 1H), 9.18 (s, 1H), 8.61 (d, J = 7.5, 1H), 8.56 (d, J = 7.5, 1H), 8.08–8.07 (m, 1H), 8.02–8.01 (m, 1H), 7.54–7.49 (m, 2H), 7.46–7.44 (m, 2H), 2.29 (d, J = 1.5 Hz, 6H), 2.14 (s, 3H), 1.89–1.82 (m, 6H), 1.39–1.32 (m, 21H). ^{13}C NMR (126 MHz, $CDCl_3$) δ 132.8, 132.2, 132.0, 131.9, 130.5, 130.0, 128.7, 128.6, 127.6, 127.3, 126.6, 126.3, 126.22, 126.16, 125.9, 125.7, 119.7, 117.4, 113.0, 105.0, 104.2, 43.2, 36.5, 31.4, 28.2, 19.0, 11.7 (one signal coincident or not observed). MALDI HRMS calcd for $C_{41}H_{46}Si$ (M^+) 566.3363, found 566.3362. DSC: Mp = 254 °C.

7.4 Experimental Data for Chapter 4

General Procedure B. A solution of lithium LiHMDS was prepared by adding *n*BuLi (15 equiv) to a solution of $[(CH_3)_3Si]_2NH$ (16 equiv) in dry THF (5 mL) at –78 °C. The solution was stirred at –78 °C for 30 min before the solution of appropriate pyridyl-endcapped acetylene (1 equiv) in dry THF (10 mL) was added at –78 °C. After stirring at –78 °C for 30 min, the solution of LiHMDS was added to a solution of compound **3.2** (1.2 equiv) in dry THF (10 mL) at –78 °C via a cannula. The resulting solution was warmed to rt and stirred for 16 h under an atmosphere of N_2. After cooling to 0 °C, satd aq NH_4Cl (10 mL) was added, followed by H_2O (50 mL), the layers were separated, and the aqueous phase was extracted with CH_2Cl_2 (3 × 50 mL). The organic phases were combined, dried ($MgSO_4$), and filtered. After removing the solvent under reduced pressure, the residue was dissolved in CH_2Cl_2, passed through a pad of silica gel (CH_2Cl_2), followed by solvent removal in vacuo. The crude product, presumably as a mixture of diastereomers, was dissolved in dry, deoxygenated THF (20 mL), to which $SnCl_2$•$2H_2O$ (3 equiv) and 10% H_2SO_4 (0.1 mL) were added at rt. The flask was wrapped in aluminum foil during the reaction to limit light exposure. The reaction mixture was stirred for 16 h under an atmosphere of N_2 and then passed through a pad

of basic alumina (THF), followed by solvent removal in vacuo. Column chromatography (silica gel) and recrystallization provided the desired products. The workup was performed in the absence of ambient light.

General Procedure C. A mixture of pyridyl tetracene (1 equiv) and **RuPc** (1.2 equiv per tetracene moiety) in $CHCl_3$ (5 mL) was stirred at room temperature for 5 min under an atmosphere of N_2. The flask was wrapped in aluminum foil during the reaction to limit light exposure. The reaction mixture was concentrated to ~1 mL under reduced pressure. Purification with size exclusion column chromatography (Bio-Beads SX1 support, $CHCl_3$), followed by solvent removal in vacuo gave the desired products.

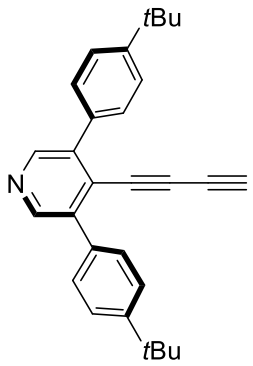

4.1 (82%)

The pyridyl-endcapped terminal diyne **4.1** was synthesized as reported in the literature.[1]

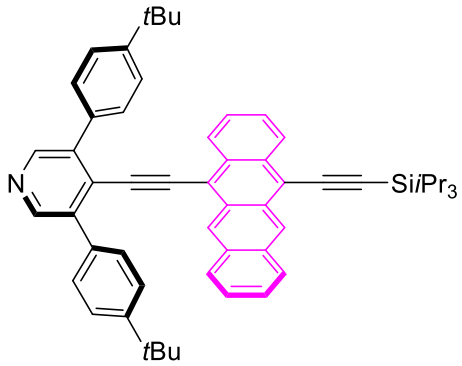

Compound TcPy-1. The pyridyl-endcapped terminal monoyne **2.7** (30 mg, 0.082 mmol), *n*BuLi (2.5 M in hexanes, 0.49 mL, 1.2 mmol), $[(CH_3)_3Si]_2NH$ (0.27 mL, 1.3 mmol), compound **3.2** (45 mg, 0.098 mmol), and $SnCl_2 \cdot 2H_2O$ (56 mg, 0.25 mmol) were used according to **General Procedure B**. The residue was purified by column chromatography (silica gel, CH_2Cl_2/hexanes 1:4), followed by solvent removal in vacuo. The resulting solid was dissolved in minimal amount of CH_2Cl_2 (~1 mL), followed by the addition of MeOH

(20 mL). The resulting suspension was filtered, and the residue was washed with MeOH (3 × 5 mL), affording **TcPy-1** as a red solid (36 mg, 57%). Mp 220–221 °C. R_f = 0.38 (EtOAc/hexanes 1:4). UV-vis (CH_2Cl_2) λ_{max} (ε) 294 (140,000), 370 (13,800), 412 (4,050), 464 (sh, 3,480), 483 (9,370), 516 (24,000), 555 nm (36,300). IR (CH_2Cl_2, cast) 3048 (w), 2962 (s), 2864 (s), 2179 (m), 2129 (s), 1569 (m) cm^{-1}. ^1H NMR (498 MHz, $CDCl_3$) δ 9.21 (s, 1H), 8.72 (s, 2H), 8.44 (d, J = 8.7 Hz, 1H), 8.39 (s, 1H), 7.94 (d, J = 8.4 Hz, 1H), 7.80 (d, J = 8.5 Hz, 4H), 7.68 (d, J = 8.7 Hz, 1H), 7.54–7.52 (m, 5H), 7.46–7.35 (m, 3H), 7.18–7.15 (m, 1H), 1.37–1.28 (m, 39H). ^{13}C NMR (126 MHz, $CDCl_3$) δ 151.6, 149.0, 138.5, 134.9, 132.7, 132.4, 132.08, 132.06, 130.2, 129.9, 129.5, 129.2, 128.4, 128.0, 127.3, 127.2, 126.6, 126.1, 126.0, 125.9, 125.8, 125.6, 119.5, 117.5, 106.5, 103.9, 100.1, 97.4, 34.8, 31.4, 19.0, 11.6 (one signal coincident or not observed). ESI HRMS calcd for $C_{56}H_{60}NSi$ ($[M + H]^+$) 774.4490, found 774.4486. DSC: Mp = 218 °C; decomposition, 309 °C (onset), 333 °C (peak).

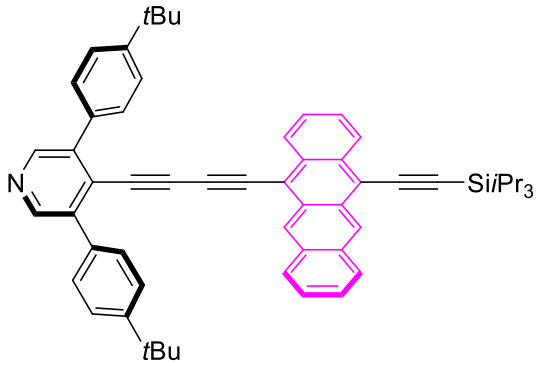

Compound TcPy-2. The pyridyl-endcapped terminal diyne **4.1** (30 mg, 0.077 mmol), *n*BuLi (2.5 M in hexanes, 0.46 mL, 1.2 mmol), $[(CH_3)_3Si]_2NH$ (0.26 mL, 1.2 mmol), compound **3.2** (42 mg, 0.092 mmol), and $SnCl_2$•$2H_2O$ (52 mg, 0.23 mmol) were used according to **General Procedure B**. The residue was purified by column chromatography (silica gel, CH_2Cl_2/hexanes 1:4), followed by solvent removal in vacuo. The resulting solid was dissolved in minimal amount of CH_2Cl_2 (~1 mL), followed by the addition of MeOH (20 mL). The resulting suspension was filtered, and the residue was washed with MeOH (3 × 5 mL), affording **TcPy-2** as a purple red solid (31 mg, 50%). Mp 201–202 °C. R_f = 0.35 (EtOAc/hexanes 1:4). UV-vis (CH_2Cl_2) λ_{max} (ε) 260 (46,800), 295 (156,000), 341 (14,600), 386 (14,600), 412 (4,680), 465 (sh, 3,310), 491 (9,260), 521 (23,100), 560 nm (33,600). IR (CH_2Cl_2, cast) 3054 (w), 3031 (w), 2961 (s), 2904 (m), 2865 (s), 2194 (w), 2133 (m), 1570 (m) cm^{-1}. ^1H NMR (498 MHz, $CDCl_3$) δ 9.31 (s,

1H), 9.02 (s, 1H), 8.69 (s, 2H), 8.62 (d, J = 7.9 Hz, 1H), 8.39 (d, J = 7.8 Hz, 1H), 8.03–8.00 (m, 2H), 7.73 (d, J = 6.6 Hz, 4H), 7.63 (d, J = 6.6 Hz, 4H), 7.56–7.47 (m, 4H), 1.42 (s, 18H), 1.39–1.29 (m, 21H). ^{13}C NMR (126 MHz, $CDCl_3$) δ 151.7, 148.7, 139.3, 134.1, 134.0, 132.5, 132.4, 132.3, 130.8, 130.2, 129.3, 128.7, 128.4, 127.7, 127.4, 126.95, 126.90, 126.8, 126.4, 126.3, 125.6, 125.5, 120.4, 116.0, 107.5, 103.7, 87.0, 84.3, 82.6, 82.2, 34.8, 31.4, 19.0, 11.6 (one signal coincident or not observed). ESI HRMS calcd for $C_{58}H_{60}NSi$ ($[M + H]^+$) 798.4490, found 798.4490. DSC: Mp = 180 °C.

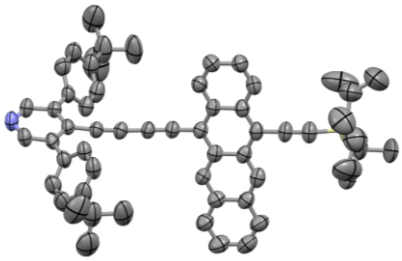

A crystal of **TcPy-2** suitable for crystallographic analysis has been grown at rt by slow evaporation of a THF/CH_2Cl_2 solution layered with MeOH. X-ray data for **TcPy-2** ($C_{58}H_{59}NSi$), F_w = 798.15; crystal dimensions 0.39 × 0.22 × 0.13 mm, monoclinic crystal system; space group $P21/c$ (No. 14); a = 12.8797(19) Å, b = 18.647(3) Å, c = 41.990(6) Å; β = 98.166(2)°; V = 9982(3) Å^3; Z = 8; ρ_{calcd} = 1.062 g/cm^3; $2\theta_{max}$ = 50.81°; μ = 0.083 mm^{-1}; T = 193 K; total data collected = 128127; R_1 = 0.0960 [8097 observed reflections with $F_o{}^2 \geq 2\sigma(F_o{}^2)$]; ωR_2 = 0.3378 for 18302 data, 1223 variables, and 843 restraints; largest difference, peak and hole = 0.758 and –0.440 e Å^{-3}. A total of 189 same distance (**SADI**) restraints were applied to the disordered tri*iso*propylsilyl groups and *tert*-butyl groups. Additionally, 180 rigid-bond (**RIGU**) and 474 similar Us (**SIMU**) restraints were applied to improve the quality of the anisotropic displacement parameters of the disordered atoms.

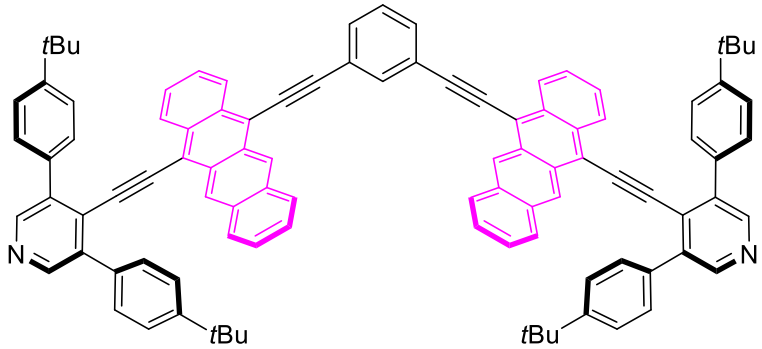

Compound mPh(TcPy)$_2$. A solution of LiHMDS was prepared by adding *n*BuLi (2.5 M in hexanes, 1.28 mL, 3.2 mmol) to a solution of $[(CH_3)_3Si]_2NH$ (0.70 mL, 3.3 mmol) in dry THF (5 mL) at –78 °C. The solution was

stirred at –78 °C for 30 min, and a solution of **2.7** (134 mg, 0.36 mmol) in dry THF (10 mL) was added at –78 °C. After stirring at –78 °C for 30 min, the resulting solution was added to a solution of 5,12-naphthacenequinone (86 mg, 0.33 mmol) in dry THF (10 mL) at –78 °C via a cannula. The resulting solution was warmed to rt and stirred for 4 h. After cooling to –78 °C, 1,3-diethynylbenzene (**3.3b**, 20 mg, 0.16 mmol) in dry THF (10 mL) was added. The solution was warmed to rt and stirred for 16 h under an atmosphere of N_2. After cooling to 0 °C, satd aq NH_4Cl (10 mL) was added, followed by H_2O (50 mL), the layers were separated, and the aqueous phase was extracted with CH_2Cl_2 (3 × 50 mL). The organic phases were combined, dried ($MgSO_4$), and filtered. After removing the solvent under reduced pressure, the residue was dissolved in CH_2Cl_2 and then passed through a pad of silica gel (EtOAc/hexanes 1:2), followed by solvent removal in vacuo. The crude product, presumably as a mixture of diastereomers, was dissolved in dry, deoxygenated THF (20 mL), to which $SnCl_2$•$2H_2O$ (220 mg, 0.95 mmol) and 10% H_2SO_4 (0.1 mL) were added at rt. The flask was wrapped in aluminum foil during the reaction to limit light exposure. The reaction mixture was stirred for 16 h under an atmosphere of N_2 and then passed through a pad of basic alumina (THF), followed by solvent removal in vacuo. The residue was purified by column chromatography (silica gel, EtOAc/hexanes 1:3), followed by solvent removal in vacuo, and the solid was dissolved in minimal amount of CH_2Cl_2 (~1 mL), followed by the addition of MeOH (20 mL). The resulting suspension was filtered, and the residue was washed with MeOH (3 × 5 mL), affording **mPh(TcPy)$_2$** as a dark purple solid (122 mg, 59%). Mp >350 °C (no obvious change). R_f = 0.30 (EtOAc/hexanes 1:3). UV-vis (CH_2Cl_2) λ_{max} (ε) 294 (203,000), 337 (28,200), 374 (31,800), 411 (8,470), 465 (sh, 6,080), 493 (16,800), 528 (41,600), 570 nm (64,300). IR (CH_2Cl_2, cast) 3053 (w), 3029 (w), 2962 (s), 2904 (m), 2868 (w), 2180 (w), 1591 (m) cm^{-1}. ^1H NMR (498 MHz, $CDCl_3$) δ 9.23 (s, 2H), 8.73 (s, 4H), 8.64 (d, J = 8.9 Hz, 2H), 8.43 (s, 2H), 8.23 (s, 1H), 8.08 (d, J = 8.5 Hz, 2H), 7.87 (dd, J = 8.8 Hz, 1.6 Hz, 2H), 7.82 (d, J = 6.8 Hz, 8H), 7.73 (d, J = 8.7 Hz, 2H), 7.60 (t, J = 7.8 Hz, 1H), 7.55 (d + m, J = 8.5 Hz, 10H), 7.53–7.49 (m, 2H), 7.45–7.38 (m, 4H), 7.23–7.20 (m, 2H), 1.30 (s, 36H). ^{13}C NMR (126 MHz, $CDCl_3$) δ 151.7, 149.0, 138.5, 134.9, 134.6, 132.7, 132.3, 132.20, 132.16, 132.0,

129.9, 129.8, 129.5, 129.3, 129.1, 128.4, 128.0, 127.4, 127.1, 126.71, 126.68, 126.2, 125.9, 125.7, 124.1, 118.7, 118.0, 102.6, 100.4, 97.4, 88.0, 34.8, 31.4. (two signals coincident or not observed). MALDI HRMS calcd for $C_{100}H_{80}N_2$ (M^+) 1308.6316, found 1308.6322. DSC: Decomposition, 264 °C (onset), 325 °C (peak).

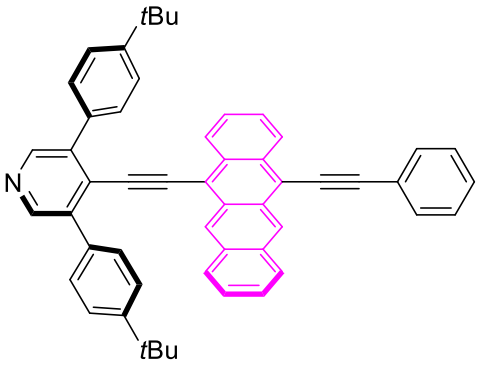

Compound PhTcPy. A solution of LiHMDS was prepared by adding *n*BuLi (2.5 M in hexanes, 0.88 mL, 2.2 mmol) to a solution of $[(CH_3)_3Si]_2NH$ (0.48 mL, 2.3 mmol) in dry THF (5 mL) at –78 °C. The solution was stirred at –78 °C for 30 min, and a solution of **2.7** (49 mg, 0.13 mmol) in dry THF (10 mL) was added at –78 °C. After stirring at –78 °C for 30 min, the solution was added to a solution of 5,12-naphthacenequinone (29 mg, 0.11 mmol) in dry THF (10 mL) at –78 °C via a cannula. The solution was warmed to rt and stirred for 4 h. After cooling to –78 °C, 4-ethynylbenzene (17 mg, 0.17 mmol) in dry THF (10 mL) was added. The solution was warmed to rt and stirred for 16 h under an atmosphere of N_2. After cooling to 0 °C, satd aq NH_4Cl (10 mL) was added, followed by H_2O (50 mL), the layers were separated, and the aqueous phase was extracted with CH_2Cl_2 (3 × 50 mL). The organic phases were combined, dried ($MgSO_4$), and filtered. After removing the solvent, the residue was dissolved in CH_2Cl_2 and passed through a pad of silica gel (EtOAc/hexanes 1:2), followed by solvent removal in vacuo. The crude product, presumably as a mixture of diastereomers, was dissolved in dry, deoxygenated THF (20 mL), to which $SnCl_2$•$2H_2O$ (74 mg, 0.33 mmol) and 10% H_2SO_4 (0.1 mL) were added at rt. The flask was wrapped in aluminum foil during the reaction to limit light exposure. The reaction mixture was stirred for 16 h under an atmosphere of N_2 and then passed through a pad of basic alumina (THF), followed by solvent removal in vacuo. The residue was purified by column chromatography (silica gel, EtOAc/hexanes 1:3), followed by solvent removal in vacuo. The resulting solid was dissolved in minimal amount of CH_2Cl_2 (~1 mL), followed by the addition of MeOH (20 mL). The resulting suspension was filtered, and

the residue was washed with MeOH (3 × 5 mL), affording **PhTcPy** as a scarlet solid (60 mg, 76%). Decomposition 272 °C. R_f = 0.32 (EtOAc/hexanes 1:3). UV-vis (CH_2Cl_2) λ_{max} (ε) 295 (110,000), 322 (13,800), 374 (14,200), 412 (3,500), 463 (sh, 2,900), 492 (4,830), 525 (21,700), 565 nm (31,900). IR (CH_2Cl_2, cast) 3055 (w), 3034 (w), 2965 (s), 2903 (m), 2867 (w), 2189 (m), 1613 (w), 1597 (m), 1569 (s) cm^{-1}. ^1H NMR (498 MHz, $CDCl_3$) δ 9.19 (s, 1H), 8.72 (s, 2H), 8.59 (d, J = 8.7 Hz, 1H), 8.41 (s, 1H), 8.03 (d, J = 8.4 Hz, 1H), 7.81 (d, J = 8.4 Hz, 6H), 7.71 (d, J = 8.5 Hz, 1H), 7.56–7.38 (m, 11H), 7.21–7.18 (m, 1H), 1.30 (s, 18H). ^{13}C NMR (126 MHz, $CDCl_3$) δ 151.6, 149.0, 138.5, 134.9, 132.8, 132.11, 132.06, 131.8, 129.9, 129.8, 129.5, 129.2, 128.9, 128.7, 128.4, 128.0, 127.3, 127.2, 126.6, 126.5, 126.1, 125.81, 125.75, 125.6, 123.5, 119.3, 117.5, 103.7, 100.2, 97.5, 87.1, 34.8, 31.4. (two signals coincident or not observed). MALDI HRMS calcd for $C_{53}H_{43}N$ (M^+) 693.3396, found 693.3390. DSC: Decomposition, 273 °C (onset), 280 °C (peak).

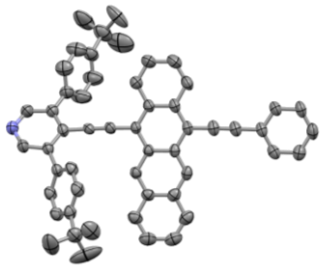

A crystal of **PhTcPy** suitable for crystallographic analysis has been grown at rt by slow evaporation of a $CDCl_3/CH_2Cl_2$ solution layered with MeOH. X-ray data for **PyTcPy** ($C_{53}H_{43}N$), F_w = 693.88; crystal dimensions 0.25 × 0.15 × 0.02 mm, triclinic crystal system; space group $P\bar{1}$ (No. 2); a = 9.5667(3) Å, b = 13.6165(3) Å, c = 15.6536(4) Å; α = 83.3598(16)°, β = 83.3598(16)°, γ = 83.3598(16)°; V = 1956.94(9) $Å^3$; Z = 2; ρ_{calcd} = 1.178 g/cm^3; $2\theta_{max}$ = 140.94°; μ = 0.508 mm^{-1}; T = 173 K; total data collected = 49759; R_1 = 0.0548 [4970 observed reflections with $F_o^2 \geq 2\sigma(F_o^2)$]; ωR_2 = 0.1705 for 7204 data, 833 variables, and 899 restraints; largest difference, peak and hole = 0.286 and –0.223 e $Å^{-3}$. A total of 185 same distance (**SADI**) restraints were applied to the following sets of atoms to improve the geometry of the minor component of the nearly whole-molecule disorder: C3–C26 and C3–C26A; the C–C distances within the *tert*-butyl group containing atoms C12 to C15A; the C–C distances within the phenyl group C16 to C20 and C16A to C20A; C19–C22 and C19A–C22A; the C–C distances within the *tert*-butyl group containing atoms C22 to C25 and C22A to C25A; the C19–C22 and C19A–C22A distances; the C18…C22,

C20…C22, C18A…C22A and C20A…C22A distances; the C…C distances of the methyl carbon atoms of the *tert*-butyl group containing atoms C22 to C25 and C22A to C25A; the C–C distances within the phenyl group C48 to C53 and C48A to C53A. The rigid-bond restraint (**RIGU**) was applied to the anisotropic displacement parameters of carbon atoms C12 to C53A (i.e. the entirety of the disordered molecule; 642 restraints). Finally, the **SIMU** restraint was applied to atoms C12 to C15 and C13A to C15A to improve the quality of the ADPs for the atoms of the two disordered parts (72 restraints).

Ru(II) 1,4,8,11,15,18,22,25-octabutoxyphthalocyanine (**RuPc**) was synthesized as previously reported.[11]

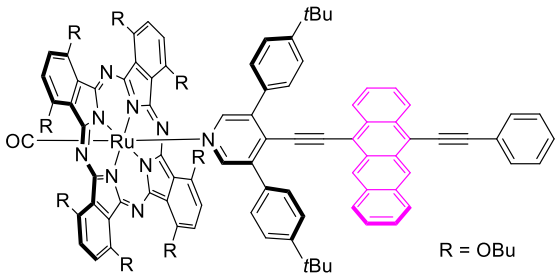

Compound PhTcPy-RuPc. The pyridyl tetracene **PhTcPy** (20 mg, 0.029 mmol) and **RuPc** (42 mg, 0.035 mmol) were used according to **General Procedure C**. The product **PhTcPy-RuPc** was obtained as a dark purple solid (55 mg, quant). Mp >350 °C (no obvious change). UV-vis (CH_2Cl_2) λ_{max} (ε) 275 (sh, 81,600), 297 (194,000), 317 (sh, 52,100), 332 (sh, 41,000), 370 (22,600), 404 (sh, 18,700), 438 (13,100), 502 (14,800), 534 (24,200), 576 (34,400), 633 (40,500), 678 (sh, 45,400), 704 nm (170,000). IR (CH_2Cl_2, cast) 3052 (w), 2957 (s), 2933 (s), 2867 (w), 2871 (s), 2672 (w), 2571 (w), 2464 (w), 2365 (w), 2175 (m), 2046 (w), 1973 (s), 1597 (s) cm^{-1}. ^1H NMR (498 MHz, $CDCl_3$) δ 8.98 (s, 1H), 8.39 (d, J = 8.6 Hz, 1H), 7.87 (d, J = 8.6 Hz, 1H), 7.70–7.68 (m, 3H), 7.47 (s, 8H), 7.40–7.38 (m, 3H), 7.30–7.26 (m, 2H), 7.26–7.18 (m, 1H), 7.17–7.12 (m, 2H), 6.94–6.92 (m, 5H), 6.34 (d, J = 8.4 Hz, 4H), 4.95 (dt, J = 11.5, 7.5 Hz, 8H), 4.84 (dt, J = 11.5, 7.4 Hz, 8H), 2.40 (s, 2H), 2.23 (quint, J = 7.5 Hz, 16H), 1.69 (sext, J = 7.5 Hz, 16H), 1.11 (t, J = 7.4 Hz, 24H), 1.03 (s, 18H). ^{13}C NMR (126 MHz, $CDCl_3$) δ 180.6, 151.3, 150.8, 143.8, 143.0, 137.4, 132.5, 132.0, 131.8, 131.74, 131.69, 129.7, 129.5, 129.4, 129.0, 128.9, 128.5, 128.4, 128.2, 127.8,

126.93, 126.89, 126.4, 126.3, 125.9, 125.6, 125.5, 125.0, 123.3, 119.4, 116.6, 116.4, 103.7, 98.7, 98.6, 86.9, 71.4, 34.4, 31.8, 31.1, 19.6, 19.4, 14.2. MALDI HRMS calcd for $C_{118}H_{123}N_2O_9{}^{102}Ru$ (M^+) 1911.8482, found 1911.8488. DSC: No change <350 °C.

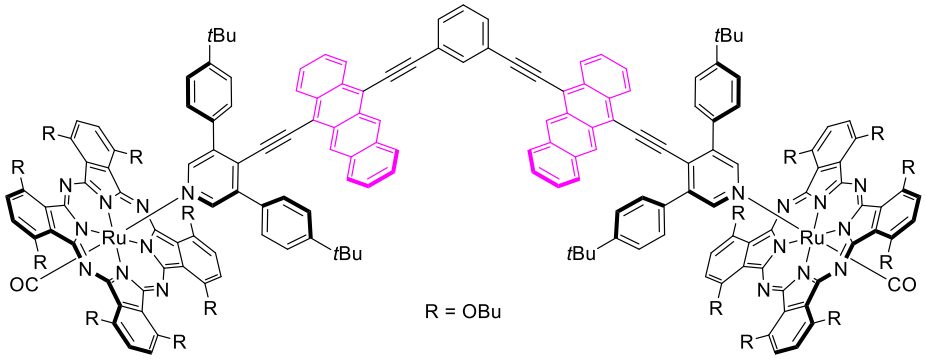

Compound mPh(TcPy-RuPc)$_2$. The pyridyl tetracene **mPh(TcPy)$_2$** (10 mg, 0.0076 mmol) and **RuPc** (22 mg, 0.018 mmol) were used according to **General Procedure C**. The product **mPh(TcPy-RuPc)$_2$** was obtained as a dark purple solid (28 mg, quant). Mp >350 °C (no obvious change). UV-vis (CH_2Cl_2) λ_{max} (ε) 275 (sh, 169,000), 296 (238,000), 323 (sh, 88,700), 338 (sh, 71,100), 367 (sh, 49,400), 437 (sh, 26,800), 505 (29,600), 539 (47,100), 581 (68,400), 639 (46,900), 680 (sh, 60,300), 704 nm (209,000). IR (CH_2Cl_2, cast) 3051 (w), 2958 (s), 2933 (s), 2870 (s), 2680 (w), 2558 (w), 2461 (w), 2352 (w), 2175 (m), 2015 (s), 1970 (s), 1593 (s) cm^{-1}. ^1H NMR (498 MHz, $CDCl_3$) δ 8.96 (s, 2H), 8.37 (d, J = 8.9 Hz, 2H), 8.00 (s, 1H), 7.86 (d, J = 8.7 Hz, 2H), 7.69 (dd, J = 7.8 Hz, 1.6 Hz, 2H), 7.67 (s, 2H), 7.46 (s, 16H), 7.28–7.11 (m, 11H), 6.32 (d, J = 8.3 Hz, 8H), 4.94 (dt, J = 11.5, 7.4 Hz, 16H), 4.83 (dt, J = 11.4, 7.3 Hz, 16H), 2.39 (s, 4H), 2.22 (quint, J = 7.4 Hz, 16H), 1.68 (sext, J = 7.6 Hz, 16H), 1.10 (t, J = 7.5 Hz, 48H), 1.01 (s, 36H). DSC: Decomposition, 120 °C (onset), 145 °C (peak).

7.5 Experimental Data for Chapter 5

5,7,12,14-Tetraphenyl-6,13-pentacenequinone (**5.1**) was synthesized as reported in the literatures.[12–13]

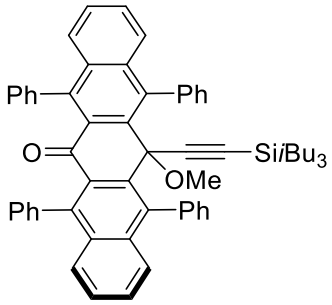

Compound 5.10. To a solution of (tri*iso*butylsilyl)acetylene (370 mg, 1.6 mmol) in dry Et_2O (5 mL), *n*BuLi (2.5 M in hexanes, 0.65 mL, 1.6 mmol) was added dropwise at –78 °C. The solution was stirred for 30 min at –78 °C and then added via a cannula to a suspension of **5.1** (100 mg, 0.16 mmol) in dry Et_2O (15 mL) at –78 °C. The solution was warmed to rt and stirred for 5 h under an atmosphere of N_2. After cooling to –78 °C, Me_2SO_4 (0.31 mL, 0.23 g, 3.2 mmol) was added. The solution was warmed to rt and stirred for 16 h. After cooling to 0 °C, satd aq NH_4Cl (10 mL) was added, followed by H_2O (50 mL). The layers were separated, and the aqueous phase was extracted with CH_2Cl_2 (3 × 50 mL). The organic phases were combined, dried ($MgSO_4$), and filtered. The pale-yellow crude product was carried on to the next step without further purification. R_f = 0.66 (EtOAc/hexanes 1:4).

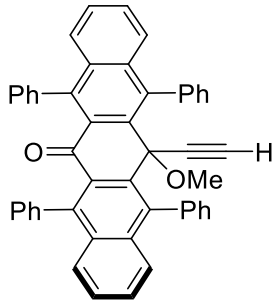

Compound 5.11. To a solution of **5.10** (60 mg, 0.070 mmol) in wet THF (5 mL) was added tetrabutylammonium fluoride (TBAF, 0.078 ml, 0.078 mmol, 1.0 M in THF) at –78 °C. The reaction mixture was warmed to rt and stirred for 3 h. After cooling to 0 °C, satd aq NH_4Cl (10 mL) was added, followed by H_2O (20 mL), the layers were separated, and the aqueous phase was extracted with CH_2Cl_2 (3 × 25 mL). The organic phases were combined, dried ($MgSO_4$), and filtered. After removing the solvent under reduced pressure, the residue was purified by column chromatography (silica gel, EtOAc/hexanes 1:4), followed by solvent removal in vacuo. Compound **5.11** was afforded as a white solid (36 mg, 78%). R_f = 0.30 (EtOAc/hexanes 1:4). ^{1}H NMR (498 MHz, $CDCl_3$) δ 7.48–7.27 (m, 24H), 7.24–7.21 (m, 2H), 6.93 (d, J = 6.1 Hz, 2H), 3.04 (br s, 3H), 1.73 (br s, 1H).

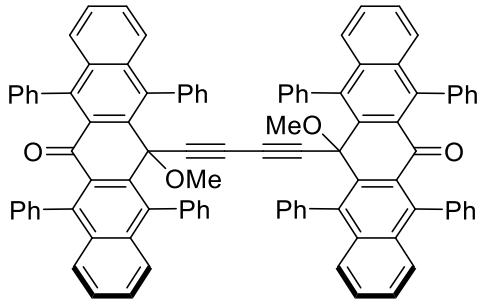

Compound **5.12.** To a solution of **5.11** (60 mg, 0.092 mmol) in pyridine (1 mL) was added $Cu(OAc)_2$ (33 mg, 0.18 mmol), CuCl (1.8 mg, 0.018 mmol), and 4 Å sieves (50 mg). The solution was stirred for 16 h at 100 °C. The reaction mixture was cooled to rt, H_2O (50 mL) and CH_2Cl_2 (25 mL) were added, the layers were separated, and the aqueous phase was extracted with CH_2Cl_2 (3 × 25 mL). The organic phases were combined, dried ($MgSO_4$), and filtered. After removing the solvent under reduced pressure, the residue was purified by column chromatography (silica gel, EtOAc/hexanes 1:4), followed by solvent removal in vacuo. Compound **5.11** was afforded as a white solid (55 mg, 92%). R_f = 0.24 (EtOAc/hexanes 1:4). ^{1}H NMR (498 MHz, $CDCl_3$) δ 7.62–7.17 (m, 56H), 2.92 (s, 6H).

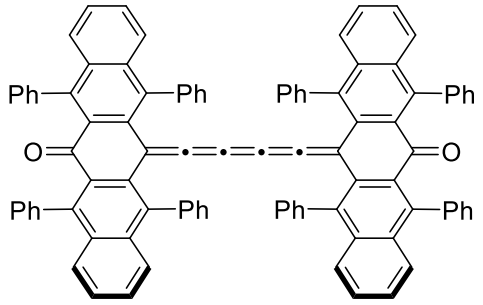

Compound **[5]tetraPh**. Compound **5.12** (30 mg, 0.023 mmol) was dissolved in dry, deoxygenated CH_2Cl_2 (5 mL), to which anhydrous $SnCl_2$ (13 mg, 0.070 mmol) and HCl (2 M in Et_2O, 0.046 mL, 0.092 mmol were added at rt. The reaction mixture was stirred for 16 h under an atmosphere of N_2 and then passed through a pad of basic alumina (CH_2Cl_2), followed by solvent removal in vacuo. The residue was dissolved in minimal amount of CH_2Cl_2 (~1 mL), followed by the addition of MeOH (20 mL). The resulting suspension was filtered, and the residue was washed with MeOH (3 × 5 mL), affording **[5]tetraPh** as a scarlet solid (20 mg, 70%). R_f = 0.32 (EtOAc/hexanes 1:4). ^{1}H NMR (498 MHz, CD_2Cl_2) δ 7.56–7.48 (m, 16H), 7.44–7.34 (m, 16H), 7.32–7.27 (m, 8H), 7.15 (d, J = 7.5 Hz, 4H), 7.11–7.07 (m, 8H), 7.01 (t, J = 7.5 Hz, 4H). ^{13}C NMR (126 MHz, $CDCl_3$) δ 190.7, 159.6, 139.9, 138.6, 137.9, 137.7, 133.33, 133.29, 133.0, 132.0, 131.7, 131.2, 130.3, 129.5, 129.2, 128.7, 128.5, 128.14, 128.10, 127.62, 127.58, 127.53, 127.3, 127.0, 116.8. MALDI HRMS calcd for $C_{96}H_{56}O_2$ (M^+) 1240.4275, found 1240.4281.

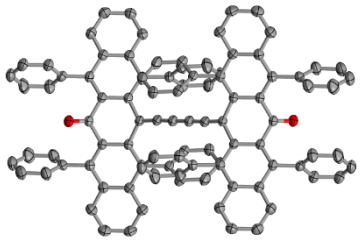

A crystal of **[5]tetraPh** suitable for crystallographic analysis has been grown at rt by slow evaporation of a CH_2Cl_2 solution layered with MeOH. X-ray data for **[5]tetraPh**•$2CH_2Cl_2$ ($C_{96}H_{56}O_2$•$2CH_2Cl_2$), F_w = 1411.26; crystal dimensions 0.44 × 0.03 × 0.03 mm, triclinic crystal system; space group $P\bar{1}$ (No. 2); a = 10.9232(3) Å, b = 13.9217(4) Å, c = 13.9946(3) Å; α = 69.3654(19)°, β = 76.9352(17)°, γ = 67.6155(17)°; V = 1831.15(9) Å^3; Z = 2; ρ_{calcd} = 1.280 g/cm^3; $2\theta_{max}$ = 140.39°; μ = 1.880 mm^{-1}; T = 173 K; total data collected = 41432; R_1 = 0.0578 [4687 observed reflections with $F_o{}^2 \geq 2\sigma(F_o{}^2)$]; ωR_2 = 0.1750 for 6715 data, 442 variables, and 0 restraints; largest difference, peak and hole = 0.275 and –0.396 e Å^{-3}.

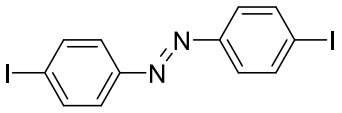

5.32

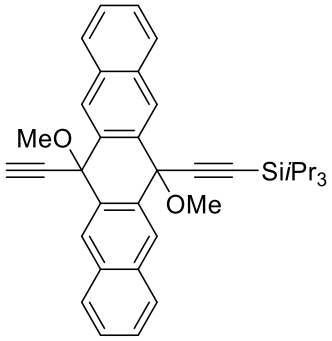

5.33

Compound **5.32**[14] and **5.33**[15] were synthesized as described in the literature.

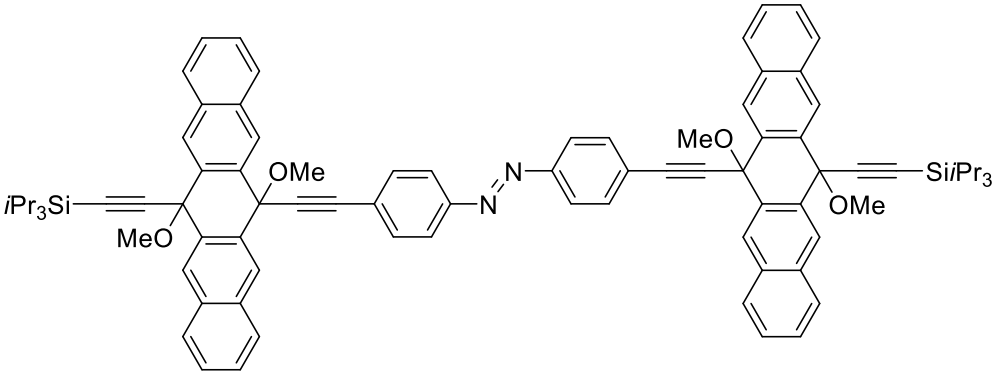

Compound 5.34. A solution of compound **5.32** (70 mg, 0.16 mmol) in dry THF 6 (mL) and HN*i*Pr$_2$ (5 mL) was deoxygenated under a flow of N_2 for 20 min. To this solution was sequentially added **5.33** (200 mg, 0.37 mmol), Pd(PPh$_3$)$_4$ (19 mg, 0.016 mmol),

and CuI (5 mg, 0.024 mmol). The mixture was stirred for 16 h at rt under an atmosphere of N_2. The reaction mixture was cooled to rt, H_2O (50 mL) and CH_2Cl_2 (50 mL) were added, the layers were separated, and the aqueous phase was extracted with CH_2Cl_2 (2 × 50 mL). The organic phases were combined, washed with satd aq NH_4Cl (50 mL), dried ($MgSO_4$), and filtered. Solvent removal and purification by column chromatography (silica gel, EtOAc/hexanes 1:4) afforded **5.34** (178 mg, 87%) as a white solid. R_f = 0.54 (EtOAc/hexanes 1:4). ^{1}H NMR (498 MHz, $CDCl_3$) δ 8.62 (s, 2H), 8.33 (s, 2H), 7.92–7.87 (m, 4H), 7.53–7.51 (m, 4H), 2.99 (s, 3H), 2.95 (s, 3H), 1.21–1.16 (m, 21H).

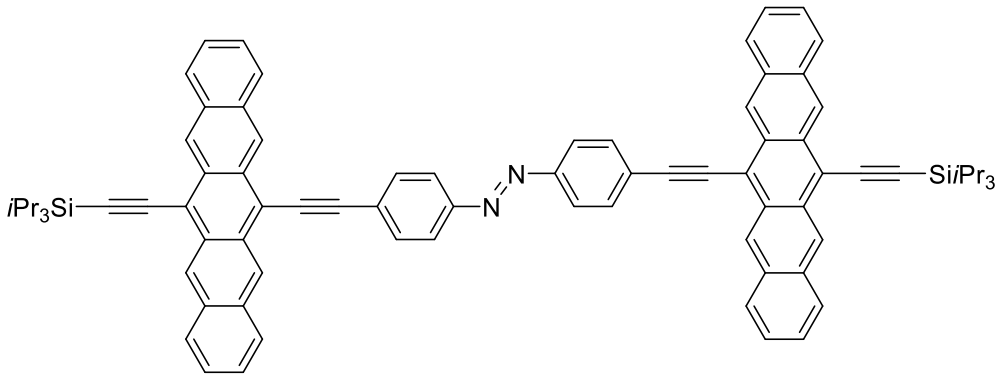

Compound ***trans*-azo-Pc$_2$.** To a solution of a mixture of isomers of **5.34** (44 mg, 0.035 mmol) in dry, deoxygenated THF (10 mL) was added $SnCl_2$•$2H_2O$ (47 mg, 0.21 mmol) and 10% H_2SO_4 (0.1 mL) at rt. The flask was wrapped in aluminum foil during the reaction to limit light exposure. The reaction mixture was stirred for 16 h under an atmosphere of N_2 and then passed through a pad of basic alumina (THF), followed by solvent removal in vacuo. The residue was purified by column chromatography (silica gel, CH_2Cl_2/hexanes 1:1), followed by solvent removal in vacuo. The resulting solid was dissolved in minimal amount of CH_2Cl_2 (~1 mL), followed by the addition of MeOH (20 mL). The resulting suspension was filtered, and the residue was washed with MeOH (3 × 5 mL), affording ***trans*-azo-Pc$_2$** as a dark blue solid (25 mg, 62%). R_f = 0.72 (CH_2Cl_2/hexanes 1:1). ^{1}H NMR (498 MHz, $CDCl_3$) δ 9.33 (s, 2H), 9.31 (s, 2H), 8.18–8.17 (m, 2H), 8.10–8.09 (m, 4H), 8.01–7.99 (m, 2H), 1.46–1.39 (m, 21H).

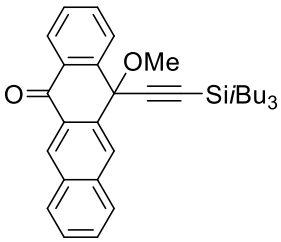

Compound 5.36. To a solution of (tri*iso*butylsilyl)acetylene (0.50 g, 2.2 mmol) in dry THF (5 mL), *n*BuLi (2.5 M in hexanes, 0.90 mL, 2.2 mmol) was added dropwise at –78 °C. The solution was stirred at –78 °C for 30 min and then added via a cannula to a suspension of 5,12-napthacenequinone (0.52 g, 2.0 mmol) in dry THF (15 mL) at –78 °C. The solution was warmed to rt and stirred for 5 h under an atmosphere of N_2. After cooling to –78 °C, MeI (0.70 mL, 11 mmol) was added. The solution was warmed to rt and stirred for 16 h. After cooling to 0 °C, satd aq NH_4Cl (10 mL) was added, followed by H_2O (50 mL). The layers were separated, and the aqueous phase was extracted with CH_2Cl_2 (3 × 50 mL). The organic phases were combined, dried ($MgSO_4$), and filtered. After removing the solvent, the residue was purified by column chromatography (silica gel, EtOAc/hexanes 1:10). The resulting pale-yellow solid was collected by vacuum filtration and washed with hexanes (3 × 5 mL), affording **5.36** as a pale yellow solid (0.72 g, 75%). R_f = 0.54 (EtOAc/hexanes 1:4). ^{1}H NMR (498 MHz, $CDCl_3$) δ 8.82 (s, 1H), 8.53 (s, 1H), 8.31 (dd, J = 7.7, 1.2 Hz, 1H), 8.13 (dd, J = 7.8, 0.59 Hz, 1H), 8.05 (d, J = 8.1 Hz, 1H), 7.94 (d, J = 8.1 Hz, 1H), 7.70 (td, J = 7.6, 1.2 Hz, 1H), 7.65 (td, J = 6.9, 1.1 Hz, 1H), 7.61–7.55 (m, 2H), 3.02 (s, 3H), 1.91 (nonet, J = 6.7 Hz, 3H), 0.99 (d, J = 6.6 Hz, 9H), 0.98 (d, J = 6.6 Hz, 9H), 0.72 (d, J = 6.9 Hz, 6H). ^{13}C NMR (126 MHz, $CDCl_3$) δ 184.0, 141.1, 135.7, 135.3, 133.43, 132.9, 132.0, 129.8, 129.4, 129.3, 129.0, 128.9, 128.8, 128.6, 128.2, 127.6, 127.4, 105.4, 94.0, 73.5, 51.9, 26.32, 26.30, 25.2, 24.9.

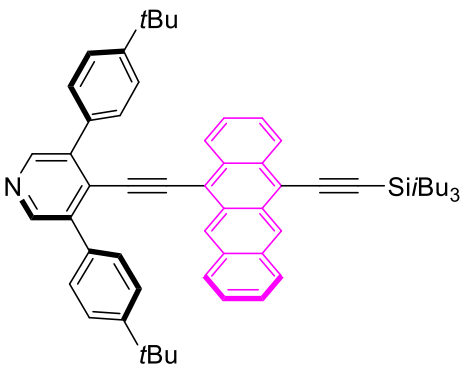

Compound L_{tc} A solution of LiHMDS was prepared by adding *n*BuLi (2.5 M in hexanes, 3.2 mL, 8.0 mmol) to a solution of $[(CH_3)_3Si]_2NH$ (1.9 mL, 9.1 mmol) in dry THF (10 mL) at –78 °C. After stirring at –78 °C for 30 min, the solution was added to a mixture of **2.7** (0.20 g, 0.54 mmol) and **5.36** (0.32 g, 0.64 mmol) in dry THF (15 mL) at –78 °C via a

cannula. The solution was warmed to rt and stirred for 16 h under an atmosphere of N_2. After cooling to 0 °C, satd aq NH_4Cl (10 mL) was added, followed by H_2O (50 mL), the layers were separated, and the aqueous phase was extracted with CH_2Cl_2 (3 × 50 mL). The organic phases were combined, dried ($MgSO_4$), and filtered. After removing the solvent under reduced pressure, the residue was dissolved in CH_2Cl_2, passed through a pad of silica gel (CH_2Cl_2), followed by solvent removal in vacuo. The crude product, presumably as a mixture of diastereomers, was dissolved in dry, deoxygenated THF (20 mL), to which $SnCl_2$•$2H_2O$ (0.35 g, 1.6 mmol) and 10% H_2SO_4 (0.1 mL) were added at rt. The flask was wrapped in aluminum foil during the reaction to limit light exposure. The reaction mixture was stirred for 16 h under an atmosphere of N_2 and then passed through a pad of basic alumina (THF), followed by solvent removal in vacuo. The residue was purified by column chromatography (silica gel, CH_2Cl_2/hexanes 1:4), followed by solvent removal in vacuo. The resulting solid was dissolved in minimal amount of CH_2Cl_2 (~1 mL), followed by the addition of MeOH (20 mL). The resulting suspension was filtered, and the residue was washed with MeOH (3 × 5 mL), affording **L**$_{\mathbf{tc}}$ as a red solid (280 mg, 63%). R_f = 0.45 (CH_2Cl_2). UV-vis (CH_2Cl_2) λ_{max} (ε) 370 (12,400), 483 (8,320), 517 (21,700), 555 nm (32,900), 370 (12,400), 483 (8,320), 517 (21,700), 555 nm (32,900). ^{1}H NMR (498 MHz, $CDCl_3$) δ 9.16 (s, 1H), 8.71 (s, 2H), 8.51 (d, J = 8.7 Hz, 1H), 8.38 (s, 1H), 7.93 (d, J = 8.4 Hz, 1H), 7.95 (d, J = 8.4 Hz, 4H), 7.675 (d, J = 8.8 Hz, 1H), 7.535 (d, J = 8.4 Hz, 4H), 7.52 (d, 1H), 7.45–7.40 (m, 2H), 7.39–7.34 (m, 1H), 7.18–14 (m, 1H), 2.11 (nonet, J = 6.7 Hz, 3H), 1.29 (s, 18H), 1.13 (d, J = 6.8 Hz, 18H), 0.90 (d, J = 6.9 Hz, 6H). ^{13}C NMR (126 MHz, $CDCl_3$) δ 151.6, 149.0, 138.5, 134.9, 132.7, 132.5, 132.1, 132.0, 130.2, 129.9, 129.5, 129.2, 128.2, 128.0, 127.3, 127.2, 126.6, 126.5, 126.1, 126.0, 125.9, 125.8, 125.6, 119.5, 117.5, 109.3, 103.8, 100.1, 97.4, 34.8, 31.4, 26.5, 25.40, 25.38. ESI HRMS calcd for $C_{59}H_{66}NSi$ ($[M + H]^+$) 816.4959, found 816.4964. ESI HRMS calcd for $C_{59}H_{66}NSi$ ($[M + H]^+$) 816.4959, found 816.4964. DSC: Mp = 210 °C; decomposition, 326 °C (onset), 346 °C (peak).

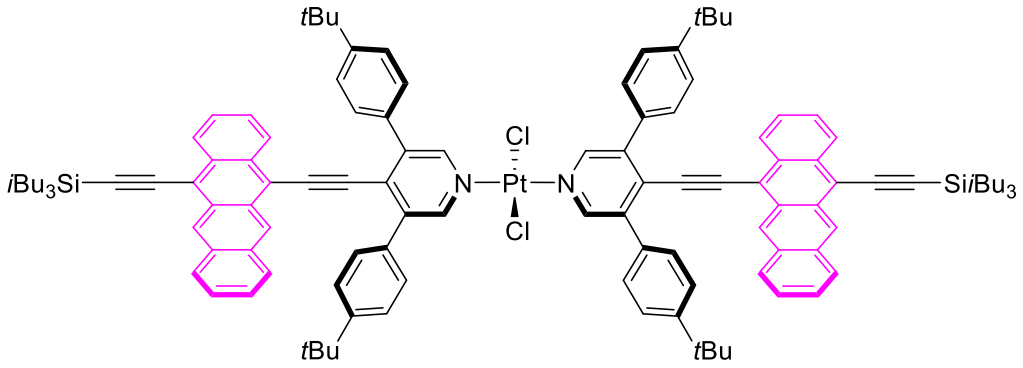

Compound Pt(L_{tc})$_2$Cl$_2$. A mixture of **L_{tc}** (20 mg, 0.025 mmol) and Pt(PhCN)$_2$Cl$_2$ (5 mg, 0.011 mmol) in dry PhMe (5 mL) was stirred at 80 °C for 16 h under an atmosphere of argon. The flask was wrapped in aluminum foil during the reaction to limit light exposure. The reaction mixture was cooled to rt, and the solvent was removed under reduced pressure. The residue was purified by column chromatography (alumina, CH_2Cl_2). The eluent volume was reduced in vacuo to ~1 mL followed by the addition of hexanes (15 mL). The resulting suspension was filtered, and the residue was washed with hexanes (3 × 2 mL), affording **Pt(L_{tc})$_2$Cl$_2$** as a dark purple solid (20 mg, 82%). R_f = 0.50 (CH_2Cl_2/hexanes 1:2). UV-vis (CH_2Cl_2) λ_{max} (ε) 390 (sh, 27,200), 398 (28,800), 500 (17,300), 533 (44,500), 573 nm (72,200). ^{1}H NMR (498 MHz, $CDCl_3$) δ 9.18 (s, 2H), 8.98 (s, 4H), 8.52 (d, J = 8.5 Hz, 2H), 8.33 (s, 2H), 7.94 (d, J = 8.5 Hz, 2H), 7.82 (d, J = 8.6 Hz, 8H), 7.61 (d, J = 8.7 Hz, 2H), 7.55 (d, J = 8.4 Hz, 8H), 7.50 (d, J = 8.5 Hz, 2H), 7.46–7.41 (m, 4H), 7.40–7.36 (m, 2H), 7.19–7.15 (m, 2H), 2.11 (nonet, J = 6.6 Hz, 6H), 1.31 (s, 36H), 1.13 (d, J = 6.6 Hz, 36H), 0.91 (d, J = 6.9 Hz, 12H). ^{13}C NMR (126 MHz, $CDCl_3$) δ 152.5, 151.9, 140.3, 133.1, 132.4, 132.2, 132.1, 130.7, 130.1, 129.9, 129.5, 129.2, 128.3, 127.3, 127.02, 126.96, 126.5, 126.20, 126.16, 126.0, 125.9, 125.7, 120.6, 116.6, 110.0, 103.7, 101.0, 99.1, 34.9, 31.4, 26.5, 25.40, 25.35 (one signal coincident or not observed). MALDI HRMS (DCTB) calcd for $C_{118}H_{130}{}^{35}Cl_2N_2{}^{195}PtSi_2$ (M^+) 1895.8792, found 1895.8770. DSC: Mp = 279 °C; decomposition, 310 °C (onset), 313 °C (peak).

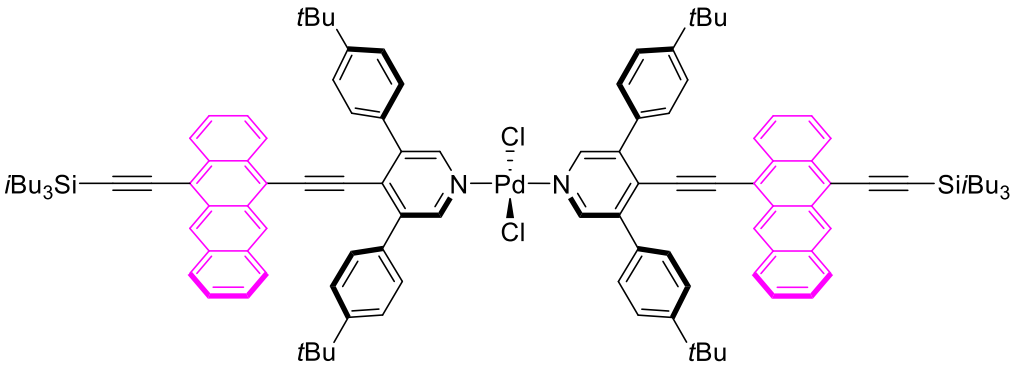

Compound Pd(L_{tc})$_2$Cl$_2$. A mixture of **L_{tc}** (24 mg, 0.029 mmol) and Pd(PhCN)$_2$Cl$_2$ (6 mg, 0.014 mmol) in dry CH_2Cl_2 (5 mL) was stirred at rt for 16 h under an atmosphere of argon. The flask was wrapped in aluminum foil during the reaction to limit light exposure. The reaction mixture was plugged through a pad of alumina (CH_2Cl_2). The eluent volume was reduced in vacuo to ~1 mL followed by the addition of hexanes (15 mL). The resulting suspension was filtered, and the residue was washed with hexanes (3 × 2 mL), affording **Pd(L_{tc})$_2$Cl$_2$** as a dark purple solid (21 mg, 79%). R_f = 0.75 (CH_2Cl_2/hexanes 1:1). UV-vis (CH_2Cl_2) λ_{max} (ε) 380 (sh, 26,400), 388 (27,000), 498 (19,300), 531 (48,400), 571 nm (77,000). ^{1}H NMR (498 MHz, $CDCl_3$) δ 9.17 (s, 2H), 8.90 (s, 4H), 8.515 (d, J = 8.7 Hz, 2H), 8.32 (s, 2H), 7.935 (d, J = 8.7 Hz, 2H), 7.81 (d, J = 8.3 Hz, 8H), 7.60 (d, J = 8.6 Hz, 2H), 7.55 (d, J = 8.4 Hz, 8H), 7.50 (d, J = 8.3 Hz, 2H), 7.46–7.41 (m, 4H), 7.40–7.36 (m, 2H), 7.18–7.14 (m, 2H), 2.11 (nonet, J = Hz, 6H), 1.31 (s, 36H), 1.13 (d, J = 6.6 Hz, 36H), 0.91 (d, J = 6.8 Hz, 12H). ^{13}C NMR (126 MHz, $CDCl_3$) δ 152.5, 151.5, 140.1, 133.2, 133.1, 132.4, 132.2, 132.1, 130.9, 130.0, 129.9, 129.5, 129.2, 128.3, 127.3, 126.99, 126.96, 126.5, 126.20, 126.16, 126.0, 125.9, 125.7, 120.6, 116.5, 110.0, 103.7, 100.9, 98.99, 34.9, 31.4, 26.5, 25.4, 25.3. MALDI HRMS (DCTB) calcd for $C_{118}H_{130}{}^{35}Cl_2N_2{}^{106}PdSi_2$ (M^+) 1806.8184, found 1806.8179. DSC: Decomposition, 276 °C (onset), 306 °C (peak).

7.6 Spectra Appendix

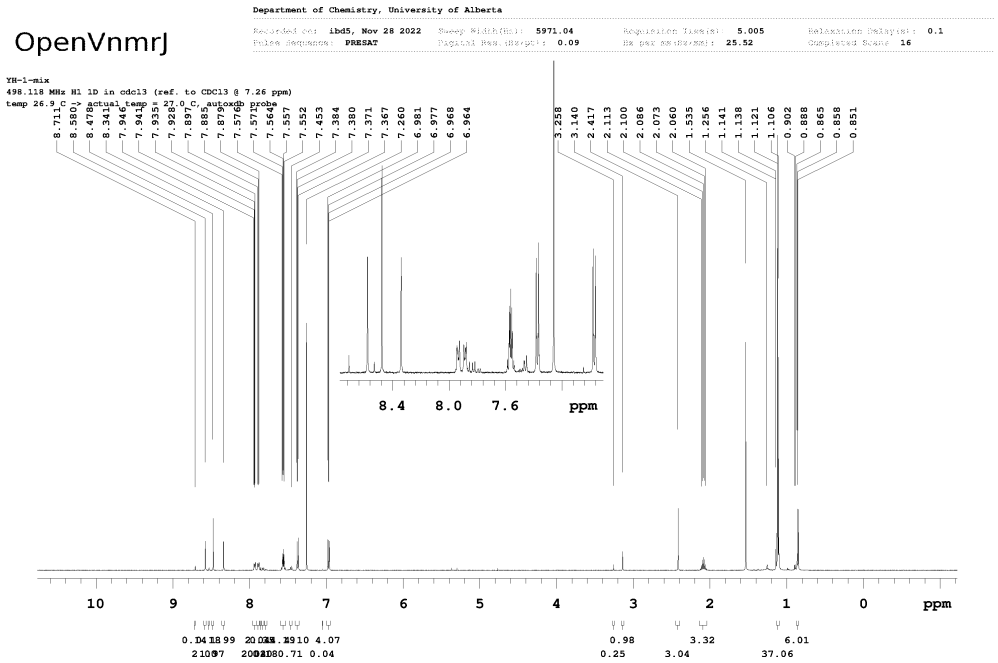

Figure 7.1. ^{1}H NMR spectrum of a mixture of isomers of compound **2.10** in $CDCl_3$.

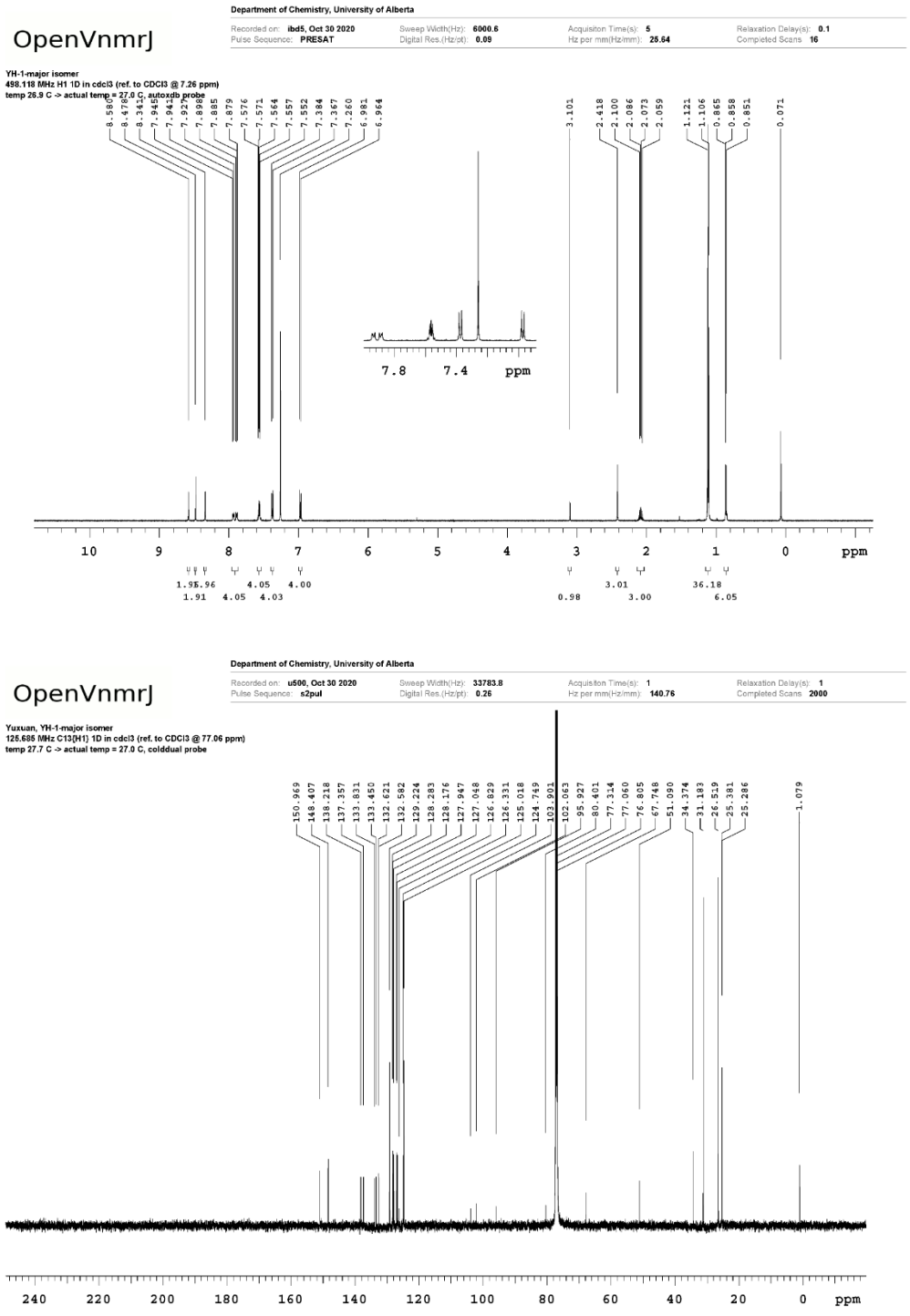

Figure 7.2. ^{1}H NMR and ^{13}C NMR spectra of the major isomer of compound **2.10** in $CDCl_3$.

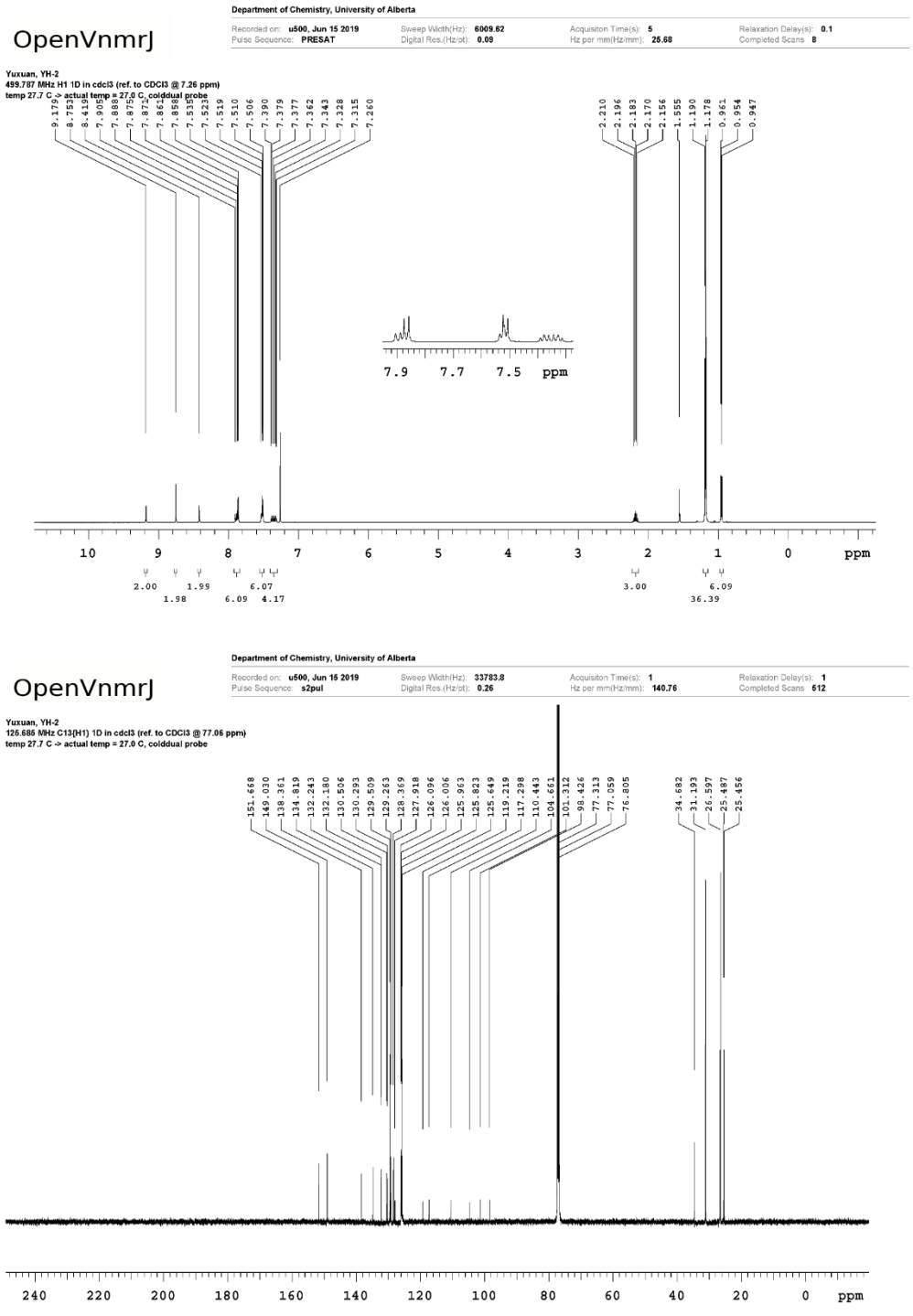

Figure 7.3. ^{1}H NMR and ^{13}C NMR spectra of $\mathbf{L_{pc}}$ in $CDCl_3$.

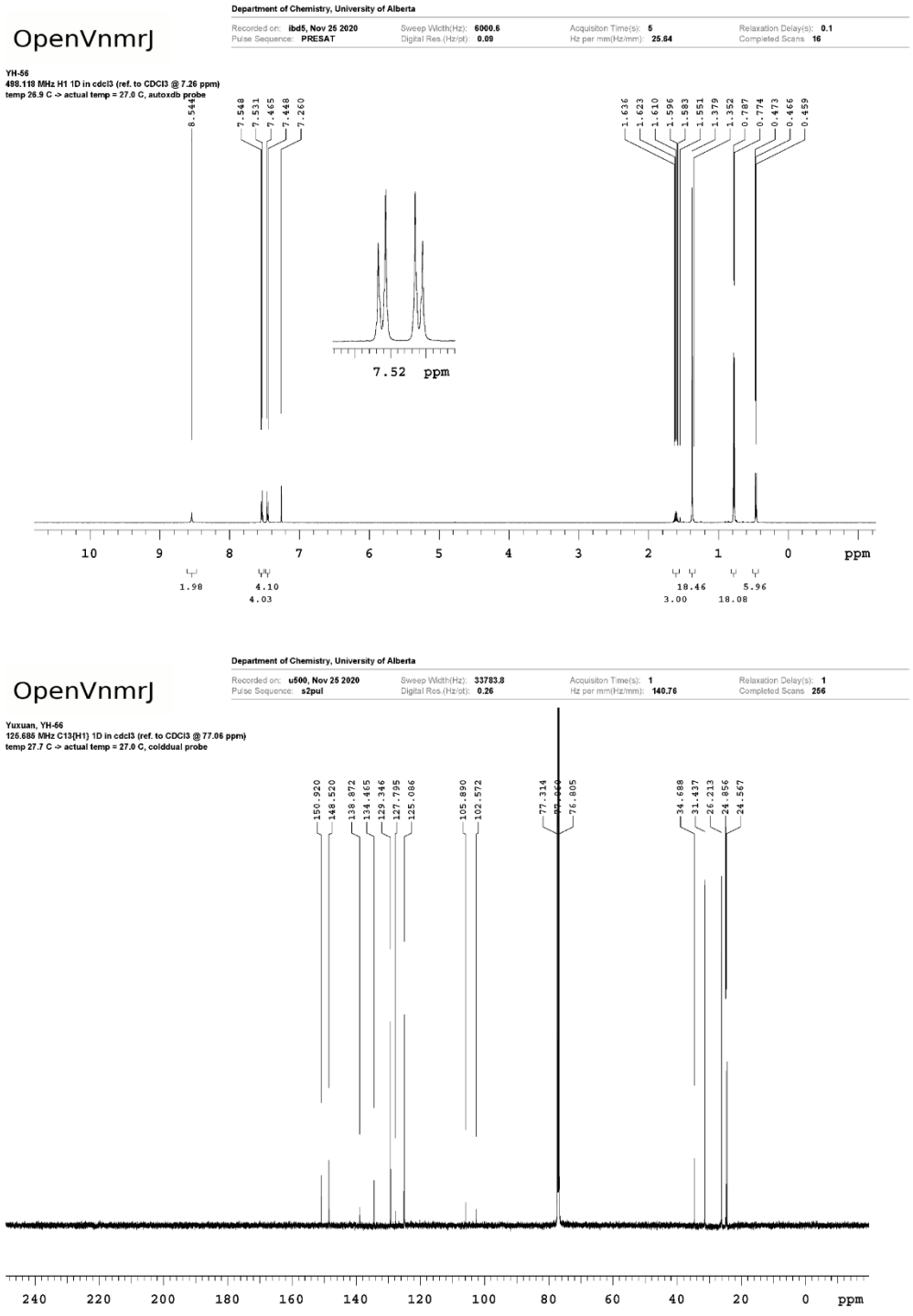

Figure 7.4. ^{1}H NMR and ^{13}C NMR spectra of $\mathbf{L_{ref}}$ in $CDCl_3$.

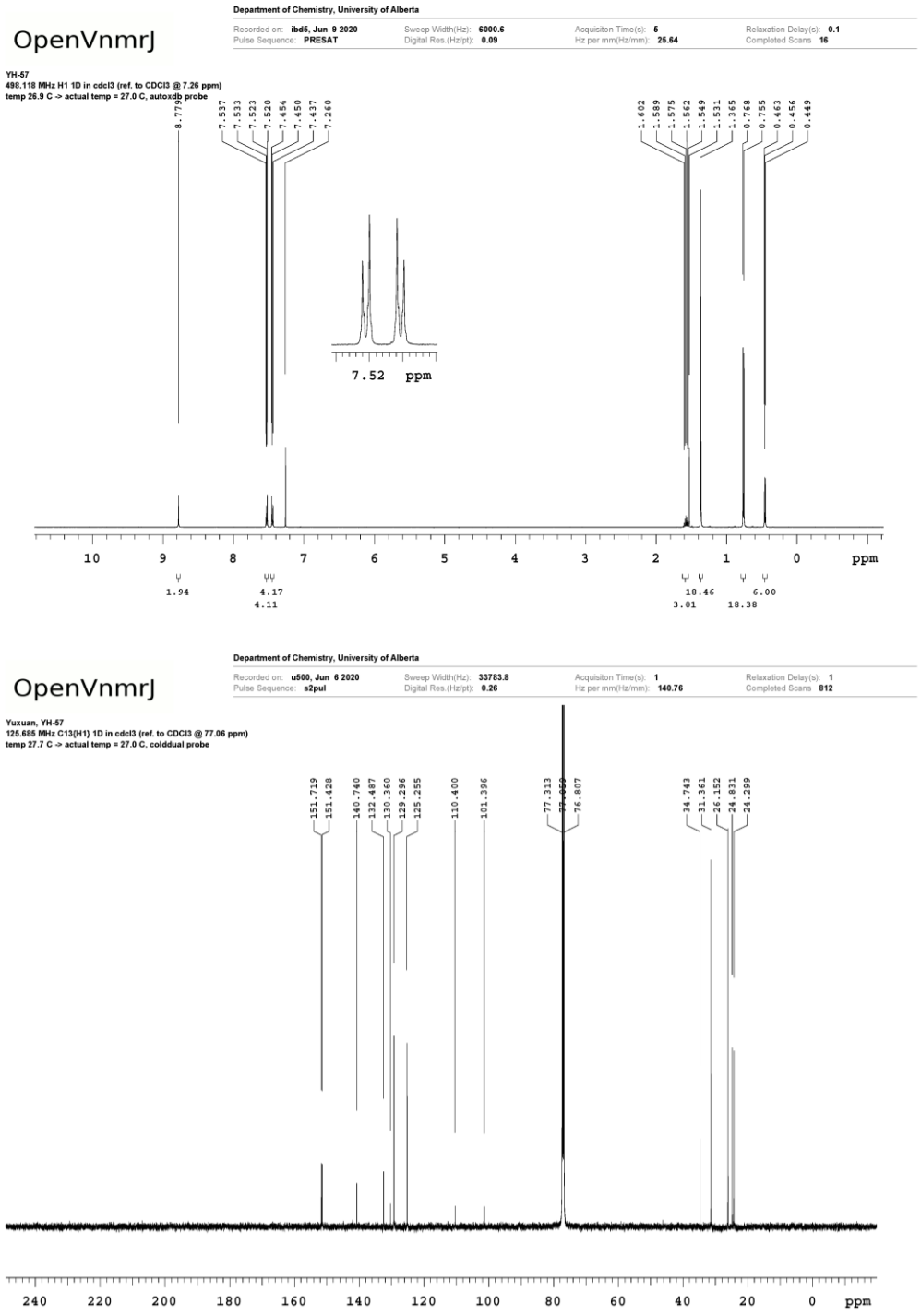

Figure 7.5. ^{1}H NMR and ^{13}C NMR spectra of **Pt(L$_{ref}$)$_2$Cl$_2$** in $CDCl_3$.

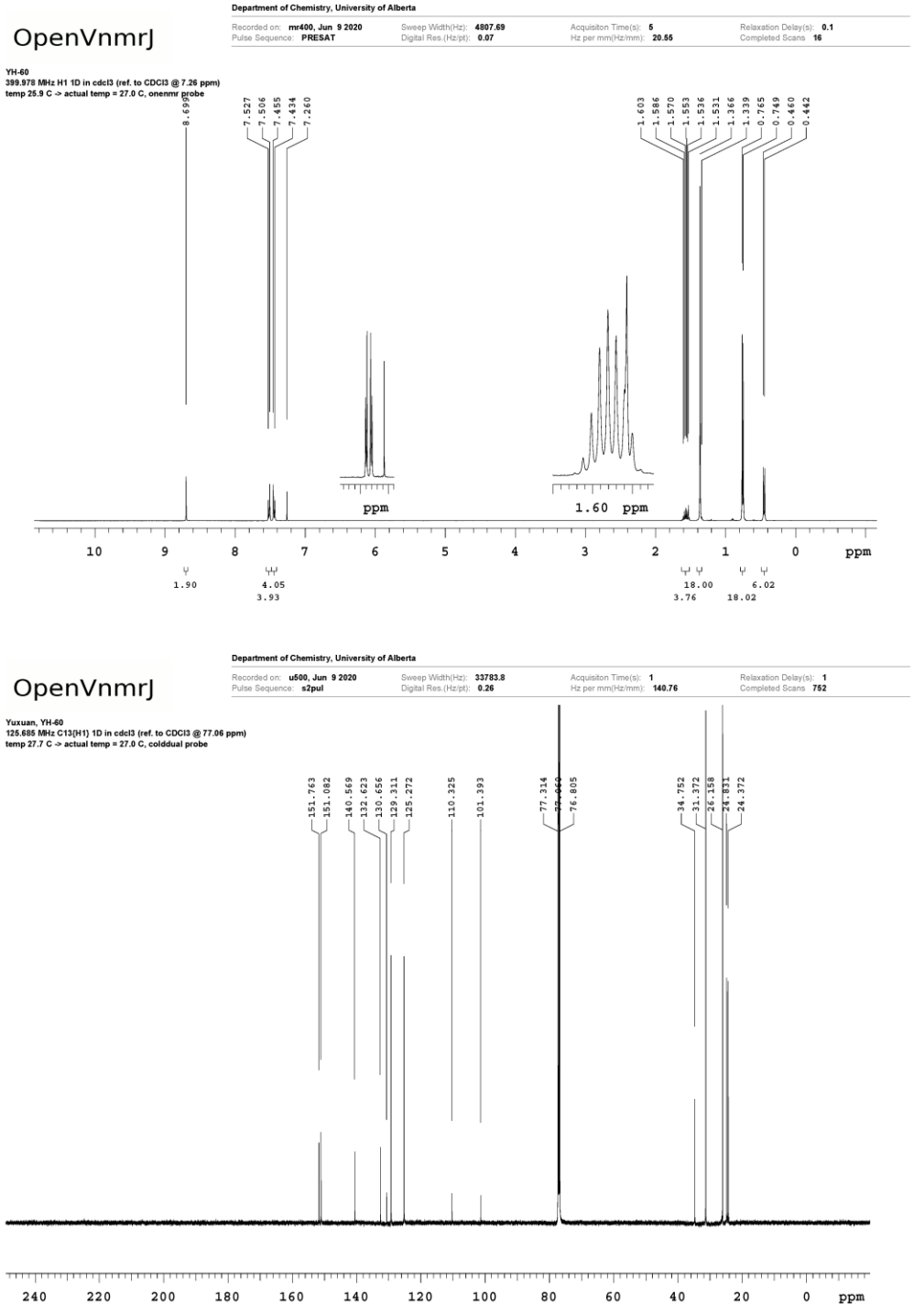

Figure 7.6. ^{1}H NMR and ^{13}C NMR spectra of **Pd(L$_{ref}$)$_2$Cl$_2$** in $CDCl_3$.

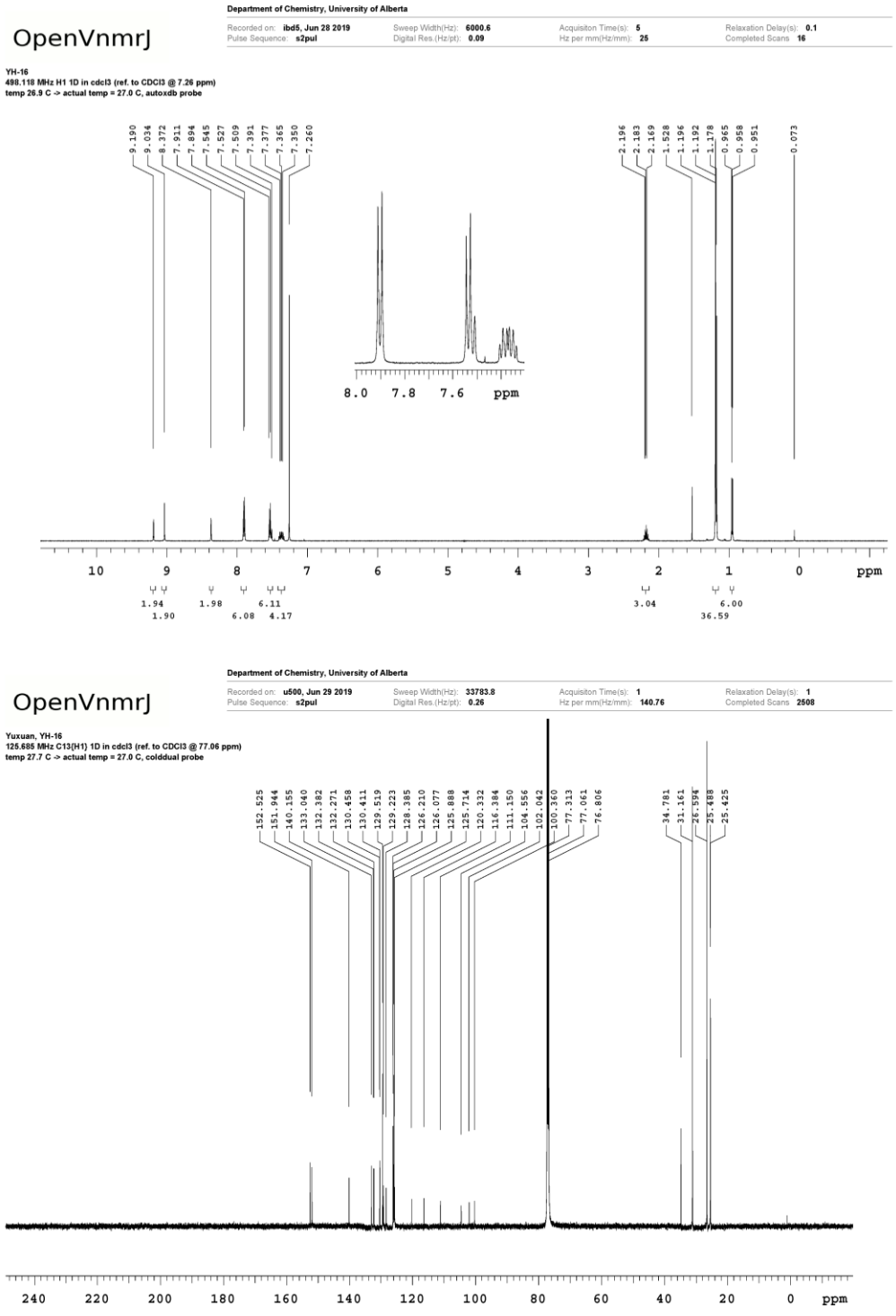

Figure 7.7. ^{1}H NMR and ^{13}C NMR spectra of **Pt(L_{pc})$_2$Cl$_2$** in $CDCl_3$.

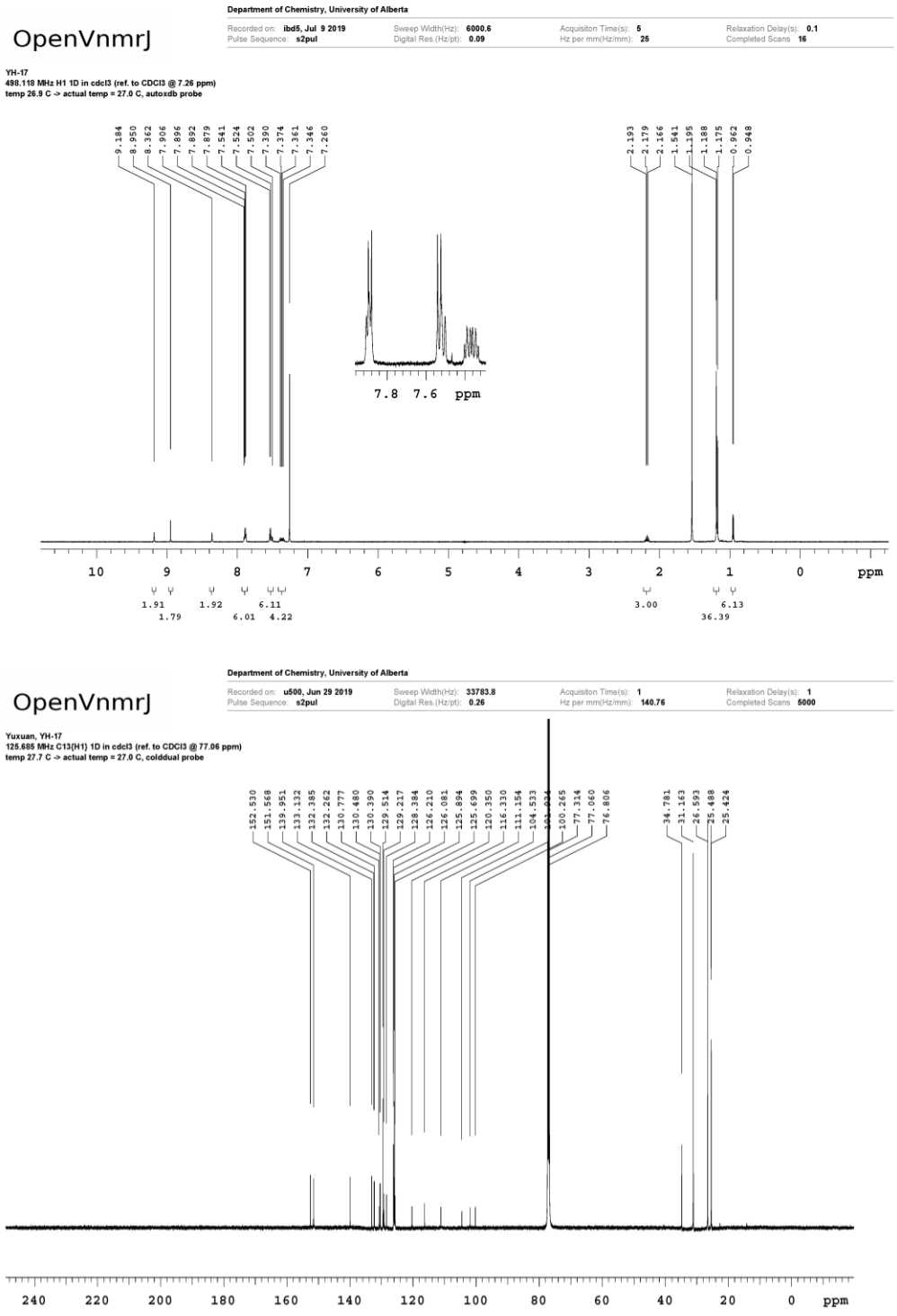

Figure 7.8. ^{1}H NMR and ^{13}C NMR spectra of **Pd(L$_{pc}$)$_2$Cl$_2$** in $CDCl_3$.

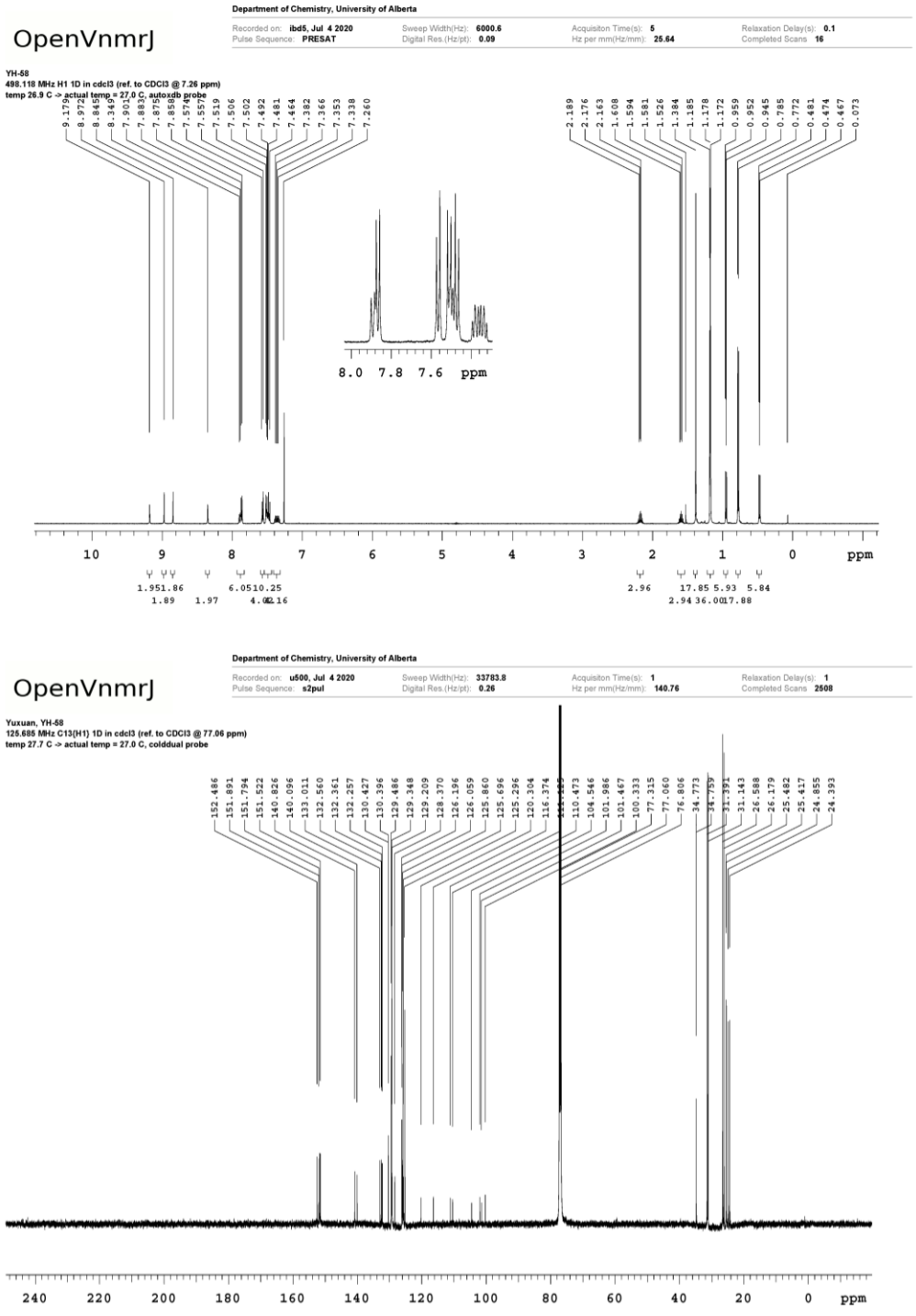

Figure 7.9. ^{1}H NMR and ^{13}C NMR spectra of **Pt(L$_{pc}$)(L$_{ref}$)Cl$_2$** in $CDCl_3$.

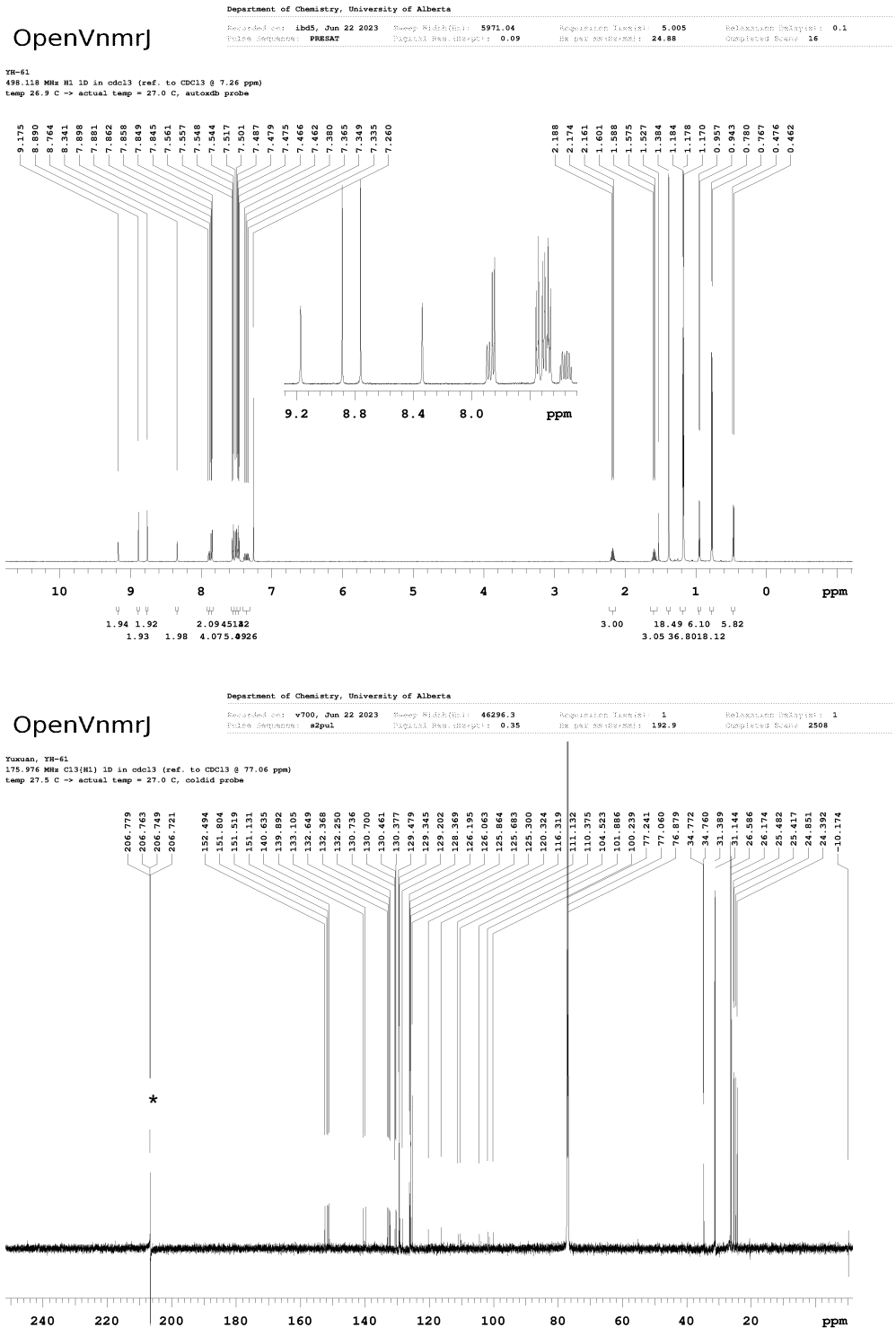

Figure 7.10. ^{1}H NMR and ^{13}C NMR spectra of **Pd(L_{pc})(L_{ref})Cl_2** in $CDCl_3$ (*artifact peak from the environment).

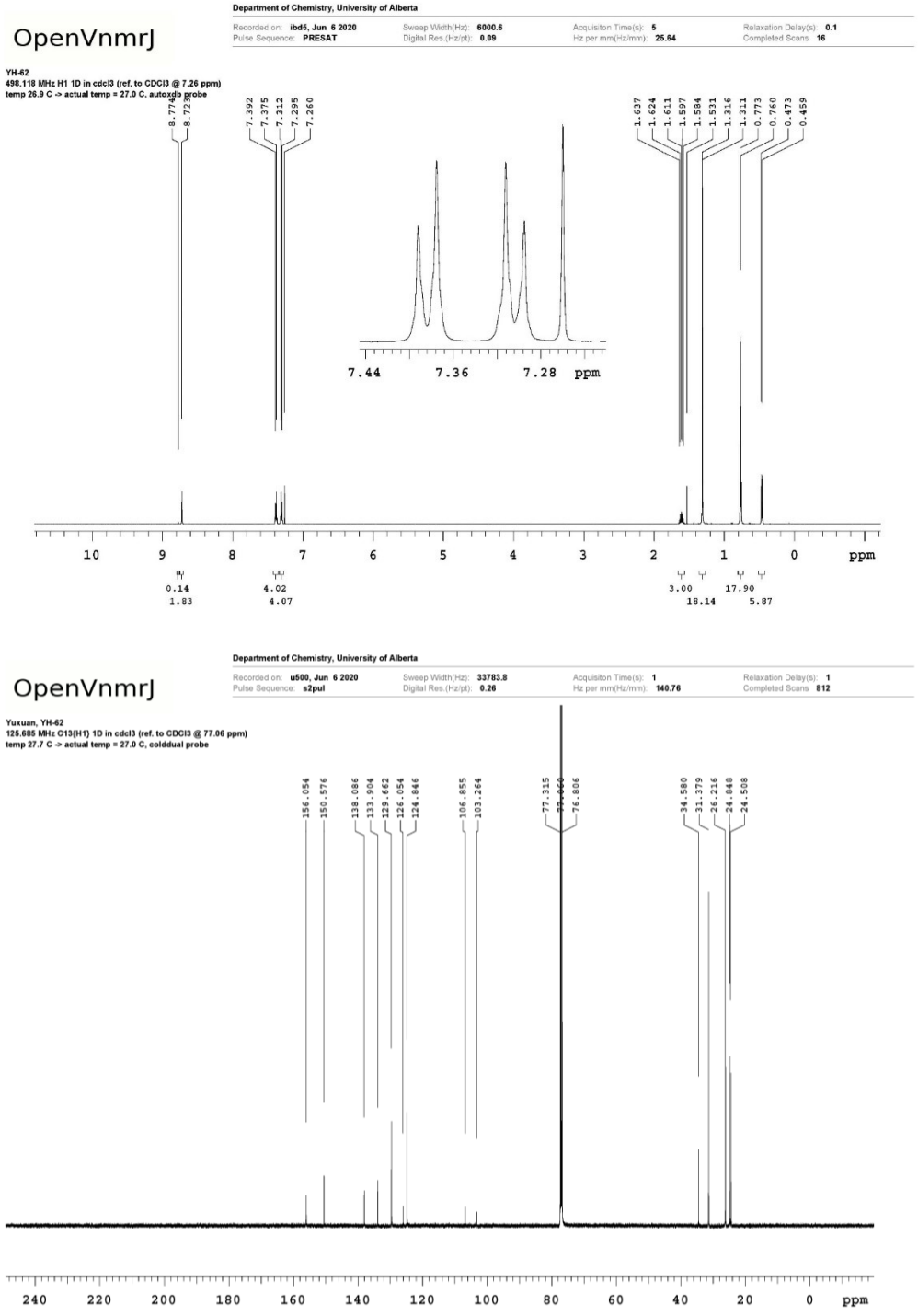

Figure 7.11. ^{1}H NMR and ^{13}C NMR spectra of **Ru(L$_{ref}$)$_4$Cl$_2$** in $CDCl_3$.

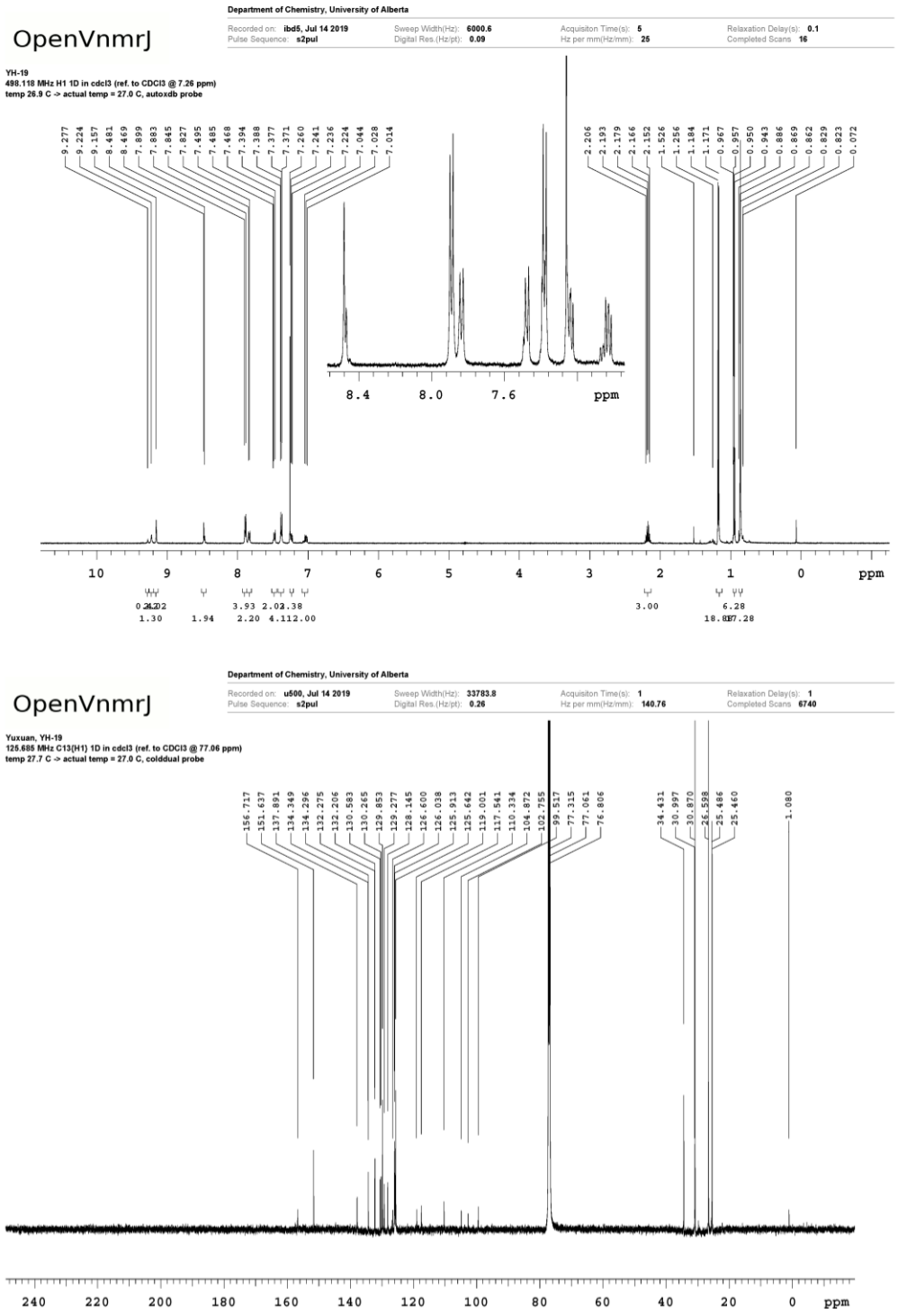

Figure 7.12. ^{1}H NMR and ^{13}C NMR spectra of **Ru(L$_{pc}$)$_4$Cl$_2$** in $CDCl_3$.

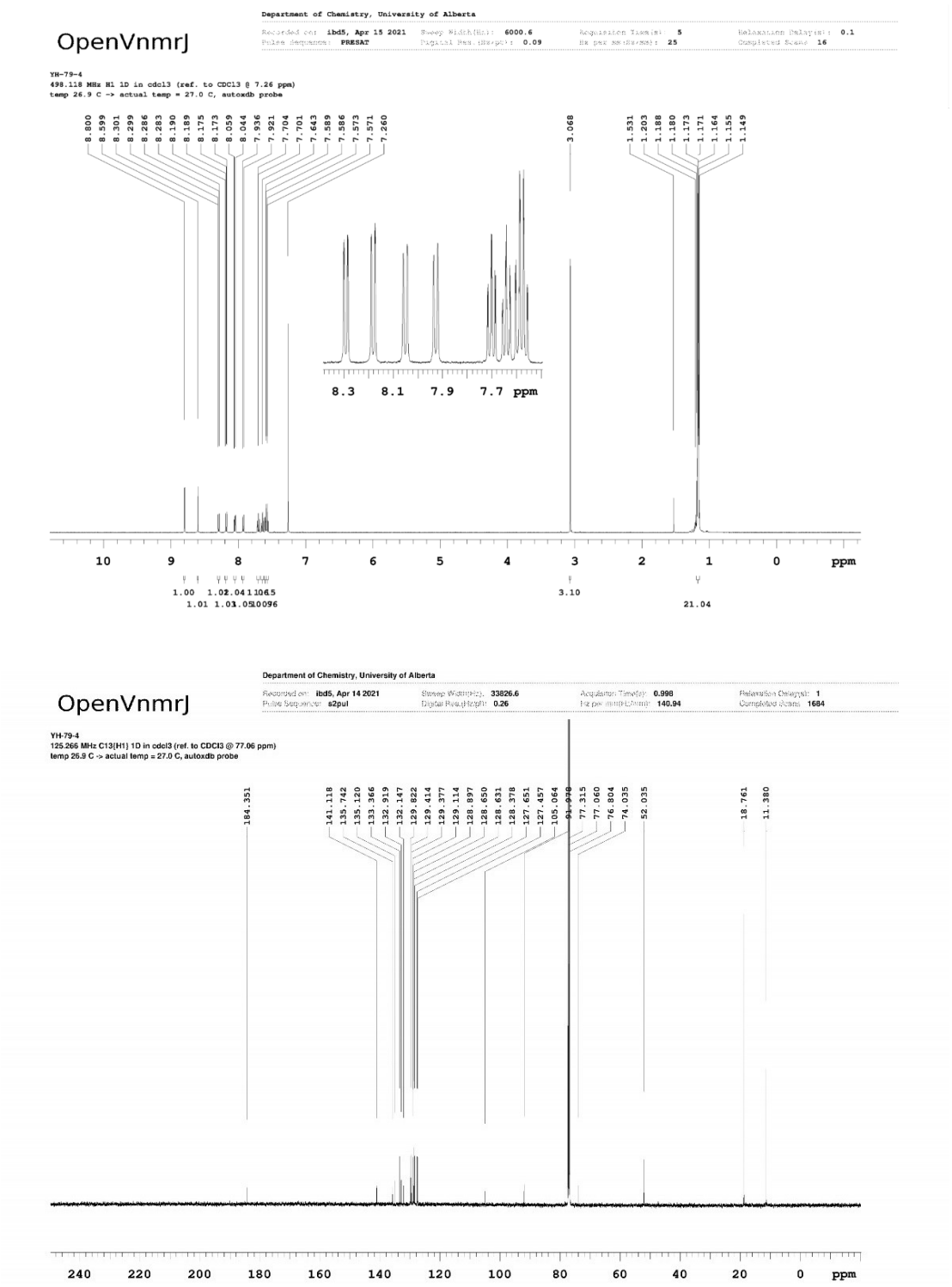

Figure 7.13. ^{1}H NMR and ^{13}C NMR spectra of compound **3.2** in $CDCl_3$.

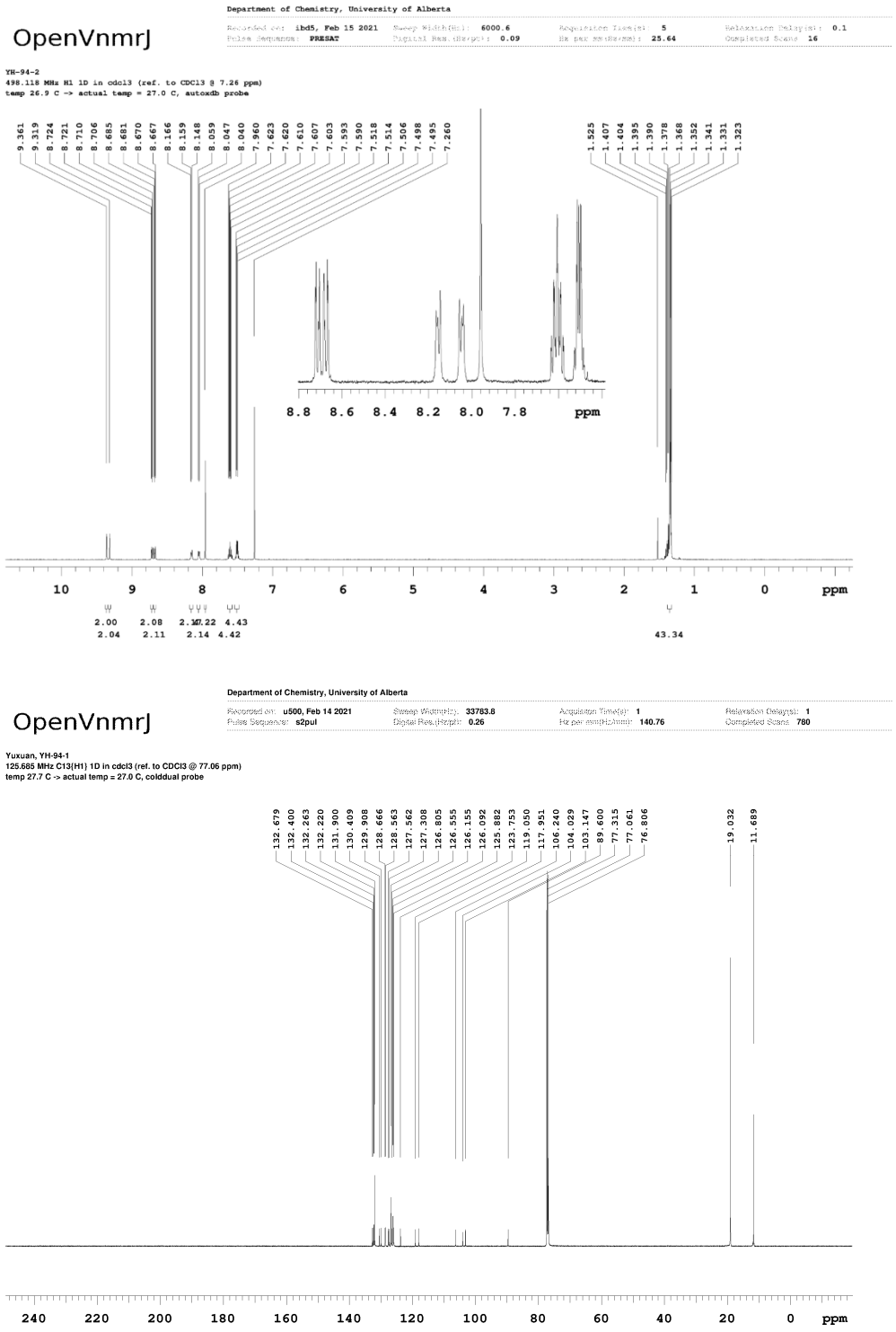

Figure 7.14. ^{1}H NMR and ^{13}C NMR spectra of **pPhTc2** in $CDCl_3$.

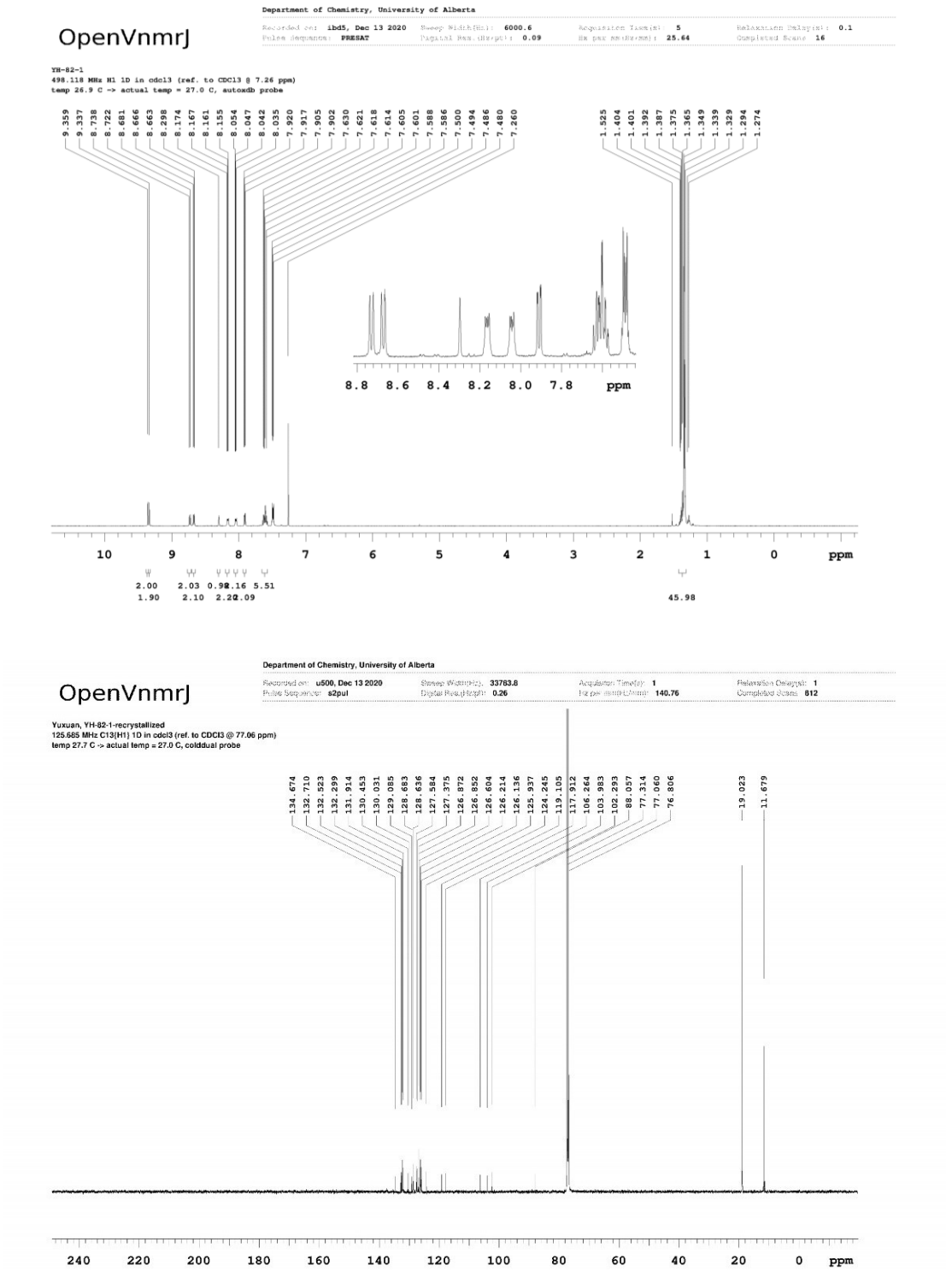

Figure 7.15. ^{1}H NMR and ^{13}C NMR spectra of **mPhTc$_2$** in $CDCl_3$.

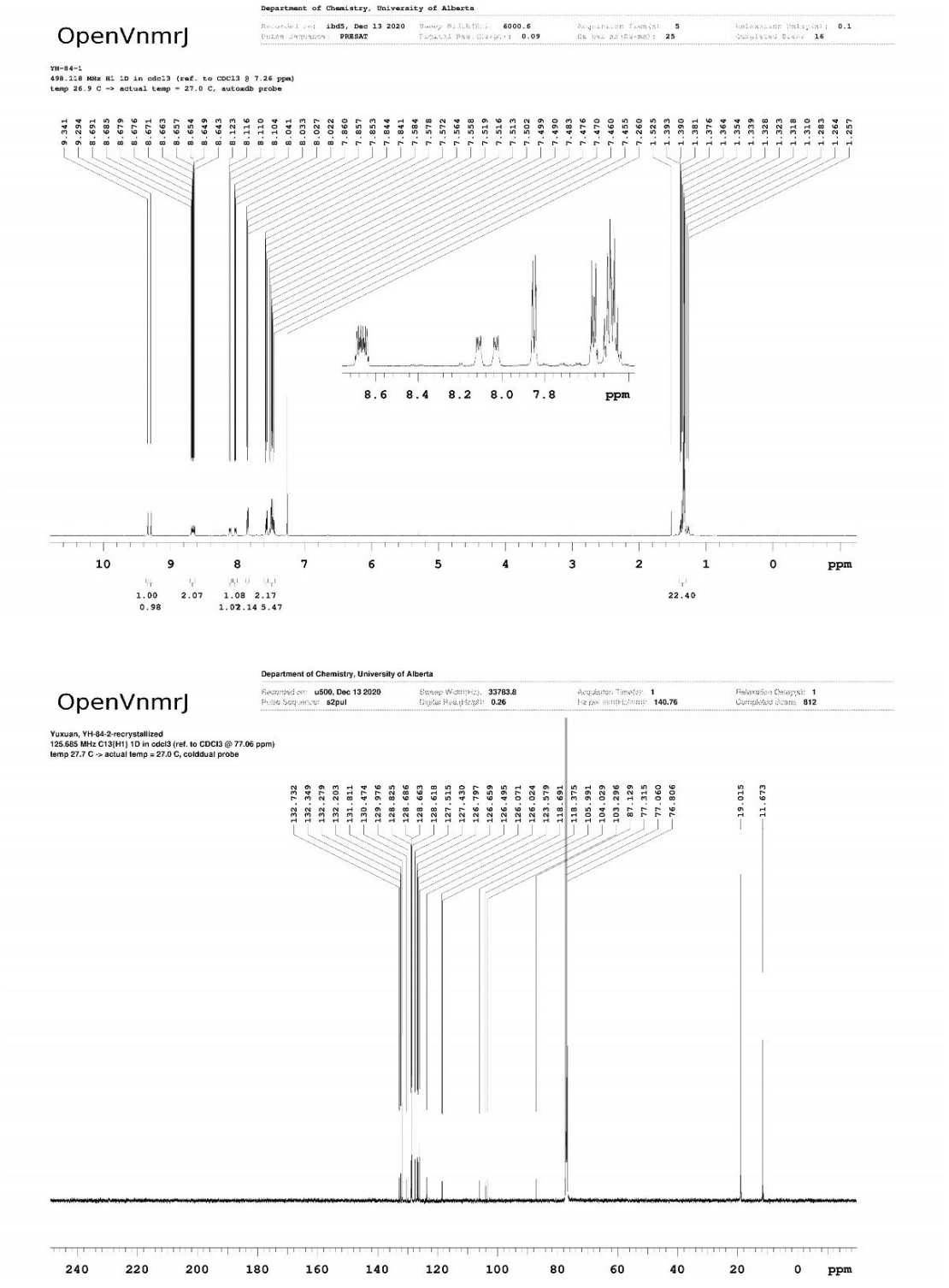

Figure 7.16. ^{1}H NMR and ^{13}C NMR spectra of **PhTc** in $CDCl_3$.

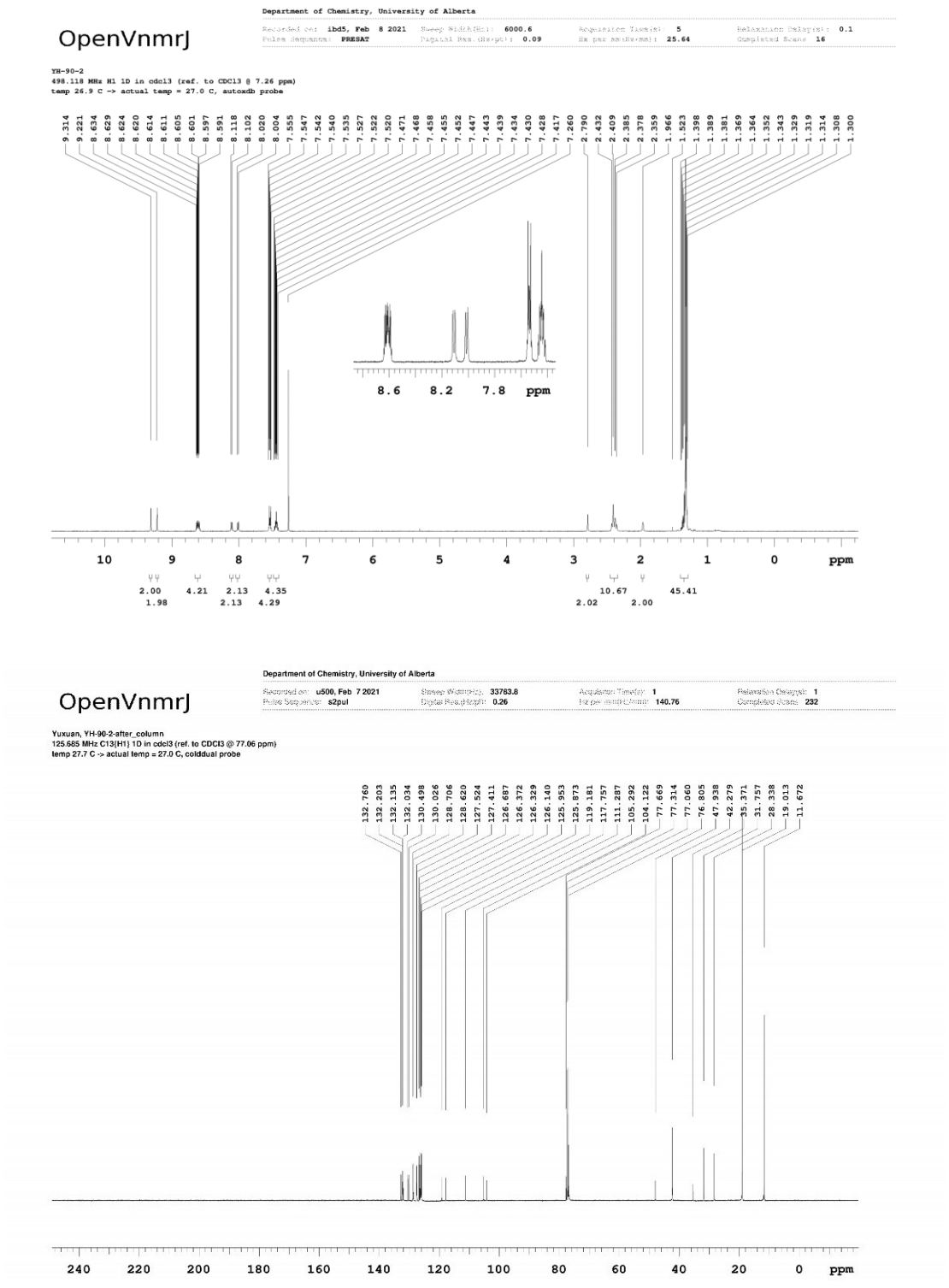

Figure 7.17. ^{1}H NMR and ^{13}C NMR spectra of **mAdTc2** in $CDCl_3$.

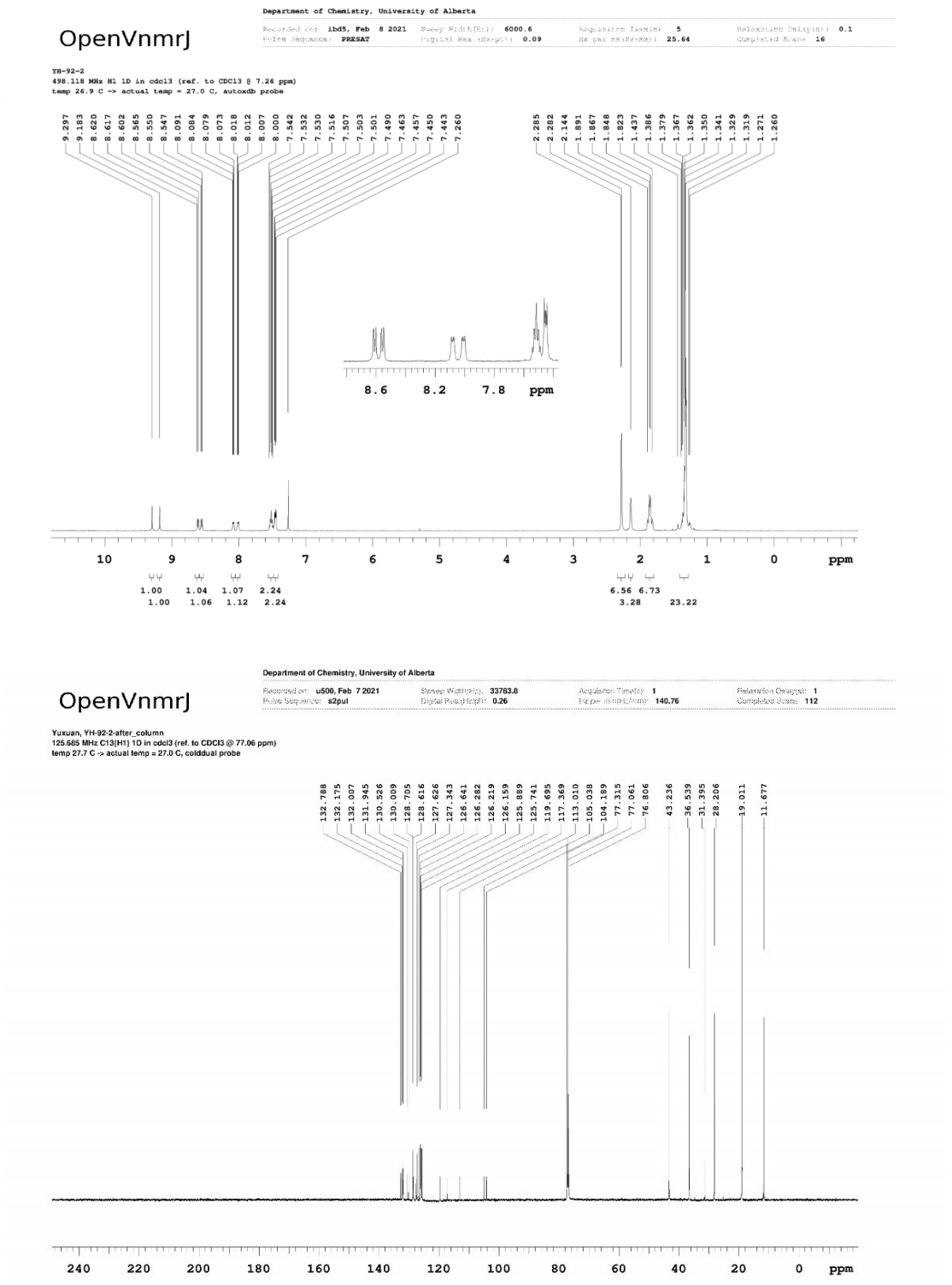

Figure 7.18. ^{1}H NMR and ^{13}C NMR spectra of **AdTc** in $CDCl_3$.

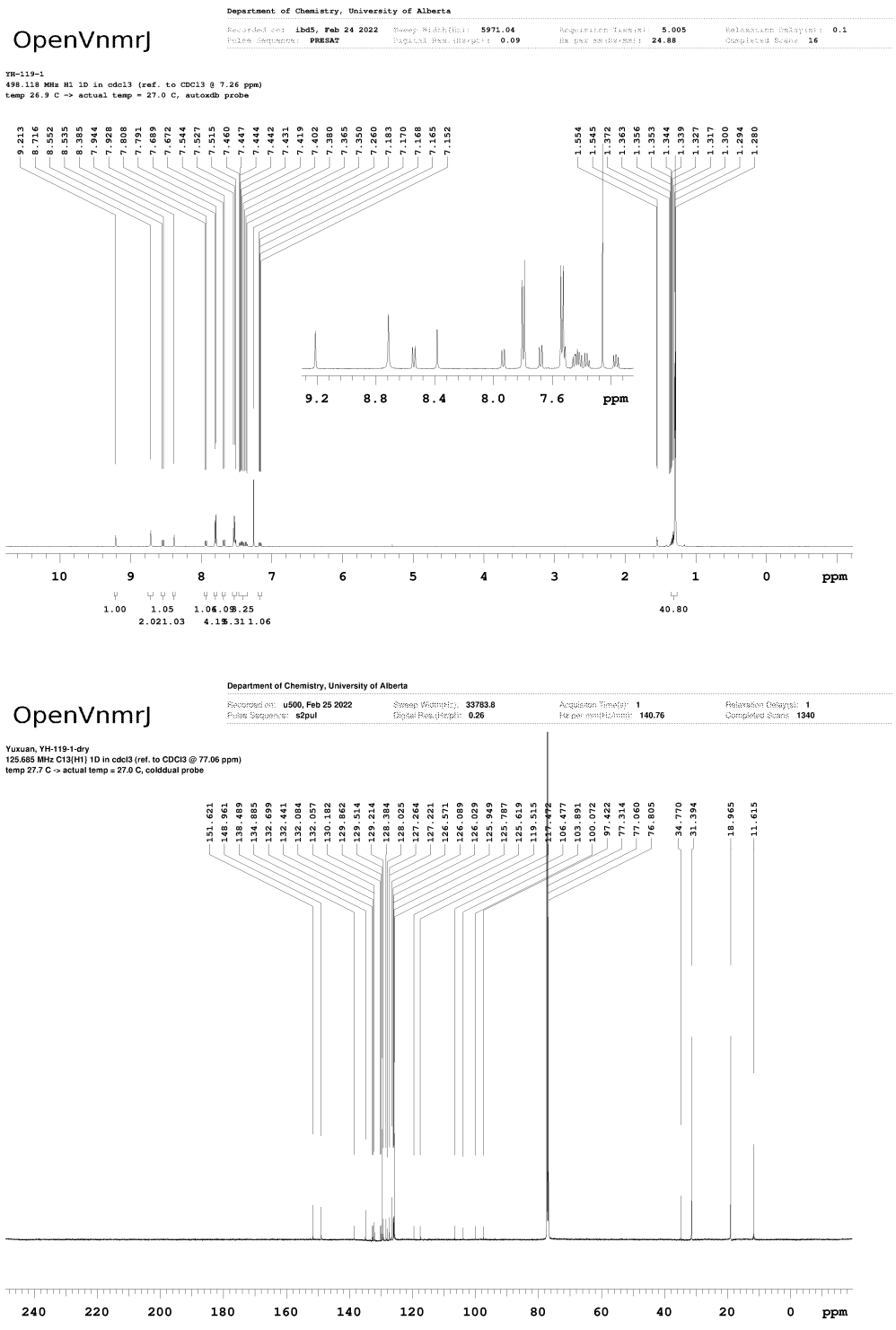

Figure 7.19. ^{1}H NMR and ^{13}C NMR spectra of **TcPy-1** in $CDCl_3$.

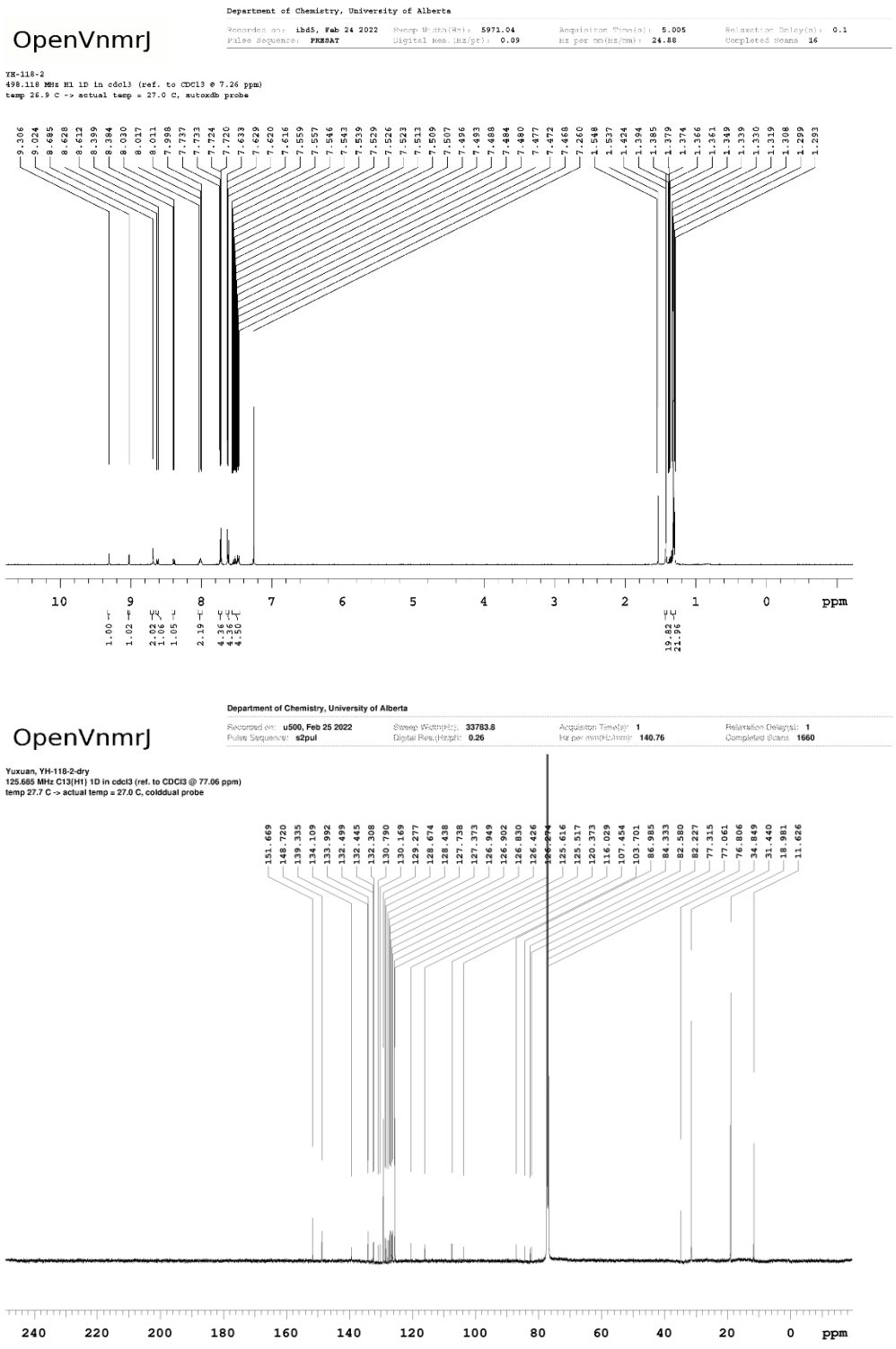

Figure 7.20. ^{1}H NMR and ^{13}C NMR spectra of **TcPy-2** in $CDCl_3$.

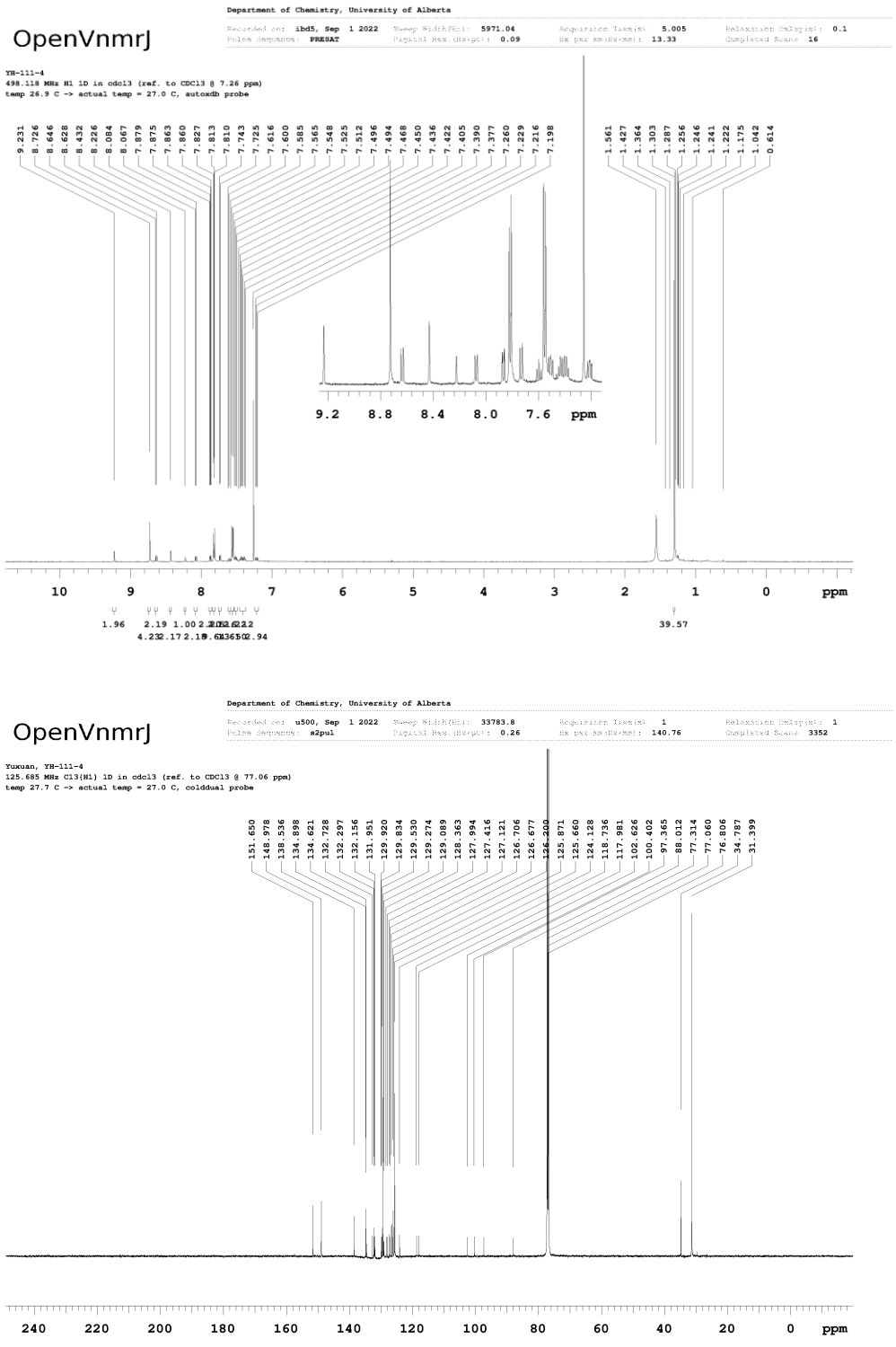

Figure 7.21. ^{1}H NMR and ^{13}C NMR spectra of **mPh(TcPy)$_2$** in $CDCl_3$.

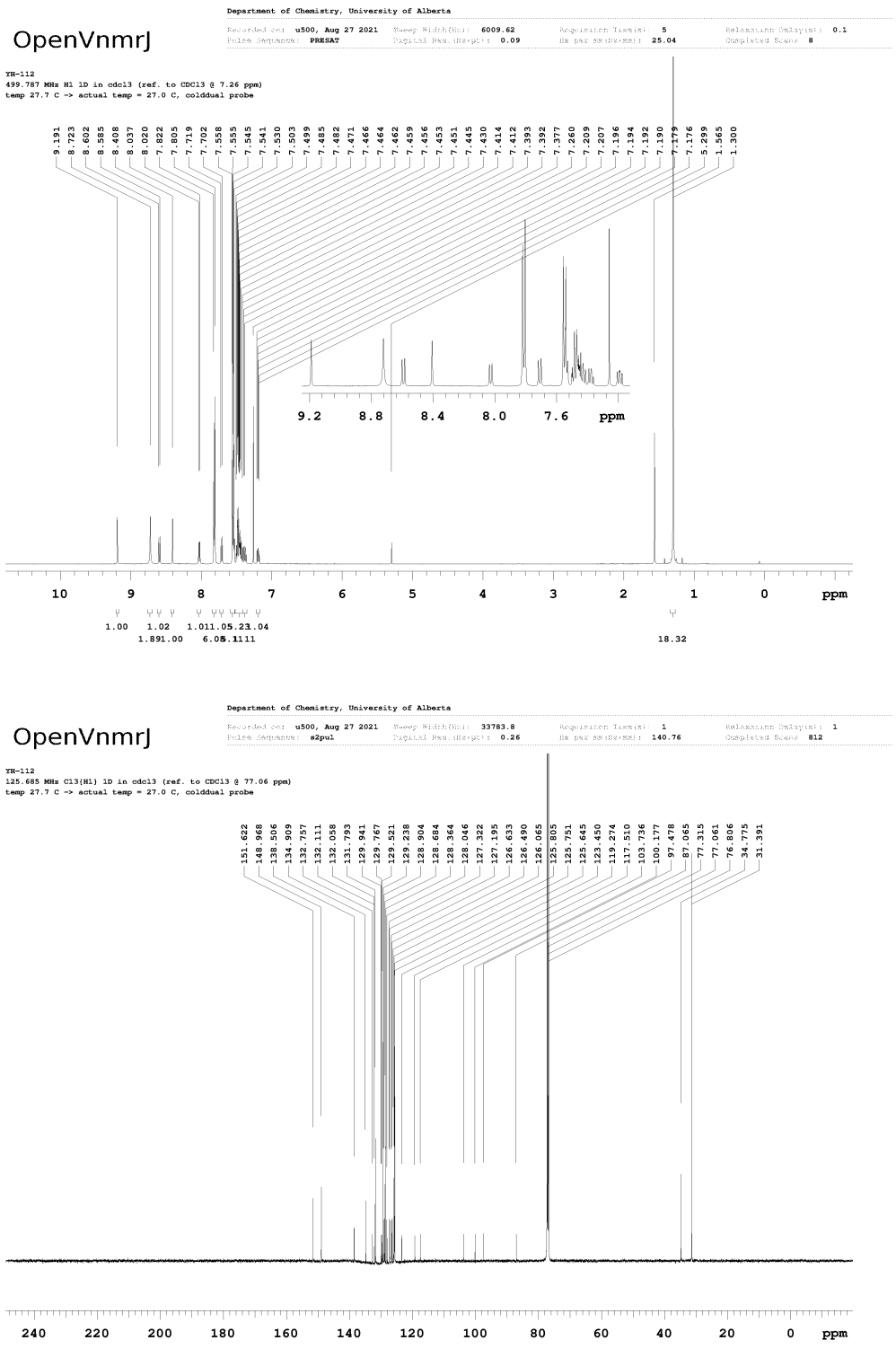

Figure 7.22. ^{1}H NMR and ^{13}C NMR spectra of **PhTcPy** in $CDCl_3$.

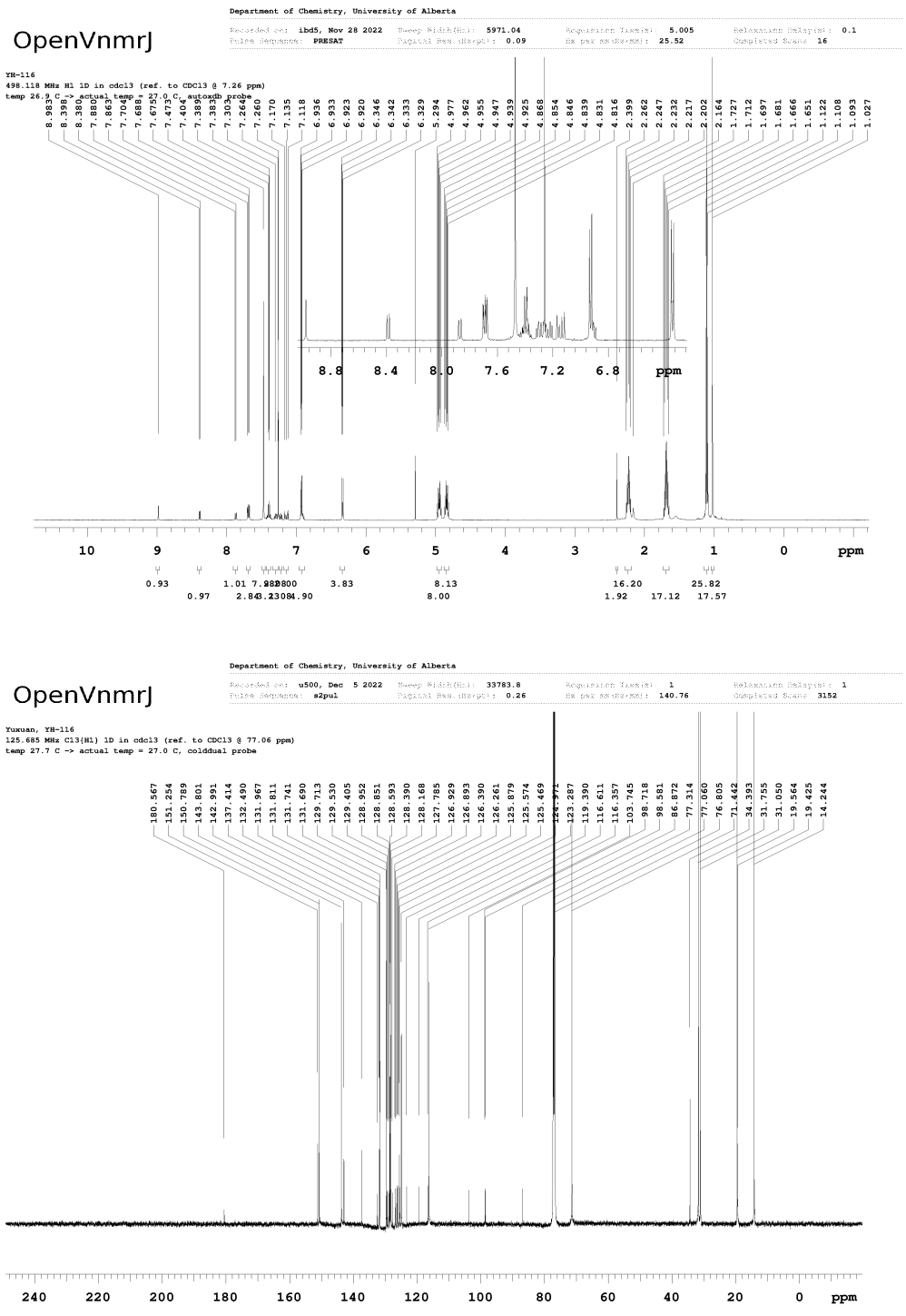

Figure 7.23. ^{1}H NMR and ^{13}C NMR spectra of **PhTcPy-RuPc** in $CDCl_3$.

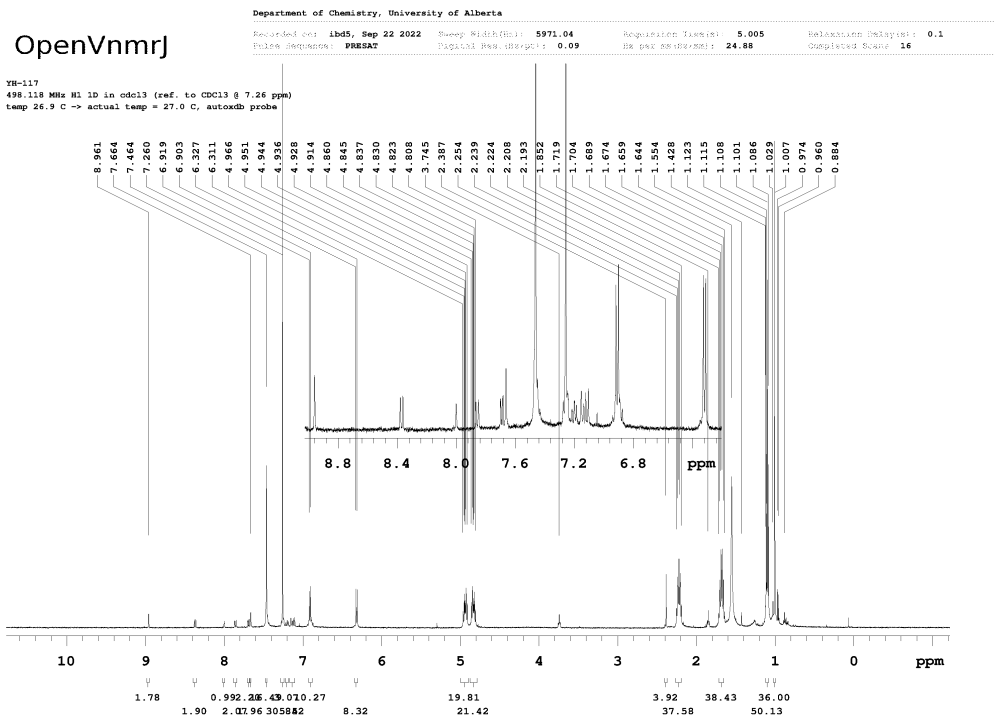

Figure 7.24. ^{1}H NMR spectrum of **mPh(TcPy-RuPc)$_2$** in $CDCl_3$.

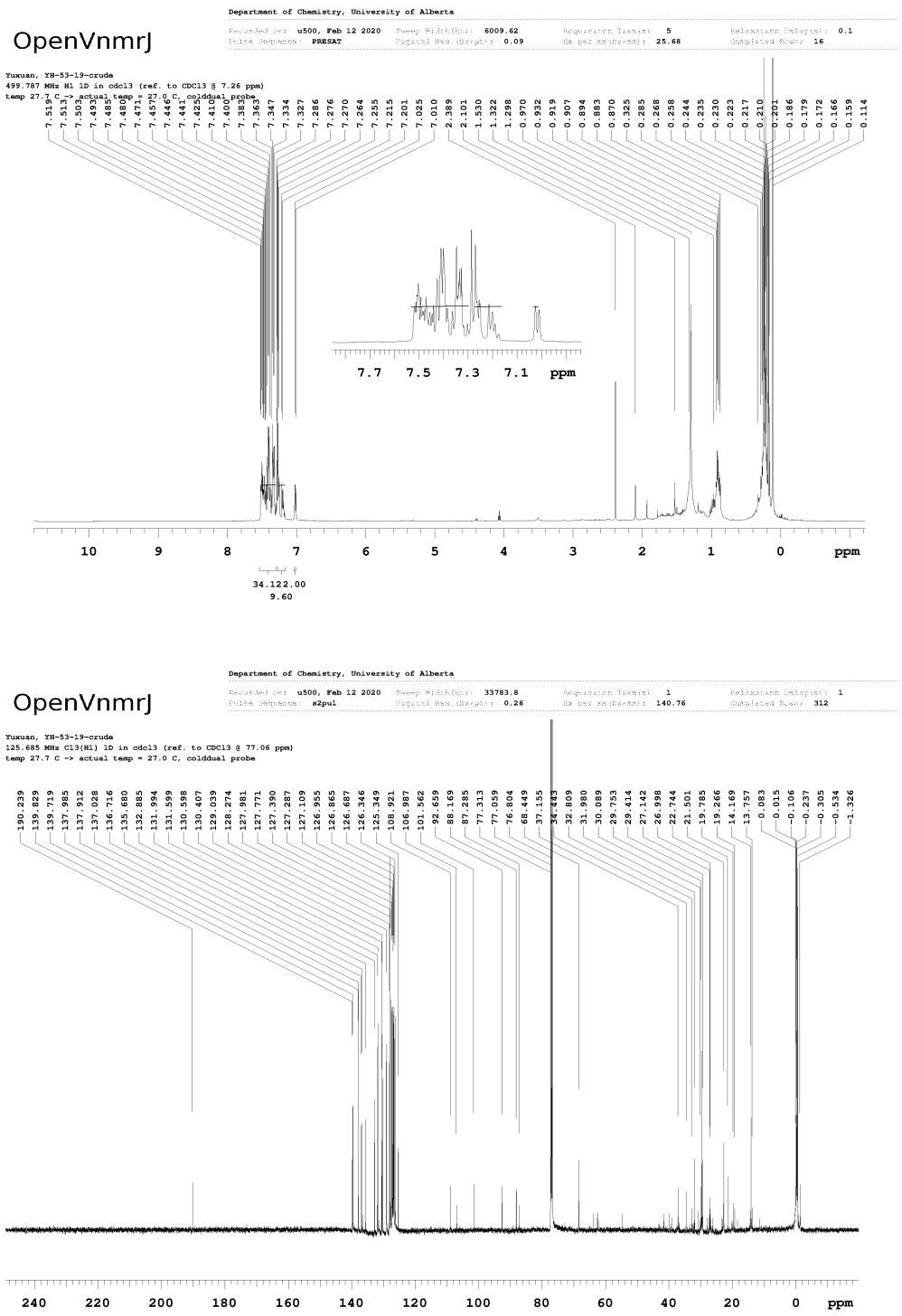

Figure 7.25. ^{1}H NMR and ^{13}C NMR spectra of compound **5.10** in $CDCl_3$.

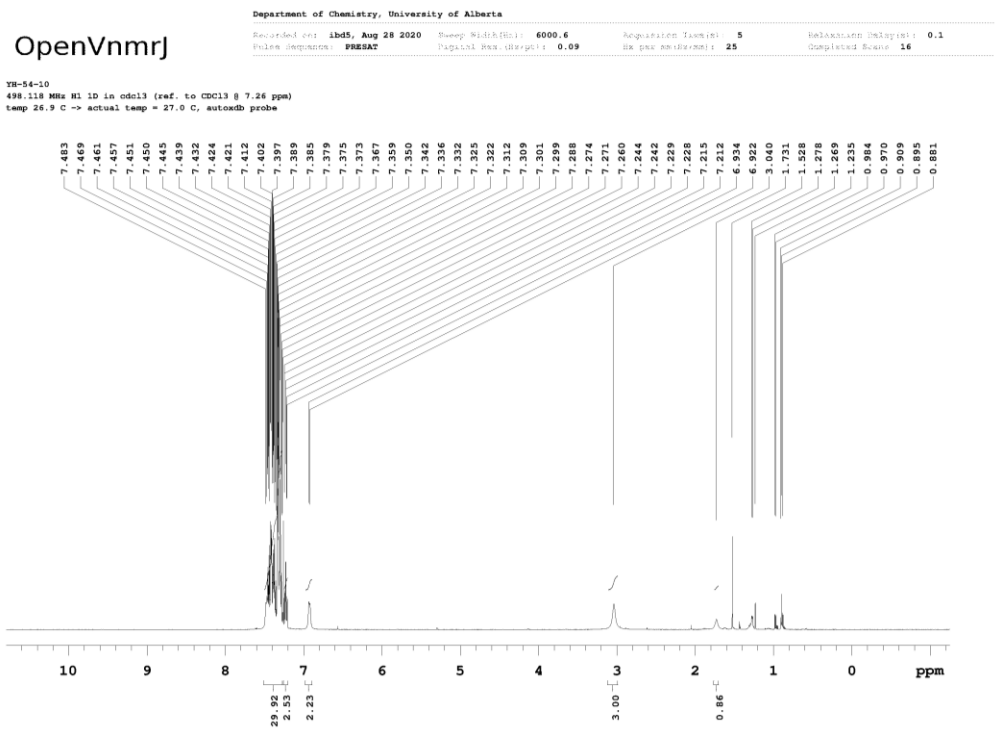

Figure 7.26. ^{1}H NMR spectrum of compound **5.11** in $CDCl_3$.

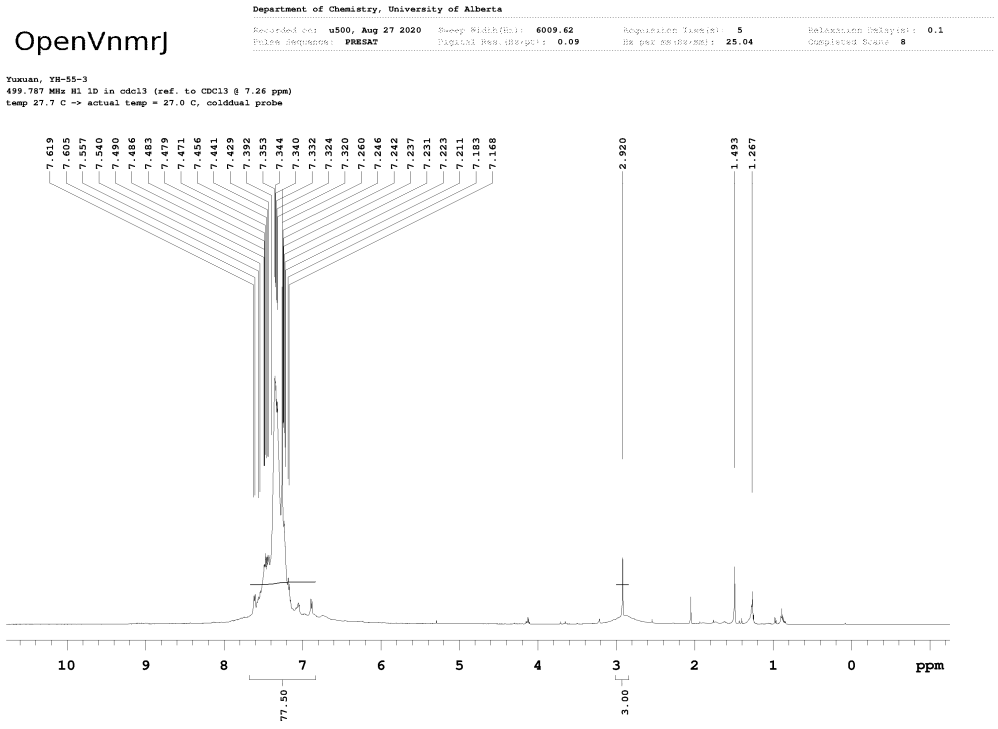

Figure 7.27. ^{1}H NMR spectrum of compound **5.12** in $CDCl_3$.

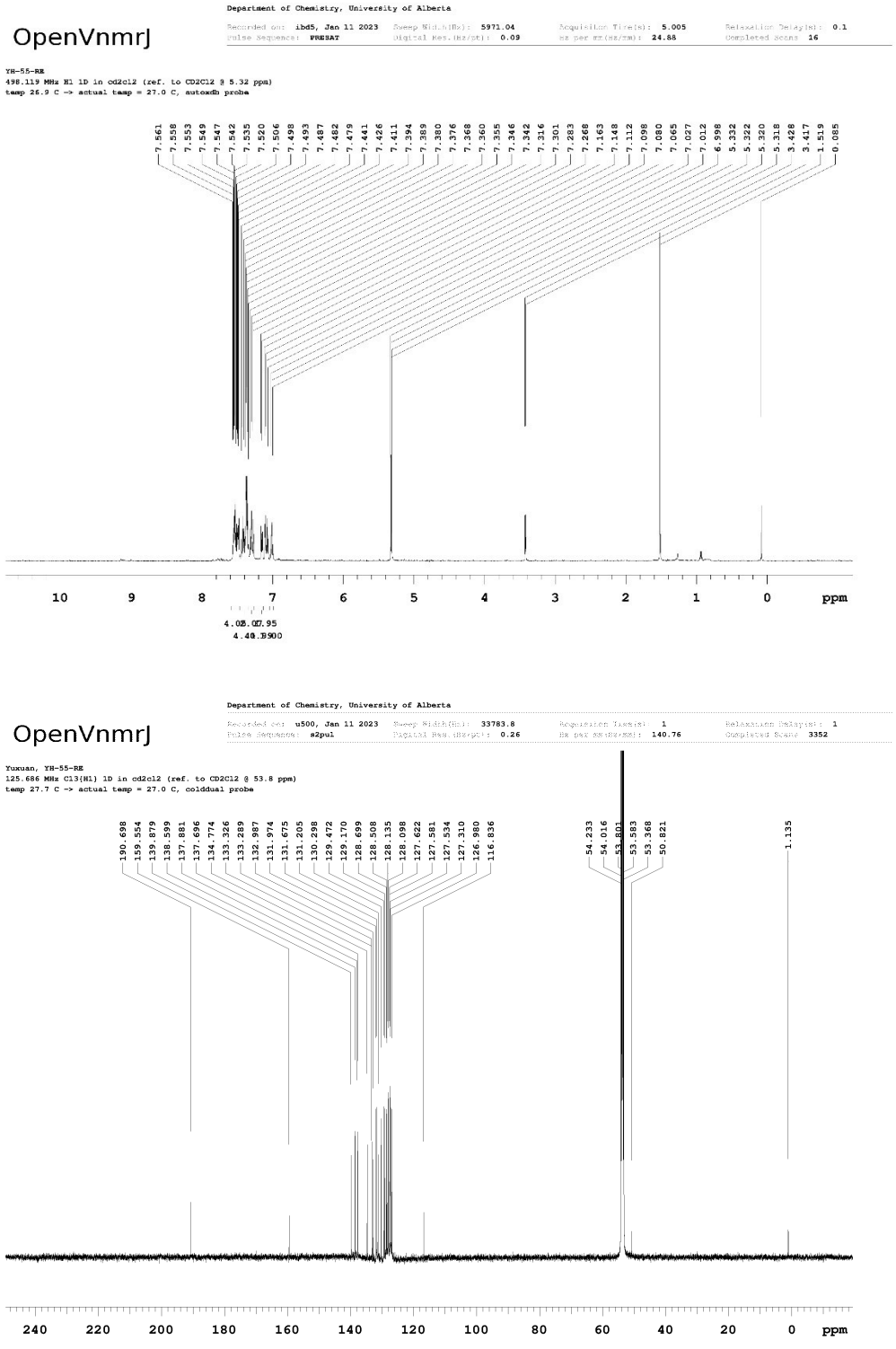

Figure 7.28. ^{1}H NMR and ^{13}C NMR spectra of **[5]tetraPh** in CD_2Cl_2.

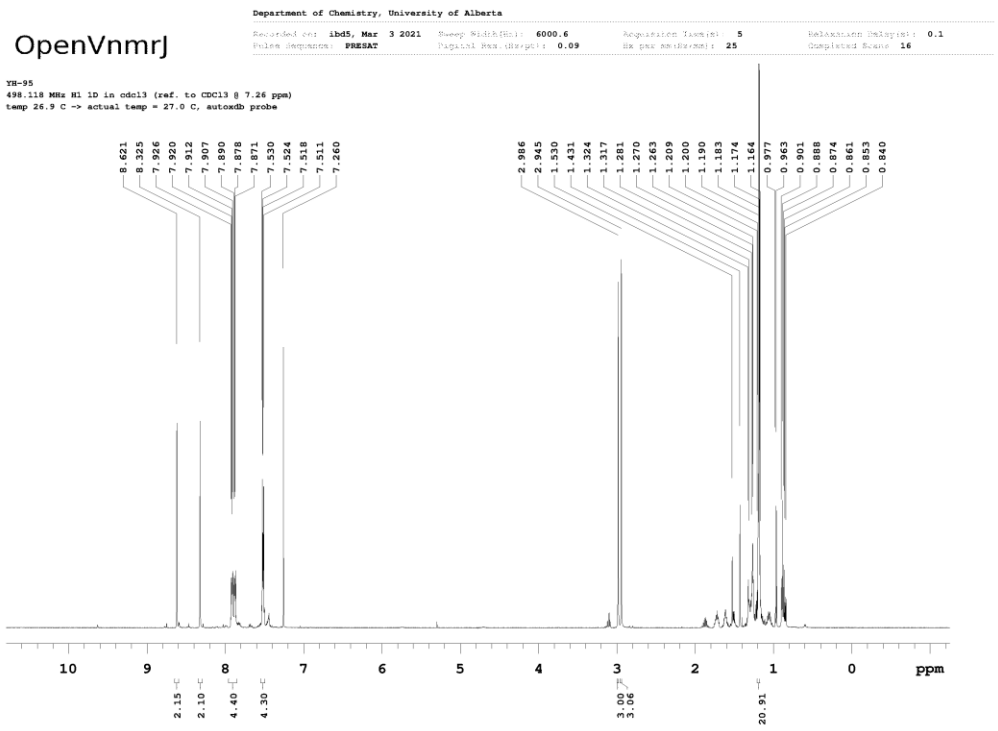

Figure 7.29. ^{1}H NMR spectrum of compound **5.34** in $CDCl_3$.

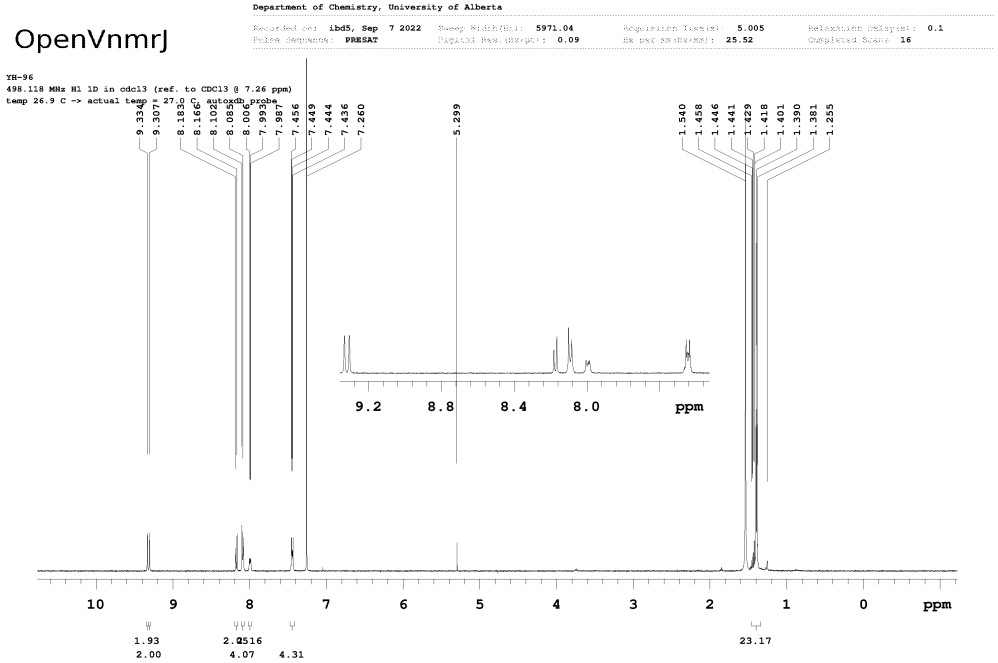

Figure 7.30. ^{1}H NMR spectrum of ***trans*-azo-Pc$_2$** in $CDCl_3$.

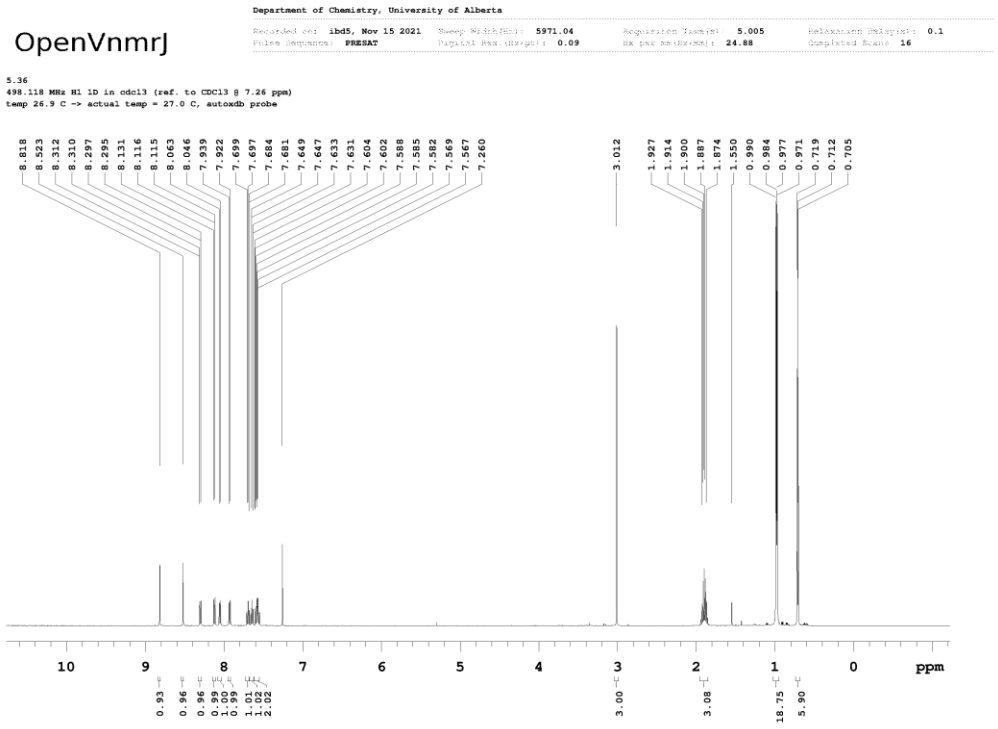

Figure 7.31. ^{1}H NMR spectrum of compound **5.36** in $CDCl_3$.

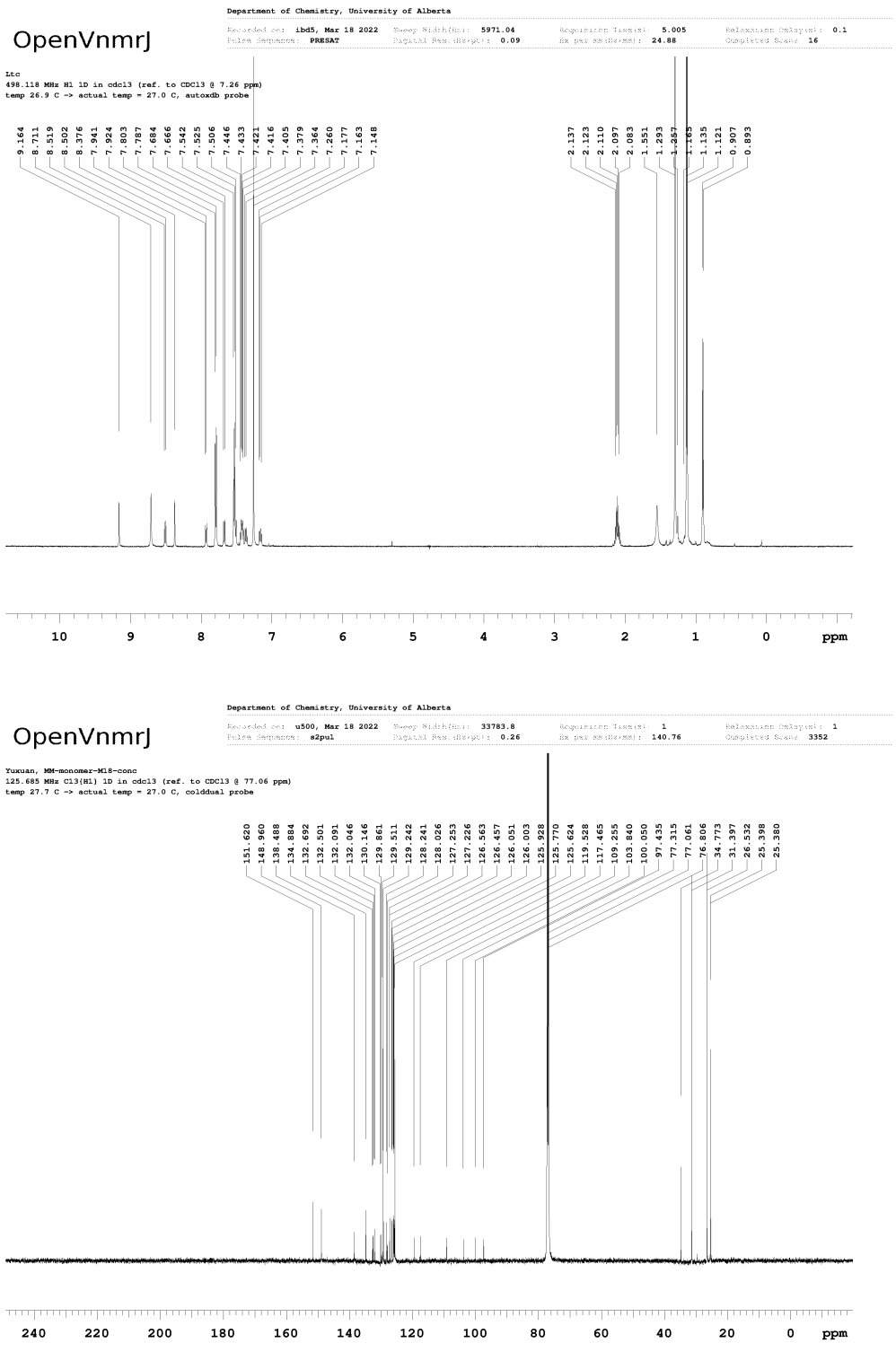

Figure 7.32. ^{1}H NMR and ^{13}C NMR spectra of $\mathbf{L_{tc}}$ in $CDCl_3$.

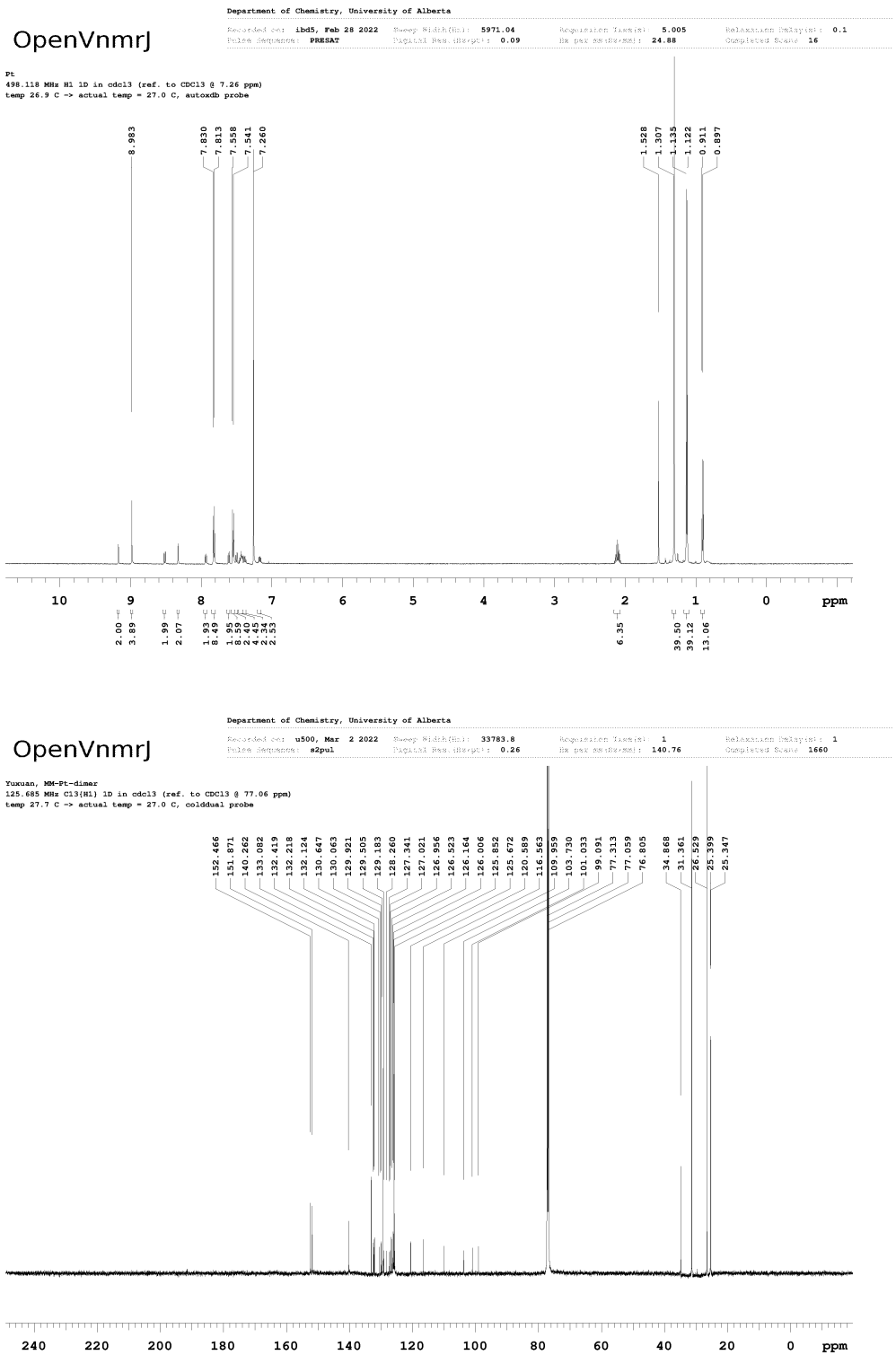

Figure 7.33. ^{1}H NMR and ^{13}C NMR spectra of **Pt(L_{tc})$_2$Cl$_2$** in $CDCl_3$.

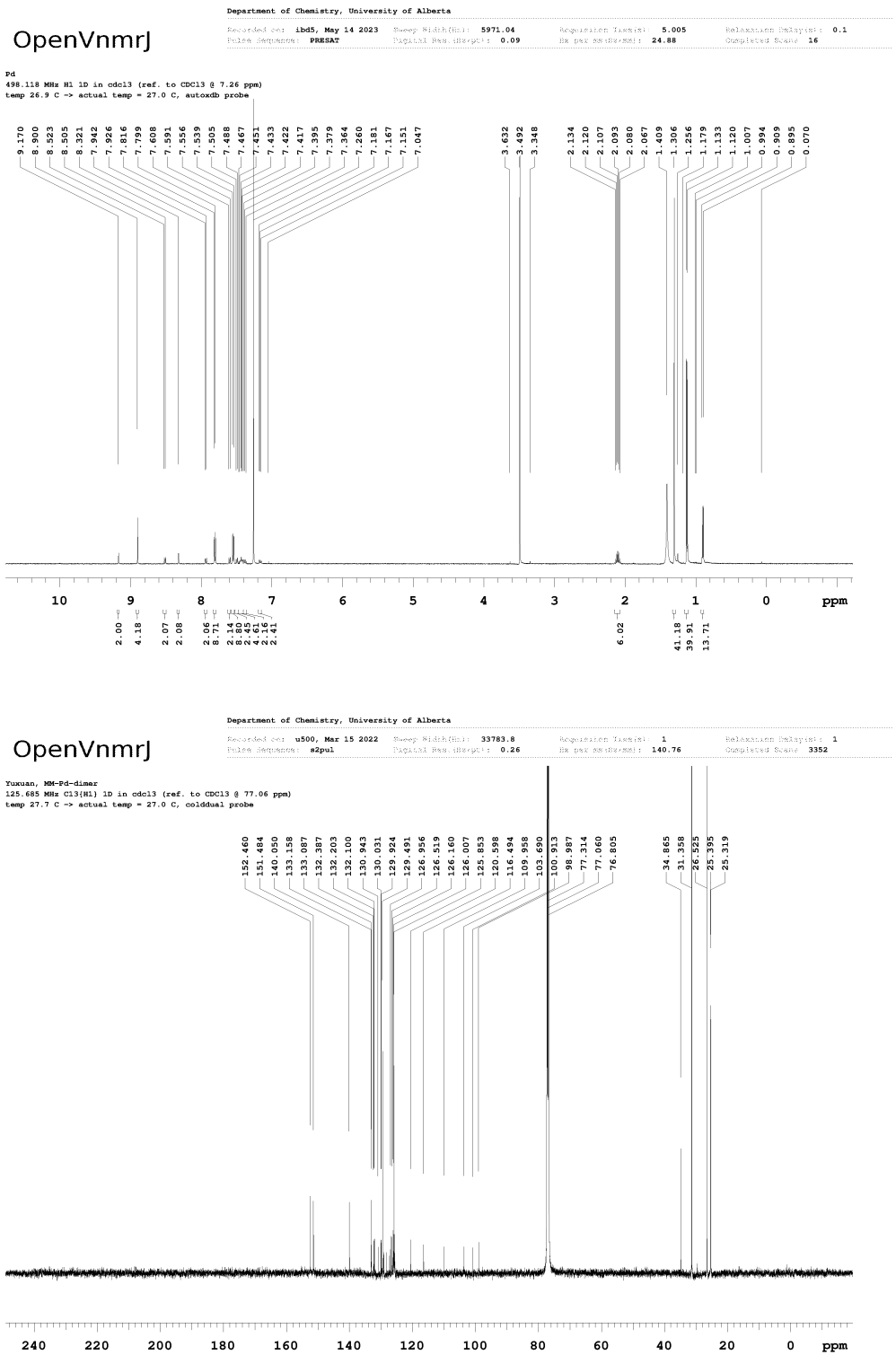

Figure 7.34. ^{1}H NMR and ^{13}C NMR spectra of **Pd(L$_{tc}$)$_2$Cl$_2$** in $CDCl_3$.

References

[1] Y. Gao, Y. Hou, F. Gordillo Gámez, M. J. Ferguson, J. Casado, R. R. Tykwinski, *Nat. Chem.* **2020**, *12*, 1143–1149.

[2] B. S. Basel, J. Zirzlmeier, C. Hetzer, B. T. Phelan, M. D. Krzyaniak, S. R. Reddy, P. B. Coto, N. E. Horwitz, R. M. Young, F. J. White, F. Hampel, T. Clark, M. Thoss, R. R. Tykwinski, M. R. Wasielewski, D. M. Guldi, *Nat. Commun.* **2017**, *8*, 15171.

[3] J. Sarju, J. Arbour, J. Sayer, B. Rohrmoser, W. Scherer, G. Wagner, *Dalton Trans.* **2008**, 5302–5312.

[4] L. P. Wu, Y. Suenaga, T. KurodaSowa, M. Maekawa, K. Furuichi, M. Munakata, *Inorg. Chim. Acta* **1996**, *248*, 147–152.

[5] C. M. Duff, G. A. Heath, *J. Chem. Soc., Dalton Trans.* **1991**, 2401–2411.

[6] A. L. Spek, *Acta Crystallogr. Sect. C: Struct. Chem.* **2015**, *71*, 9–18.

[7] T. X. Neenan, G. M. Whitesides, *J. Org. Chem.* **1988**, *53*, 2489–2496.

[8] D. W. Price, S. M. Dirk, F. Maya, J. M. Tour, *Tetrahedron* **2003**, *59*, 2497–2518.

[9] T. G. Archibald, A. A. Malik, K. Baum, M. R. Unroe, *Macromolecules* **1991**, *24*, 5261–5265.

[10] M. Bregnhoj, M. Westberg, F. Jensen, P. R. Ogilby, *Phys. Chem. Chem. Phys.* **2016**, *18*, 22946–22961.

[11] A. P. Kroitor, A. A. Dmitrienko, A. G. Martynov, Y. G. Gorbunova, A. B. Sorokin, *Org. Biomol. Chem.* **2023**, *21*, 69–74.

[12] C. F. H. Allen, J. W. Gates, *J. Am. Chem. Soc.* **1943**, *65*, 1502–1503.

[13] G. P. Miller, J. Briggs, in *Fullerenes--Volume 12: The Exciting World of Nanocages and Nanotubes, Vol. 12* (Eds.: P. V. Kamat, D. M. Guldi, K. M. Kadish), Electrochemical Society, New Jersey, **2002**, pp. 279–284.

[14] D. Lehnherr, A. H. Murray, R. McDonald, R. R. Tykwinski, *Angew. Chem. Int. Ed.* **2010**, *49*, 6190–6194.

[15] J. Strueben, P. J. Gates, A. Staubitz, *J. Org. Chem.* **2014**, *79*, 1719–1728.

Bibliography

CHAPTER 1

[1] S. Singh, W. J. Jones, W. Siebrand, B. P. Stoicheff, W. G. Schneider, *J. Chem. Phys.* **1965**, *42*, 330–342.

[2] R. P. Groff, P. Avakian, R. E. Merrifield, *Phys. Rev. B* **1970**, *1*, 815–817.

[3] H. Marciniak, M. Fiebig, M. Huth, S. Schiefer, B. Nickel, F. Selmaier, S. Lochbrunner, *Phys. Rev. Lett.* **2007**, *99*, 176402.

[4] J. Gao, F. A. Hegmann, *Appl. Phys. Lett.* **2008**, *93*, 223306.

[5] J. J. Burdett, A. M. Muller, D. Gosztola, C. J. Bardeen, *J. Chem. Phys.* **2010**, *133*, 144506.

[6] C. Gao, W. W. H. Wong, Z. Qin, S. C. Lo, E. B. Namdas, H. Dong, W. Hu, *Adv. Mater.* **2021**, *33*, 2100704.

[7] K. T. Munson, E. R. Kennehan, J. B. Asbury, *J. Mater. Chem. C* **2019**, *7*, 5889–5909.

[8] J. M. Aubry, C. Pierlot, J. Rigaudy, R. Schmidt, *Acc. Chem. Res.* **2003**, *36*, 668–675.

[9] S. Dong, A. Ong, C. Chi, *J. Photochem. Photobiol., C* **2019**, *38*, 27–46.

[10] T. Wang, B. Y. Zhang, H. L. Zhang, *Macromol. Rapid. Commun.* **2022**, *43*, 2200326.

[11] J. Li, H. Cao, Z. Zhang, S. Liu, Y. Xia, *Photonics* **2022**, *9*, 689.

[12] M. J. Dumas, *Ann. Chim. Phys.* **1832**, *50*, 182–197.

[13] X. Qiao, D. Ma, *Mater. Sci. Eng., R* **2020**, *139*, 100519.

[14] A. N. Aleshin, J. Y. Lee, S. W. Chu, J. S. Kim, Y. W. Park, *Appl. Phys. Lett.* **2004**, *84*, 5383–5385.

[15] M. Chen, L. Yan, Y. Zhao, I. Murtaza, H. Meng, W. Huang, *J. Mater. Chem. C* **2018**, *6*, 7416–7444.

[16] L. Jiang, H. Dong, W. Hu, *J. Mater. Chem.* **2010**, *20*, 4994–5007.

[17] T. R. Battersbya, P. Gantzela, K. K. Baldridge, J. S. Siegel, *Tetrahedron Lett.* **1995**, *36*, 845–848.

[18] T. Geiger, A. Haupt, C. Maichle-Mössmer, C. Schrenk, A. Schnepf, H. F. Bettinger, *J. Org. Chem.* **2019**, *84*, 10120–10135.

[19] M. Ehrenberg, *Acta Crystallogr.* **1966**, *20*, 177–182.

[20] O. C. Musgrave, *Chem. Rev.* **2002**, *69*, 499–531.

[21] T. Takahashi, T. Takenobu, J. Takeya, Y. Iwasa, *Adv. Funct. Mater.* **2007**, *17*, 1623–1628.

[22] J. J. Burdett, C. J. Bardeen, *Acc. Chem. Res.* **2013**, *46*, 1312–1320.

[23] R. Lapouyade, A. Nourmamode, H. Bouas-Laurent, *Tetrahedron* **1980**, *36*, 2311–2316.

[24] E. Clar, F. John, *Ber. Dtsch. Chem. Ges.* **1929**, *62*, 3021–3029.

[25] E. Clar, F. John, *Ber. Dtsch. Chem. Ges.* **1930**, *63*, 2967–2977.

[26] N. Vets, M. Smet, W. Dehaen, *Tetrahedron Lett.* **2004**, *45*, 7287–7289.

[27] O. Berg, E. L. Chronister, T. Yamashita, G. W. Scott, R. M. Sweet, J. Calabrese, *J. Phys. Chem. A* **1999**, *103*, 2451–2459.

[28] I. Kaur, G. P. Miller, *New J. Chem.* **2008**, *32*, 459–463.

[29] A. Maliakal, K. Raghavachari, H. Katz, E. Chandross, T. Siegrist, *Chem. Mater.* **2004**, *16*, 4980–4986.

[30] S. S. Zade, M. Bendikov, *J. Phys. Org. Chem.* **2012**, *25*, 452–461.

[31] J. B. Briggs, G. P. Miller, *C. R. Chim.* **2006**, *9*, 916–927.

[32] J. E. Anthony, *Angew. Chem. Int. Ed.* **2008**, *47*, 452–483.
[33] R. E. Blankenship, D. M. Tiede, J. Barber, G. W. Brudvig, G. Fleming, M. Ghirardi, M. R. Gunner, W. Junge, D. M. Kramer, A. Melis, T. A. Moore, C. C. Moser, D. G. Nocera, A. J. Nozik, D. R. Ort, W. W. Parson, R. C. Prince, R. T. Sayre, *Science* **2011**, *332*, 805–809.
[34] J. Hansen, P. Kharecha, M. Sato, V. Masson-Delmotte, F. Ackerman, D. J. Beerling, P. J. Hearty, O. Hoegh-Guldberg, S. L. Hsu, C. Parmesan, J. Rockstrom, E. J. Rohling, J. Sachs, P. Smith, K. Steffen, L. Van Susteren, K. von Schuckmann, J. C. Zachos, *PLoS One* **2013**, *8*, e81648.
[35] L. Tsakalakos, L. C. Hirst, N. J. Ekins-Daukes, in *Next Gener. Photonic Cell Technol. Sol. Energy Convers., Vol. 7772*, **2010**, p. 777211.
[36] R. Rawat, R. Lamba, S. C. Kaushik, *Renewable and Sustainable Energy Rev.* **2017**, *71*, 630–638.
[37] W. Shockley, H. J. Queisser, *J. Appl. Phys.* **1961**, *32*, 510–519.
[38] S. Rühle, *Sol. Energy* **2016**, *130*, 139–147.
[39] A. Rao, R. H. Friend, *Nat. Rev. Mater.* **2017**, *2*, 17063.
[40] J. Xia, S. N. Sanders, W. Cheng, J. Z. Low, J. Liu, L. M. Campos, T. Sun, *Adv. Mater.* **2017**, *29*, 1601652.
[41] M. B. Smith, J. Michl, *Annu. Rev. Phys. Chem.* **2013**, *64*, 361–386.
[42] T. Sharma, P. Mahajan, M. Adil Afroz, A. Singh, Yukta, N. Kumar Tailor, S. Purohit, S. Verma, B. Padha, V. Gupta, S. Arya, S. Satapathi, *ChemSusChem* **2022**, *15*, e202101067.
[43] M. C. Hanna, A. J. Nozik, *J. Appl. Phys.* **2006**, *100*, 074510.
[44] D. Beery, T. W. Schmidt, K. Hanson, *ACS Appl. Mater. Interfaces* **2021**, *13*, 32601–32605.
[45] E. M. Gholizadeh, S. K. K. Prasad, Z. L. Teh, T. Ishwara, S. Norman, A. J. Petty, J. H. Cole, S. Cheong, R. D. Tilley, J. E. Anthony, S. Huang, T. W. Schmidt, *Nat. Photonics* **2020**, *14*, 585–590.
[46] M. Uji, T. J. B. Zahringer, C. Kerzig, N. Yanai, *Angew. Chem. Int. Ed.* **2023**, *62*, e202301506.
[47] M. B. Smith, J. Michl, *Chem. Rev.* **2010**, *110*, 6891–6936.
[48] J. Michl, *Mol. Front. J.* **2019**, *03*, 84–91.
[49] M. K. Gish, N. A. Pace, G. Rumbles, J. C. Johnson, *J. Phys. Chem. C* **2019**, *123*, 3923–3934.
[50] K. Miyata, F. S. Conrad-Burton, F. L. Geyer, X. Y. Zhu, *Chem. Rev.* **2019**, *119*, 4261–4292.
[51] B. S. Basel, J. Zirzlmeier, C. Hetzer, B. T. Phelan, M. D. Krzyaniak, S. R. Reddy, P. B. Coto, N. E. Horwitz, R. M. Young, F. J. White, F. Hampel, T. Clark, M. Thoss, R. R. Tykwinski, M. R. Wasielewski, D. M. Guldi, *Nat. Commun.* **2017**, *8*, 15171.
[52] C. Hetzer, D. M. Guldi, R. R. Tykwinski, *Chem. - Eur. J.* **2018**, *24*, 8245–8257.
[53] H. Sakai, R. Inaya, H. Nagashima, S. Nakamura, Y. Kobori, N. V. Tkachenko, T. Hasobe, *J. Phys. Chem. Lett.* **2018**, *9*, 3354–3360.
[54] R. J. Hudson, A. N. Stuart, D. M. Huang, T. W. Kee, *J. Phys. Chem. C* **2022**, *126*, 5369–5377.
[55] B. S. Basel, J. Zirzlmeier, C. Hetzer, S. R. Reddy, B. T. Phelan, M. D. Krzyaniak, M. K. Volland, P. B. Coto, R. M. Young, T. Clark, M. Thoss, R. R. Tykwinski, M. R. Wasielewski, D. M. Guldi, *Chem* **2018**, *4*, 1092–1111.
[56] M. Chen, M. D. Krzyaniak, J. N. Nelson, Y. J. Bae, S. M. Harvey, R. D. Schaller, R. M. Young, M. R. Wasielewski, *Proc. Natl. Acad. Sci. U. S. A.* **2019**, *116*, 8178–8183.
[57] T. S. C. MacDonald, M. J. Y. Tayebjee, M. I. Collins, E. Kumarasamy, S. N. Sanders, M. Y. Sfeir, L. M. Campos, D. R. McCamey, *J. Am. Chem. Soc.* **2023**, *145*, 15275–15283.
[58] T. Hasobe, *Chem. Lett.* **2021**, *50*, 615–622.

[59] S. N. Sanders, A. B. Pun, K. R. Parenti, E. Kumarasamy, L. M. Yablon, M. Y. Sfeir, L. M. Campos, *Chem* **2019**, *5*, 1988–2005.
[60] T. Minami, S. Ito, M. Nakano, *J. Phys. Chem. Lett.* **2012**, *3*, 2719–2723.
[61] J. Zirzlmeier, D. Lehnherr, P. B. Coto, E. T. Chernick, R. Casillas, B. S. Basel, M. Thoss, R. R. Tykwinski, D. M. Guldi, *Proc. Natl. Acad. Sci. U. S. A.* **2015**, *112*, 5325–5330.
[62] R. Ringstrom, F. Edhborg, Z. W. Schroeder, L. Chen, M. J. Ferguson, R. R. Tykwinski, B. Albinsson, *Chem. Sci.* **2022**, *13*, 4944–4954.
[63] T. Hasobe, S. Nakamura, N. V. Tkachenko, Y. Kobori, *ACS Energy Lett.* **2021**, *7*, 390–400.
[64] R. Casillas, I. Papadopoulos, T. Ullrich, D. Thiel, A. Kunzmann, D. M. Guldi, *Energy Environ. Sci.* **2020**, *13*, 2741–2804.
[65] T. Wang, H. Liu, X. Wang, L. Tang, J. Zhou, X. Song, L. Lv, W. Chen, Y. Chen, X. Li, *J. Mater. Chem. A* **2023**, *11*, 8515–8539.
[66] A. J. Carrod, V. Gray, K. Börjesson, *Energy Environ. Sci.* **2022**, *15*, 4982–5016.
[67] P. Bharmoria, H. Bildirir, K. Moth-Poulsen, *Chem. Soc. Rev.* **2020**, *49*, 6529–6554.
[68] S. E. Seo, H.-S. Choe, H. Cho, H.-i. Kim, J.-H. Kim, O. S. Kwon, *J. Mater. Chem. C* **2022**, *10*, 4483–4496.
[69] L. Zeng, L. Huang, J. Han, G. Han, *Acc. Chem. Res.* **2022**, *55*, 2604–2615.
[70] *Proc. R. Soc. London, Ser. A* **1962**, *269*, 574–584.
[71] T. Trupke, M. A. Green, P. Würfel, *J. Appl. Phys.* **2002**, *92*, 4117–4122.
[72] R. R. Islangulov, J. Lott, C. Weder, F. N. Castellano, *J. Am. Chem. Soc.* **2007**, *129*, 12652–12653.
[73] L. Wei, C. Yang, W. Wu, *Mater. Chem. Front.* **2023**, *7*, 3194–3208.
[74] L. Naimovicius, P. Bharmoria, K. Moth-Poulsen, *Mater. Chem. Front.* **2023**, *7*, 2297–2315.
[75] T. Schloemer, P. Narayanan, Q. Zhou, E. Belliveau, M. Seitz, D. N. Congreve, *ACS Nano* **2023**, *17*, 3259–3288.
[76] J. Feng, J. Alves, D. M. de Clercq, T. W. Schmidt, *Annu. Rev. Phys. Chem.* **2023**, *74*, 145–168.
[77] G. Klein, R. Voltz, M. Schott, *Chem. Phys. Lett.* **1972**, *16*, 340–344.
[78] H. L. Stern, A. Cheminal, S. R. Yost, K. Broch, S. L. Bayliss, K. Chen, M. Tabachnyk, K. Thorley, N. Greenham, J. M. Hodgkiss, J. Anthony, M. Head-Gordon, A. J. Musser, A. Rao, R. H. Friend, *Nat. Chem.* **2017**, *9*, 1205–1212.
[79] F. Edhborg, H. Bildirir, P. Bharmoria, K. Moth-Poulsen, B. Albinsson, *J. Phys. Chem. B* **2021**, *125*, 6255–6263.
[80] A. Olesund, V. Gray, J. Martensson, B. Albinsson, *J. Am. Chem. Soc.* **2021**, *143*, 5745–5754.
[81] R. Ieuji, K. Goushi, C. Adachi, *Nat. Commun.* **2019**, *10*, 5283.
[82] T. Ullrich, D. Munz, D. M. Guldi, *Chem. Soc. Rev.* **2021**, *50*, 3485–3518.
[83] B. J. Walker, A. J. Musser, D. Beljonne, R. H. Friend, *Nat. Chem.* **2013**, *5*, 1019–1024.
[84] S. R. Yost, J. Lee, M. W. B. Wilson, T. Wu, D. P. McMahon, R. R. Parkhurst, N. J. Thompson, D. N. Congreve, A. Rao, K. Johnson, M. Y. Sfeir, M. G. Bawendi, T. M. Swager, R. H. Friend, M. A. Baldo, T. Van Voorhis, *Nat. Chem.* **2014**, *6*, 492–497.
[85] N. V. Korovina, N. F. Pompetti, J. C. Johnson, *J. Chem. Phys.* **2020**, *152*, 040904.
[86] I. Papadopoulos, J. Zirzlmeier, C. Hetzer, Y. J. Bae, M. D. Krzyaniak, M. R. Wasielewski, T. Clark, R. R. Tykwinski, D. M. Guldi, *J. Am. Chem. Soc.* **2019**, *141*, 6191–6203.
[87] A. Kunzmann, M. Gruber, R. Casillas, J. Zirzlmeier, M. Stanzel, W. Peukert, R. R. Tykwinski, D. M. Guldi, *Angew. Chem. Int. Ed.* **2018**, *57*, 10742–10747.
[88] B. S. Basel, I. Papadopoulos, D. Thiel, R. Casillas, J. Zirzlmeier, T. Clark, D. M. Guldi, R. R. Tykwinski, *Trends Chem.* **2019**, *1*, 11–21.

[89] N. V. Korovina, J. Joy, X. Feng, C. Feltenberger, A. I. Krylov, S. E. Bradforth, M. E. Thompson, *J. Am. Chem. Soc.* **2018**, *140*, 10179–10190.

[90] R. S. Mattos, I. Burghardt, A. J. A. Aquino, T. M. Cardozo, H. Lischka, *J. Am. Chem. Soc.* **2022**, *144*, 23492–23504.

[91] S. Mardazad, Y. Xu, X. Yang, M. Grundner, U. Schollwock, H. Ma, S. Paeckel, *J. Chem. Phys.* **2021**, *155*, 194101.

[92] E. A. Buchanan, Z. Havlas, J. Michl, *Bull. Chem. Soc. Jpn.* **2019**, *92*, 1960–1971.

[93] M. W. B. Wilson, A. Rao, K. Johnson, S. Gelinas, R. di Pietro, J. Clark, R. H. Friend, *J. Am. Chem. Soc.* **2013**, *135*, 16680–16688.

[94] D. N. Congreve, J. Y. Lee, N. J. Thompson, E. Hontz, S. R. Yost, P. D. Reusswig, M. E. Bahlke, S. Reineke, T. Van Voorhis, M. A. Baldo, *Science* **2013**, *340*, 334–337.

[95] X. Feng, A. I. Krylov, *Phys. Chem. Chem. Phys.* **2016**, *18*, 7751–7761.

[96] T. C. Wu, N. J. Thompson, D. N. Congreve, E. Hontz, S. R. Yost, T. Van Voorhis, M. A. Baldo, *Appl. Phys. Lett.* **2014**, *104*.

[97] A. B. Pun, S. N. Sanders, E. Kumarasamy, M. Y. Sfeir, D. N. Congreve, L. M. Campos, *Adv. Mater.* **2017**, *29*, 1701416–n/a.

[98] H. Liu, Z. Wang, X. Wang, L. Shen, C. Zhang, M. Xiao, X. Li, *J. Mater. Chem. C* **2018**, *6*, 3245–3253.

[99] A. B. Pun, S. N. Sanders, M. Y. Sfeir, L. M. Campos, D. N. Congreve, *Chem. Sci.* **2019**, *10*, 3969−3975.

[100] K. J. Fallon, E. M. Churchill, S. N. Sanders, J. Shee, J. L. Weber, R. Meir, S. Jockusch, D. R. Reichman, M. Y. Sfeir, D. N. Congreve, L. M. Campos, *J. Am. Chem. Soc.* **2020**, *142*, 19917−19925.

[101] C. J. Imperiale, P. B. Green, E. G. Miller, N. H. Damrauer, M. W. B. Wilson, *J. Phys. Chem. Lett.* **2019**, *10*, 7463–7469.

[102] J. E. Anthony, J. S. Brooks, D. L. Eaton, S. R. Parkin, *J. Am. Chem. Soc.* **2001**, *123*, 9482–9483.

[103] D. Lehnherr, A. H. Murray, R. McDonald, R. R. Tykwinski, *Angew. Chem. Int. Ed.* **2010**, *49*, 6190–6194.

[104] T. Iwanaga, Y. Yamamoto, K. Nishioka, S. Toyota, *Synthesis* **2015**, *47*, 3997–4007.

[105] D. Lehnherr, M. Adam, A. H. Murray, R. McDonald, F. Hampel, R. R. Tykwinski, *Can. J. Chem.* **2016**, *95*, 303–314.

[106] D. R. Maulding, B. G. Roberts, *J. Org. Chem.* **1969**, *34*, 1734–1736.

[107] R. N. Baral, S. W. Thomas, III, *J. Org. Chem.* **2015**, *80*, 11086–11091.

[108] T. Takahashi, K. Kashima, S. Li, K. Nakajima, K.-i. Kanno, *J. Am. Chem. Soc.* **2007**, *129*, 15752–15753.

[109] E. Kumarasamy, S. N. Sanders, A. B. Pun, S. A. Vaselabadi, J. Z. Low, M. Y. Sfeir, M. L. Steigerwald, G. E. Stein, L. M. Campos, *Macromolecules* **2016**, *49*, 1279–1285.

[110] H. Yu, Y. He, Y. Wu, Y. He, C. He, H. Meng, *Org. Electron.* **2020**, *85*.

[111] E. G. Fuemmeler, S. N. Sanders, A. B. Pun, E. Kumarasamy, T. Zeng, K. Miyata, M. L. Steigerwald, X. Y. Zhu, M. Y. Sfeir, L. M. Campos, N. Ananth, *ACS Cent. Sc.* **2016**, *2*, 316–324.

[112] M. J. Y. Tayebjee, S. N. Sanders, E. Kumarasamy, L. M. Campos, M. Y. Sfeir, D. R. McCamey, *Nat. Phys.* **2017**, *13*, 182–188.

[113] D. Casanova, *Chem. Rev.* **2018**, *118*, 7164–7207.

[114] S. Khan, S. Mazumdar, *Phys. Rev. B* **2018**, *98*, 165202.

[115] L. Abu-Sen, J. J. Morrison, A. B. Horn, S. G. Yeates, *Adv. Opt. Mater.* **2014**, *2*, 636–640.

[116] W. Fudickar, T. Linker, *J. Am. Chem. Soc.* **2012**, *134*, 15071–15082.
[117] C. P. Bénard, Z. Geng, M. A. Heuft, K. VanCrey, A. G. Fallis, *J. Org. Chem.* **2007**, *72*, 7229–7236.
[118] P. Coppo, S. G. Yeates, *Adv. Mater.* **2005**, *17*, 3001–3005.
[119] S. Li, Z. Li, K. Nakajima, K.-i. Kanno, T. Takahashi, *Chem. - Asian J.* **2009**, *4*, 294–301.
[120] S. S. Zade, N. Zamoshchik, A. R. Reddy, G. Fridman-Marueli, D. Sheberla, M. Bendikov, *J. Am. Chem. Soc.* **2011**, *133*, 10803–10816.
[121] M. Garcia-Borràs, A. Konishi, A. Waterloo, Y. Liang, Y. Cao, C. Hetzer, D. Lehnherr, F. Hampel, K. N. Houk, R. R. Tykwinski, *Chem. - Eur. J.* **2017**, *23*, 6111–6117.
[122] M. M. Rauhut, B. G. Roberts, D. R. Maulding, W. Bergmark, R. Coleman, *J. Org. Chem.* **1975**, *40*, 330–335.
[123] J. E. Anthony, D. L. Eaton, S. R. Parkin, *Org. Lett.* **2002**, *4*, 15–18.
[124] D. Lehnherr, J. Gao, F. A. Hegmann, R. R. Tykwinski, *Org. Lett.* **2008**, *10*, 4779–4782.
[125] S. A. Odom, S. R. Parkin, J. E. Anthony, *Org. Lett.* **2003**, *5*, 4245–4248.
[126] D. Lehnherr, R. McDonald, M. J. Ferguson, R. R. Tykwinski, *Tetrahedron* **2008**, *64*, 11449–11461.
[127] N. Monahan, X. Y. Zhu, *Annu. Rev. Phys. Chem.* **2015**, *66*, 601–618.
[128] K. M. Felter, F. C. Grozema, *J. Phys. Chem. Lett.* **2019**, *10*, 7208–7214.
[129] R. Casillas, M. Adam, P. B. Coto, A. R. Waterloo, J. Zirzlmeier, S. R. Reddy, F. Hampel, R. McDonald, R. R. Tykwinski, M. Thoss, D. M. Guldi, *Adv. Energy Mater.* **2019**, *9*, 1802221.
[130] M. J. Y. Tayebjee, K. N. Schwarz, R. W. MacQueen, M. Dvořák, A. W. C. Lam, K. P. Ghiggino, D. R. McCamey, T. W. Schmidt, G. J. Conibeer, *J. Phys. Chem. C* **2016**, *120*, 157–165.
[131] A. N. Stuart, P. C. Tapping, E. Schrefl, D. M. Huang, T. W. Kee, *J. Phys. Chem. C* **2019**, *123*, 5813–5825.
[132] C. Gao, S. K. K. Prasad, B. Zhang, M. Dvořák, M. J. Y. Tayebjee, D. R. McCamey, T. W. Schmidt, T. A. Smith, W. W. H. Wong, *J. Phys. Chem. C* **2019**, *123*, 20181–20187.
[133] S. Ito, T. Nagami, M. Nakano, *J. Phys. Chem. A* **2016**, *120*, 6236–6241.
[134] J. Hu, K. Xu, L. Shen, Q. Wu, G. He, J.-Y. Wang, J. Pei, J. Xia, M. Y. Sfeir, *Nat. Commun.* **2018**, *9*, 2999.
[135] E. Busby, J. Xia, Q. Wu, J. Z. Low, R. Song, J. R. Miller, X. Y. Zhu, L. M. Campos, M. Y. Sfeir, *Nat. Mater.* **2015**, *14*, 426–433.
[136] T. Zeng, P. Goel, *J. Phys. Chem. Lett.* **2016**, *7*, 1351–1358.
[137] S. Mattiello, S. Mecca, A. Ronchi, A. Calascibetta, G. Mattioli, F. Pallini, F. Meinardi, L. Beverina, A. Monguzzi, *ACS Energy Lett.* **2022**, *7*, 2435–2442.
[138] A. M. Müller, Y. S. Avlasevich, W. W. Schoeller, K. Müllen, C. J. Bardeen, *J. Am. Chem. Soc.* **2007**, *129*, 14240–14250.
[139] Y. Matsui, S. Kawaoka, H. Nagashima, T. Nakagawa, N. Okamura, T. Ogaki, E. Ohta, S. Akimoto, A. Sato-Tomita, S. Yagi, Y. Kobori, H. Ikeda, *J. Phys. Chem. C* **2019**, *123*, 18813–18823.
[140] J. C. Miller, J. S. Meek, S. J. Strickler, *J. Am. Chem. Soc.* **1977**, *99*, 8175–8179.
[141] L. Lin, J. Zhu, *Inorg. Chem. Front.* **2022**, *9*, 914–924.
[142] D. Lubert-Perquel, E. Salvadori, M. Dyson, P. N. Stavrinou, R. Montis, H. Nagashima, Y. Kobori, S. Heutz, C. W. M. Kay, *Nat. Commun.* **2018**, *9*, 4222.
[143] B. S. Basel, R. M. Young, M. D. Krzyaniak, I. Papadopoulos, C. Hetzer, Y. Gao, N. T. La Porte, B. T. Phelan, T. Clark, R. R. Tykwinski, M. R. Wasielewski, D. M. Guldi, *Chem. Sci.* **2019**, *10*, 11130–11140.

[144] N. Maity, W. Kim, N. A. Panjwani, A. Kundu, K. Majumder, P. Kasetty, D. Mishra, R. Bittl, J. Nagesh, J. Dasgupta, A. J. Musser, S. Patil, *Nat. Commun.* **2022**, *13*, 5244.
[145] D. Sasikumar, A. T. John, J. Sunny, M. Hariharan, *Chem. Soc. Rev.* **2020**, *49*, 6122–6140.
[146] A. J. Musser, M. Al-Hashimi, M. Heeney, J. Clark, *J. Chem. Phys.* **2019**, *151*, 044902.
[147] I. Papadopoulos, Y. Gao, C. Hetzer, R. R. Tykwinski, D. M. Guldi, *Chemphotochem* **2020**, *4*, 5168–5174.
[148] W. L. Chan, J. R. Tritsch, X. Y. Zhu, *J. Am. Chem. Soc.* **2012**, *134*, 18295–18302.
[149] B. Daiber, K. van den Hoven, M. H. Futscher, B. Ehrler, *ACS Energy Lett.* **2021**, *6*, 2800–2808.
[150] S. N. Sanders, E. Kumarasamy, A. B. Pun, M. T. Trinh, B. Choi, J. Xia, E. J. Taffet, J. Z. Low, J. R. Miller, X. Roy, X. Y. Zhu, M. L. Steigerwald, M. Y. Sfeir, L. M. Campos, *J. Am. Chem. Soc.* **2015**, *137*, 8965–8972.
[151] S. N. Sanders, E. Kumarasamy, A. B. Pun, M. L. Steigerwald, M. Y. Sfeir, L. M. Campos, *Chem* **2016**, *1*, 505–511.
[152] G. He, L. M. Yablon, K. R. Parenti, K. J. Fallon, L. M. Campos, M. Y. Sfeir, *J. Am. Chem. Soc.* **2022**, *144*, 3269–3278.
[153] J. Kim, H. T. Teo, Y. Hong, J. Oh, H. Kim, C. Chi, D. Kim, *Angew. Chem. Int. Ed.* **2020**, *59*, 20956–20964.
[154] L. M. Yablon, S. N. Sanders, H. Li, K. R. Parenti, E. Kumarasamy, K. J. Fallon, M. J. A. Hore, A. Cacciuto, M. Y. Sfeir, L. M. Campos, *J. Am. Chem. Soc.* **2019**, *141*, 9564–9569.
[155] C. Hetzer, B. S. Basel, S. M. Kopp, F. Hampel, F. J. White, T. Clark, D. M. Guldi, R. R. Tykwinski, *Angew. Chem. Int. Ed.* **2019**, *58*, 15263–15267.
[156] R. D. Ribson, G. Choi, R. G. Hadt, T. Agapie, *ACS Cent. Sci.* **2020**, *6*, 2088–2096.
[157] Y. Gao, Y. Hou, F. Gordillo Gámez, M. J. Ferguson, J. Casado, R. R. Tykwinski, *Nat. Chem.* **2020**, *12*, 1143–1149.
[158] Y. Li, Y. Wu, P. Liu, Z. Prostran, S. Gardner, B. S. Ong, *Chem. Mater.* **2007**, *19*, 418–423.
[159] T. Theiss, S. Buss, I. Maisuls, R. López-Arteaga, D. Brünink, J. Kösters, A. Hepp, N. L. Doltsinis, E. A. Weiss, C. A. Strassert, *J. Am. Chem. Soc.* **2023**, *145*, 3937–2951.
[160] C. A. Strassert, M. Mauro, L. De Cola, *Adv. Inorg. Chem.* **2011**, *63*, 47–103.
[161] A. K. Pal, G. S. Hanan, *Chem. Soc. Rev.* **2014**, *43*, 6184–6197.
[162] B. Pashaei, H. Shahroosvand, M. Graetzel, M. K. Nazeeruddin, *Chem. Rev.* **2016**, *116*, 9485–9564.
[163] I. Papadopoulos, S. R. Reddy, P. B. Coto, D. Lehnherr, D. Thiel, M. Thoss, R. R. Tykwinski, D. M. Guldi, *J. Phys. Chem. Lett.* **2022**, 5094–5100.

CHAPTER 2

[1] R. D. Ribson, G. Choi, R. G. Hadt, T. Agapie, *ACS Cent. Sci.* **2020**, *6*, 2088–2096.
[2] Y. Gao, Y. Hou, F. Gordillo Gámez, M. J. Ferguson, J. Casado, R. R. Tykwinski, *Nat. Chem.* **2020**, *12*, 1143–1149.
[3] O. Berg, E. L. Chronister, T. Yamashita, G. W. Scott, R. M. Sweet, J. Calabrese, *J. Phys. Chem. A* **1999**, *103*, 2451–2459.
[4] J. E. Anthony, *Angew. Chem. Int. Ed.* **2008**, *47*, 452–483.
[5] Y. Li, Y. Wu, P. Liu, Z. Prostran, S. Gardner, B. S. Ong, *Chem. Mater.* **2007**, *19*, 418–423.
[6] J. B. Briggs, G. P. Miller, *C. R. Chim.* **2006**, *9*, 916–927.
[7] A. K. Pal, G. S. Hanan, *Chem. Soc. Rev.* **2014**, *43*, 6184–6197.

[8] B. Pashaei, H. Shahroosvand, M. Graetzel, M. K. Nazeeruddin, *Chem. Rev.* **2016**, *116*, 9485–9564.

[9] C. Hetzer, B. S. Basel, S. M. Kopp, F. Hampel, F. J. White, T. Clark, D. M. Guldi, R. R. Tykwinski, *Angew. Chem. Int. Ed.* **2019**, *58*, 15263–15267.

[10] B. S. Basel, J. Zirzlmeier, C. Hetzer, B. T. Phelan, M. D. Krzyaniak, S. R. Reddy, P. B. Coto, N. E. Horwitz, R. M. Young, F. J. White, F. Hampel, T. Clark, M. Thoss, R. R. Tykwinski, M. R. Wasielewski, D. M. Guldi, *Nat. Commun.* **2017**, *8*, 15171.

[11] J. Sarju, J. Arbour, J. Sayer, B. Rohrmoser, W. Scherer, G. Wagner, *Dalton Trans.* **2008**, 5302–5312.

[12] L. P. Wu, Y. Suenaga, T. KurodaSowa, M. Maekawa, K. Furuichi, M. Munakata, *Inorg. Chim. Acta* **1996**, *248*, 147–152.

[13] M. M. Olmstead, P.-p. Wei, A. S. Ginwalla, A. L. Balch, *Inorg. Chem.* **2000**, *39*, 4555–4559.

[14] T. Nakagawa, H. Danjo, M. Kawahata, K. Yamaguchi, *Tetrahedron* **2019**, *75*, 315–323.

[15] M. J. Mayoral, C. Rest, V. Stepanenko, J. Schellheimer, R. Q. Albuquerque, G. Fernández, *J. Am. Chem. Soc.* **2013**, *135*, 2148–2151.

[16] D. Fujita, A. Takahashi, S. Sato, M. Fujita, *J. Am. Chem. Soc.* **2011**, *133*, 13317–13319.

[17] C. M. Duff, G. A. Heath, *J. Chem. Soc., Dalton Trans.* **1991**, 2401–2411.

[18] C. Tessier, F. D. Rochon, *Inorg. Chim. Acta* **1999**, *295*, 25–38.

[19] L. Pazderski, J. Toušek, J. Sitkowski, K. Maliňáková, L. Kozerski, E. Szłyk, *Magn. Reson. Chem.* **2009**, *47*, 228–238.

[20] L. Pazderski, T. Pawlak, J. Sitkowski, L. Kozerski, E. Szłyk, *Magn. Reson. Chem.* **2010**, *48*, 417–426.

[21] N. A. Lewis, S. Pakhomova, P. A. Marzilli, L. G. Marzilli, *Inorg. Chem.* **2017**, *56*, 9781–9793.

[22] G. Kurpik, A. Walczak, M. Gołdyn, J. Harrowfield, A. R. Stefankiewicz, *Inorg. Chem.* **2022**, *61*, 14019–14029.

[23] C. A. Strassert, M. Mauro, L. De Cola, *Adv. Inorg. Chem.* **2011**, *63*, 47–103.

[24] T. Theiss, S. Buss, I. Maisuls, R. López-Arteaga, D. Brünink, J. Kösters, A. Hepp, N. L. Doltsinis, E. A. Weiss, C. A. Strassert, *J. Am. Chem. Soc.* **2023**, *145*, 3937–2951.

[25] D. Lehnherr, A. H. Murray, R. McDonald, R. R. Tykwinski, *Angew. Chem. Int. Ed.* **2010**, *49*, 6190–6194.

[26] B. S. Basel, R. M. Young, M. D. Krzyaniak, I. Papadopoulos, C. Hetzer, Y. Gao, N. T. La Porte, B. T. Phelan, T. Clark, R. R. Tykwinski, M. R. Wasielewski, D. M. Guldi, *Chem. Sci.* **2019**, *10*, 11130–11140.

[27] I. Papadopoulos, Y. Gao, C. Hetzer, R. R. Tykwinski, D. M. Guldi, *Chemphotochem* **2020**, *4*, 5168–5174.

[28] M.-H. Nguyen, J. H. K. Yip, *Organometallics* **2012**, *31*, 7522–7531.

[29] Z. Bu, Z. Wang, L. Yang, S. Cao, *Appl. Organomet. Chem.* **2010**, *24*, 813–816.

[30] W. T. Wong, T. C. Lau, *Acta Crystallogr. Sect. C: Struct. Chem.* **1994**, *50*, 1406–1407.

[31] M. R. J. Elsegood, D. A. Tocher, *Acta Crystallogr. Sect. C: Struct. Chem.* **1995**, *51*, 40–42.

[32] J. G. Małecki, M. Jaworska, R. Kruszynski, R. Gil-bortnowska, *Polyhedron* **2005**, *24*, 1445–1453.

[33] A. Vertova, I. Cucchi, P. Fermo, F. Porta, D. M. Proserpio, S. Rondinini, *Electrochim. Acta* **2007**, *52*, 2603–2611.

[34] A. Cadranel, J. H. Hodak, *J. Coord. Chem.* **2015**, *68*, 1452–1464.

[35] M. Nishio, *CrystEngComm* **2004**, *6*, 130–158.

CHAPTER 3

[1] J. Zirzlmeier, D. Lehnherr, P. B. Coto, E. T. Chernick, R. Casillas, B. S. Basel, M. Thoss, R. R. Tykwinski, D. M. Guldi, *Proc. Natl. Acad. Sci. U. S. A.* **2015**, *112*, 5325–5330.

[2] B. S. Basel, J. Zirzlmeier, C. Hetzer, B. T. Phelan, M. D. Krzyaniak, S. R. Reddy, P. B. Coto, N. E. Horwitz, R. M. Young, F. J. White, F. Hampel, T. Clark, M. Thoss, R. R. Tykwinski, M. R. Wasielewski, D. M. Guldi, *Nat. Commun.* **2017**, *8*, 15171.

[3] C. Hetzer, D. M. Guldi, R. R. Tykwinski, *Chem. - Eur. J.* **2018**, *24*, 8245–8257.

[4] A. M. Müller, Y. S. Avlasevich, W. W. Schoeller, K. Müllen, C. J. Bardeen, *J. Am. Chem. Soc.* **2007**, *129*, 14240–14250.

[5] Y. Matsui, S. Kawaoka, H. Nagashima, T. Nakagawa, N. Okamura, T. Ogaki, E. Ohta, S. Akimoto, A. Sato-Tomita, S. Yagi, Y. Kobori, H. Ikeda, *J. Phys. Chem. C* **2019**, *123*, 18813–18823.

[6] A. J. Carrod, V. Gray, K. Börjesson, *Energy Environ. Sci.* **2022**, *15*, 4982–5016.

[7] T. Iwanaga, Y. Yamamoto, K. Nishioka, S. Toyota, *Synthesis* **2015**, *47*, 3997–4007.

[8] D. Lehnherr, R. McDonald, R. R. Tykwinski, *Org. Lett.* **2008**, *10*, 4163–4166.

[9] T. X. Neenan, G. M. Whitesides, *J. Org. Chem.* **1988**, *53*, 2489–2496.

[10] D. W. Price, S. M. Dirk, F. Maya, J. M. Tour, *Tetrahedron* **2003**, *59*, 2497–2518.

[11] T. G. Archibald, A. A. Malik, K. Baum, M. R. Unroe, *Macromolecules* **1991**, *24*, 5261–5265.

[12] M. Bregnhoj, M. Westberg, F. Jensen, P. R. Ogilby, *Phys. Chem. Chem. Phys.* **2016**, *18*, 22946–22961.

[13] Z. Liang, W. Zhao, S. Wang, Q. Tang, S.-C. Lam, Q. Miao, *Org. Lett.* **2008**, *10*, 2007–2010.

[14] K. T. Weber, K. Karikis, M. D. Weber, P. B. Coto, A. Charisiadis, D. Charitaki, G. Charalambidis, P. Angaridis, A. G. Coutsolelos, R. D. Costa, *Dalton Trans.* **2016**, *45*, 13284–13288.

[15] N. V. Korovina, J. Joy, X. Feng, C. Feltenberger, A. I. Krylov, S. E. Bradforth, M. E. Thompson, *J. Am. Chem. Soc.* **2018**, *140*, 10179–10190.

[16] M. Lippitz, C. G. Hübner, T. Christ, H. Eichner, P. Bordat, A. Herrmann, K. Müllen, T. Basché, *Phys. Rev. Lett.* **2004**, *92*, 103001.

CHAPTER 4

[1] E. M. Gholizadeh, S. K. K. Prasad, Z. L. Teh, T. Ishwara, S. Norman, A. J. Petty, J. H. Cole, S. Cheong, R. D. Tilley, J. E. Anthony, S. Huang, T. W. Schmidt, *Nat. Photonics* **2020**, *14*, 585–590.

[2] T. Trupke, M. A. Green, P. Würfel, *J. Appl. Phys.* **2002**, *92*, 4117–4122.

[3] R. R. Islangulov, J. Lott, C. Weder, F. N. Castellano, *J. Am. Chem. Soc.* **2007**, *129*, 12652–12653.

[4] A. B. Pun, S. N. Sanders, M. Y. Sfeir, L. M. Campos, D. N. Congreve, *Chem. Sci.* **2019**, *10*, 3969−3975.

[5] K. J. Fallon, E. M. Churchill, S. N. Sanders, J. Shee, J. L. Weber, R. Meir, S. Jockusch, D. R. Reichman, M. Y. Sfeir, D. N. Congreve, L. M. Campos, *J. Am. Chem. Soc.* **2020**, *142*, 19917−19925.

[6] C. J. Imperiale, P. B. Green, E. G. Miller, N. H. Damrauer, M. W. B. Wilson, *J. Phys. Chem. Lett.* **2019**, *10*, 7463–7469.
[7] S. Mattiello, S. Mecca, A. Ronchi, A. Calascibetta, G. Mattioli, F. Pallini, F. Meinardi, L. Beverina, A. Monguzzi, *ACS Energy Lett.* **2022**, *7*, 2435–2442.
[8] I. Papadopoulos, S. R. Reddy, P. B. Coto, D. Lehnherr, D. Thiel, M. Thoss, R. R. Tykwinski, D. M. Guldi, *J. Phys. Chem. Lett.* **2022**, 5094–5100.
[9] Y. Gao, Y. Hou, F. Gordillo Gámez, M. J. Ferguson, J. Casado, R. R. Tykwinski, *Nat. Chem.* **2020**, *12*, 1143–1149.
[10] S. J. Havens, P. M. Hergenrother, *J. Org. Chem.* **1985**, *50*, 1763–1765.
[11] A. S. Hay, *J. Org. Chem.* **1962**, *27*, 3320–3321.
[12] D. Lehnherr, A. H. Murray, R. McDonald, R. R. Tykwinski, *Angew. Chem. Int. Ed.* **2010**, *49*, 6190–6194.
[13] T. Iwanaga, Y. Yamamoto, K. Nishioka, S. Toyota, *Synthesis* **2015**, *47*, 3997–4007.
[14] A. P. Kroitor, A. A. Dmitrienko, A. G. Martynov, Y. G. Gorbunova, A. B. Sorokin, *Org. Biomol. Chem.* **2023**, *21*, 69–74.
[15] M. Hanack, Y. G. Kang, *Chem. Ber.* **1991**, *124*, 1607–1612.
[16] M. Hanack, S. Knecht, R. Polley, *Chem. Ber.* **1995**, *128*, 929–933.
[17] T. Rawling, A. McDonagh, *Coord. Chem. Rev.* **2007**, *251*, 1128–1157.
[18] A. N. Cammidge, G. Berber, I. Chambrier, P. W. Hough, M. J. Cook, *Tetrahedron* **2005**, *61*, 4067–4074.

CHAPTER 5

[1] M. B. Smith, J. Michl, *Chem. Rev.* **2010**, *110*, 6891–6936.
[2] T. Wang, H. Liu, X. Wang, L. Tang, J. Zhou, X. Song, L. Lv, W. Chen, Y. Chen, X. Li, *J. Mater. Chem. A* **2023**, *11*, 8515–8539.
[3] N. V. Korovina, N. F. Pompetti, J. C. Johnson, *J. Chem. Phys.* **2020**, *152*, 040904.
[4] R. Casillas, M. Adam, P. B. Coto, A. R. Waterloo, J. Zirzlmeier, S. R. Reddy, F. Hampel, R. McDonald, R. R. Tykwinski, M. Thoss, D. M. Guldi, *Adv. Energy Mater.* **2019**, *9*, 1802221.
[5] C. Hetzer, D. M. Guldi, R. R. Tykwinski, *Chem. - Eur. J.* **2018**, *24*, 8245–8257.
[6] A. M. Alvertis, S. Lukman, T. J. H. Hele, E. G. Fuemmeler, J. Feng, J. Wu, N. C. Greenham, A. W. Chin, A. J. Musser, *J. Am. Chem. Soc.* **2019**, *141*, 17558–17570.
[7] L. M. Yablon, S. N. Sanders, K. Miyazaki, E. Kumarasamy, G. He, B. Choi, N. Ananth, M. Y. Sfeir, L. M. Campos, *Mater. Horiz.* **2022**, *9*, 462–470.
[8] R. Ringstrom, F. Edhborg, Z. W. Schroeder, L. Chen, M. J. Ferguson, R. R. Tykwinski, B. Albinsson, *Chem. Sci.* **2022**, *13*, 4944–4954.
[9] P. Siemsen, R. C. Livingston, F. Diederich, *Angew. Chem. Int. Ed.* **2000**, *39*, 2632–2657.
[10] D. Lehnherr, A. H. Murray, R. McDonald, R. R. Tykwinski, *Angew. Chem. Int. Ed.* **2010**, *49*, 6190–6194.
[11] I. Papadopoulos, S. R. Reddy, P. B. Coto, D. Lehnherr, D. Thiel, M. Thoss, R. R. Tykwinski, D. M. Guldi, *J. Phys. Chem. Lett.* **2022**, 5094–5100.
[12] C. F. H. Allen, J. W. Gates, *J. Am. Chem. Soc.* **1943**, *65*, 1502–1503.
[13] G. P. Miller, J. Briggs, in *Fullerenes--Volume 12: The Exciting World of Nanocages and Nanotubes, Vol. 12* (Eds.: P. V. Kamat, D. M. Guldi, K. M. Kadish), Electrochemical Society, New Jersey, **2002**, pp. 279–284.

[14] A. S. Hay, *J. Org. Chem.* **1962**, *27*, 3320–3321.
[15] B. Sun, PhD Thesis, University of Alberta (Edmonton), **2022**.
[16] Y. Gao, Y. Hou, F. Gordillo Gámez, M. J. Ferguson, J. Casado, R. R. Tykwinski, *Nat. Chem.* **2020**, *12*, 1143–1149.
[17] J. P. C. M. van Dongen, M. J. A. de Bie, R. Steur, *Tetrahedron Lett.* **1973**, *14*, 1371–1374.
[18] M. Gruber, K. Padberg, J. Min, A. R. Waterloo, F. Hampel, H. Maid, T. Ameri, C. J. Brabec, R. R. Tykwinsk, *Chem. - Eur. J.* **2017**, *23*, 17829–17835.
[19] R. G. Clevenger, B. Kumar, E. M. Menuey, G. H. Lee, D. Patterson, K. V. Kilway, *Chem. - Eur. J.* **2018**, *24*, 243–250.
[20] G. R. Llorente, M. B. Dufourg-Madec, D. J. Crouch, R. G. Pritchard, S. Ogier, S. G. Yeates, *Chem. Commun.* **2009**, 3059–3061.
[21] H. Matsubara, S. Yasuda, H. Sugiyama, I. Ryu, Y. Fujii, K. Kita, *Tetrahedron* **2002**, *58*, 4071–4076.
[22] R. P. Kopreski, J. B. Briggs, W. Lin, M. Jazdzyk, G. P. Miller, *J. Org. Chem.* **2012**, *77*, 1308–1315.
[23] M. Nishio, *CrystEngComm* **2004**, *6*, 130–158.
[24] H. Fischer, *The chemistry of alkenes*, John Wiley & Sons Ltd., New York, **1964**.
[25] C. Zong, Y. Zhao, H. Ji, X. Han, J. Xie, J. Wang, Y. Cao, S. Jiang, C. Lu, *Angew. Chem. Int. Ed.* **2016**, *55*, 3931–3935.
[26] Y. Dong, P. E. S. Silva, J. V. I. Timonen, J. Vapaavuori, *Chemphyschem* **2023**, *24*, e202300153.
[27] I. C. D. Merritt, D. Jacquemin, M. Vacher, *Phys. Chem. Chem. Phys.* **2021**, *23*, 19155–19165.
[28] J. Strueben, P. J. Gates, A. Staubitz, *J. Org. Chem.* **2014**, *79*, 1719–1728.
[29] J. M. Mativetsky, G. Pace, M. Elbing, M. A. Rampi, M. Mayor, P. Samori, *J. Am. Chem. Soc.* **2008**, *130*, 9192–9193.
[30] A. N. Oldacre, C. A. Pointer, S. M. Martin, A. Kemmerer, E. R. Young, *Chem. Commun.* **2019**, *55*, 5874–5877.
[31] B. S. Basel, J. Zirzlmeier, C. Hetzer, B. T. Phelan, M. D. Krzyaniak, S. R. Reddy, P. B. Coto, N. E. Horwitz, R. M. Young, F. J. White, F. Hampel, T. Clark, M. Thoss, R. R. Tykwinski, M. R. Wasielewski, D. M. Guldi, *Nat. Commun.* **2017**, *8*, 15171.
[32] J. Sarju, J. Arbour, J. Sayer, B. Rohrmoser, W. Scherer, G. Wagner, *Dalton Trans.* **2008**, 5302–5312.
[33] L. P. Wu, Y. Suenaga, T. KurodaSowa, M. Maekawa, K. Furuichi, M. Munakata, *Inorg. Chim. Acta* **1996**, *248*, 147–152.
[34] C. Tessier, F. D. Rochon, *Inorg. Chim. Acta* **1999**, *295*, 25–38.
[35] L. Pazderski, J. Toušek, J. Sitkowski, K. Maliňáková, L. Kozerski, E. Szłyk, *Magn. Reson. Chem.* **2009**, *47*, 228–238.
[36] L. Pazderski, T. Pawlak, J. Sitkowski, L. Kozerski, E. Szłyk, *Magn. Reson. Chem.* **2010**, *48*, 417–426.
[37] N. A. Lewis, S. Pakhomova, P. A. Marzilli, L. G. Marzilli, *Inorg. Chem.* **2017**, *56*, 9781–9793.
[38] G. Kurpik, A. Walczak, M. Gołdyn, J. Harrowfield, A. R. Stefankiewicz, *Inorg. Chem.* **2022**, *61*, 14019–14029.
[39] C. A. Strassert, M. Mauro, L. De Cola, *Adv. Inorg. Chem.* **2011**, *63*, 47–103.
[40] T. Theiss, S. Buss, I. Maisuls, R. López-Arteaga, D. Brünink, J. Kösters, A. Hepp, N. L. Doltsinis, E. A. Weiss, C. A. Strassert, *J. Am. Chem. Soc.* **2023**, *145*, 3937–2951.

CHAPTER 6

[1] N. V. Korovina, N. F. Pompetti, J. C. Johnson, *J. Chem. Phys.* **2020**, *152*, 040904.

[2] D. Sasikumar, A. T. John, J. Sunny, M. Hariharan, *Chem. Soc. Rev.* **2020**, *49*, 6122–6140.

[3] B. Daiber, K. van den Hoven, M. H. Futscher, B. Ehrler, *ACS Energy Lett.* **2021**, *6*, 2800–2808.

[4] E. Zojer, C. Winkler, *J, Phys. Chem. Lett.* **2021**, *12*, 7002–7009.

[5] R. J. Hudson, A. N. Stuart, D. M. Huang, T. W. Kee, *J. Phys. Chem. C* **2022**, *126*, 5369–5377.

[6] T. Wang, H. Liu, X. Wang, L. Tang, J. Zhou, X. Song, L. Lv, W. Chen, Y. Chen, X. Li, *J. Mater. Chem. A* **2023**, *11*, 8515–8539.

[7] D. Lehnherr, A. H. Murray, R. McDonald, R. R. Tykwinski, *Angew. Chem. Int. Ed.* **2010**, *49*, 6190–6194.

[8] O. Alduhaish, R. B. Lin, H. L. Wang, B. Li, H. D. Arman, T. L. Hu, B. L. Chen, *Cryst. Growth Des.* **2018**, *18*, 4522–4527.

[9] A. V. Desai, S. Sharma, S. Let, S. K. Ghosh, *Coord. Chem. Rev.* **2019**, *395*, 146–192.

[10] M. Mostaghimi, C. R. C. Rêgo, R. Haldar, C. Wöll, W. Wenzel, M. Kozlowska, *Front. Mater.* **2022**, *9*, 840644.

[11] S. S. Rajasree, J. Yu, F. Fajardo-Rojas, H. C. Fry, R. Anderson, X. Li, W. Xu, J. Duan, S. Goswami, K. Maindan, D. A. Gomez-Gualdron, P. Deria, *J. Am. Chem. Soc.* **2023**, *145*, 17678–17688.

[12] R. Haldar, M. Kozlowska, M. Ganschow, S. Ghosh, M. Jakoby, H. Chen, F. Ghalami, W. Xie, S. Heidrich, Y. Tsutsui, J. Freudenberg, S. Seki, I. A. Howard, B. S. Richards, U. H. F. Bunz, M. Elstner, W. Wenzel, C. Woll, *Chem. Sci.* **2021**, *12*, 4477–4483.

[13] E. Zojer, C. Winkler, *J. Phys. Chem. Lett.* **2021**, *12*, 7002–7009.

[14] L. Naimovicius, P. Bharmoria, K. Moth-Poulsen, *Mater. Chem. Front.* **2023**, *7*, 2297–2315.

[15] T. Schloemer, P. Narayanan, Q. Zhou, E. Belliveau, M. Seitz, D. N. Congreve, *ACS Nano* **2023**, *17*, 3259–3288.

[16] M. Uji, T. J. B. Zahringer, C. Kerzig, N. Yanai, *Angew. Chem. Int. Ed.* **2023**, *62*, e202301506.

[17] L. Wei, C. Yang, W. Wu, *Mater. Chem. Front.* **2023**, *7*, 3194–3208.

[18] M. Wu, D. N. Congreve, M. W. B. Wilson, J. Jean, N. Geva, M. Welborn, T. Van Voorhis, V. Bulović, M. G. Bawendi, M. A. Baldo, *Nat. Photonics* **2015**, *10*, 31–34.

[19] E. M. Gholizadeh, S. K. K. Prasad, Z. L. Teh, T. Ishwara, S. Norman, A. J. Petty, J. H. Cole, S. Cheong, R. D. Tilley, J. E. Anthony, S. Huang, T. W. Schmidt, *Nat. Photonics* **2020**, *14*, 585–590.

[20] M. W. Brett, C. K. Gordon, J. Hardy, N. Davis, *ACS Phys. Chem. Au* **2022**, *2*, 364–387.

[21] V. Gray, W. Drake, J. R. Allardice, Z. Zhang, J. Xiao, D. G. Congrave, J. Royakkers, W. Zeng, S. Dowland, N. C. Greenham, H. Bronstein, J. E. Anthony, A. Rao, *J. Mater. Chem. C Mater.* **2022**, *10*, 16321–16329.

[22] L. Zeng, L. Huang, J. Han, G. Han, *Acc. Chem. Res.* **2022**, *55*, 2604–2615.

[23] V. Gray, J. R. Allardice, Z. Zhang, A. Rao, *Chem. Phys. Rev.* **2021**, *2*, 031305.

[24] C. Ye, D.-S. Zhang, B. Chen, C.-H. Tung, L.-Z. Wu, *Chem. Phys. Rev.* **2023**, *4*, 011304.

[25] C. C. Huang, Y. Tang, M. van der Laan, J. van de Groep, A. F. Koenderink, K. Dohnalova, *ACS Appl. Nano Mater.* **2021**, *4*, 288–296.

CHAPTER 7

[1] Y. Gao, Y. Hou, F. Gordillo Gámez, M. J. Ferguson, J. Casado, R. R. Tykwinski, *Nat. Chem.* **2020**, *12*, 1143–1149.

[2] B. S. Basel, J. Zirzlmeier, C. Hetzer, B. T. Phelan, M. D. Krzyaniak, S. R. Reddy, P. B. Coto, N. E. Horwitz, R. M. Young, F. J. White, F. Hampel, T. Clark, M. Thoss, R. R. Tykwinski, M. R. Wasielewski, D. M. Guldi, *Nat. Commun.* **2017**, *8*, 15171.

[3] J. Sarju, J. Arbour, J. Sayer, B. Rohrmoser, W. Scherer, G. Wagner, *Dalton Trans.* **2008**, 5302–5312.

[4] L. P. Wu, Y. Suenaga, T. KurodaSowa, M. Maekawa, K. Furuichi, M. Munakata, *Inorg. Chim. Acta* **1996**, *248*, 147–152.

[5] C. M. Duff, G. A. Heath, *J. Chem. Soc., Dalton Trans.* **1991**, 2401–2411.

[6] A. L. Spek, *Acta Crystallogr. Sect. C: Struct. Chem.* **2015**, *71*, 9–18.

[7] T. X. Neenan, G. M. Whitesides, *J. Org. Chem.* **1988**, *53*, 2489–2496.

[8] D. W. Price, S. M. Dirk, F. Maya, J. M. Tour, *Tetrahedron* **2003**, *59*, 2497–2518.

[9] T. G. Archibald, A. A. Malik, K. Baum, M. R. Unroe, *Macromolecules* **1991**, *24*, 5261–5265.

[10] M. Bregnhoj, M. Westberg, F. Jensen, P. R. Ogilby, *Phys. Chem. Chem. Phys.* **2016**, *18*, 22946–22961.

[11] A. P. Kroitor, A. A. Dmitrienko, A. G. Martynov, Y. G. Gorbunova, A. B. Sorokin, *Org. Biomol. Chem.* **2023**, *21*, 69–74.

[12] C. F. H. Allen, J. W. Gates, *J. Am. Chem. Soc.* **1943**, *65*, 1502–1503.

[13] G. P. Miller, J. Briggs, in *Fullerenes--Volume 12: The Exciting World of Nanocages and Nanotubes, Vol. 12* (Eds.: P. V. Kamat, D. M. Guldi, K. M. Kadish), Electrochemical Society, New Jersey, **2002**, pp. 279–284.

[14] D. Lehnherr, A. H. Murray, R. McDonald, R. R. Tykwinski, *Angew. Chem. Int. Ed.* **2010**, *49*, 6190–6194.

[15] J. Strueben, P. J. Gates, A. Staubitz, *J. Org. Chem.* **2014**, *79*, 1719–1728.